High Spin Entities – A Supramolecular Approach via Pure Organic and Coordination Chemistry

Vom Fachbereich Chemie
der Technischen Universität Darmstadt

zur Erlangung des akademischen Grades eines
Doktor rerum naturalium [Dr. rer. nat.]

genehmigte
Dissertation

vorgelegt von
Chandrasekar Rajadurai, M.Sc., M.Tech.,
aus Madurai, India

Berichterstatter:	Prof. Dr. H. Plenio
Mitberichterstatter:	Prof. Dr. W. Haase
Tag der Einreichung:	3.12.2003
Tag der mündlichen Prüfung:	26.1.2004

Darmstadt 2004
D 17

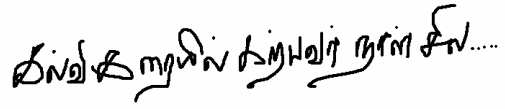

Kalvi Karayil Karpavar Nalsila.....
Naladiyar, 2:14:135

Learning is endless, (and) life so short....
Excerpt from Tamil Anthology of Quartets
Naladiyar, Circa, 50 B.C – 150 A.D

TABLE OF CONTENTS

Zusammenfassung

Ziel dieser Arbeit war die Synthese neuer Radikale und ihre supramolekulare Anordnung im Festkörper über Wasserstoffbrückenbindung, π-Stapelung und Metallkoordination.

So wurden im Rahmen dieser Dissertation zwei neue Hochspinliganden (**1** und **2**) basierend auf Nitronylnitroxiden, Monoradikale **3**-**5** und ein symmetrisches Trisnitronylnitroxid synthetisiert, sowie ausführlich charakterisiert.

Die absorptionsspektroskopischen Untersuchungen ergaben, dass eine Pyridin Komponente im Vergleich zu Benzol die Extinktionskoeffizienten verkleinert und die vibronische Kopplung bei direkter Verknüpfung mit den Radikalzentren verloren geht.

Aus den ESR-Spektren der Mono-, Bi- und Triradikale in flüssiger Lösung konnte direkt auf eine grosse Austauschwechselwirkung zwischen den Radikalzentren der Bi- und Triradikale geschlossen werden (J >> An). Für die Biradikale wurden Nullfeldaufspaltungen von D/hc ~ 0.24 $\times 10^{-4}$ cm^{-1} gemessen, die einem gemitteltem Dipolabstand von r ~ 1.02 nm entspricht. Dieser Abstand ist wesentlich kleiner als der aus den Röntgenstrukturen ermittelte (r ~ 1.5 nm) und weist die Spindelokalisation in das konjugierte System nach. Mithilfe temperaturabhängiger ESR-Messungen der Δms = 2 Übergänge wurde ein Curieverhalten gefunden, das im Einklang mit einer positiven Austauschwechselwirkung von J ~ 10 –15 K steht. Der Triplettgrundzustand wurde auch aus semiempirischen Rechnungen vorhergesagt.

Im 4. Kapitel werden die Zugänge zu neuen Metallkoordinationsverbindungen mit den Radikalen beschrieben. Als erstes wurde ein dreikerniger Kupfer Komplex **22** kristallisiert, der zwei verschiedene $Cu(hfac)_2$-Bindungsstellen aufweist und einen Spin von S = 5/2. Anschliessend wurden lineare Koordinationspolymere aus Monoradikal **4** durch Komplexierung mit $Cu(hfac)_2$ und $Mn(hfac)_2$ hergestellt. Für die alternierenden Kupferketten ergab sich eine ferromagnetische Kopplung (J = 6 cm^{-1}) und für die ferrimagnetischen Manganketten eine antiferromagnetische Kopplung, die über eine dipolare Wechselwirkung mit Nachbarketten erklärt werden konnte (zJ' = -0.33 cm^{-1}).

Unter Verwendung des Biradikals **1** zur Komplexierung mit $Cu(hfac)_2$ gelang es schliesslich auch, ein kompliziertes Netzwerk zu kristallisieren mit sieben Kupferzentren pro zwei Biradikalen. Die magnetischen Messungen ergaben hier

allerdings ein antiferromagnetisches Verhalten von 300 K bis zu 14 K und dann erst einen Anstieg der Suszeptibilitäten, der auf einen ferromagnetischen Übergang hindeutet.

Die rein organischen Ansätze zur supramolekularen Ordnung werden im 5. Kapitel beschrieben. Hier wurden als H-bindende Synthons die acetylenhaltigen Radikale **26** und **27** kristallisiert, deren Röntgenstrukturen lineare kettenförmige Anordnungen über schwache H-Brücken vom freien Acetylen-H zum Sauerstoff des Radikals aufweisen. Bei Temperaturen unterhalb 30 K werden die Wechselwirkungen allerdings antiferromagnetisch.

Schliesslich wurde auch die Stapelung von π-Systemen untersucht. Als erstes Beispiel wurde das Monoradikal **22** verwendet, das eine relativ grosse Stapeldistanz von 3.7 Å aufweist, und zusätzliche H-Verbrückung über Wassermoleküle. Obwohl die Radikale im Stapel um jeweils genau 60^{o} verdreht sind, was gut für eine ferromagnetische Anordnung ist, ergaben die magnetischen Messungen einen starken Abfall der Suszeptibilitäten unterhalb 50 K, und ein Ansteigen erst wieder unterhalb von 3 K.

Am Ende wurde noch ein symmtrisches Triradikal dargestellt, dessen reine π-Struktur (ohne NIT) als Stapel bereits literaturbekannt war. Allerdings waren die zugänglichen Mengen nicht gross genug, um auch die Festkörpereigenschaften näher zu bestimmen.

A - Hyperfine coupling
$a_{iso} = A_{iso}$ -Isotropic hyperfine splitting (Fermi contact term)
A_{dip} - Dipolar hyperfine coupling
$A_N = a_N$ - Nitrogen hyperfine splitting
$A_H = a_H$ - Proton hyperfine splitting
ΔB_{PP} - Difference in peak to peak line width
C - Curie constant
c - Concentration
D - Zero field splitting
d - Distance between the stacks
ΔE - Difference in energy
ΔE_{ST} - Singlet-triplet energy difference
ΔE_{DQ} - Doublet - quartet energy difference
g_e - Electron g factor
g_n - Nuclear g factor
h - Planck's constant
H - Magnetic field strength
$\hat{H}$ - Spin Hamiltonian
H_{dc} - Static field
I - Nuclear spin quantum number
$\hat{I}$ - Nuclear spin operator
J - Total angular momentum
J - Spin-spin exchange coupling energy
K_B - Boltzmann constant
K_{12} - Exchange integral
L - Orbital angular momentum
L/G - Lorentzion- Gaussian ratio
M – Magnetization
m - Distance vector
ms - Magnetic quantum number
mI - Nuclear spin quantum number
N_A - Avogadro´s number
Q_{12} - Coulomb integral
r - Distance between two atoms
S - Spin quantum number
$\hat{S}$ - Electron spin operator
T - Temperature
T_c - Curie temperature
z_i - Magnetic neighbors

χ - Susceptibility
χ_M - Molar susceptibility
χ_{ac} - susceptibility measured by applying alternating current
χ_{dc} - susceptibility measured by applying direct current
χ' - Real susceptibility
χ'' - Imaginary susceptibility
χ_{ESR} - Integrated ESR signal intensity
$\beta = \beta_e$ - Bohr Magneton
β_n - Nuclear Magneton
θ - Weiss constant
θ - Stack rotational angle
Θ - Torsion angle
μ_{eff} - Effective magnetic moment
$\underline{\varepsilon}$ - Energy of SOMO
ε - Extinction coefficient
ρ - Spin density of electron
ν - Frequency
$|\psi(0)|^2$ - Unpaired electron density at the nucleus
$\Delta\nu$ - Frequency shift in wave number

AF - Antiferromagnetic
AO - Atomic orbital
ArO - Phenoxides
b.p. - Boiling point
chp - 6-Chloro-2-pyridonate
cm - Centimeter
CI - Configuration interaction
CU - Coupling unit
CW - Continuous wave
DMF - Dimethylformamide
ENDOR - Electron nuclear double resonance
ESR - Electron spin resonance
FAB - Fast atom bombardment
FC - Ferromagnetic coupler
FD - Field desorption
g - Gram
h - Hour
hfac - Hexafluroacetylacetonate
hfc - Hyperfine coupling
IN - Iminonitroxide
IR – Infrared
M - Mole
MeOH - Methanol
MO - Molecular orbital
min - Minute
mp - Melting point
mol - Mole
mW - Milliwatt
NBMO - Non-bonding molecular orbitals
NIT - Nitronylnitroxide
nm - Nanometer
NMR - Nuclear magnetic resonance
NO - ^{t}Butyl nitroxide
pbaOH - 2-hydroxy-1,3-propane-diylbis(oxamato)
PNN - *p*-nitrophenylnitronylnitroxide
PIMR – Pyroxyliminonitroxides
ROHF - Restricted open shell Hartee-Fock
RT - Room temperature
SMMs - Single Molecular Magnets
SOMO - Singly occupied molecular orbital
SQUID - Super conducting quantum interference device
TCNE - Tetracyanoethylene
THF - Tetrahydrofuran
TLC - Thin Layer Chromatography
TMSA -Trimethylsilylacetylene
TPM - Triphenylmethylradical
UV/Vis - Ultraviolet/Visible
VZ - Verdazylradicals
zfs - Zero field splitting

CHAPTER 1

Introduction

Abstract: *This introductory chapter reviews some basic aspects of magnetism*[1a,b] *and classes of magnetic molecules (pure organic, organic-inorganic and single molecule magnets). The first two classes of molecule-based magnets are described in more detail: design of high spin molecules, pure organic supramolecular magnetic structures, intra- and intermolecular magnetic exchange interactions, and higher dimensional organic-inorganic magnetic architectures. The magneto-structural relationships are recognized, and this demonstrates the relevance of well defined supramolecular motifs. These considerations served to formulate the aim and outline of this thesis.*

1.1 Aspects of magnetism

Magnetism is one of the nature's most fascinating and evergreen phenomena. Magnetism was first discovered by the ancient Greeks and was used by the Chinese to create the compass for directional findings in 300-200 BC. The magnetic behavior of solids is complex and many different types of magnetism have been distinguished: *diamagnetism, paramagnetism, antiferromagnetism, ferromagnetism, canted ferromagnetism,* etc. [Fig.1.1.]. The many different forms of magnetic phenomena arise as a result of the diverse number of ways in which the electron moments in molecular and supramolecular assemblies can be coupled together.

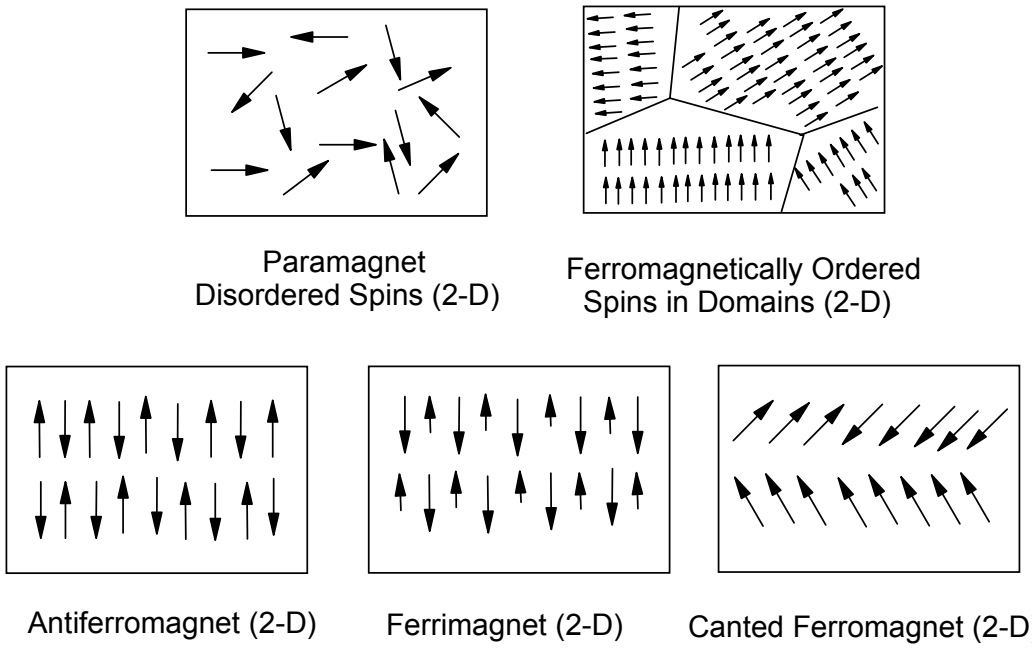

Figure 1.1. *Schematic diagram of different spin coupling behaviors [where T-Temperature, D - Dimension]*

Magnetism is frequently measured by the material's response (attraction and repulsion) to a magnet. It is a consequence of the spin associated with an unpaired electron and how near by unpaired electrons interacts with each other. Molecules are typically sufficiently large and far apart that their spin-spin exchange coupling energy J is smaller compared to the coupling breaking thermal energy. Their spins do not couple, but instead form a very weak *paramagnet*. When the spins are closer, J can be sufficiently large to enable an efficient parallel (or antiparallel) alignment, this

increases (or decreases) the measured susceptibility χ. The susceptibility is defined as the ratio of the induced magnetic moment per unit volume to the applied magnetic field:

$$\chi = M / H \qquad \ldots 1$$

Where M is the magnetization (magnetic moment per unit volume) and H is the magnetic field strength. χ is dimensionless. The molar susceptibility [χ_M] of a paramagnetic substance is proportional to the thermodynamic temperature [T], i.e.

$$\chi_M = C/T \qquad \ldots 2$$

where C is the Curie constant, which is given by,

$$C = N_A\beta^2g^2\, S\,(S+1)/\, 3K_B \text{ [or] } C = 0.125\, g^2\, S(S+1)\, cm^3\, K\, /mol^{-1} \qquad \ldots 3$$

where N_A is Avogadro's number, K_B is Boltzmann constant, β is a constant unit called the Bohr magneton (BM). The Curie constant provides the convenient check of the spin concentration of the sample (C = 0.375 emu K/mol for S = ½).

A modification of the Curie law, which takes into account the interactions among the individual magnetic moments, is the Curie-Weiss law. It states that,

$$\chi_M = C/(T - \theta) \qquad \ldots 4$$

where θ is the Weiss constant in temperature units, a characteristic of the material. It relates the total dipole-dipole exchange interactions [*J*] of magnetically active centers with all its magnetic neighbors *z* (nearest, next nearest, etc.)

$$\theta = [2S(\, S+1) / 3K_B\,] \sum_i z_i\, J_i \qquad \ldots 5$$

When the spins coupled in a parallel manner χ is enhanced i.e. θ > 0 [ferromagnetic], and when the spins are coupled in antiparallel manner χ is suppressed i.e. θ < 0 [antiferromagnetic].

$$\chi_M = N_A\beta^2g^2\, S\,(S+1)/\, 3K_B\,(T-\theta) \qquad \ldots 6$$

In substances with interacting magnetic moments and where the orbital contribution to the magnetic moment is significant, the molar susceptibility is given by,

$$\chi_M = N_A\beta^2g^2\, J\,(J+1)/\, 3K_B\,(T-\theta) \qquad \ldots 7$$

Here the resultant total angular momentum [J] is given by,

$$J(J+1) = L(L+1) + S(S+1) \qquad \ldots 8$$

The quantum number L is the resultant orbital angular momentum of all unpaired electrons present in the atom (i.e. L is zero for a completely filled orbital). For most compounds of the first row transition metal series, the orbital contribution to the magnetic moment is negligible, such that J = S and eqn. 7 is identical to eqn. 6. Simplification of eqn. 3 can be done by defining the effective magnetic moment μ_{eff} as $g\sqrt{S(S+1)}$ or $\mu^2_{eff} = g^2S(S+1)$ and combining all of the constants to give,

$$\chi_M = [N_A\beta^2 / 3K_B]\ \mu^2_{eff}/(T-\theta) \approx 0.125\ \mu^2_{eff}/(T-\theta) \qquad \ldots 9$$

This eqn. 9 allows us to calculate the μ_{eff} of an ion or radical, which can be rewritten as,

$$\mu_{eff} = 2.828\ [\chi_M (T-\theta)]^{½} \qquad \ldots 10$$

A typical plot of the effective magnetic moment [μ_{eff}] as a function of temperature [T] is shown for an ideal paramagnet, ferromagnet, ferrimagnet, and antiferromagnet in Fig.1.2. For the substance that shows bulk ferromagnetism, a transition occurs at a temperature known as Curie temperature [T_c], leading to a phase in which there is long range parallel ordering of spins. Below this temperature χ_M rises abruptly to a very high value.

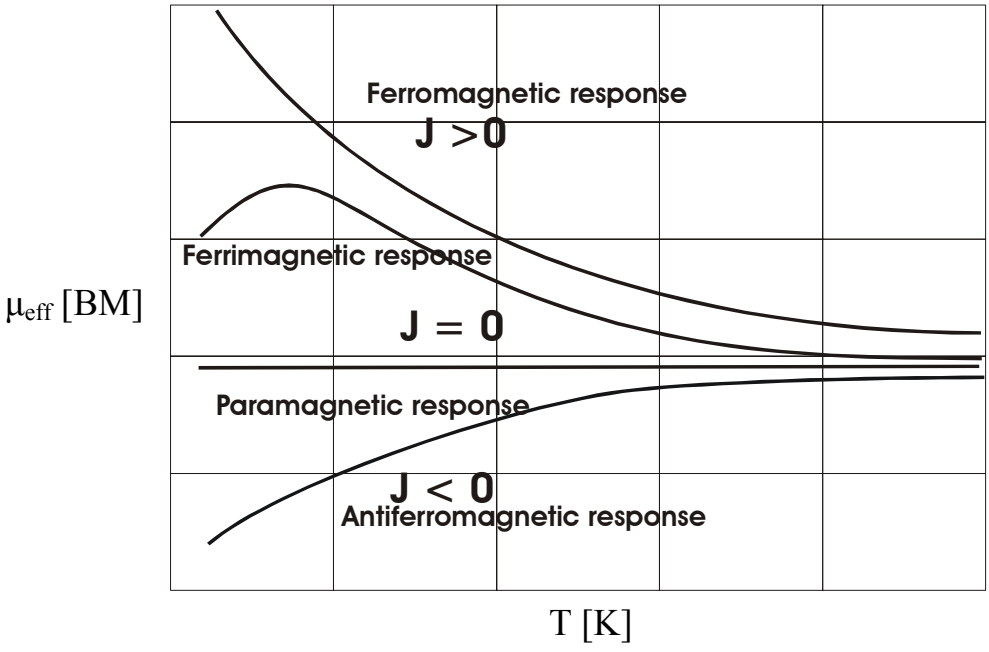

Figure 1.2. *Temperature dependence of the effective magnetic moment (μ_{eff}) in magnetic materials*

If the substance is diamagnetic containing only spin-paired electrons the magnetic response opposes the applied field and χ is small and negative. In a paramagnetic substance, i.e. one that contains unpaired electrons the normally randomized spin moments align with the external magnetic field. Here the density of the magnetic lines of force within the sample is intensified giving small but positive χ, independent of the magnetic field intensity, and χ decreases with increase in temperature. In a ferromagnetic substance, the spins are spontaneously parallel to one another in microscopic domains leading to a permanent magnetization. The application of a magnetic field causes the domains to point along the field even when the field is removed. The χ is large and positive, dependent on the magnetic field, temperature, and the history of the sample. The related phenomenon, antiferromagnetism occurs when neighboring, equal spin moments couple in an anti-parallel fashion, leading to a lowering of the magnetization, while ferrimagnetism occurs when unequal spin moments couple in a way to leave a net magnetization.

Ferro-, antiferro-, and ferrimagnetic materials often show a hysteresis, which is an irreversibility of the magnetic behavior as the applied magnetic field is changed [see Fig.1.3.]. Although ferromagnets, below T_c exhibit long-range ordering of spins,

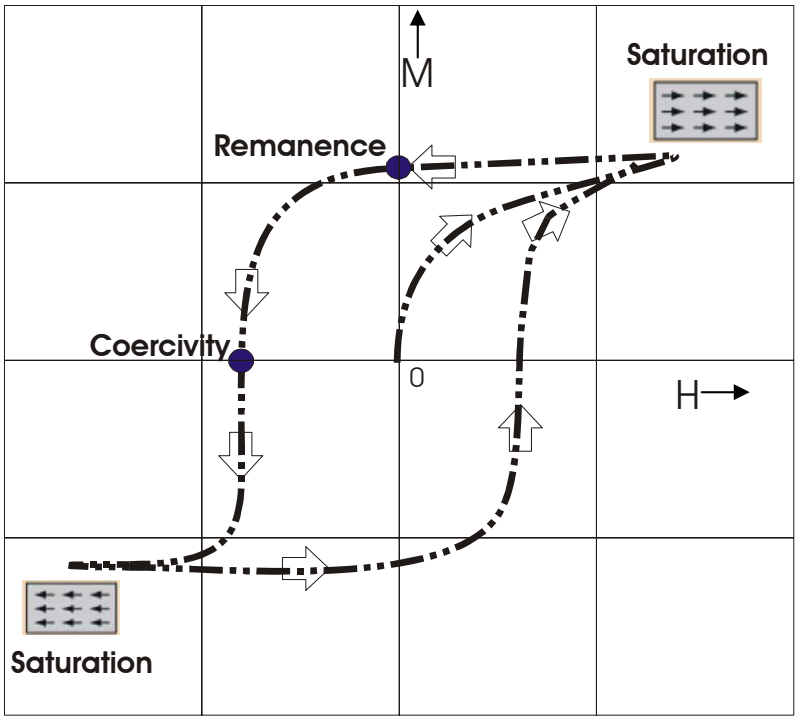

Figure 1.3. *Hysteresis curve of a ferromagnetically ordered material with memory*

a sample may still not behave like a magnet, unless this ordering occurs within "domains". The domain themselves are randomly oriented and cancel each other out, however application of magnetic field will magnetize the sample. When the field is turned off, the magnetization curve shows hysteresis and the sample retains some magnetization. The amount of magnetization the sample retains at zero driving field is called remanence. It must be driven back to zero by a field in the opposite direction; the amount of reverse driving field required to demagnetize it is called coercivity. If an alternating magnetic field is applied to the material, its magnetization will trace out a loop called hysteresis loop. The area of the hysteresis loop is related to the amount of energy dissipation upon reversal of the field. It is important to emphasize that highly magnetic behavior is not a property of an isolated molecule. It is a cooperative solid-state (bulk) property. This can be achieved through strong intermolecular interactions in 3-D space. The magnetic susceptibility χ can be measured using Faraday-type balance or Super conducting quantum interference device - SQUID susceptometer down to liquid helium temperature.

Today the greatest challenge in the field of magnetic materials research remains in the design and synthesis of ferromagnets. Many strategies have currently been followed towards molecular magnets, 1) the pure organic approach with spin carrying molecules, 2) the organic-inorganic hybrid approach and 3) the cluster approach or single molecular magnets (SMMs). These strategies will be outlined in the following chapter 1.2. This whole work focuses on the first two approaches, which will be discussed, in the chapters 3-5.

1.2 Classes of magnetic molecules

1.2.1 Organic magnets

Atoms in organic molecules are held together with covalent bonds consisting of electron pairs with anti-parallel electron spins. Typical organic materials are diamagnetic for this reason. There are, however, exceptional species, so-called free radicals, which carry an unpaired electron. Most radicals are very reactive and mainly play a role as intermediates in chemical transformation. Fortunately, stable radicals do exist, and these species enable the investigation of possible electron spin-spin

interactions in organic magnetic materials. In the area of molecular magnetism, purely organic materials based on radicals are still under active investigation. Therefore, magnets with multiple properties can be synthesized *(i.e. plastic magnets)*. These molecular compounds will have no presence of metal ions, but rather rely solely on electron spins residing only in the s and p orbitals. They must also maintain long-range order of spins in at least two dimensions to produce ferromagnetic behavior. Many spin carrying units are in active use toward building organic based magnets. Examples are, Nitronylnitroxides (NIT), Iminonitroxides (IN), ^{t}Butyl-Nitroxides (NO), Verdazyl radicals (VZ), Carbenes, Nitrenes, Phenoxides (ArO), Ketyl radicals, Triphenylmethyl radical (TPM) [Fig.1.4.].

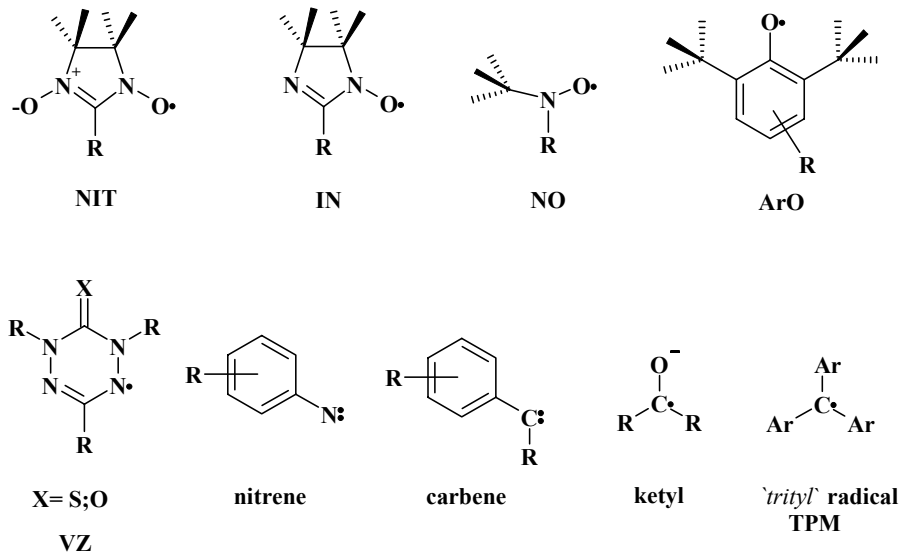

Figure 1.4. *Some common organic radical units*

Stable nitronylnitroxide radicals were synthesized by Ullman et al.[1c,d] upon reacting 2,3-dimethyl-2,3-bis(hydroxylamino)-butane **I** with aliphatic aldehydes to give anhydro adduct **II** as white solid, which upon oxidation with $NaIO_4$ or PbO_2 give nitronylnitroxide **IV**. If oxidation of **II** with lead oxide was not carried out to completion, a highly reactive intermediate **III** could be isolated. The color of the nitronylnitroxides varies depending upon the R group [Scheme.1.1]. Aliphatic radicals are red in color and aromatic compounds are blue or violet, depending on whether the solvent is polar or nonpolar[1c,d].

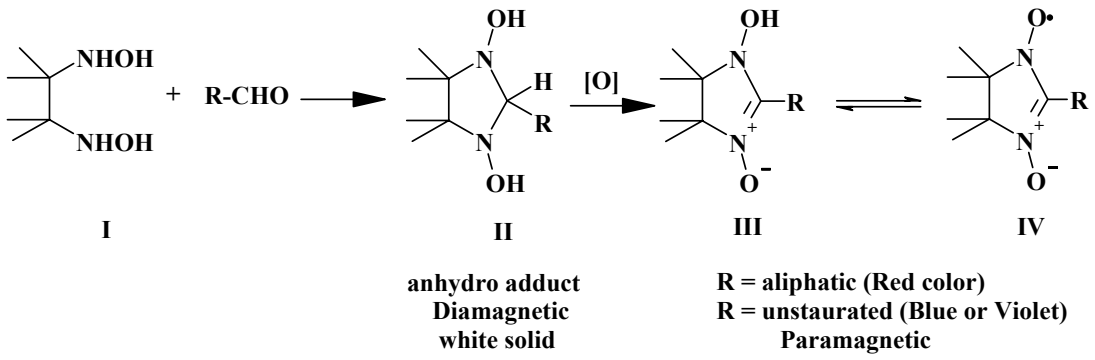

Scheme 1.1. Ullman's reaction[1c,d]

The unpaired electron is delocalized mainly between nitrogen and oxygen and between both N-O groups, it is stabilized by protecting the radical center with geminal dimethyl groups. These methyl groups also prevent NIT from becoming dinitrone[1c,d]. Nitroxide radicals have an inherently stable electronic configuration and can be further stabilized by conjugation with π electrons of aromatic systems and/or by shielding with bulky substituents. The SOMOs of the mononitroxides (NO) are localized mainly on the N-O moiety and the unpaired electron mainly resides there. The general strategy for designing nitroxide containing magnetic materials has been to prepare molecules with large intermolecular spin polarizations, and to minimize the intermolecular overlap integrals between the SOMOs of adjacent radical centers, and the vacant or doubly occupied molecular orbital of neighboring molecules. Each radical unit has its merits and demerits. Amongst the radicals units mentioned above NIT, IN, NO, VZ are stable spin carrying units at ambient conditions. Many molecules have been synthesized based on NIT, IN, NO radicals due to their synthesis, purification and characterization advantages in presence of oxygen[1c,d].

The first pure organic based magnet was reported in 1991 by Kinoshita and co-workers[2], i.e. the *β*-Phase of *p*-nitrophenyl nitronylnitroxide (PNN) with T_c = 0.65 K, exhibiting low magnetic anisotropy and small coercive forces. This discovery evoked the successive rapid development and discovery of other ferromagnets. Most of them are based on nitroxide radicals. After PNN an elegant example was provided by Rassat and his coworkers[3] in 1993, namely 1,3,5,7-tetramethyl-2,6-diazaadamantane-*N*,*N*′-dioxyl with T_c = 1.48 K. This compound was expected to possess intermolecular ferromagnetic interactions from the orthogonality of the two N-O groups of the

biradical, and owing to the favorable 3-D network of NO chains for an intermolecular ferromagnetic interactions. Later in 1995, thiaverdazyl based organic magnet was reported with T_c = 0.67 K[4]. The dithiadiazolyl radical has also displayed properties smaller than expected for a ferromagnet, but has one of the highest T_c = 36 K so far reported[5] [Fig.1.5.].

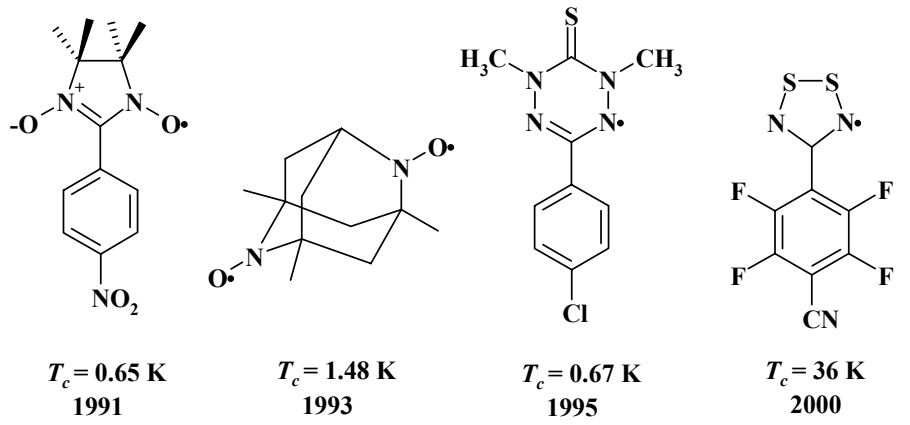

Figure 1.5. *Pure organic based magnets obtained from NIT, NO, VZ and Dithiadiazolyl radicals*

1.2.2 Intramolecular interaction

There are two driving forces, which have emerged in the development of the field of molecular magnetism. One is, to align many electron spins of polyradicals ferromagnetically to create high spin entities, and the other is, to align one or more electron spins of an organic radical moiety intermolecularly to create organic ferromagnetic materials. The landmark in the study of spin alignment in organic molecules, belonging to the former category, is the discovery of the quintet *meta*-Phenylenebis(phenylmethylene)[6].

The strategy of preparing high spin molecules is to utilize degenerated non-bonding molecular orbitals (NBMOs) derived from the π-topology of odd alternant hydrocarbons. According to molecular orbital (MO) theory two atomic orbitals (AOs) form bonding and anti-bonding orbitals when they interact with an effective overlap integral [Fig.1.6A.]. This is called non-orthogonal interaction. In this case, two electrons with anti-parallel spin occupy the bonding orbital, forming a chemical bond.

On the contrary, when two AOs interact with zero overlap integral, the two unperturbed orbitals are occupied by one electron each with parallel spins in accordance with Hund's rule [Fig.1.6B.]. If two orthogonal orbitals belong to the same atom, a one-centered biradical is obtained.

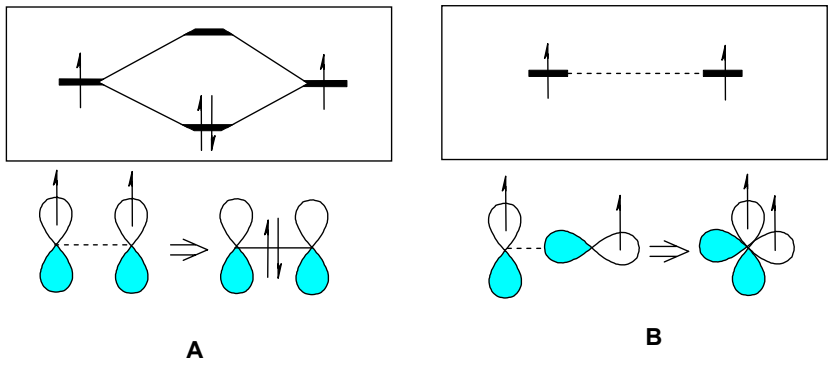

Figure 1.6. *(A) "non-orthogonal" orbital interaction; (B) "orthogonal" orbital interaction*

1.2.3 Hund's rule and exchange integral

According to Hund's rule, when two orthogonal atomic orbitals are singly occupied, the orbital energies of these orbitals are the same or so called degenerate, and can be expressed as $\underline{\varepsilon}_1 + \underline{\varepsilon}_2$ ($\underline{\varepsilon}_1 = \underline{\varepsilon}_2$ in the present case), regardless of the configuration of mutual spins. The electronic repulsion energies between electrons (1) and (2) consist of two terms, Coulomb integral (Q_{12}), and exchange integral (K_{12}). The Coulomb integral between electron (1) in orbital φ_a and electron (2) in orbital φ_b can be expressed by the following equation, where $\varphi_a(1)\,\varphi_a(1)$ is called "*overlap density*".

$$Q_{12} = \int \varphi_a(1)\,\varphi_a(1)\,\frac{e^2}{r_{12}}\,\varphi_b(2)\,\varphi_b(2)\,d\tau_1\,d\tau_2 \qquad \ldots 11$$

For evaluation of the electron repulsion between the two electrons, the exchangeability of electrons (1) and (2) has to be taken into account. Through exchange of electrons, electron (1) can jump over to φ_b, and *vice versa*. The electronic repulsion, which originates from the electronic exchange (exchange integral), can be expressed by eqn.12, where $\varphi_a(1)\,\varphi_b(1)$ is called the "*exchange overlap density*".

$$K_{12} = \int \varphi_a(1)\,\varphi_b(1)\,\frac{e^2}{r_{12}}\,\varphi_a(2)\,\varphi_b(2)\,d\tau_1\,d\tau_2 \qquad \ldots 12$$

The expression for the total energy for antiparallel spins is written as $\underline{\varepsilon_1} + \underline{\varepsilon_2} + Q_{12} + K_{12}$, whereas that for the parallel spins is written as $\underline{\varepsilon_1} + \underline{\varepsilon_2} + Q_{12} - K_{12}$. This means that the electronic state of the parallel spins is energetically more stable than that of the anti-parallel ones. The physical meaning of the difference in the repulsion energy may be rationalized as follows. Suppose the electron (1) exists at x_1 along x-axis, probability of finding electron (2) is known to be heavily dependent on the configuration of spins [Fig.1.7.]. When the spin of electron (2) is anti-parallel to that of electron (1), there is no restriction with respect to that of electron (1); it can never occupy the same space as electron (1) does. This is called Pauli's exclusion principle. As a result, the anti-parallel spins (low spin) suffer from larger mutual Coulombic repulsion than that of parallel spins. This is the reason why electrons occupy the degenerate orbital in a parallel manner.

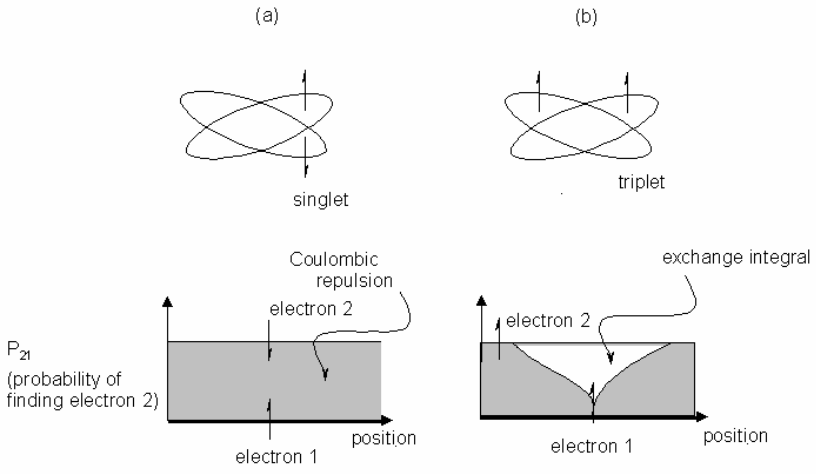

Figure 1.7. *Spin dependent Coulomb repulsion*

The triplet state (high spin) consists of three sub levels [Fig.1.8.], and they split into three separate levels due to the magnetic dipolar interaction, even in the absence of external magnetic field. This is called zero field splitting, and the degree of the splitting is in the order of $1cm^{-1}$ or less. When an external field is applied, the energy levels separate in proportion to the strength of the external magnetic field by the Zeeman effect. The spin system is analyzed by the following spin Hamiltonian according to Fig.1.8.

$$\hat{\mathbf{H}} = -2\,J\,S_1 \cdot S_2 + D\,[Sz^2 - S\,(S+1)/3] + E\,(S_x^2 - S_y^2) + S\,g\,\beta_e\,H \qquad \ldots(13)$$

This eqn. (13) will be discussed in detail in chapter 2.

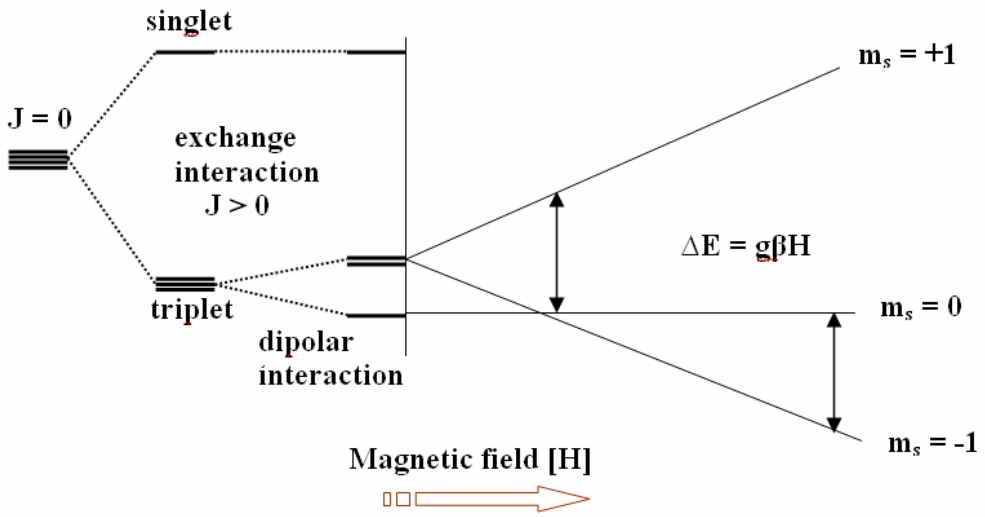

Figure 1.8. *Exchange interaction, magnetic dipolar interaction, and Zeeman effect*

1.2.4 Design of high spin molecules

In order to construct high spin molecules, it is effective to use a "*ferromagnetic coupler*" (FC), which couples two unpaired electrons on its both sides ferromagnetically. The important role of the FC unit has been underlined by a recent theoretical study[7].

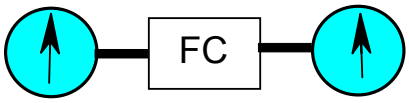

The most often used approach for high spin molecules is the control of through bond exchange interaction leading to so called non-Kekulé structures as in *m*-xylene, where no double bond between the unpaired electrons are formed. *p*- and *o*-xylenes undergo spin pairing to the more stable quinoid structures in the Kekulé forms [Fig.1.9.].

In case of *m*-xylene (non-Kekulé) the ground state is supposed to be triplet due to the presence of degenerate NBMOs of a non-disjoint type. A topological rule has been well established to predict the ground state spin multiplicities of odd alternant

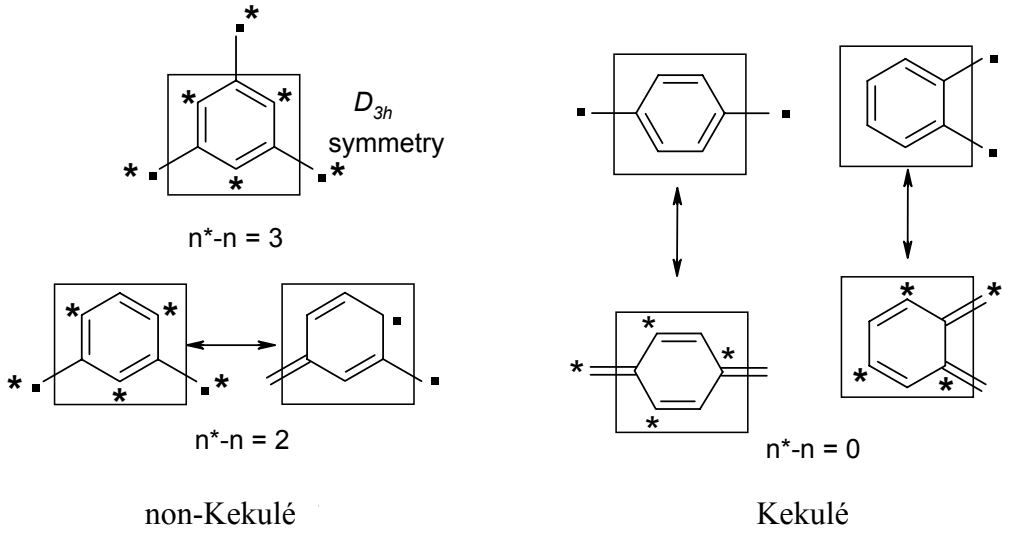

Figure 1.9. *Non-Kekulé versus Kekulé Structures*

hydrocarbons in a straightforward manner. In 1950, Longuet-Higgins[8a] proposed a rule to predict the ground state spin multiplicity on the basis of Hund's rule, as given below,

$$[nNBMO = (N-2T);\ S = 0.5\ (N-2T)] \qquad ...(14)$$

where, N is number of π-centers and T is number of double bonds. Later, Ovchinnikov[8b] proposed a spin polarization rule. According to this rule, every other carbon atoms along the conjugated carbon framework are marked with a "star" based on spin polarization. Counting "starred" and "unstarred" atoms of the π-conjugated system and applying in eqn. 15 gives the value of the net spin S.

$$S = 0.5\ (n^*-n) \qquad ...(15)$$

Since the spin multiplicity is expressed as 2S+1, the rule predicts the triplet ground state for non-Kekulé molecules.

Following these approaches many high spin molecules connected by different FC units have been designed and synthesized. Some of the NO and NIT based bi-, tri-, and tetraradicals are given in Fig.1.10[9]. Apart from the above mentioned topological rules the ground state of the molecule having more than one unpaired electrons is

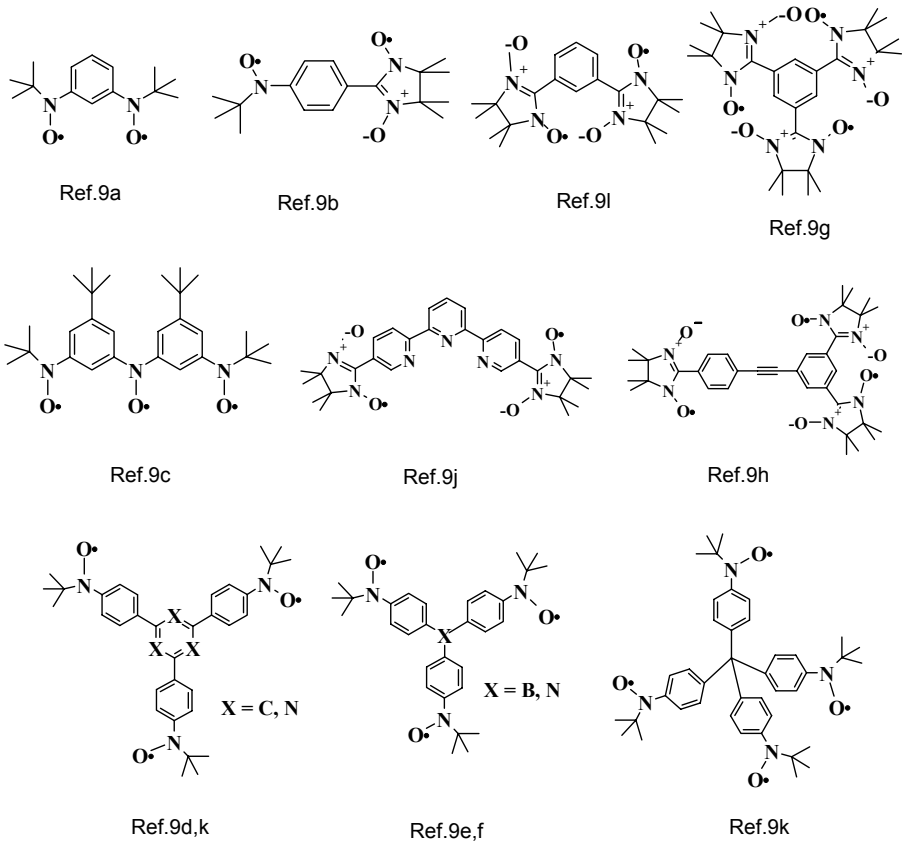

Figure 1.10. *Some non-Kekulé type molecules carrying NIT or NO radicals with different coupling units*[9]

governed by the nature of the coupling units [CU]. The effect of the CU in high spin molecular ground state of the non-Kekulé molecules varies according to their molecular geometry[10], nature and position of the substituents[11] and heteroatom influence[12]. The detailed discussion about the spin multiplicities of the molecules presented in Fig. 1.10. can be found in the corresponding articles[9].

1.2.5. Intermolecular interaction (through space interaction)

In case of purely organic molecular magnets, the magnetic force of interaction mainly occurs by direct overlap of the orbitals of the nearby units, in what is called *through space interaction*, in contrast from the *through bond interactions* found in organometallic solids. The mechanism of the through *space interactions* are not well

understood at the present moment. It depends on the relative orientation of the radicals and the packing of the radical within the crystal.

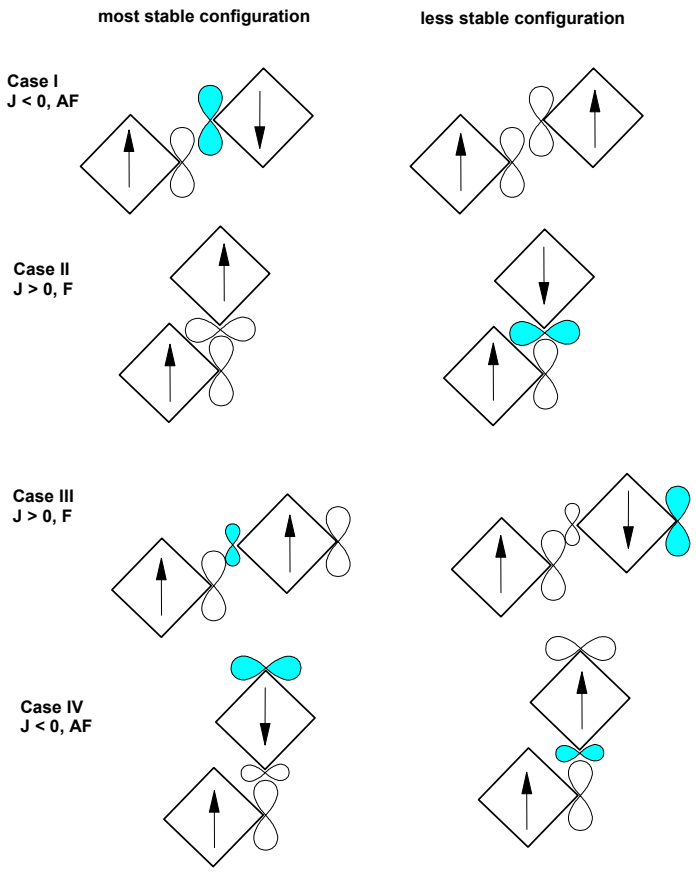

Figure 1.11. *Schematic representation of the magnetic couplings according to the McConnell spins density mechanism*[15]*. White and cyan orbitals denote the positive and negative spin densities, respectively, and smaller orbitals illustrate the spin polarization*

In 1963 McConnell[13] proposed rules based on the unpaired electron densities (spin densities) that allow prediction of the type of magnetic order expected for a given material. Four cases (I- IV) can be distinguished and are schematically given in Fig.1.11[15].

Case I is the most common. Normally, open-shell molecules interact to give antiferromagnetic coupling and no spontaneous magnetization.

Case II corresponds to ferromagnetic interactions, which are found when the magnetic orbitals (or SOMOs, singly occupied molecular orbitals) are orthogonal, either by design or by accident.

Case III, he proposed an empirical correlation the most popular magneto-structural correlation is the so-called McConnell I mechanism,

$$E^S - E^T = \langle \hat{H}^{AB} \rangle^S - \langle \hat{H}^{AB} \rangle^T = \sum_{i \in A, j \in B} J_{ij}^{AB} \rho_i^A \rho_j^B = J \qquad \text{....(16)}$$

According to this equation, *a triplet state is obtained for the interaction between two doublet fragments when the atoms making the shortest contacts present atomic spin populations of opposite sign.*

This mechanism has been experimentally confirmed several times[14]. Now, it is commonly accepted that short N-O···O-N contacts in the nitronylnitroxide crystals are indicative of the dominant antiferromagnetic interactions between the dimers in which such contacts are found.

McConnell confirmed **Case IV** as "unlikely", he just noted that then the sign of the magnetic coupling should be reversed (antiferromagnetic). Hirel et al[15]. have reported this peculiar case in cyanonitronylnitroxide radical in which the closest spin-spin contact between the molecules is of the positive–negative type but the exchange coupling is antiferromagnetic. An additional possibility is the charge-transfer (or configuration interaction) mechanism also proposed by McConnell known as McConnell mechanism II[16a,b]. This is rare, but has occasionally been used to explain the magnetic behavior in charge transfer salts[16c].

One should mention here that, having good magneto-structural correlations is only half of the problem in designing molecular magnets. In addition, one has to learn how to control the packing of the radicals within the crystal[17] to guarantee the presence of the desired magnetic interactions in the crystal. This is an example of what is now-a-days called *crystal engineering*[18]. Crystal engineering is the process of designing the three dimensional structure of solids, using non-covalent interactions. Following this approach many experimental[19b-f] and computational[19a and its Refs.] reports are available on organizing molecules in the solid state via π- π stacking and hydrogen bonding [Fig.1.12.].

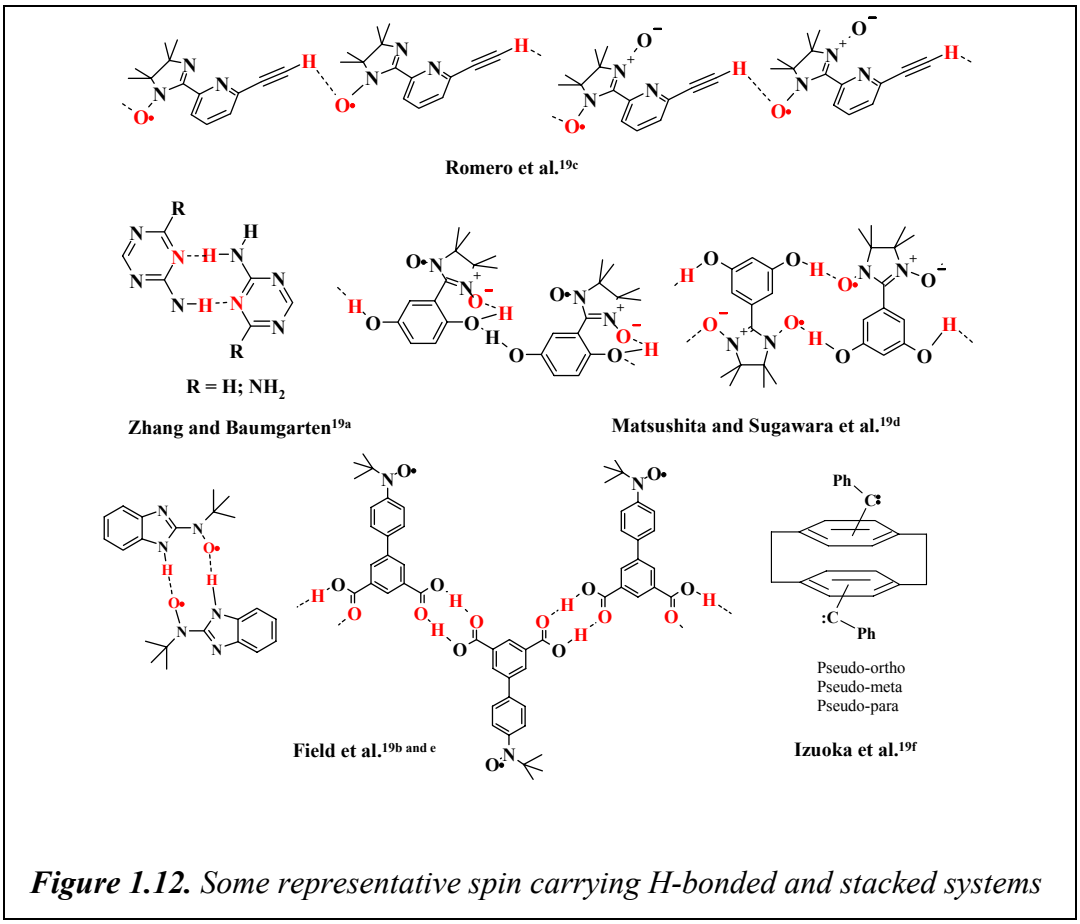

Figure 1.12. *Some representative spin carrying H-bonded and stacked systems*

1.2.6 Metal-organic approach

Miller, Epstein and co-workers[20] developed a charge transfer model compound, $[Fe^{III}(C_5Me_5)_2]^{\bullet+}$ $[TCNE]^{\bullet-}$ in which bulk ferromagnetic behavior was observed (T_c = 0.4 K). This was the first example of a magnet with spins residing in p-orbitals. It exhibited magnetic hysteresis, was soluble in organic solvents and did not require metallurgical preparative methods[20]. According to McConnell mechanism the driving force behind its ferromagnetic behavior is, the triplet ground state character of $[Fe^{III}(C_5Me_5)_2]^{2+}$. This leads to the ferromagnetic coupling between $[Fe^{III}(C_5Me_5)_2]^{\bullet+}$ and $[TCNE]^{\bullet-}$ both within the stack and between out of registry adjacent stacks giving the full three dimensional coupling of spins required for bulk ferromagnetism. Later, a variety of TCNE based organic magnets have been discovered, including the remarkable $V^{II}(TCNE)_x \cdot y(CH_2Cl_2)$, which has T_c above room temperature (ca. 400 K)[21]. In 1991 Kahn[22] developed a strategy in the design of bimetallic chains

containing metal ions of different spins held together by diamagnetic bridging ligands. This approach provided one of the earliest true molecular based magnets, namely $MnCu(pbaOH)(H_2O)_3$ [pbaOH = 2-hydroxy-1,3-propane-diylbis(oxamato)] T_c = 4.6 K. Its structure consist of alternating bimetallic chains assembled within the crystal lattice in such a way that, along the chain axis the shortest interchain separations are Mn···Cu instead of Mn···Mn and Cu···Cu. The overall ferromagnetic coupling occurs through the interaction between strong positive (S_{Mn} = 5/2) and negative (S_{Cu} = ½) spin densities belonging to neighboring ferrimagnetic chains. The Mn···Cu interaction through the oxalato bridge is, however, antiferromagnetic.

Gatteschi et al.[23] further developed this idea by choosing paramagnetic stable nitroxide ligands, and investigated the interaction between paramagnetic metal (Cu, Mn, Ni, Co) ions and nitroxide ligands. The sign of coupling (J) of a nitroxide ligand bound to a paramagnetic metal ion is dependent on the orbital overlap consideration [Fig. 1.13.[23]]. In [**a**] the interaction between the two orbitals are orthogonal to each other and the coupling is ferromagnetic. Situation [**b**] occurs in Cu(II)-nitroxide complexes, when the radical coordinates in an equatorial coordination site. If the M-

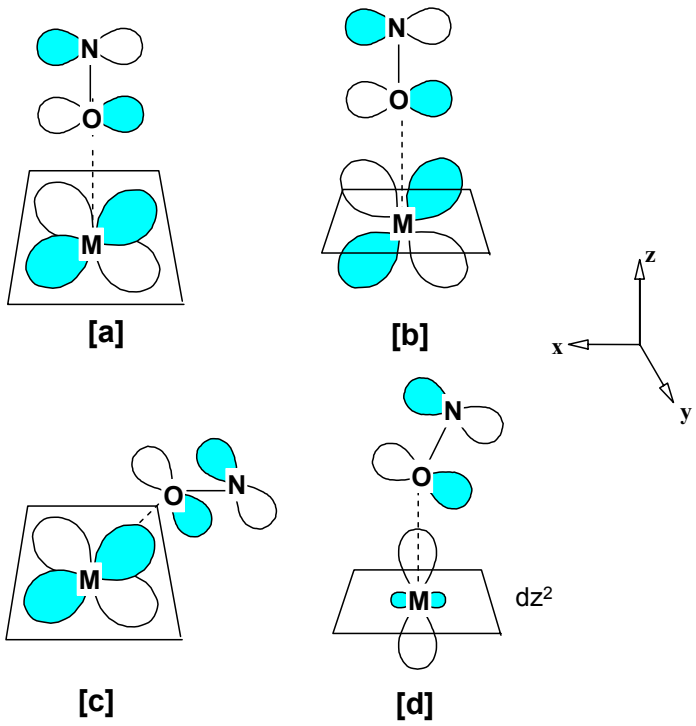

Figure 1.13. *Overlap model between nitroxide ligand and transition metal*[23]

O-N angle is different from 180°, substantial overlap occurs and the coupling must be antiferromagnetic. Cases [**c**] and [**d**] occur in complexes of Ni(II), Co(II), and Mn(II), and they invariably lead to strong antiferromagnetic coupling. The magnetic properties of Ni(II), Co(II), and Mn(II) hexafluroacetylacetonate adducts with nitroxides of formula $M(hfac)_2$(R-NIT) have indeed shown that the ground state has zero, one and three unpaired electrons, respectively.

Simple nitroxides (e.g. *t*butyl nitroxide) can interact with only one metal ion at a time and cannot form extended magnetic architectures. Gatteschi[24] synthesized a series of bidentate nitronylnitroxides (NIT) with different R functions. If the two oxygens of the NIT bind to two different metals ions, a polymeric structure could be formed with effective pathways to transmit magnetic interactions between the metal ions. NIT coordinates in different modes to metal ions as shown in Fig. 1.14[23]. In **I** they bind with one oxygen atom to one metal ion, yielding discrete mononuclear complexes[25]. In **II**, the radicals bind with one oxygen to one metal, while the other oxygen interacts weakly with one other radical, forming magnetic chains[26]. In **III**, they bind with the two oxygen atoms to two different metal ions: in this case, chains can be formed, either ferromagnetic or ferrimagnetic, depending upon the nature of metal ions[27]. In **IV**, they bind with one oxygen atom to two different metal ions, and each metal ion is bound to two radicals, with four spins arranged at the vertices of a diamond. The second oxygen atom then interacts with the oxygen atom of another radical, thus forming antiferromagnetic chains[28a].

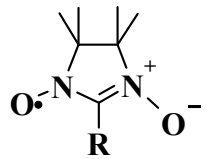

NIT

R = Me, Et, *i*-pr, n-Pr

Gatteschi discovered that above 20 K manganese with hexafluroacetylacetonate (hfac) ligands complexed to NIT-R behaved as typical ferromagnetic chains, but at low temperatures [T_c = 7.6, 8.1, 8.6 K for R = *i*-Pr, Et, n-Pr] a three dimensional ferromagnetic ordering occurred and the magnetic moments rapidly developed due to the dipolar interactions between the chains. In order to enhance the critical ordering

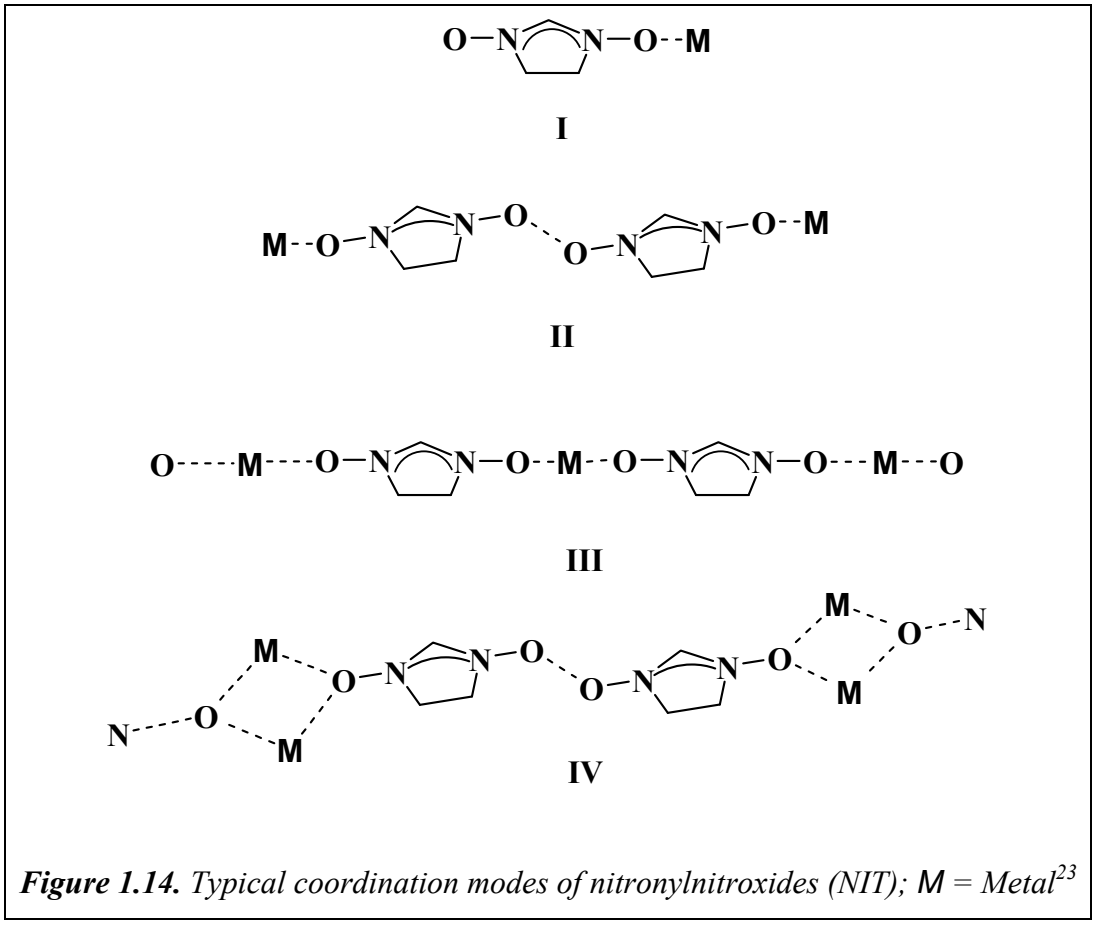

Figure 1.14. *Typical coordination modes of nitronylnitroxides (NIT); M = Metal*[23]

temperature he chose to introduce either additional donor atoms on the NIT-R radicals and hence to increase the number of metal ions or to use coligands other than hfac.[28b] Ise et al.[28c] have reported 1-D linear chains of NIT-R (R = H) with $Mn(hfac)_2$ and IN-H (R = H) with $Cu(hfac)_2$ and $Mn(hfac)_2$.

Minguet et al.[29] have synthesized crystalline enantiopure chiral 1-D linear chains of a nitronylnitroxide derivative [R = (*R*)C_6H_4Me-*p*] with $Co(hfac)_2$ which exhibit ferromagnetic phase transition at 4 K. Below 800 mK opening up of hysteresis loop was observed. Inoue and Iwamura reported[30] ferrimagnetic 2-D sheet like structure made out of trinitroxide having a quartet ground state with $Mn(hfac)_2$. Fegy et al[31] reported a 2-D honey- comb like structure based on imidazolyl-nitronylnitroxide monoradical and Mn ion. The presence of magnetic ordering below 1.4 K is confirmed by the field dependence of the magnetization at 85 mK. The curve exhibits a weak hysteresis loop with coercive field of 270 Oe and a remanent magnetization of 0.22 μ_B. Recently, Mathevet and Luneau reported[32] an interpenetrated 3-D

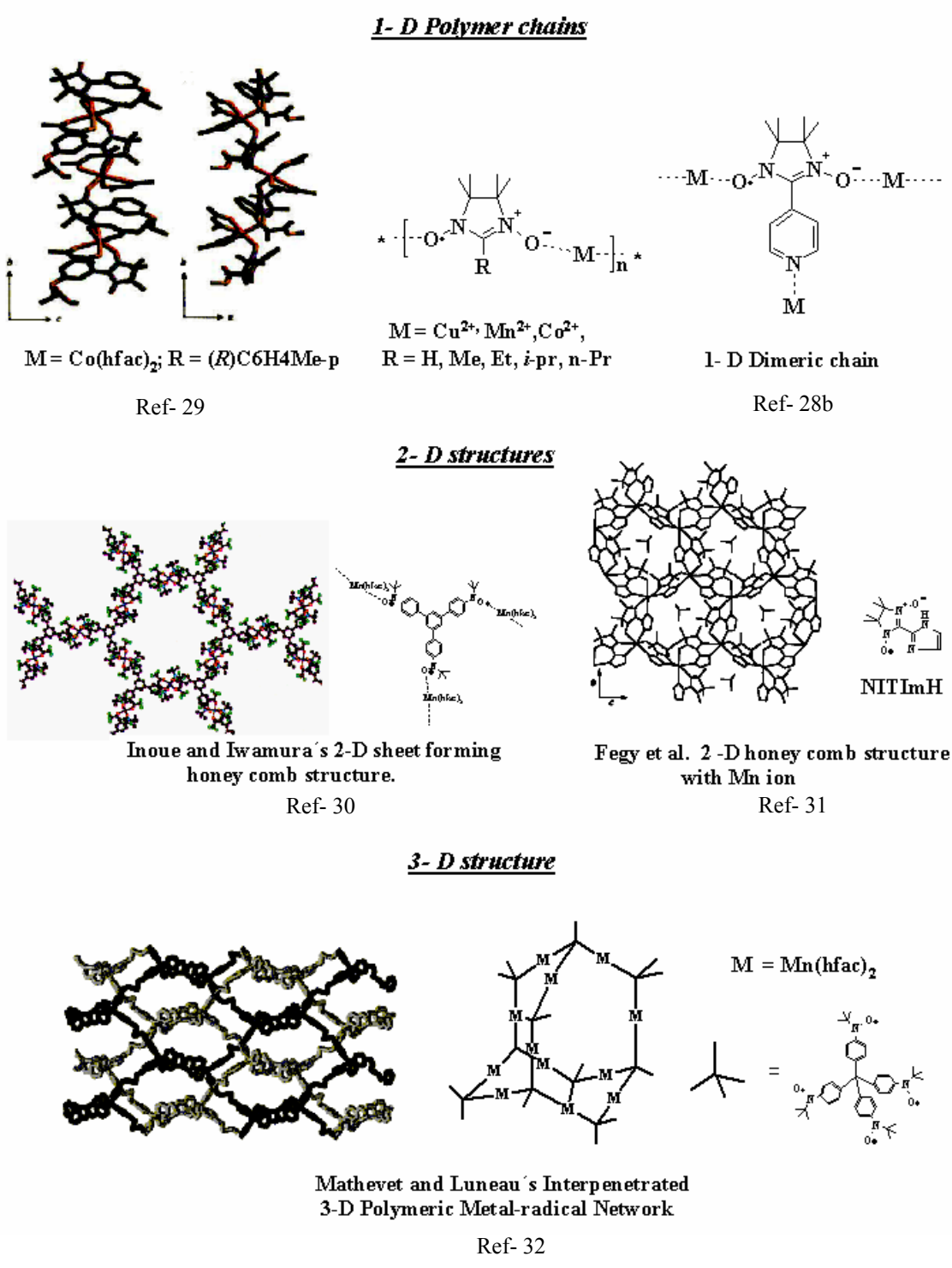

Figure 1.15. *Typical examples of metal-organic higher dimensional compounds*

polymeric network structure of tetrakis[4-(*N*-tert-butyl-*N*-oxyamino)phenyl]methane with $Mn(hfac)_2$ displaying antiferromagnetic behavior in the solid state.

1.2.7 Single Molecule Magnets (SMMs)

SMM are molecular spin clusters with an extremely slow paramagnetic relaxation rate which are able to fix magnetization on a single molecule. Such a molecule can act as a memory unit cell. One of the most extensively studied SMMs is $[Mn_{12}O_{12}(O_2CCH_3)_{16}(H_2O)_4].4H_2O.CH_3COOH$ commonly called "Mn-Ac" or simply "Mn_{12}". Mn_{12} first synthesized by Lis[33a], consists of 12 Mn ions in which eight of the Mn ions in the ring [green] are in the +3 oxidation state (S = 2) and four in the cubane [yellow] are in the +4 oxidation state (S = 3/2). These manganese ions are magnetically coupled to give S = 10 ground state[33b] [Fig.16. left]. Cyclic molecular system $[Ni_{12}(chp)_{12}(O_2CMe)_{12}(THF)_6(H_2O)_6]$ (chp = 6-chloro-2-pyridonate) contains twelve ferromagnetically coupled S = 1 nickel centers, which gives an S = 12 ground state [Fig.16. right]. It shows a slow relaxation of magnetization at low temperatures,

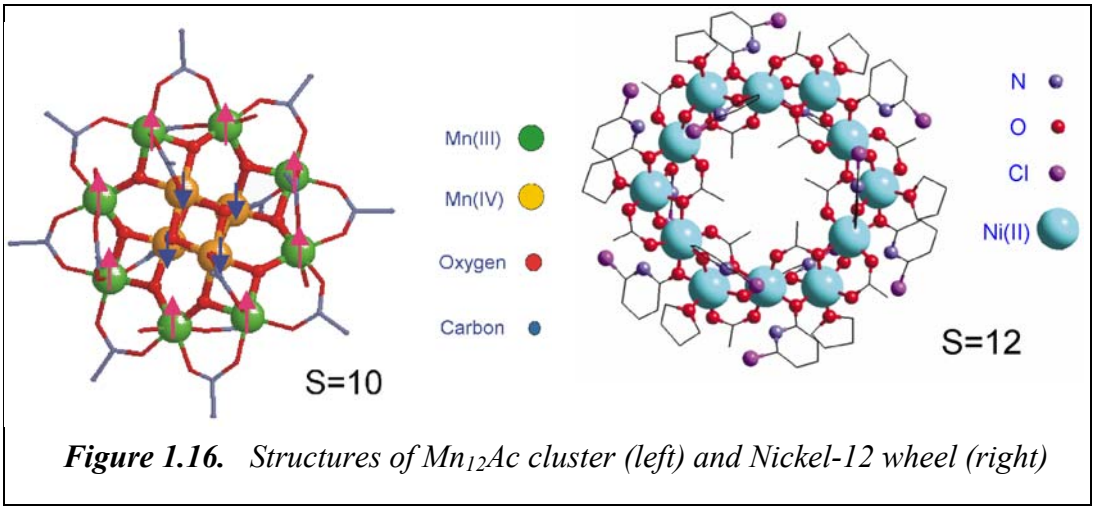

Figure 1.16. *Structures of $Mn_{12}Ac$ cluster (left) and Nickel-12 wheel (right)*

and quantum tunneling of the magnetization[34]. For SMM, the source of magnetic anisotropy arises from the molecular spin ground state combined with appreciable zero field splitting[35]. The larger the magnetic anisotropy and the spin S of the cluster, the higher the energy barrier $\boldsymbol{DS^2}$ separating the M_s = +S and M_s = -S states with opposite directions of magnetization. The magnetic moment of the molecule has two preferred orientations "up" or "down" relative to the molecular axial anisotropy axis. When the temperature is much lower than the energy barrier to flip the spin from up to down, the spins of the SMM can be magnetized in one direction. This phenomenon called magnetic bistability shows that SMM can be used as a data storage device[35].

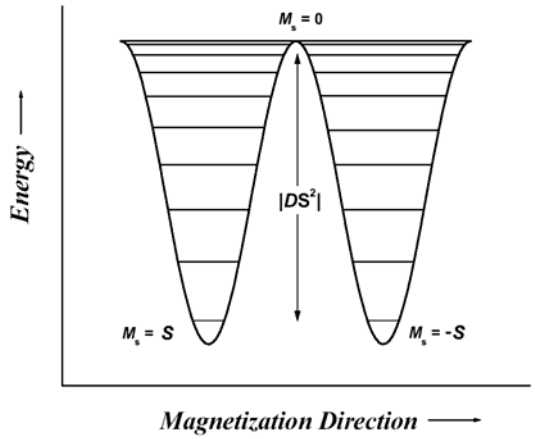

Figure 1.17. *Spin levels and the potential energy curve of a magnetically anisotropic spin cluster*

1.3 Outline of this thesis

The aim of the thesis was the organization of spin entities as supramolecular magnetic arrays in solid state. This ordering was realized in two ways i) combining organic spin entities with Cu^{II} (S = 1/2) and Mn^{II} (S = 5/2) ions to yield metal-radical covalent higher dimensional architectures via a "*metal-radical hybrid approach*" and ii) designing and aggregating organic spin carrying entities via noncovalent interactions such as H-bonding and π-π stacking in solid state following a "*pure organic approach*". The main idea behind aggregating the spins following these two approaches was to correlate the magnetic behavior of these materials with their solid-state structures. In both approaches the dimensions (1-, 2-, and 3-D) of the magnetic arrays were very important, since the bulk magnetic ordering phenomena of the magnetic material depend on the magnitude and sign of the exchange interactions (*J*) between the spins in 3-D space.

In order to follow the *metal-radical approach* it was necessary to synthesize stable spin carrying ligands; here the number of coordination sites of the ligand determines the dimension of the hybrid soild-state structure. In this vein, nitronylnitroxide radicals were fruitful because each unit carries an unpaired electron (S = 1/2) and also has two ligation sites per unit, which can yield 1-D alternating magnetic chains with metals. To get higher dimensional motifs via high spin ligands (S = 1) based on nitronylnitroxides it was vital to design and synthesize high spin building blocks 3,5-Bis[4-(1-oxyl-3-oxo-4,4,5,5- tetramethylimidazolin-2- yl)phenylethynyl)]pyridine (**1**) and

2,6-Bis[4-(1-oxyl-3-oxo-4,4,5,5-tetramethylimidazolin-2-yl)phenylethynyl)]pyridine (**2**) having five coordination sites. To understand the magneto-structural relationship of the network it was necessary to synthesize mononitronylnitroxide radicals 4-(5-Bromo-pyridine-3-ylethynyl)-1-(1-oxyl-3-oxo-4,4,5,5-tetramethylimidazolin-2-yl)benzene (**3**), 4-Trimethylsilylethynyl-1-(1-oxyl-3-oxo-4,4,5,5-tetramethylimidazoline-2-yl)benzene (**4**), and 4-Trimethylsilylethynyl-1-(1-oxyl-3-oxo-4,4,5,5-tetramethylimidazoline-2-yl)pyridine (**5**) to form 1-D chains and clusters with metals.

In addition before synthesizing the network it was crucial to establish the high spin ground state of **1** and **2** by X-band ESR spectroscopic studies down to liquid helium temperature. These experimental results were backed up by quantum mechanical computation studies, such as semi-empirical (AM1) calculations with extended configuration interaction (CI), in order to diagnose the influence of torsional angles on, i) the spin density distribution, ii) heat of formation, and iii) $\Delta E_{S\text{-}T}$ triplet-singlet energy levels. Further, magnetic susceptibility studies had to be undertaken to probe different magnetic behaviors of the clusters, chains and networks down to liquid helium temperature. In some cases, particularly in chains, it was interesting to study the dynamic and static magnetic susceptibilities and importantly hysteresis. Appropriate magnetic data were modeled to calculate the sign and the magnitude of different exchange interaction *J* values by theoretical fitting procedure.

Using a pure *organic approach* and *crystal engineering* as tools, it was challenging to develop supramolecular entities based on hydrogen bonding and π-π stacking. For the H-bonding [N-O···H-C≡C-] purposes, synthesis of hydrogen bonding synthons having ethynyl (donor) and nitronylnitroxide oxygen (acceptor) functionalities such as 2-(5-ethynyl-2-phenyl)-4,4,5,5-tetramethylimidazoline-1-oxyl (**26**) and 2-(5-ethynyl-2-pyridyl)-4,4,5,5-tetramethylimidazoline-1-oxyl (**27**) was required. To prove the formation of hydrogen bonded polymeric chains and π-π stacking it was necessary to obtain single crystal X- ray structures. Monoradical **21** also had to be crystallized for the purpose of π-π stacking. Towards realizing the stacking of a quartet spin system, a conjugated symmetric triradical, *sym*-1,3,5-tris[4-(1-oxyl-3-oxo-4,4,5,5-tetramethylimidazolin-2-yl)phenylethynyl)]benzene (**33**) was designed. To establish the propagation of spin waves of the nitronylnitroxides to the

ethynyl function of the H-bonding synthons **26** and **27**, obtaining well-resolved ESR spectra with isotropic proton hyperfine structure were necessary. The magnetic susceptibility studies had to be carried out to investigate the intra and intermolecular magnetic behaviors down to liquid helium temperature; the same applies to stacks of **21**. Good magneto-structural correlation was necessary in order to find an explanation for the different magnetic behaviors. This had to be done by correlating solution ESR data and the bulk magnetic susceptibility data with the crystal structures. For **33**, ESR studies were necessary to diagnose the thirteen line pattern of the triradical. Symmetrical triradical (**33**) had to be crystallized for π-π stacking.

1.4 References

1. (a) R. L. Carlin, *Magneto-chemistry*, Springer-Verlag, **1985**. (b) M. M. Turnbull, T. Suimoto, L. K. Thompson, *Molecular-Based Magnetic Materials*, ACS Symposium series, **1996**. (c) J. H. Osiecki, E. F. Ullman, *J. Am. Chem. Soc*. **1968**, 90, 1078. (d) E. F. Ullman, J. H. Osiecki, D. G. B. Boocock, R. Darey, *J. Am. Chem. Soc*. **1972**, 94, 7049.
2. M. Tamura, Y. Nakazawa, D. Shiomi, K. Nozawa, Y. Hosokoshi, M. Ishikawa, M. Takahashi, M. Kinshita, *Chem. Phys. Lett.* **1991**, 186, 401. For review, see: M. Kinoshita, *Jpn. J. Appl. Phys*. **1994**, 33, 5718.
3. R. Chiarelli, M. A. Novak, A. Rassat, J. L. Tholence, *Nature (London)*, **1993**, 363, 147.
4. K. Mukai, K. Konishi, K. Nedachi, K. Takeda, *J. Magn. Magn. Mater*. **1995**, 140-144, 1449.
5. P. Carretta, D. Gatteschi, A. Lascialfari, *Physica B*. **2000**, vol. 289-290, pp. 94.
6. (a) R.W. Murray, A. M. Trozollo, E. Wasserman, W. A. Yager, G. Smolisky, *J. Am. Chem. Soc.* **1967**, 89, 5079. (b) K. Itoh, *Chem. Phys. Lett*. **1967**, 1, 235.
7. P. Lafenete, J. J. Nova, M. J. Bearpark, P. Celani, M. Olivucci, M. A. Robb, *Theor. Chem. Acc*. **1999,** 102, 309.
8. (a) H. C. Longuet-Higgins, *J. Chem. Phys*. **1950**, 18, 265. (b) A. A. Ovchinnikov, *Theor. Chim. Acta*. **1978**, 47, 297.

9. (a) A. Calder, A. R. Forrester, P. G. James, G. R. Luckhurst, *J. Am. Chem. Soc*. **1969**, 91, 3724. (b) K. Inoue, H. Iwamura, *Angew. Chem. Int. Ed.* **1995**, 34, 927. (c) T. Ishida, H. Iwamura, *J. Am. Chem. Soc*. **1991**, 113, 4238. (d) F. Kanno, K. Inoue, N. Koga, H. Iwamura, *J. Phys. Chem.* **1993**, 97, 13267. (e) T. Itoh, K. Matsuda , H. Iwamura, *Angew. Chem*. **1999**, 111, 1886. (f) T. Itoh, K. Matsuda ; H. Iwamura, K. Hori, *J. Am. Chem. Soc*. **2000**, 122, 2567. (g) D. Shiomi, M. Tamura, H. Sawa, R. Kato, M. Kinoshita, *Synt. Met.* 1993, 56, 3279. (h) L. Catala, P. Turek, J. Le Moigne, A. De Cian, N. Kyrisakas, *Tetrahedron Lett*. **2000**, 41, 1015. (i) F. Mathevet, D. Luneau, *J. Am. Chem. Soc.* **2001**, 123, 7465. (j) G. Zoppellaro, A. Ivanova, V. Enkelmann, A. Geies, M. Baumgarten, *Polyhedron*. **2001**, 22, 2099. (k) S. Kayami, K. Inoue, *Chem. Lett*. **1999**, 7, 545. (l) A. Izuoka, M. Fukada, T: Sugawara, *Mol. Cryst. Liq. Cryst*. **1993**, 232, 103.
10. K. Okada, T. Imakura, M. Oda, M. Baumgarten, *J. Am. Chem. Soc.* **1996**, 118, 3047.
11. (a) M. Dvolaitzki, R. Chiarelli, A. Rassat, *Angew. Chem. Int*. *Ed. Engl.* **1992**, 31, 180. (b) F. Kanno, K. Inoue, N. Koga, H. Iwamura, *J. Am. Chem. Soc.* **1993**, 115, 847.
12. (a) A. P. Jr. West, S. K. Silverman, D. A. Dougherty, *J. Am. Chem. Soc*. **1996**, 118, 1452. (b) S. V. Chapyshev, R. Walton, J. A. Sanborn, P. M. Lahti, *J. Am. Chem. Soc.* **2000**, 122, 1580. (c) M. Rule, A. R. Matlin, D. E. Seeger, E. F. Hilinski, D. A. Dougherty, J. A. Berson, *Tetrahedron*. **1982**, *38*, 787. (d) Y. Liao, C. Xie, P. M. Lahti, R. T. Weber, J. Jiang, D. P. Barr, *J. Org. Chem*. **1999**, *64* (14), 5176.
13. H. M. McConnell, *J. Chem. Phys.* **1963**, 39, 1916.
14. O. Kahn, *Molecular Magnetism*, VCH, Weinheim, **1993**.
15. C. Hirel, D. Luneau, J. Pécaut, L. Öhrström, G. Bussière, C. Reber, *Chem. Eur. J*. **2002**, 8, No.14, 3157.
16. (a) R. Breslow, *Pure. Appl. Chem*. **1982**, 54,927; (b) H. M. McConnell, *Proc. Robert A. Welch Found. Conf. Chem. Res.* **1967**, 11, 144. (c) J. S. Miller, A. J. Epstein, *Angew. Chem. Int. Ed. Engl.* **1994**, 33, 385; *Angew. Chem.* **1994**, 106, 399.

17. Reviews of crystal packing analysis can be found in: (a) A. Gavezzotti, **1998**, *Cryst. Rev.* 7:5. (b) A. Gavezzotti, **1994**, *Acc. Chem. Res.* 27, 309, (c) G.R. Desiraju, *Angew. Chem. Int. Ed. Engl*. **1995**, 34, 23111.
18. G. Desiraju, **1989**, *Crystal Engineering, The Design of Organic Solids*. Elsevier, Amsterdam.
19. (a) J. Zhang, M. Baumgarten, *Chem. Phys.* **1997**, 222, 1. (b) J. R. Ferrer, P.M. Lahti, C. George, P. Oliete, M. Julier, F. Palacio, *Chem. Mater.* **2001,** 13 (7), 2447. (c) F. M. Romero, R. Ziessel, M. Bonnet, Y. Pontillon, E. Ressouche, J. Schweizer, B. Delley, A. Grand, C. Paulsen. *J. Am. Chem. Soc*. **2000**, 122, 1298. (d) M. M. Matsushita, A. Izuoka, T. Sugawara, T. Kobayashi, N. Wada, N. Takeda, M. Ishikawa, *J. Am. Chem. Soc*. **1997**, 119, 4369. (e) L. M. Field, P. M. Lahti, *Chem. Mater.* **2003**, 15, (15), 2861. (f) A. Izuoka, S. Murata, T. Sugawara, H. Iwamura, *J. Am. Chem. Soc.* **1985**, 107, 1786.
20. (a) J. S. Miller, J. C. Calabrese, H. Rommelmann, S. R. Chittapedi, R. W. Zhang, W. M. Reiff, A. J. Epstein, *J. Am. Chem. Soc.* **1987**, 109, 769. (b) J. S. Miller, A. J. Epstein, W. M. Reiff, *Mol. Cryst. Liq. Cryst.* **1985**, 120, 27. (c) J. S. Miller, J. C. Calabrese, A. J. Epstein, R. W. Bigelow, R. W. Zhang, W. M. Reiff, , *J. Chem. Soc., Chem. Commun.* **1986**, 1026.
21. J. M. Manriquez, G. T. Yee, R. S. Mclean, A. J. Epstein, A. J. Miller, *Science*, **1991**, 252, 1415.
22. K. Nakatani, P. Bergerat, E. Codjovi, C. Mathoniere, Y. Pei, O. Kahn, *Inorg. Chem.* **1991**, 30, 3977.
23. A. Caneschi, D. Gatteschi, R. Sessoli, P. Rey, *Acc. Chem. Res*. **1989**, 22, 392.
24. A. Caneschi, D. Gatteschi, D. Renard, P. Rey, R. Sessoli, *J. Am. Chem. Soc*. **1989**, 111, 785.
25. (a) A. Caneschi, D. Gatteschi, A. Grand, J. Laugier, P. Rey, L. Pardi, *Inorg. Chem.* **1988**, 27, 1031. (b) D. Gatteschi, J. Laugier, P. Rey, C. Zanchini, *Inorg. Chem*. **1987**, 26, 938. (c) (a) A. Caneschi, D. Gatteschi, J. Laugier, L. Pardi, P. Rey, C. Zanchini, *Inorg. Chem.* **1988**, 27, 2027.
26. J. Laugier, P. Rey, C. Benelli, D. Gatteschi, C. Zanchini, *J. Am. Chem. Soc.* **1986**, 108, 5763.

27. (a) A. Caneschi, D. Gatteschi, J. Laugier, P. Rey, *J. Am. Chem. Soc.* **1987**, 109, 2191. (b) A. Caneschi, D. Gatteschi, P. Rey, R. Sessoli, *Inorg. Chem*. **1988**, 27, 1756.
28. (a) A. Caneschi, D. Gatteschi, , J. Laugier, P. Rey, R. Sessoli, *Inorg. Chem*. **1988**, 27, 1553. (b) A. Caneschi, F. Ferraro, D. Gatteschi, P. Rey, R. Sessoli, *Inorg. Chem*. **1991**, 30, 3162. (c) T. Ise, T. Ispida, D. Hashizume, F. Iwasaki, T. Nogami, *Inorg. Chem*. **2003**, 42, 6106.
29. M. Minguet, D. Luneau, E. Lhotel, V. Viller, C. Paulsen, D. B. Amabilino, and J. Veciana, *Angew. Chem. Int. Ed*. **2002**, 41, 4, 586.
30. K. Inoue, H. Iwamura, *J. Am. Chem. Soc.* **1994**, 116,3173.
31. K. Fegy, D. Luneau, T. Ohm, C. Paulsen, P. Rey, *Angew. Chem. Int. Ed*. **1998**, 37,9, 1270.
32. F. Mathevet, D. Luneau, *J. Am. Chem. Soc.* **2001**, 123, 7465.
33. (a) T. Lis, *Acta. Crystallogr.* **1980**, B36, 2042-2046. (b) A. Caneschi, D. Gatteschi, R. Sessoli, A. L. Bara, L.C. Brunel, M. J. Guillet, *J. Am. Chem. Soc.* **1991**, 113, 5873.
34. S. Parsons, C. Paulsen, F. Semadini, V. Villar, W. Wernsdorfer, R. E. P Winpenny, *Chem. Eur. J.* **2002**, 8, 4867.
35. (a) B. Schwarzschild, *Phys. Today*. **1997**, 50, 17 (b) E. M. Chudnovsky, *Science*. **1996**, 274, 938. (c) A. Caneschi, T. Ohm, C. Paulsen, D. Rovai, C. Sangregorio, R. Sessoli, *J. Magn. Magn. Mater*. **1998**, 177, 1330. (d) A. Caneschi, D. Gatteschi, C. Sangregorio, R. Sessoli, L. Sorace, A. Corina, M. A. Novak, C. Paulsen, W. J. Wernsdorfer, *J. Magn. Magn. Mater*. **1999**, 200, 182.
36. R. Sessoli, A. Caneschi, D. Gatteschi, M. A. Novak, *Nature*. **1993**, 365, 141.

CHAPTER 2

Electron Spin Resonance

Abstract: *This chapter explains the basic principles of electron spin resonance and its applications in characterizing mono- and oligoradicals. The elaborate discussion can be found in many wonderful books[1] and reviews.[2]*

2.1 Introduction

Electron spin resonance (ESR) and electron paramagnetic resonance (EPR) are synonymous terms, which explains the resonance absorption phenomenon of microwave radiations by paramagnetic ion or molecules in a constant magnetic field. Normally, the continuous wave (CW) ESR spectrum is obtained by sweeping the magnetic field at fixed microwave frequency. The resonance absorption of energy causes a transition from the lower energy to the higher energy state. The frequency at which the absorption occurs corresponds to the energy differences of the states. Most commonly used ESR spectrometers are operating in the range of 9-10 GHz (X – band).

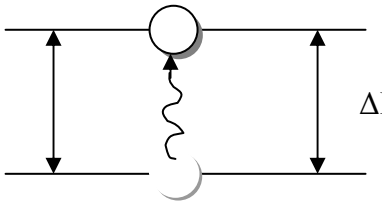

$$\Delta E = h\nu \qquad \ldots (17)$$

The differences in energies are associated with the interaction of an unpaired electron with external magnetic field produced by ESR spectrometer. This effect is called Zeeman effect. Because the electron has a magnetic moment μ, it acts like a compass in a magnetic field H. It will have a state of lowest energy where the electron moment μ is aligned along the local magnetic field (ms = -½) and a state with highest energy where μ is aligned against magnetic field (ms = +½). From quantum mechanics the derived basic equation for ESR is as follows,

$$E = m_s\, g_e\, \beta_e\, H = \pm\tfrac{1}{2}\, g_e\, \beta_e\, H$$
$$\Delta E = h\nu = g_e\, \beta_e\, H \qquad \ldots (18)$$

where g is the g-factor (unit less), β_e is the electron magnetic moment or Bohr magneton ($eh/4\pi m_e$ = 9.2740 x 10^{-24} J/T), and m_s is the magnetic quantum number. The free electron g_e value is 2.002319304386, for most of the organic radicals generally g value is ≤ 2.01, but varies depending on the electron configuration especially for transition metal ions. The selection rule for the magnetic quantum number ms; which has allowed values S. S –1…- S is.

$$\Delta m_s = \pm 1 \; ; \; \Delta m_I = 0 \qquad \ldots (19)$$

where, m_I is the nuclear spin quantum number.

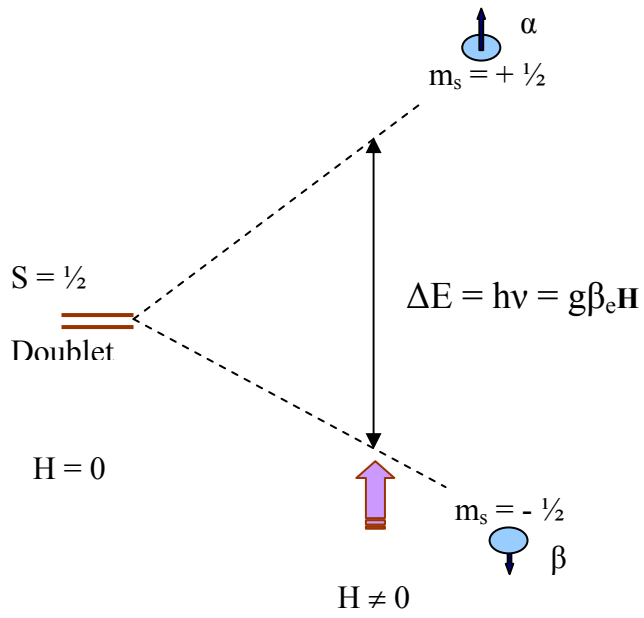

Figure 2.1. *Splitting of Zeeman levels in a magnetic field*

The condition in eqn. (19) not hold strictly, when S > ½ or the hyperfine interaction (*hfc*), including quadrupole and nuclear Zeeman interactions are present.

From eqn. (18) by substituting the values of β_e and h in appropriate units the resonance condition becomes,

$$g = \frac{71.448 \times \nu\,[\text{GHz}]}{H\,[\text{mT}]} \qquad \ldots. (20)$$

Boltzmann's distribution law governs the relative distribution of electrons over the two levels, which is given by,

$$n_{½} / n_{-½} = e^{[-\Delta E / K_B T]} = e^{[-g\beta H / K_B T]} \qquad \ldots (21)$$

where, n is the energy level, K_B is the Boltzmann's constant and T is the temperature. Here the lower level is more populated than the upper level. The difference in the present case will be larger than that between the two NMR levels, because of the larger values of ΔE. Consequently, the ESR signals are expected to be more intense than those of NMR.

The ESR g value depends upon the orientation of electron magnetic moment, the applied magnetic field makes with the molecular framework.

$$g^2 = g_x^2\, l_x^2 + g_y^2\, l_y^2 + g_z^2\, l_z^2 \qquad \ldots (22)$$

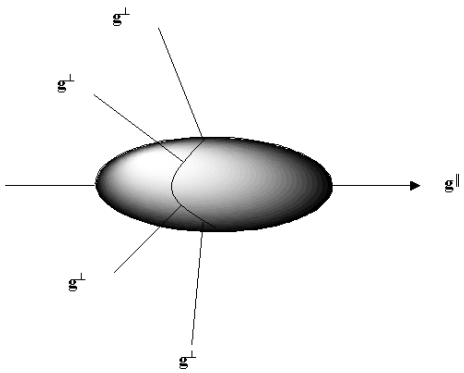

Figure 2.2. *The* $\boldsymbol{g}^{\parallel}$ *and some* $\boldsymbol{g}^{\perp}$ *axes in a crystallite with three fold and higher axis*

where, l_x, l_y and l_z are the direction cosines between the direction of H and the principle g-axes. In solid-state powder or frozen solution due to anisotropic nature of the paramagnetic site three main components can be seen for a (rhombic case) or in axial case, two anisotropic g values, [$g^{\parallel}$ and $g^{\perp}$] are required to describe the ESR spectrum. Since the paramagnetic crystallites have more $g^{\perp}$ [g_x and g_y] aligned than $g^{\parallel}$ [g_z], the most intense absorption will correspond to $g^{\perp}$ [see Fig. 2.2.]. In reality, often one finds that the overlapping features generally from $g^{\parallel}$ and $g^{\perp}$ make it difficult to obtain their values. For rhombic systems due to the lower symmetry of the crystallite the observed g values in different directions (X, Y, and Z) are no longer equal, $g_{xx} \neq g_{yy} \neq g_{zz}$. For an axial systems the solid-state anisotropic g values are [$g_z = g^{\parallel}$ and $g_x = g_y = g^{\perp}$]. In dilute liquid solution, all the g axis [$g_x = g_y = g_z$] are equal to the applied magnetic field H due to the free molecular rotation giving the isotropic g value, g_{iso}.

$$g_{iso} = [g_{xx} + g_{yy} + g_{zz}] / 3 \qquad \ldots(23)$$

2.2 Hyperfine coupling (*hfc*)

The hyperfine interaction is the sum of the "classical" dipolar term, E_{dip}, and the "quantum mechanical" Fermi-contact term E_{FC}. The magnetic interaction between an unpaired electron magnetic moment S and nuclear magnetic moment [nuclei with non-zero nuclear spin, $I \neq 0$] I is called *hyperfine coupling* A.

The general Hamiltonian describing the Zeeman and hyperfine interactions is given by,

$$\hat{\mathbf{H}} = (\beta \hat{S} \cdot g \cdot \hat{H}) + \hat{S} \cdot A \cdot \hat{I} \qquad \ldots(24)$$

Any observed hyperfine interaction theoretically consists of two terms i) isotropic and ii) anisotropic. The total hyperfine value of a system can be expressed by the following equation,

$$A = a_{iso} + A_{dip} \qquad \ldots(25)$$

The a_{iso} value also called Fermi contact term can be explained by the following quantum mechanical equation,

$$a_{iso} = \left[\frac{8\pi}{3}\right] g_e \beta_e g_n \beta_n \rho(0) \qquad \ldots(26)$$

where $\rho(0) = |\psi(0)|^2$ is the unpaired electron density at the nucleus, β_n is the nuclear magneton [$5.0507866 * 10^{-27}$ J T^{-1}]. Equation 26 measures the magnetic interaction energy (in joules) between the electron and nucleus. The A_{dip} term arises due to the interaction between the electron and nuclear dipoles, and is time-averaged to zero in liquid solution due to the random molecular motions. The observed isotropic hyperfine value in liquid solution is exclusively due to the Fermi contact term, E_{FC}. In this situation the A_{dip} value in eqn. 25 vanishes, leaving only the isotropic hyperfine value a_{iso},

$$a_{iso} = [A_{xx} + A_{yy} + A_{zz}] / 3 \qquad \ldots(27)$$

In solid or frozen rigid systems, it is precisely the dipole-dipole interaction between the electron and nuclear dipoles that gives anisotropic component of hyperfine coupling.

The magnitude of the A component is like the g component, orientation dependent. The Hamiltonian describing the anisotropic interaction takes the following form,

$$\hat{\mathbf{H}} = (\beta \hat{S} \cdot g \cdot \hat{H}) + (\hat{S}_z \cdot A_{zz} \cdot \hat{I}_z + \hat{S}_x \cdot A_{xx} \cdot \hat{I}_x + \hat{S}_y \cdot A_{yy} \cdot \hat{I}_y) \qquad \ldots(28)$$

Thus we can obtain the principle hyperfine values A_{xx}, A_{yy}, and A_{zz} for each directional cosines for all three directions or the $A_{zz} = A^{\parallel}$ and $A_{xx} = A_{yy} = A^{\perp}$ in case of axial symmetry. Most often g axis and the A axis are collinear.

Hyperfine interactions usually result in splitting of lines in an ESR spectrum. The number of hyperfine lines grows multiplicatively with the number n of magnetic nuclei, because each additional nucleus splits every line into equidistant 2I+1 lines of the same intensity. The n equivalent nucleus thus gives rise to $(2I+1)^n$ lines. However, when n nuclei are equivalent, some of the lines coincide and their number is reduced to 2nI+1. The hyperfine pattern then exhibits a characteristic distribution of intensities for I =1 with n = 1– 6, which are given [Pascal's triangle] below,

n =	**0**	I=	1					1						
	1						1	1	1					
	2					**1**	**2**	**3**	**2**	**1**				
	3				1	3	6	7	6	3	1			
	4			**1**	**4**	**10**	**16**	**19**	**16**	**10**	**4**	**1**		
	5		1	5	15	36	45	51	45	36	15	5	1	
	6	**1**	**6**	**21**	**56**	**96**	**132**	**141**	**132**	**96**	**56**	**21**	**6**	**1**

2.3 Species with more than one unpaired electron (S ≥ 1)

According to Kramer's rule, if an ion has an odd number of electrons the degeneracy of energy level must remain at least two fold in the absence of a magnetic field. Therefore, any ion with an odd number of unpaired electrons must always have as its lowest levels at least a doublet called a Kramer's doublet. This degeneracy can be removed by a magnetic field and an ESR spectrum should be observed [Fig. 2.1.]. On the other hand, for a system with an even number of electrons, e.g., two non-interacting electrons, four orientation dependent configurations are possible, with α and β described as spin up and spin down, respectively [see Fig. 2.1.].

$$\alpha(1)\alpha(2) \quad \alpha(1)\beta(2) \quad \beta(1)\alpha(2) \quad \beta(1)\beta(2)$$

When interaction occurs between the two electrons, symmetric and asymmetric states are possible,

α(1)α(2)	
1 /√2 (α(1)β(2) + β(1)α(2))	1 /√2 (α(1)β(2) - β(1)α(2))
β(1)β(2)	
Symmetric (Triplet; S = 1)	Asymmetric (Singlet; S = 0)

The spin multiplicity of the states with S = 1 is called a triplet state [(2S+1) = 3]. When S = 0 is analogously called a singlet state [(2S+1) = 1]. The asymmetric features arises when two electrons occupy the same spatial orbital, it gives S = 0. However, if the two electrons occupy different orbitals then both the singlet and triplet state exists. The total spin Hamiltonian for this system is given by,

$$\hat{\mathbf{H}} = (\beta\, \hat{S} \,.\, g \,.\, \hat{H}) + \hat{S}.\, A \,.\hat{I} + \hat{S} \,.\, D \,.\, \hat{S} - 2\, J\, S_1 \,.\, S_2 \qquad \ldots(29)$$

2.3.1 Exchange interactions (J)

The simulated isotropic solution state ESR spectrum of a mono- (n = 2), bi- (n = 4) and trinitronylnitroxide (n = 6) radicals are given in Fig. 2.3. In a monoNITradical interaction of electron spin with two equivalent nitrogen nuclei [I = 1], yields five lines pattern with intensity distribution 1:2:3:2:1 in solution, which contains, only information about the nitrogen *hfc* (**I**). A well resolved spectrum with hydrogen hyperfine interaction [A_H] can be obtained by using argon bubbled solution of concentration $c \leq 10^{-4}$ M and low modulation frequency (**II**). This spectrum gives rich information about the spin density of different carbons attached to hydrogens in other words spin polarization pathways. A biNITradical with four equivalent nitrogen nuclei [I = 1], gives nine lines in solution yielding intensity ratios close to 1:4:10:16:19:16:10:4.1, when the intramolecular exchange interaction [*J*] between the two radical units exceeds the A_N value (**III**). The integrated intensity of the signal is 2.66 times that of a monoradical, which provides information about the spin concentration. For a triNITradical, when the $J >> hfc$, interaction of six equivalent nitrogens with the electron spin affords thirteen line pattern (**IV**) with the intensity ratio close to 1:6:21:56:96:132:141:132:96:56:21:6:1.

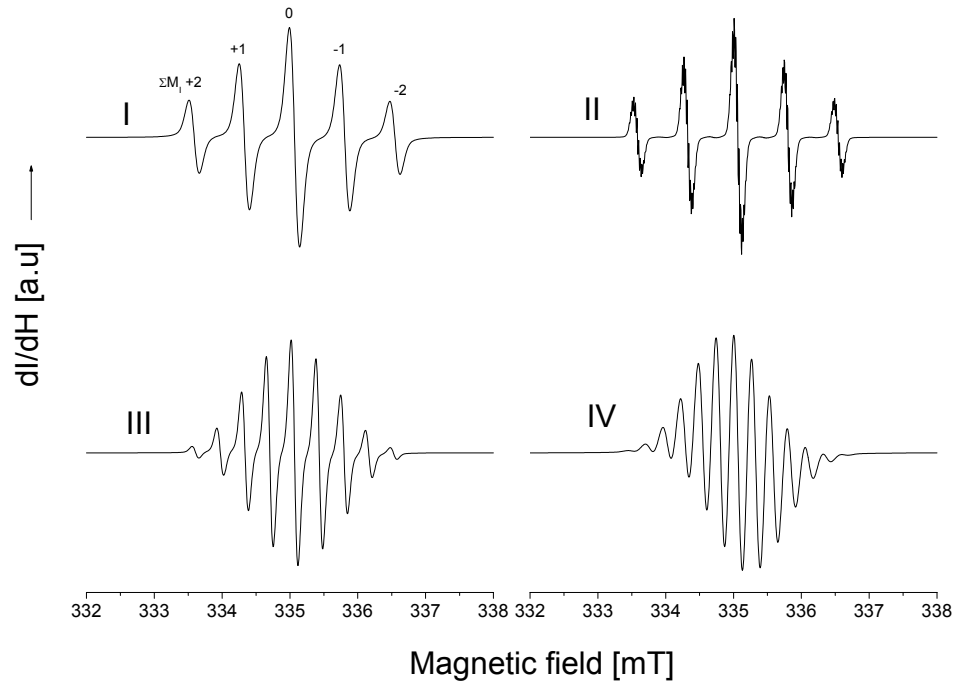

Figure 2.3. *Simulated solution state ESR spectrum of the Δms = ±1 transition of (I) monoNITradical - poorly resolved [a_N = 7.4 G; ΔB_{PP} = 1.5 G; L/G = 0.33], (II) monoNITradical - well resolved [a_N = 7.4 G; 12 H = 0.21G; 2 H = 0.51 G; ΔB_{PP} = 0.18 G; L/G = 0.33], (III) biNITradical [a_N = 3.65 G; ΔB_{PP} = 1.5 G; L/G = 0.33] in the limit of J >> a_N and (IV) triNIT radical [a_N 2.6 G; ΔB_{PP}=1.5 G; L/G = 0.33] in the limit of J >> a_N*

The total spin Hamiltonian governing the number of lines of a two-spin system is given by,

$$\hat{\mathbf{H}} = g\beta H (S_{1z} + S_{2z}) + A (\hat{S}_1\hat{I}_1 + \hat{S}_2\hat{I}_2) - 2J \hat{S}_1 . \hat{S}_2 \quad \text{....(30)}$$

The influence of intraradical exchange interaction J in relation with A_N value on the number of lines for a bisnitroxide radical $[NO]_2$ with two equivalent nitrogens [I =1] are given in Fig. 2.4. When the exchange interaction between the two spins are zero (J = 0), the spectrum looks like a mononitroxide showing three lines of equal intensity but with double the intensity of a monoradical. When the exchange interaction is much larger than the hyperfine interaction it shows five lines with intensity close to 1:2:3:2:1 ratio. Importantly with same spectral width as for

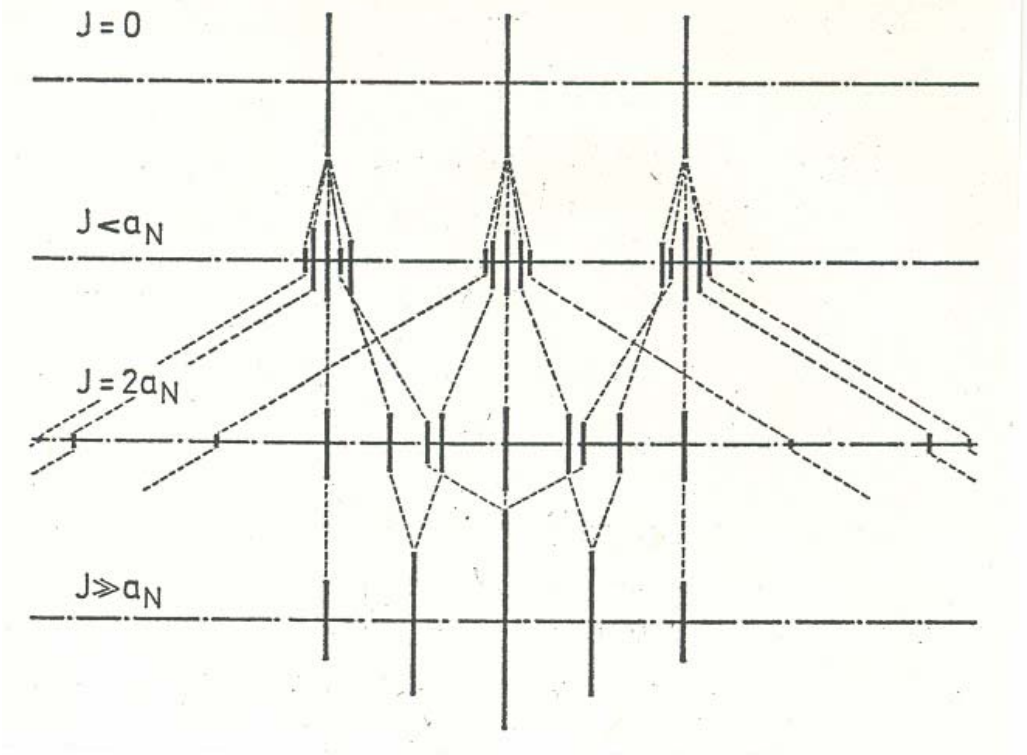

Figure 2.4. *Hyperfine coupling of a two spin system having coupling with nuclear spin (I =1) with different J values*[Fig. taken from Ref.1b]

monoradical, where the spacing between the lines of the biradical is half of the corresponding monoradical ($a_N/2$). Intermediate cases like $J < a_N$ or $J = 2a_N$ changes the total spectral width higher than for the respective monoradical, with a number of additional lines with different intensities. When the exchange interaction between the two radicals is large the *J* value increases, in other words the energy gap between the singlet and triplet state increases. However, when the exchange is weak the singlet and the triplet states are almost degenerate. There also exists an electronspin-electronspin contact interaction analogous to the Fermi contact interaction that is the mechanism of isotropic hyperfine interaction. However, the magnitude of this term is very small. To the extent it is present, it contributes to *J*.

2.3.2 Zero field splitting (zfs)

For a system with two or more unpaired electrons, the degeneracy of the spin states (e.g., two electron system; between S = 0 and S = 1) may be removed even in the absence of magnetic field. This phenomenon is referred to as *zfs* represented as D,

which is a dipolar tensor. The *zfs* arise from the dipolar interaction of the two or more electron spin moments can be explained by the following equation.

$$\hat{S} \cdot \mathbf{D} \cdot \hat{S} = D [\hat{S}_z^2 - \tfrac{1}{3} \hat{S} (\hat{S}+1)] + E (\hat{S}_x^2 - \hat{S}_y^2) \quad \ldots(31)$$

The values of D and E are not unique. They depend on which axis is chosen as Z. For a system in axial symmetry one has $D_x = D_y$ and hence E = 0. so, equation 31 becomes

$$zfs = D [\hat{S}_z^2 - \tfrac{1}{3} \hat{S} (\hat{S}+1)] \quad \ldots(32)$$

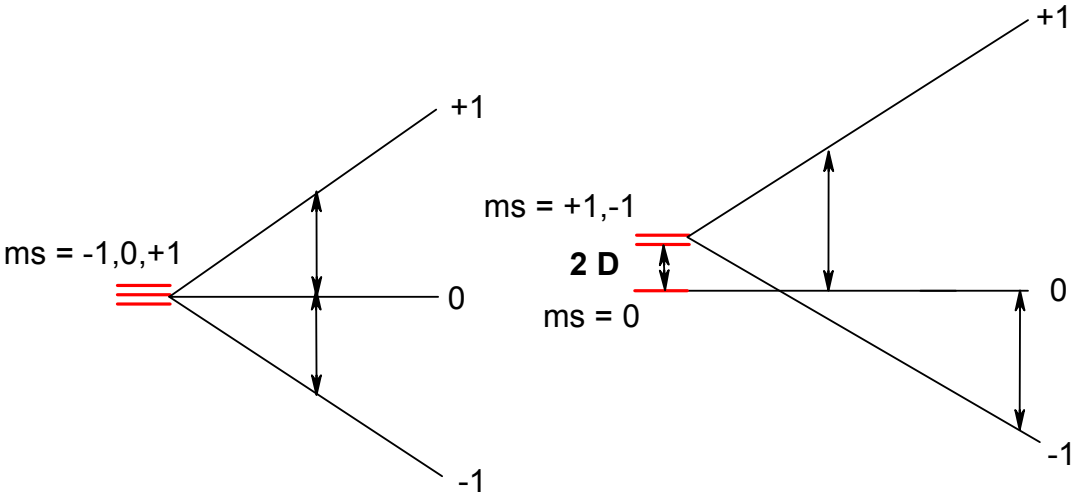

Figure 2.5. *Schematic diagram of a triplet state zero field splitting (D>0; E=0)*

In case of a distortion to lower symmetry (rhombic) in organic radicals, $E \neq 0$. so all the states are degenerate at zero field. If the molecule has cubic symmetry one has $D = E = 0$.

Calculating *zfs* parameters D and E as a function molecular geometry are useful to elucidate the conformation of the organic molecules. It is convenient to express D and E in magnetic field units [$D' \equiv D/g_e\beta_e$ and $E' \equiv E/g_e\beta_e$] or in cm^{-1} [$\underline{D} \equiv D/hc$ and $\underline{E} \equiv E/hc$]. Various approximations are used for the theoretical determination of D, the frequently used equation by Mukai[3] and co-workers is,

$$D = \tfrac{3}{4} g^2 \beta^2 \sum [r_{ij}^2 - 3 m_{ij}^2] \rho_i \rho_j / r_{ij}^5 \quad \ldots(33)$$

The *zfs* parameter or fine structure (D) gives an indication about the dipolar interaction of unpaired electrons in a molecule and is related to the intraradical distance (r) by $1 / r^3$. Where r_{ij} is the distance between atoms of i and j, m_{ij} is the

distance vector along the axis which gives rise to the largest dipole-dipole interaction and ρ_i and ρ_j are the spin densities on atoms i and j. The eqn. 33 give reasonable D value approximation for biradicals with localized electron distributions that can be separated into monoradical halves with atoms i and j belonging to different halves (localized biradicals). Sandberg and Shultz[4] considered the dipolar interactions in delocalized radical systems (S>1) having shared spin densities, then atom i is a spin-containing atom in one SOMO and atom j is a spin-containing atom in the other SOMO, and r_{ij} refers to the distance between spin-containing atoms in the SOMOs instead of the monoradical halves since the biradical cannot be separated into monoradical halves. The spin density is determined by summing the squared coefficients (obtained from AM1-RHF-triplet calculation) of each atom in the SOMO. Since the sum of the product of $\rho_i\rho_j$ is approximately unity, its inclusion in eqn. 33 is unnecessary. Here the dipole-dipole interactions, and thus the D value, strongly depend on the "average" distance. The value of r can be calculated using the simplified equation given below,

$$r^{1/3}\ [\text{Å}] = 7.8 \times 10^4 / D\ [\text{MHz}] \qquad ...(34)$$

In the absence of *zfs*, the two allowed ESR transitions ($\Delta ms = \pm 1$) occur at the same magnetic field but in the presence of *zfs* these transitions are no longer degenerate and may be observed separately (with fine structures). The separation depends upon the magnitude of the *zfs* parameter D.

The simulated ESR spectra[5] of a triplet species with D′ value 50 G is given in Fig. 2.5. The distance between the outer most lines corresponds to 2 D′ value. If the *zfs* is larger than the microwave transition energy no *zfs* is observed. According to eqn. 33 the D value is indirectly proportional to the distance (r) between the two radicals. For large distance separated radicals the outer most lines are difficult to locate, since the value of D is small and may not be resolved.

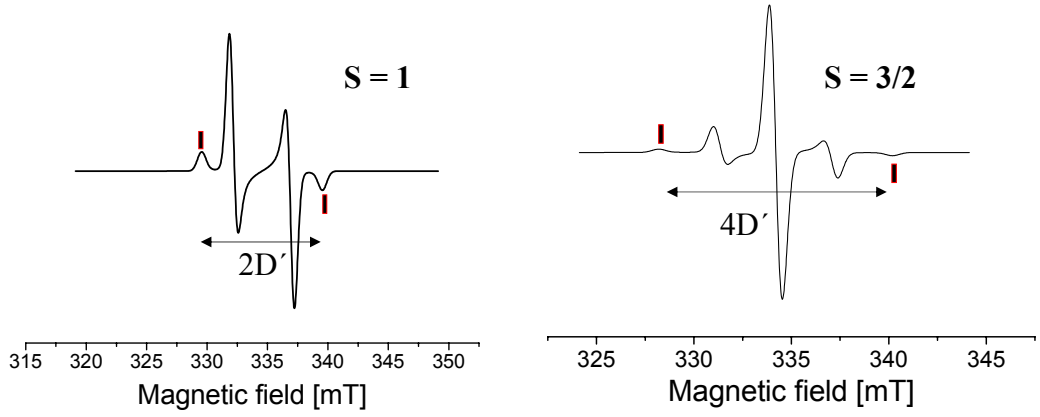

Figure 2.5. *Simulated solid state ESR spectra of an axially symmetric Δms = ±1 transition of (a) triplet species with D´ = 50 G; E = 0; g_{av} = 2.0066 and (b) a quartet species D´ = 30 G; E = 0; g_{av} = 2.0066 randomly oriented species in frozen state*

2.3.3 Ground state spin multiplicity

For fast electron exchange (i.e., strong coupling) the ground state of the biradical will be either a singlet or a triplet. The ground state of a biradical can be explored by plotting the double integrated signal intensities of the Δms = ±1 transitions or the Δms = ±2 transitions (forbidden transition - the selection rule Δms = ±1 is no longer valid at lower fields; this signal appears exactly at half field of the Δms = ±1 transition, also called half field transition) versus inverse temperatures (down to liquid helium temperature). In order to establish the pure intramolecular spin ground state, it is necessary to use lower concentrated solutions [c ≥ 10^{-3} M] to avoid intermolecular contacts between the molecules. Usually, peak-to-peak signal intensities or better double integrated Δms = ±2 transition signal intensities (χ_{ESR}) are plotted as a function of inverse temperature, since the saturation of the signal can be easily avoided by using lower microwave power, which can be monitored by plotting the observed signal intensities with respect to the square root of the microwave power. For a species having triplet ground state or triplet-singlet nearly degenerate states the signal intensity follows Curie law [χ_{ESR} = C/T]. The difference between the singlet-triplet (ΔE_{S-T}) energy levels is equal to 2*J* and its magnitude and sign can be estimated by

fitting the curve of the product of Δms = ±2 signal intensity and the temperature ($\chi_{ESR} \times T$) versus temperature using the Bleany-Bower equation[6].

$$\chi = [2Ng^2\beta^2/3K_BT][1+(⅓)\exp(-2J/K_BT)]^{-1} \quad ...(35)$$

The value of *J* is related to the ΔE_{S-T} energy levels by the equation given below,

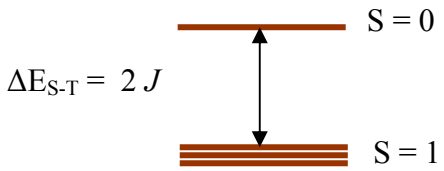

...(36)

Usually J is expressed in Kcal /mol or cm^{-1} or in Kelvin.

2.4. References

1. a) J. A. Weil, J. R. Bolton, J. E. Wertz, *Electron Paramgnetic Resonance – Elementary Theory and Practical Applications*, John Wiley & Sons, **1994**. b) M. M. Porio, J. H. Freed, *EPR and Advanced Resonance Spectroscopy*, Plenum Press, **1979**. c) F. E. Mabbs, D. Collison, *Studies in Inorganic Chemistry 16, Electron Paramagnetic Resonance of d Transition Metal Compounds*, Elsevier, **1992**. d) K. Scheffler, H. B. Stegmann, *Elektronenspinresonanz, Organische Chemie in Einzeldarstellungen*,*12,* Springer-Verlag. **1970**. e) W. Welner. Jr., *Magnetic Atoms and Molecules*, Scientific and Academic edition, **1983**. f) A. Schweiger, G. Jeschke, *Principles of pulse paramagnetic resonance*, Oxford University Press, **2001**.
2. M. Baumgarten, *Molecular Magnets*, Chapter 2 in *EPR of free radicals in Solids*, Lund, A.; Shiotani, M. (eds), Kluwer, **2003** in press.
3. K. Mukai, T. Tamaki*, Bull. Chem. Soc. Jpn*. **1977**, 50, 1239. (b) K. Mukai, J. Sakamoto, *J. Chem. Phys*. **1978**, 68, 1432. (c) K. Mukai, N. Inagaki, *Bull. Chem. Soc. Jpn*. **1980**, 53, 2695.
4. K. A. Sandberg, D. A. Shultz, *J. Phy. Org. Chem.* **1998**, 11, 819.
5. All the ESR spectral simulations were performed in Bruker Win-SymFonia programme.
6. B. Bleaney, K. D. Bowers, *Proc. R. Soc. London A*. **1952**, 214

CHAPTER 3

Organic High Spin Ligands with Extended π - Systems

Abstract: *Novel non-Kekulé type high spin biradical ligands were designed and synthesized using two extended phenylethynyl building blocks coupled with 3,5- and 2,6-pyridines. The main notion behind these designs, is to understand the influence of pyridyl nitrogens on ground state spin multiplicities in comparison with previous results. Further, these biradicals have a pivotal role in the formation of magnetic supramolecular architectures with transition metals. which will be described extensively in Chapter 4.*

3.1 Backgrounds and design

For the design of high spin molecules control of geometry and topology are crucial[1]. The sign of molecular exchange interaction (*J*) can be either positive or negative depending on the coupling unit between the radical sites and their steric demands. Most often, *meta* - phenylene bridging, leading to non - Kekulé structures, have been used for high spin ground state formation.[2] To obtain a ferromagnetically coupled system, apart from topology, the geometry of the molecules[3], the nature and position of the substituents,[4] and heteroatom influence[5,6] are to be considered in the design of high spin molecules. Understanding the effect of the heteroatom position like nitrogen in the ground state spin multiplicity is important, since the role of nitrogen is pivotal for metal complexation in constructing higher dimensional magnetic architectures. In this context, Dougherty's group[5a] have probed the influence of heteroatom in non - Kekulé systems and reported stable quintet ground state for a series of neutral pyridine based tetraradicals (3,5-, 2,6-, and 2,4-isomers) generated by the photolysis of the corresponding neutral bisdiazenes [Fig. 3.1]. It was found that the position of the pyridyl nitrogen in all the three isomers has no influence

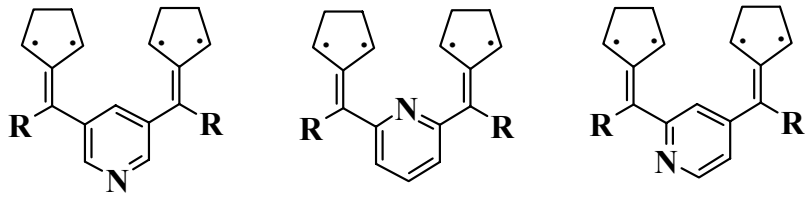

Figure 3.1. *Dougherty's Tetraradicals*

on the ground states spin multiplicities. Also Lahti et al.[5b] have described high spin ground states for dinitrenes attached to pyridines in 2,6- and 2,4- positions. Interestingly in contrast to the above reports, Takui et al.[6a] have examined the molecular ground state of NIT biradicals substituted to 2,6- and 3,5- pyridines and reported the S = 1 ground state for 2,6-pyridine NIT radicals based on magnetic susceptibility measurements and S = 0 state for the corresponding 3,5-pyridine biradicals based on ESR and magnetic susceptibility measurements [Fig. 3.2 B]. While for carbenes as spin sources[6b] reverted high spin stabilities were found as compared to NIT, the low spin ground state was described for 2,6-pyridine bridging

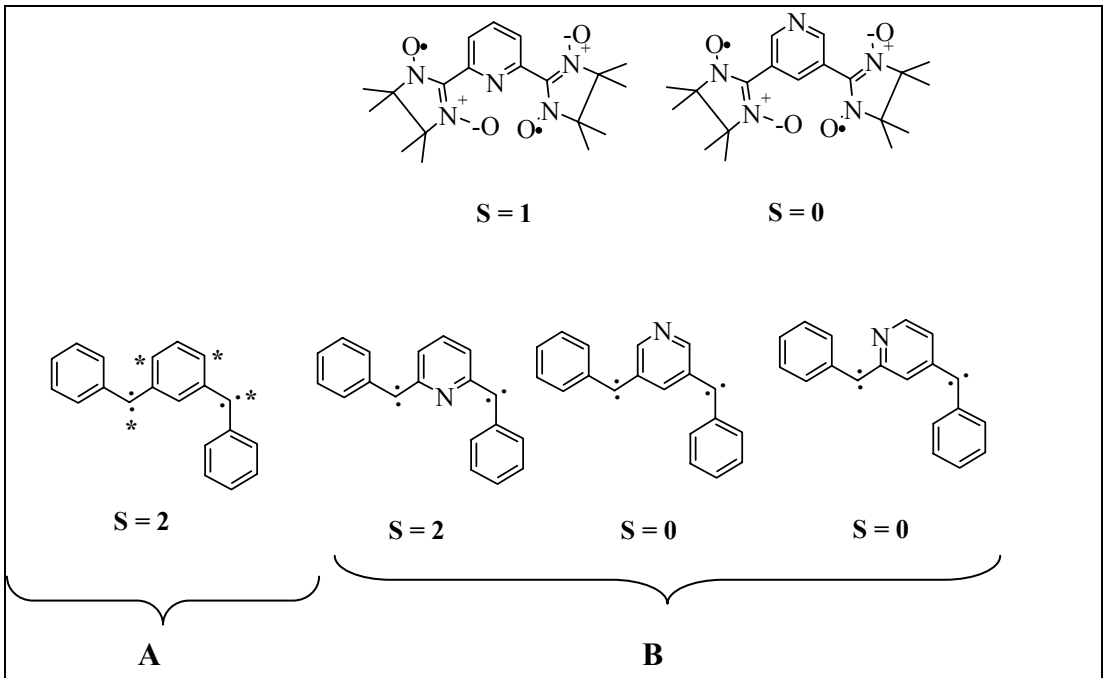

Figure 3.2. *(A) Itoh and Wasserman tetracarbeneradicals and (B) Takui's bisNIT and tetracarbene radicals*

and high spin quintet ground state for the 3,5-pyridine bridging, reasoned by opposite effects of the heteroatom locations. Where as in 1967, Itoh and Wasserman individually prepared and reported tetracarbene radicals with S = 2 state with benzene bridging[6c] [Fig. 3.2A.]. Wautelet et al[6c]. have reported the singlet ground state for the methyl and methoxy carrying bisimino nitroxide derivative of **T** (1,3-Bis[4-(1-oxyl-3-oxo-4,4,5,5-tetramethylimidazolin-2-yl)phenylethynyl)]benzene). The interplay between the spin polarization and the spin delocalization (π-conjugation) mechanisms were reasoned for the observed singlet ground state. Accidentally the half field signal was not observed by ESR and no comparison with the stronger exchange coupled bisnitronylnitroxide was made[7].

3.2 Design strategy

We have designed the NIT biradicals (**1** and **2**) using phenylethynyl spacers attached to 2,6- and 3,5-pyridine units to uncover the influence of pyridyl nitrogen position on the molecular ground state spin multiplicities [Fig. 2.3.]. Radicals, which are separated intramolecularly by longer distance, on the other hand (e.g., **1** and **2**) need good π conjugation for achieving strong intramolecular exchange interaction

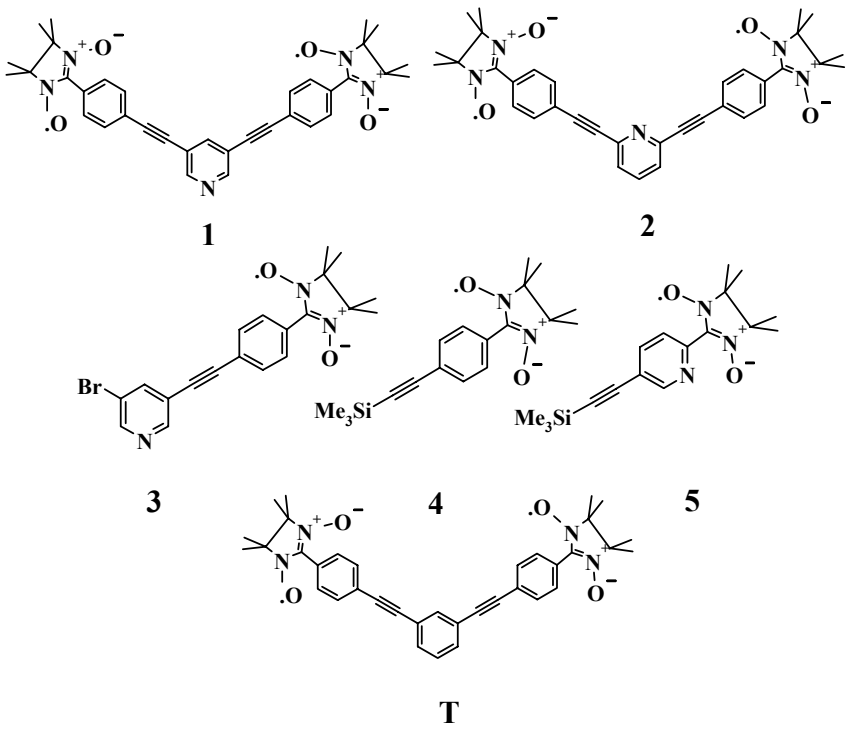

Figure 3.3. *Mono- and bisnitronylnitroxides*

(*J>hfc*). In this aspect, arylethynyl units are versatile and useful building blocks for spatially separated radical units in a molecule for their rigid and conjugated nature[6c,d]. Formation of alternating spin density waves along the near planar conjugated spacer is good for high spin formation.

3.3 Synthesis of 1- 5

The main precursor for the Ullman's radical[8] is 2,3-dimethyl-2,3-bis(hydroxylamino)-butane **6**, which was prepared adopting modified procedure of Ovacharenko[9], from 2,3-dimethyl-2,3-bis(hydroxylamino)-butane sulphate salt. The reaction sequence is given in Scheme 3.1.

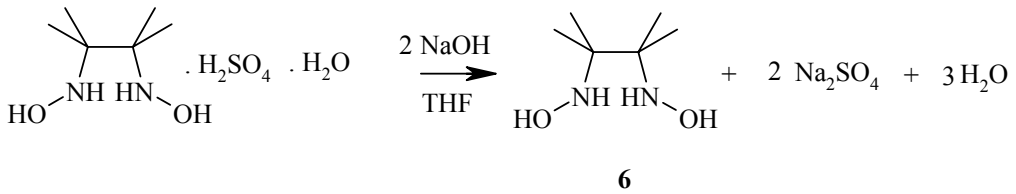

6

Scheme 3.1. *Synthesis of the radical precursor* ***6***

Salt freebase from the sulphate salt was prepared by stirring with the drop-by-drop addition of cooled aq. NaOH solution into the 2,3-dimethyl-2,3-bis(hydroxylamino)-butane sulphate salt in THF at room temperature. The purity of the free base is important for the success and the yield of the condensation reaction, especially with the dialdehydes and trialdehydes.

The synthetic sequence towards high spin biradicals **1** and **2**, is based on the key building block **9**[10a-b] [Fig. 3.2.], which was prepared via Sonogashira coupling of *para*-bromobenzaldehyde with trimethylsilylacetylene (TMSA) to give **7**, followed by deprotection of the silyl group[10c] upon stirring with K_2CO_3 in methanol under argon to afford the key compound **9**. The model monoradical **4** was prepared by subsequent condensation reaction of **7** with **6** by stirring at RT for one day in THF/ MeOH solvents to afford condensed white precipitate of **8**. The oxidation reaction of **8** was performed in phase transfer solution ($CHCl_3$ / H_2O) with $NaIO_4$ as oxidant to give monoradical **4** as blue powder.

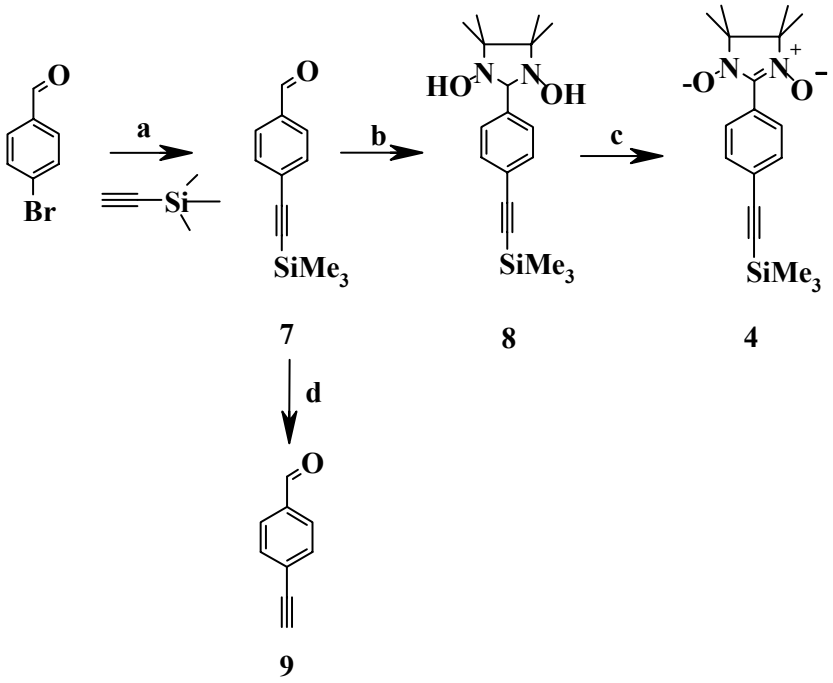

Scheme 3.2. *Synthesis of Monoradical **4** and the key building block **9**. Reagents and conditions: (a) TMSA / $Pd(PPh_3)_2Cl_2$ / CuI / Et_3N / THF (b) 2,3-Dimethyl-2,3-bis(hydroxylamino)butane / MeOH / THF / RT / Overnight (c) $NaIO_4$ / $CHCl_3$ / H_2O(d) K_2CO_3 / MeOH*

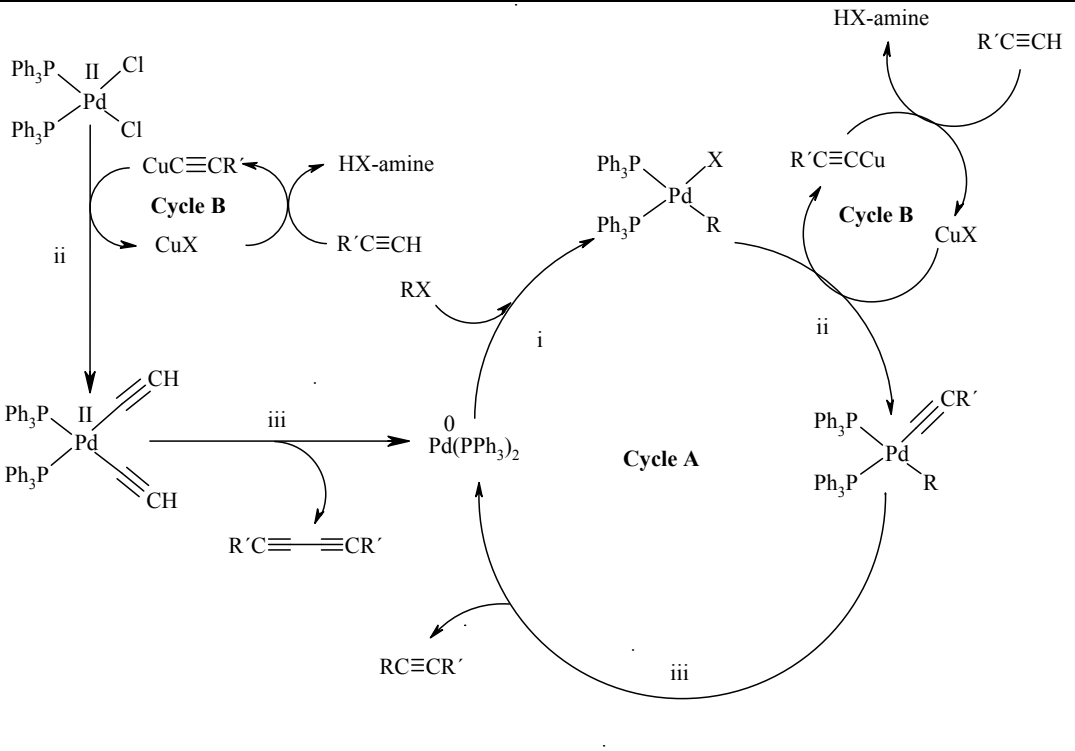

Scheme 3.3. *Sonogashira´s Coupling Mechanism. Pd(II)-catalyzed cross-coupling reaction of terminal acetylenes with sp^2 halides: i) Oxidative addition, ii) Transmetallation, iii) Reductive elimination*

The reaction to couple the key arylethynyl spacer **9** to 2,6-, and 3,5-dibromopyridines to synthesize the dialdehydes, mainly involves Sonogashira coupling reaction conditions[10a]. Therefore, it is important to understand the mechanism and conditions of the reaction before proceeding to other multiple step reactions involved to achieve the final products. The detailed mechanism is given in the Scheme 3.3. The total cross-coupling reaction has three steps before releasing the final cross-coupled product from the Pd catalyst namely, 1) Oxidative addition reaction 2) Insertion reaction and 3) Reductive elimination reaction. In the reaction cycles, the cycle A determines the cross-coupled product yield, in our case the yields of cross-coupled products 2,6-, and 3,5-dialdehydes mainly depends on pure dry argon atmosphere and degassed base and co-solvents. Failure to take the necessary conditions leads to undesirable monocoupled products **11, 16** and homo-coupled dimer as side products **12** [Scheme. 3.4 and 3.5].

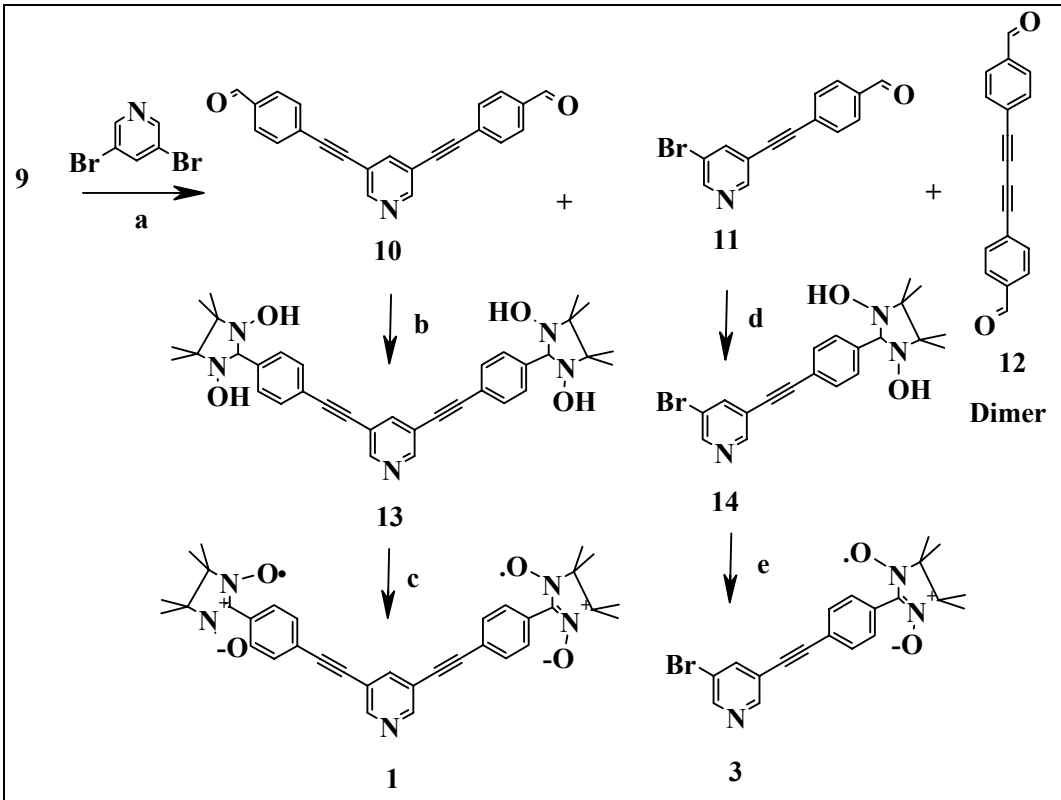

Scheme 3.4. *Synthesis of **1** and **3**. Reagents and conditions: (a) / $Pd(PPh_3)_2Cl_2$ / CuI / Et_3N / THF / 80°C / Argon / yield 27% (b) 2,3-Dimethyl-2,3-bis(hydroxylamino)butane / MeOH / Dichloromethane / Reflux/ Argon bubbling / 12 h / Yield 37% (c) $NaIO_4$ / $CHCl_3$ / H_2O / Yield 35% (d) 2,3-Dimethyl-2,3-bis(hydroxylamino)butane / MeOH / Toluene / 90°C / Argon / Yield 46% (e) $NaIO_4$ / $CHCl_3$ / H_2O / Yield 20%*

Key molecule **9** was used to build the dialdehydes **10** and **15** using 3,5-, and 2,6-dibromopyridines in presence of catalysts $Pd(PPh_3)_2Cl_2$, CuI, THF and Triethylamine. The cross-coupling reactions towards dialdehydes involve absolute dry argon conditions obtained by freeze-pump-thaw cycles. This is necessary to avert homocoupling of **9** to form dimer **12** [m/z (%) 258.0 (100%)]. The dimers become the predominant product if the oxygen is not properly excluded from the reaction vessel. Together with the dialdehydes, mono coupled products **11** and **16** [m/z (%) 285.2 (~89%) and 287.2 (100%)] were also obtained. The dialdehydes have low R_f values as compared to dimers and monocoupled products in chloroform and dichloromethane. The low R_f values of the dialdehydes are due to the poor solubility in the eluent at

room temperature. Alternatively this low R_f values of the dialdehydes have some advantages, after removing the first two fractions, the final desired product could also be easily taken from the silica column by washing with acetone.

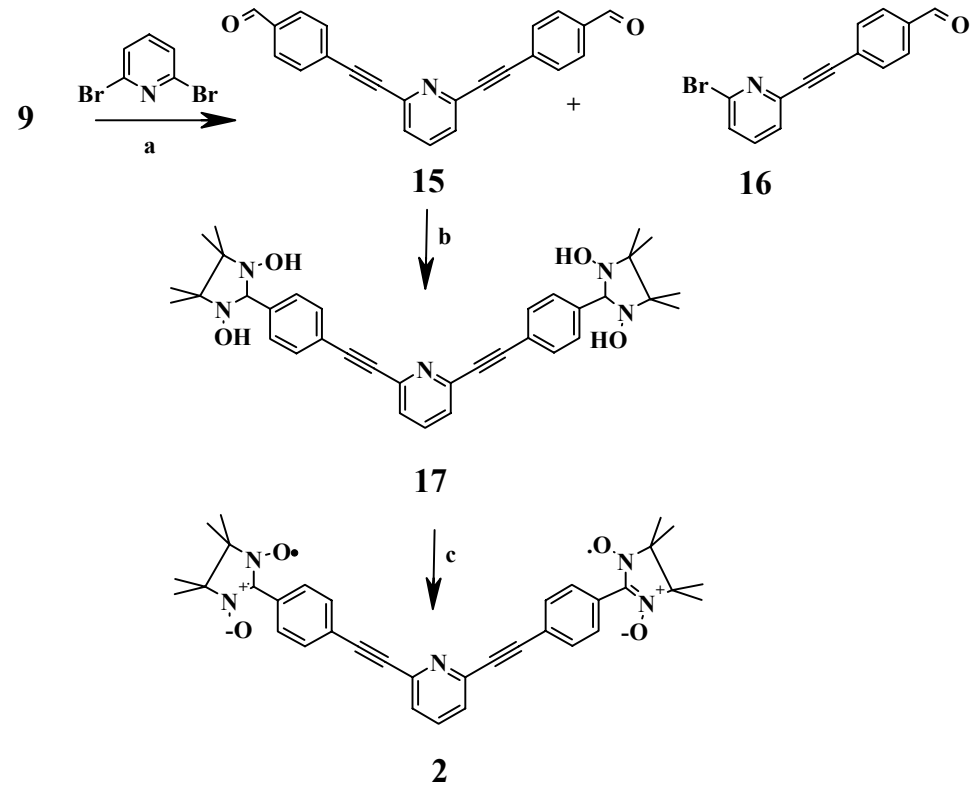

Scheme 3.5. *Synthesis of* ***2****. Reagents and conditions: (a) / $Pd(PPh_3)_2Cl_2$ / CuI / Et_3N / THF / 60°C / Argon / 3 days / yield 60% (b) 2,3-Dimethyl-2,3-bis(hydroxylamino)butane / MeOH / Toluene / Reflux/ Argon bubbling / Yield 61% (c) $NaIO_4$ / $CHCl_3$ / H_2O / Yield 34%*

The condensation reactions of aldehydes (**10, 11** and **15)** with 2,3-dimethyl-2,3-bis(hydroxylamino)-butane were performed in methanol with co-solvents, dichloromethane for **10**, and toluene for both **11** and **15** respectively. Mild reflux under constant argon bubbling lead to the precipitation of the condensation products. The oxidation reactions of the condensed product were performed in phase transfer solution (water / $CHCl_3$) with $NaIO_4$ by stirring at RT for just 10 min to prevent the over oxidation of NIT to the imino nitroxides. The biradicals **1** and **2** were purified by preparative thin layer chromatography. The radicals are blue in color and are stable up to one year even in toluene solution. The biradicals were crystallized in toluene

and the obtained blue color single crystals were used for X - ray crystal and molecular structure analysis.

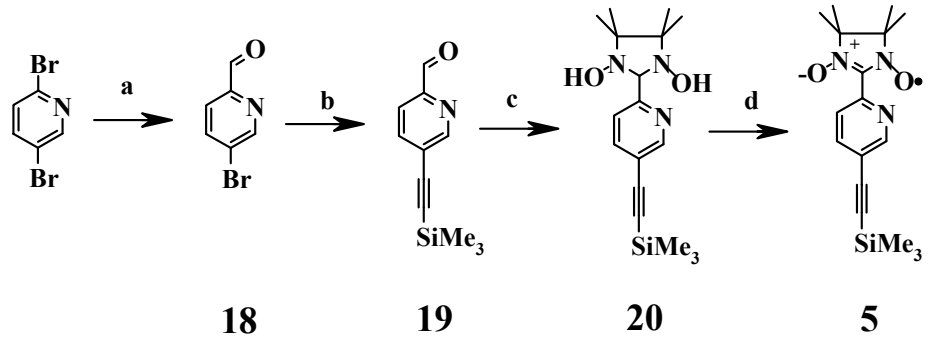

18 **19** **20** **5**

Scheme 3.6. *Synthesis of monoradical **5**. Reagents and conditions: (a) 1. n-BuLi / -78°C / Toluene 2. DMF (b) TMSA / $Pd(PPh_3)_2Cl_2$ / CuI / Et_3N / THF (c) 2,3-Dimethyl-2,3-bis(hydroxylamino)butane / MeOH (d) $NaIO_4$ / $CHCl_3$ / H_2O*

Monoradical **5** was prepared in four steps [Scheme.3.6]. The first step involves synthesis of 2-formyl-5-bromopyridine[11], which was carried out in 2 steps, (1) Selective mono lithiation of 2,5-dibromopyridine in 2-position to generate 5-bromo-2-lithiopyridine using n-BuLi (1.6 M in hexane) at -78°C in toluene (50 mL for 1 g of 2,5-dibromopyridine); (2) followed by addition of dry DMF and quenching with saturated solution of NH_4Cl. The yield was up to 23% after column chromatography on silica. The coupling reaction of the aldehyde **18** with TMSA in order to form **19** was performed via Sonogashira coupling reaction. The TMSA-coupled product was obtained as sticky dark brown mass, which was difficult to purify by regular workup and column chromatography. Alternatively, direct sublimation of the dark brown mass was carried out in order to get analytically pure, light brown crystalline powder up to 33% yield. During condensation reaction of **19** with 2,3-Dimethyl-2,3-bis(hydroxylamino)-butane, no precipitate was obtained after two days stirring in methanol. Following solvent evaporation, the obtained crude product was used for the oxidation reaction with $NaIO_{4\ in}$ $CHCl_3$ / water to afford **5**.

3.4 Optical properties

The UV/Vis spectra of the NIT radicals are very useful tool to estimate approximately the number of radical units in a single molecule based on the extinction coefficient of the n-π* transition in the visible range of the spectrum at ~ 600 nm, provided that the functionality and the back bones are quite similar. Prior results from our group have established the use of UV/Vis studies to distinguish benzene based mono, bi and tri NIT radicals besides ESR spectroscopic technique. In this scope we have attempted to compare the extinction coefficients (n-π* transition) of **4** with those of **1** and **2** [Fig. 2.4.]. In contrast to our expectation, the biradicals **1** and **2** have extinction coefficients 470 M^{-1} cm^{-1} and 530 M^{-1} cm^{-1} respectively which are not exactly twice as compared to the extinction coefficient of **4** which is 339 M^{-1} cm^{-1} at 611 nm. On the other hand the vibronic coupling pattern is very similar for **1, 2** and **4.** The lowered extinction coefficients of **1** and **2** compared to **4** may be due to the presence of pyridine unit.

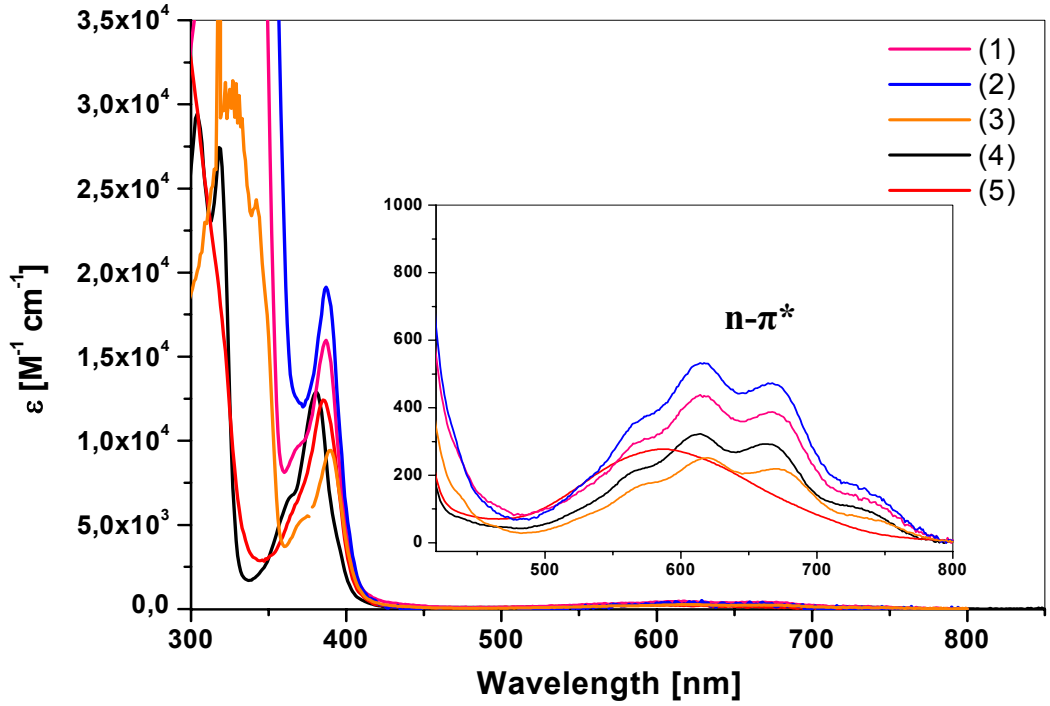

Figure 3.4. *UV/Vis spectra of mono and biradicals (in toluene, at RT) inset shows the n-π* transition molar extinction coefficients differences*

Indeed monoradicals **3** and **5** have extinction coefficient, 252 M^{-1} cm^{-1} at 620 nm and 266 M^{-1} cm^{-1} at 581 nm (blue shifted without vibronic coupling due to loss in symmetry) respectively. Which are much lower than the benzene based monoradical **4**. The extinction coefficients of **3** and **5** are now reasonable as compared to the doubled extinction coefficients of **1** and **2**, proving that, the pyridine unit has predominant role in lowering some of the extinction coefficient of the biradicals even in the presence of phenylethynyl spacers.

3.5 ESR studies

The ESR (X-band) investigations of the degassed toluene solutions of the mono and biradicals were performed. The monoradicals (**1 - 5**) show five lines due to the hyperfine coupling (*hfc*) of the electron spin with two equivalent NIT nitrogens (I = 1) with g_{iso} values 2.0067. The spectra of the monoradicals were best simulated with *hfc* values ($|a_N|$) 7.40 G, 7.40 G, 7.36 G for **3 - 5** respectively. In order to observe proton *hfc* in the monoradicals, argon bubbled dilute toluene solutions ($c \geq 10^{-4}$ M)

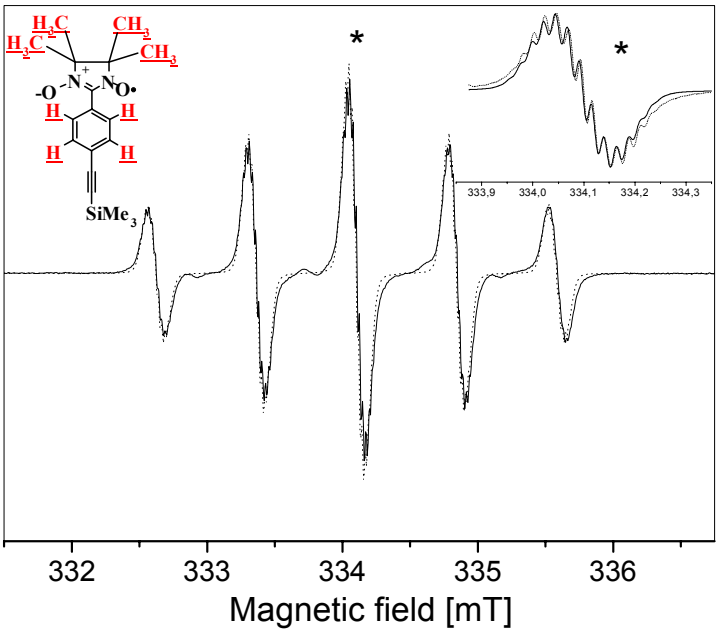

Figure 3.5. *ESR solution spectra of **4** at c = 1×10^{-4} M in toluene (5 mW, 16 dB, 1 scan) inset show the enlarged portion of the central line (right).——expt,....sim*

were used. Figure 3.5. shows, that each major lines of the monoradicals **4 - 5** were further splitted by protons hyperfine coupling. The enlarged portion of the central lines clearly shows the proton *hfc* of the 12 NIT methyl groups and aromatic protons. Interestingly, the central field is in the middle of a single line in **4** and it is between the two lines in **5** with some additional lines. This difference in central line position arises because of the symmetric and asymmetric structures of **4** and **5** respectively.

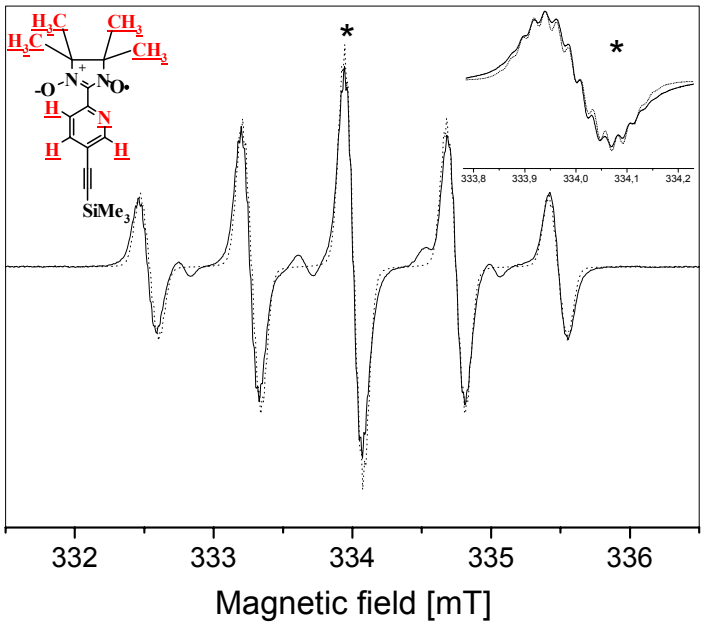

Figure 3.6. *ESR solution spectra of* ***5*** *at c = 1×10^{-4}M in toluene (5 mW, 16 dB, 1 scan) inset show the enlarged portion of the central line (right).——expt,....sim*

The detailed simulation of the protons hyperfine interactions in both **4** and **5** will be analyzed elaborately in chapter 5.

Biradicals **1** and **2** display nine line patterns at all the concentrations (10^{-2} M to 10^{-4} M), in liquid solution phase with g_{iso} = 2.0067 yielding intensity ratios close to 1:4:10:16:19:16:10:4:1 [Fig. 3.8.]. Temperature-dependant spectral behavior of the $\Delta ms = \pm 1$ transition from 300-200 K clearly ruled out the possibility of *J*-modulation effect in both **1** and **2** [Fig. 3.7.]. These nine line patterns seen at all dilute concentrations (c = 10^{-3} - 10^{-5} M) further supports that the interaction between the radicals are purely intramolecular.

For these cases of strong exchange coupling within the ESR limits, the simulation perfectly fits by assuming four nitrogens with half the hyperfine coupling with $J >> 7 \times 10^{-4}$ cm^{-1} ($J / a_N >> 1$). The lower limit of J value was ~ 400 MHz, estimated by

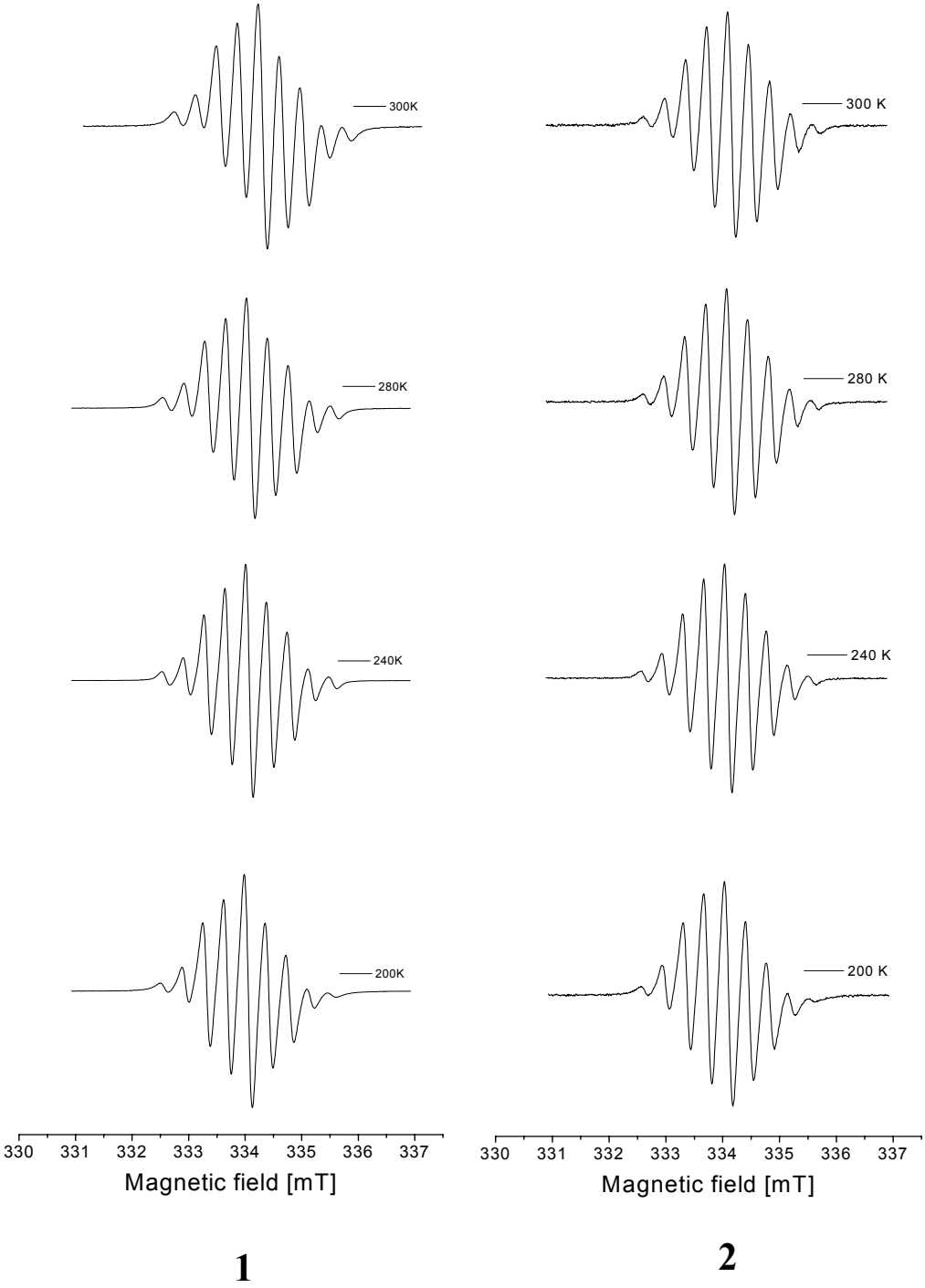

Figure 3.7. *ESR spectra of **1** and **2** at (c = 10^{-3} M in toluene) 300 – 200 K*

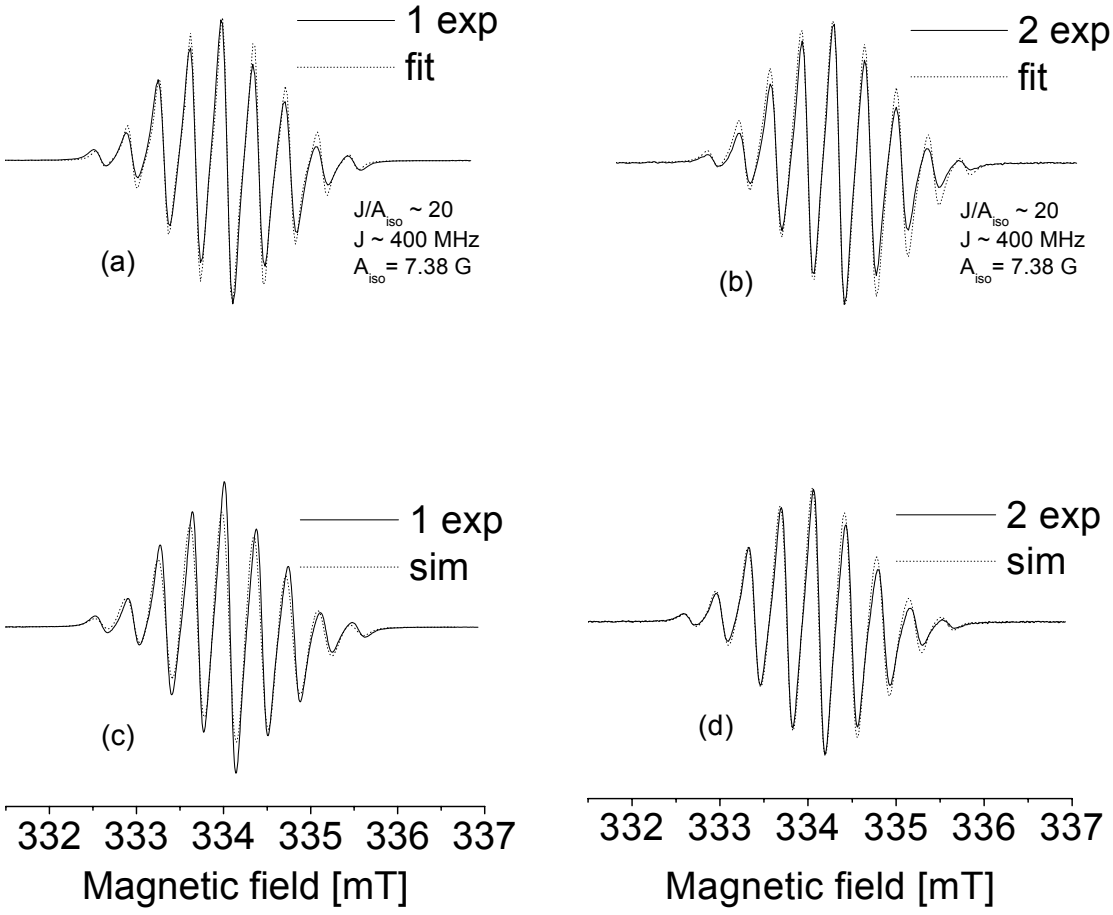

Figure 3.8. *Experimental ESR spectra (Δms = ±1) of **1** and **2** in toluene (c =10^{-3} M) at 240 K (— line). In (a) and (b)…line show the fitting analysis for the estimation of the low limit of J, (c) and (d)…line show the simulated spectra for the estimation of $a_N/2$ values. This is an illustration of the case $J >> a_N$*

fitting the solution state spectra of **1** and **2** using BiRad programme.[12] This further supports that $J >> a_N$ value.

In order to ensure pure anisotropic intramolecular magnetic dipole-dipole interaction, 10^{-4} M toluene solutions were used to observe the fine structures (at 120 K using 0.2 mW microwave power) [Fig. 3.9.]. The zero field splitting parameter or fine structure (D) gives an indication about the dipolar interaction of unpaired electrons in a molecule and is related to the intra radical distance (r) by $1 / r^3$. The

r-value is related to the approximation used by Mukai[13] and co-workers,

$$D = \tfrac{3}{4}\, g^2\, \beta^2 \sum [r^2_{ij} - 3m^2_{ij}]\rho_i\, \rho_j / r^5_{ij} \qquad ...(33)$$

Where r_{ij} is the distance between atoms of i and j , m_{ij} is the distance vector along the axis, which gives rise to the largest dipole-dipole interaction and ρ_i and ρ_j are the spin densities on atoms i and j. Here the value of D not only depends on r but also ρ. In NIT the spin densities are mainly localized on the O-N-C-N-O bonds, besides that for extended π-conjugated system like **1** and **2**, some spins are localized along the conjugated pathways. The experimentally measured D values are the average of all the dipolar interactions among the delocalized spin densities at different atoms.

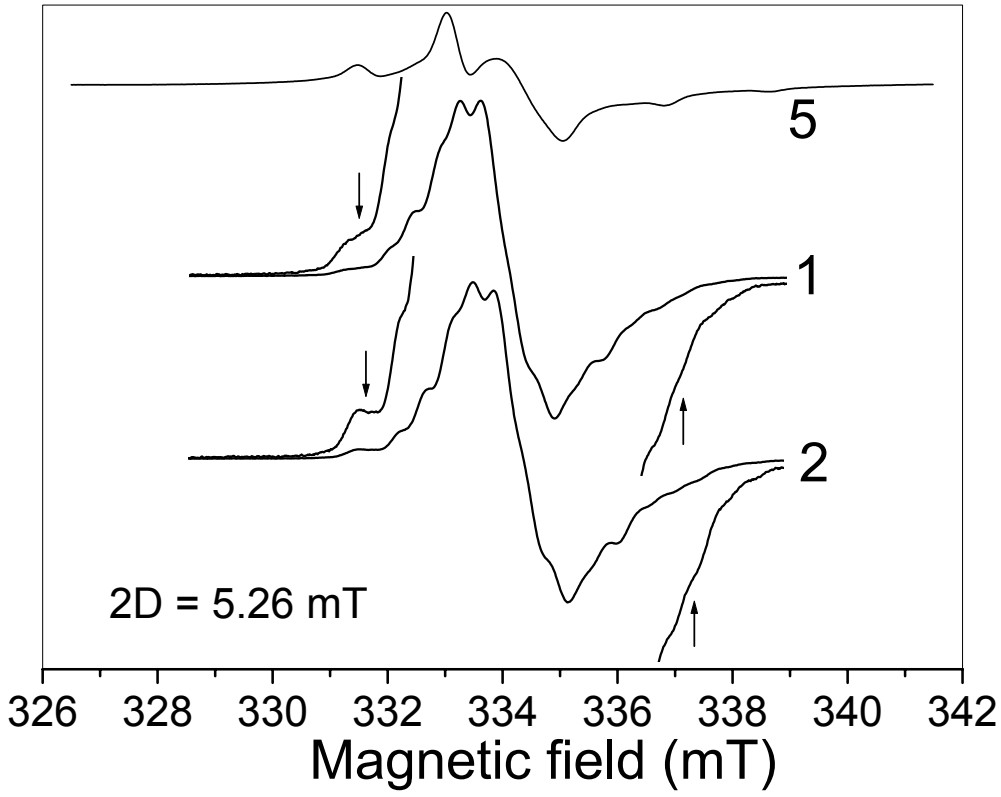

Figure 3.9. *ESR spectra (Δms = ±1) of **1** and **2** in toluene glass (c =10^{-4} M) at 120 K (0.2 mW microwave power) in comparison with monoradical **5** (arrow marks show the enlarged outermost zfs components)*

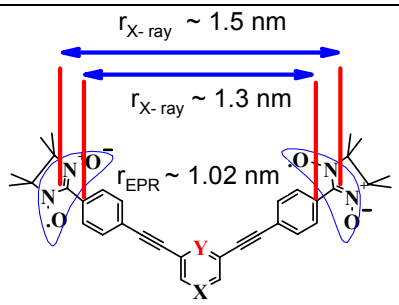

Figure 3.10. *Illustration of the distance measurements by zero field splitting and by X- ray for the biradicals* ***1*** *and* ***2****. [X = N and Y = C for* ***1****; X= C and Y = N for* ***2****]*

Even though the fine structure spectra of **1** and **2** still contained some nitrogen hyperfine interactions, we can be sure that the approximate D values taken from the fine structures are from the biradicals, since the total width of the spectra are different from that of mono radical **5**, where the spectrum is asymmetric. For the biradicals the spectra are nearly symmetric. The measured $\underline{D}$ values for both biradicals are ~ 0.24×10^{-4} cm^{-1} and the average distances derived using the point-dipolar approximation are r ~ 1.02 nm [Fig. 3.9. and 3.10.]. They are much closer than those between the C centers of the radical or the neighboring C centers of the phenyl ring, indicating considerable spin delocalization into the conjugated part [Fig. 3.10.].

To ascertain the intramolecular biradical nature of **1** and **2**, 10^{-3} M concentrations were used to measure (microwave power = 3.9 mW, number of scans = 10, receiver gain = 8×10^5, modulation frequency = 100 kHz, modulation amplitude = 0.4 mT) the forbidden half field transitions ($\Delta ms = \pm 2$) down to liquid helium temperature. The measurements were repeated at different microwave powers in order to ensure that the signals were not saturated. By plotting the observed signal intensities with respect to the square root of the microwave power used a linear behavior was observed. The plot of the doubly integrated signal intensity of the $\Delta ms = \pm 2$ signal versus inverse temperature [Fig. 3.11.] followed a Curie pattern with strong increase in signal intensity down to liquid helium temperature indicating triplet ground state or its near degeneracy with the singlet state. Certainly the exchange coupling J cannot be very large, but a ferromagnetic exchange of $J \sim$ 10-15 K is in line with the results, while an antiferromagnetic exchange could only be as small as $|J| < 2$ K.

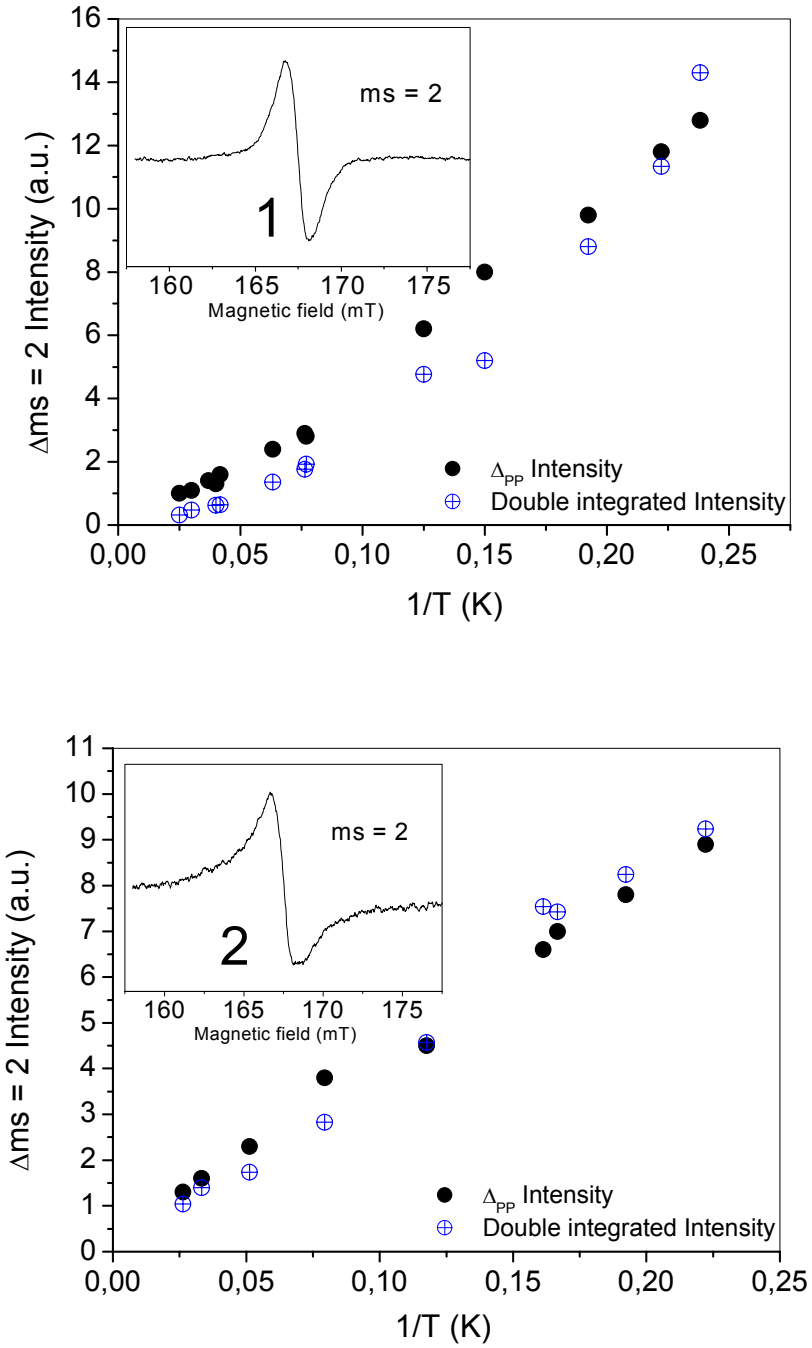

Figure 3.11. *Temperature dependence of ESR forbidden transition signal intensities (Curie plot) of* ***1*** *and* ***2****, inset show the Δms = ±2 transitions at 4 K*

3.6 Molecular structures of 1 and 2 in solid state

Single crystals suitable for X-ray studies were selected and the structures were determined and confirmed with monoclinic crystal system in *C*2/*c* and $P2_1/a$ space groups for **1** and **2** (with toluene molecule), respectively. As shown in the ORTEP diagram [Fig. 3.13.], radical **1** is symmetric and the radical **2** slightly distorted from the planarity. The intramolecular distance between the two radical carbon centers (O-N-**C**-N-O) was measured for **1** and **2**, which are 1.54 and 1.47 nm respectively. Per unit cell four molecules of **1** and three molecules of **2** (with four toluene) were found and the molecules of **1** and **2** are packed in *c* - axis. The torsional angles between the benzene ring and radical plane are 28.41° (C11-C10-C13-N4), and due to the location of toluene molecule close to the radical the plane is distorted by 33.15° (C24-C25-C28-N5) for **2**, and in **1** both arms have 21.03° (C10-C9-C12-N3). The O-N-C-N-O moiety is planar; with nearly equivalent O-N bond lengths of 1.296 Å (O1-N3); 1.286 Å (O2-N4); 1.289 Å (O3-N5); 1.292 Å (O4-N6) for **2** and 1.278 Å (N2-O1); 1.280 Å (N3-O2) for **1**. The bond angles are 125.7(9)° (O2-N3-C12) and 126.2(6)° (O1-N2-C12) for **1** and 127.6(1)° (O1-N3-C13); 124.7(2)° (O2-N4-C13); 123.8(8)° (O3-N5-C28); 125.6(5)° (O4-N6-C28) for **2**. The C≡C lengths are 1.196Å (C5-C4) for **1** and 1.187 Å (C6-C5) and 1.190 Å (C20-C21) for **2**. The torsional angles of **1** were found to be $\Theta_1 = 21°$, $\Theta_2 = 2.4°$, and $\Theta_3 = 5.7°$ [Fig. 3.12.].

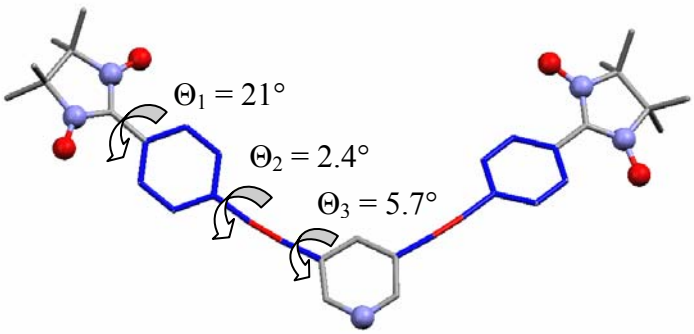

Figure 3.12. *Capped sticks representation of **1** with torsional angles*

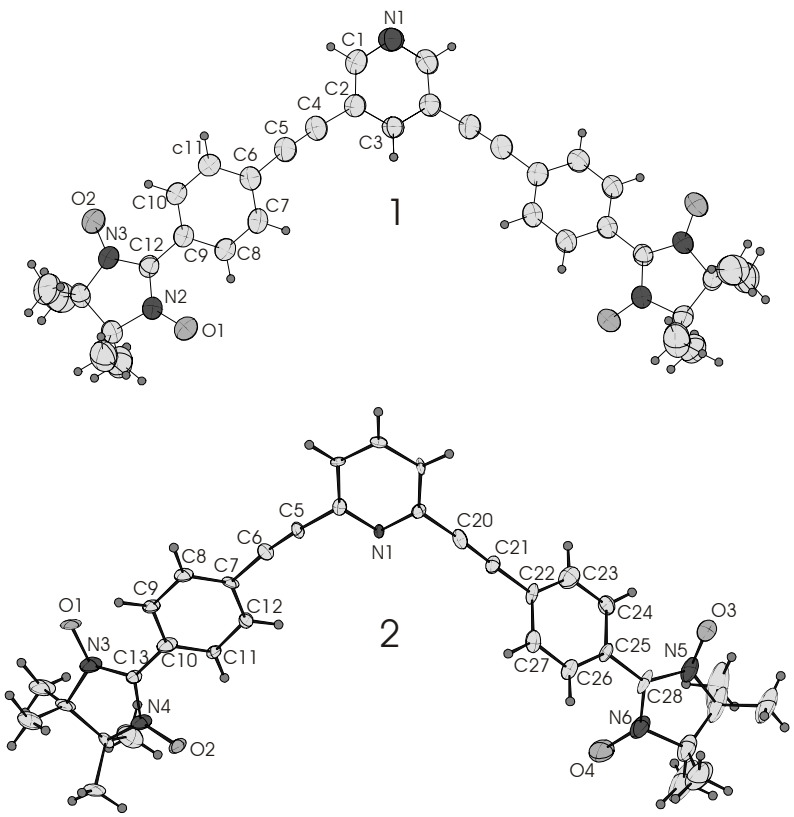

Figure 3.13. *ORTEP diagrams of* ***1*** *and* ***2*** *with thermal ellipsoid plot (50 % probability) with numbering scheme*

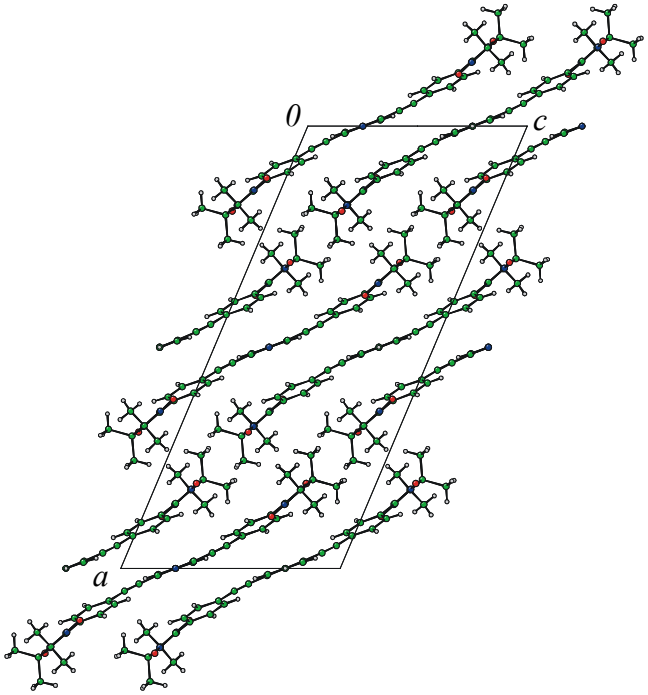

Figure 3.14. *Crystal packing of* ***1*** *along a, b - plane*

3.7 Theoretical calculations

Semi-empirical (AM1) calculations with extended configuration interaction (CI) were performed for the biradicals **1**, **2** and **T** (the analogue of **1** and **2** with three benzene rings in the spacer). The singlet-triplet splitting (ΔE_{ST}) and the spin densities were determined. The influence of structure alternation on the magnitude of ΔE_{ST} was estimated as well.

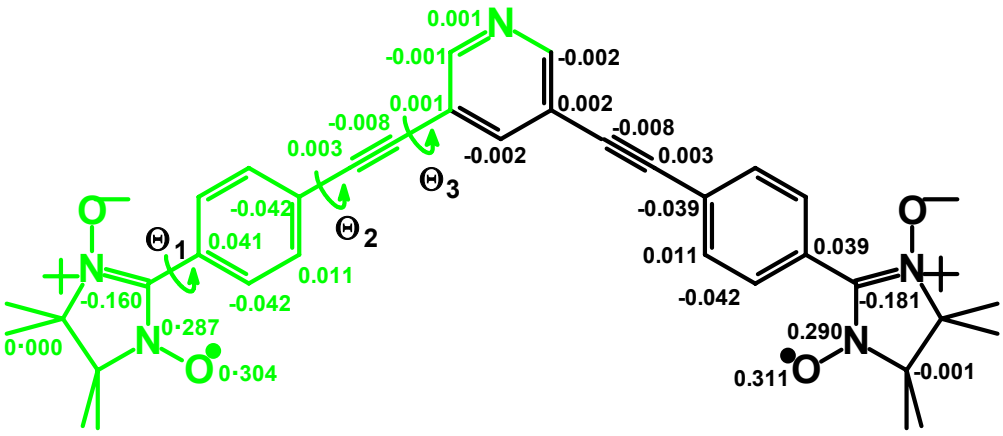

Figure 3.15. *Spin density distribution of biradicals **1** (green) and **T** (black) calculated with ROHF/AM1/CIS (20, 20)*

The geometry of the biradicals was optimized with inclusion of 6 frontier MOs occupied by 6 electrons into the active space of the CI. Two minima of **T** with close energy were detected [see Table 3.2.]: one corresponding to a planar structure [$\Theta_1 = \Theta_2 = \Theta_3 = 0^o$, see Fig. 3.15.] separated by ~2.7 kJ/mol from a molecule with $\Theta_1 = 20^o$, $\Theta_2 = 21^o$ and $\Theta_3 = 3^o$. Substitution of one carbon atom in the central benzene ring with nitrogen led to slightly larger difference between the energies of the planar form [~3 kJ/mol] as compared to the respective twisted conformation. To determine more accurately ΔE_{ST}, single-point energy calculations of the optimized structures with extended CI were made. The correlation included configurations resulting from the mixing of 8 electrons in 8 MOs (or CAS (8, 8)). The effect of the out-of-plane rotation on the magnitude of the singlet - triplet splitting was estimated by

consideration of two intermediate structures, one with $\Theta_1 = 20^o$ and $\Theta_2 = \Theta_3 = 0^o$ and the other with $\Theta_1 = 0^o$, $\Theta_2 = 21^o$ and $\Theta_3 = 3^o$. For comparison X- ray for the dihedral angles of **1** were found with $\Theta_1 = 21^o$, $\Theta_2 = 2.4^o$ and $\Theta_3 = 5.7^o$ [see Fig. 3.12.]. The results for ΔE_{ST} are summarized in Table 3.1. The heat of formation of all molecules is given in Table 3.2.

Table 3.1. *Singlet-triplet splitting (ΔE_{ST}) calculated with ROHF/ AM1 / CAS (8, 8). The values are in kJ/mol.*

Molecule Geometry	**1**	**2**	**T**
$\Theta_1 = \Theta_2 = \Theta_3 = 0^o$	3.6160	2.8524	3.7943
$\Theta_1 = 0^o, \Theta_2 = 21^o, \Theta_3 = 3^o$	3.2638	2.4690	3.1781
$\Theta_1 = 20^o, \Theta_2 = \Theta_3 = 0^o$	4.1582	3.3262	4.5220
$\Theta_1 = 20^o, \Theta_2 = 21^o, \Theta_3 = 3^o$	1.4007	0.9369	1.2700

Table 3.2. *Heats of formation calculated with ROHF/ AM1 / CAS (8, 8). The values are in kJ/mol.*

Molecule Geometry	**1**	**2**	**T**
$\Theta_1 = \Theta_2 = \Theta_3 = 0^o$	1227.611	1262.359	1187.645
$\Theta_1 = 0^o, \Theta_2 = 21^o, \Theta_3 = 3^o$	1252.284	1292.634	1210.456
$\Theta_1 = 20^o, \Theta_2 = \Theta_3 = 0^o$	1232.322	1267.827	1191.888
$\Theta_1 = 20^o, \Theta_2 = 21^o, \Theta_3 = 3^o$	1224.602	1259.351	1184.900

All values in Table 3.1 are positive, which means that all biradicals have triplet ground state, in accordance with the topological predictions. It can be seen that the replacement of the central benzene ring from the pyridine has a moderate effect on the exchange interaction. The 3,5-substituted pyridine is comparable to benzene as

a coupling unit. The 2,6-substituted biradical features slightly smaller singlet - triplet gap but the triplet is still well below the singlet. The variation of the singlet - triplet splitting can be explained in terms of MOs involved in the interaction. A scheme of the frontier MOs of **1** included in the active space is shown in Fig. 3.16. The same MO pattern was preserved in the other two radicals as well.

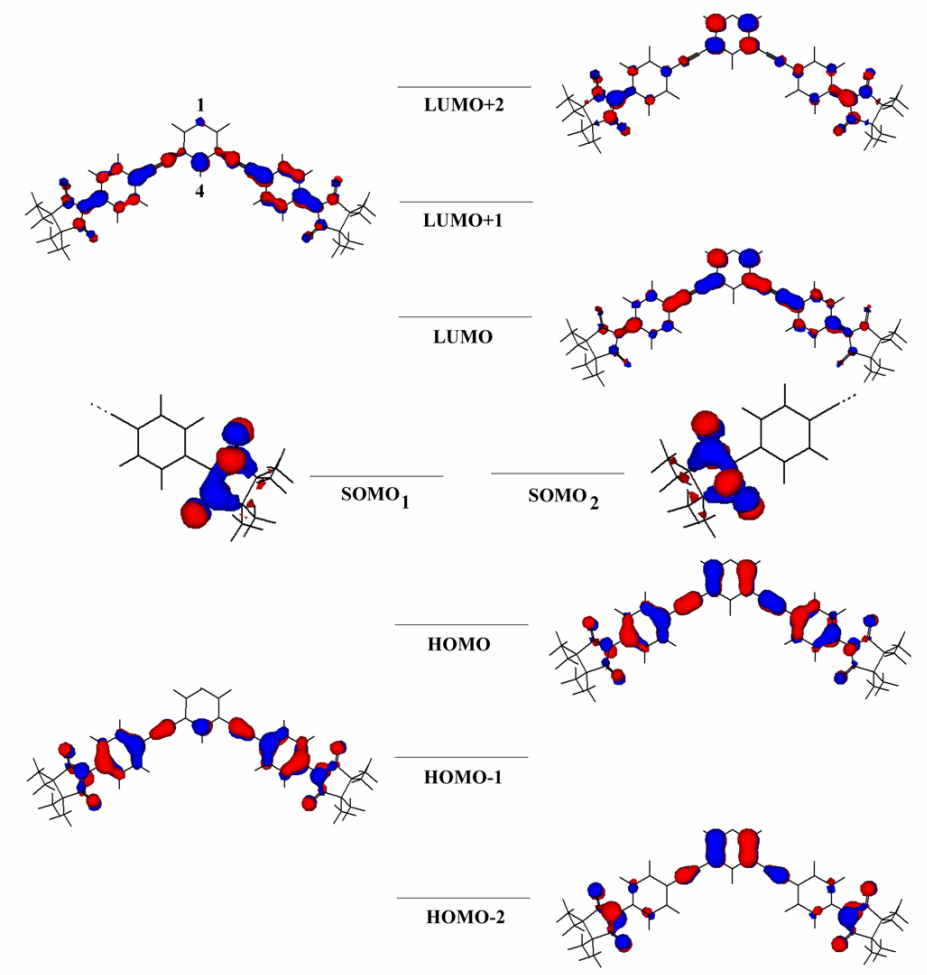

Figure 3.16. *ROHF /AM1 calculated frontier MOs of biradical* ***1****; pictured with contour value of 0.035 and 64 x 64 grid points.*

Substitution of carbon with nitrogen at position 1 or 4 in the central ring of the coupler constitutes the only structural difference between the three biradicals, which should be reflected in the exchange interaction. From all depicted MOs, only two have non-zero coefficients on one of these atomic sites, namely HOMO - 1 and LUMO + 1. Moreover, the value in position 4 is much larger than that in 1. Therefore,

the 3,5-substitution of pyridine in **1** practically does not alter the singlet-triplet separation. On the other hand, the 2,6-pattern in **2** results in MOs with nitrogen contribution. This could be responsible for the slight decrease of ΔE_{ST}. The largest ΔE_{ST} is obtained when the bridging π-system is planar. This is an indication that the high-spin ground state is stabilized by the spin-polarization through the bridge.

Good illustrations of this phenomenon are the calculated spin densities. The values for the structures with largest ΔE_{ST} of **1** (green) and **T** (black) are shown in the [Figure 3.15].

It can be seen that:

- there is sign alternation throughout the molecules, characteristic of the ferromagnetic coupling of the unpaired electrons;
- introduction of nitrogen affects only the energy of the system but does not change the spin density distribution.

Thus, nitrogen can be considered as suitable replacement of carbon in the coupling unit, sustaining the triplet ground state and furthermore offering ligation advantages.

3.8 Conclusions

The two NIT attached to phenylethynyl spacer, which are linked (*meta*-type) at both ends of 3,5- and 2,6-Pyridines by ~1.5 nm distance (X - ray) are strongly intramolecularly exchange coupled (**1** and **2**) with $J >> hfc$. Biradicals **1** and **2** have approximately the same zero field splitting values independent of the position of the pyridyl nitrogen. In both molecules **1** and **2**, the position of the pyridyl nitrogen has no influence on the molecular ground state as evidenced by cryogenic ESR measurements. These experimental findings point toward triplet ground state or its near-degeneracy with a singlet state while the theoretical calculations support the triplet entities. In addition to ESR, the extinction coefficient of the n-π* transition of the UV/Vis spectra in the visible region can also be used to estimate roughly the number of radical units in a molecule. This approach can be used to distinguish a monoradical from a biradical or even a triradical.

3.9 References

1. (a) H. C. Longuet-Higgins, *J. Chem. Phys*. **1950**, 18, 265. (b) H. M. McConnell, *J. Chem. Phys.* **1963**, 39, 1916. (c) A. A. Ovchinnikov, *Theor. Chim. Acta*. **1978**, 47, 297. (d) M. Baumgarten, *Acta. Chem. Scan.* **1997**, 51, 193. (e) W. M. Nau, *Angew. Chem. Int*. *Ed. Engl.* **1997**, 36, 2445.
2. a) T. Ishida, H. Iwamura, *J. Am. Chem. Soc.* **1991**, 113, 4238. (b) F. Kanno, K. Inoue, N. Koga, H. Iwamura, *J. Phy. Chem*. **1997**, 97, 13267. (c) K. Inoue, H. Iwamura, *J. Am. Chem. Soc,* **1994**, 116, 3173. (d) K. Inoue, H. Iwamura, *Adv. Mater*. **1996**, 8, 73. (e) K. Inoue, H. Iwamura, *Angew. Chem. Int*. *Ed. Engl.* **1995**, 34, 927. (f) W. T. Borden, H. Iwamura, J. A. Berson, *Acc. Chem. Res*. **1994**, 27, 109. (g) W. T. Borden, E. R. Davidson, *J. Am. Chem. Soc.* **1977**, 99, 4587 .
3. K. Okada, T. Imakura, M. Oda, M. Baumgarten, *J. Am. Chem. Soc.* **1996**, 118, 3047.
4. a) M. Dvolaitzki, R. Chiarelli, A. Rassat, *Angew. Chem. Int*. *Ed. Engl.* **1992**, 31, 180. b) F. Kanno, K. Inoue, N. Koga, H. Iwamura, *J. Am. Chem. Soc.* **1993**, 115, 847.
5. (a) A. P. Jr. West, S. K. Silverman, D. A. Dougherty, *J. Am. Chem. Soc*. **1996**, 118, 1452. (b) S. V. Chapyshev, R. Walton, J. A. Sanborn, P. M. Lahti, *J. Am. Chem. Soc.* **2000**, 122, 1580. (c) M. Rule, A. R. Matlin, D. E. Seeger, E. F. Hilinski, D. A. Dougherty, J. A. Berson, *Tetrahedron.* **1982**, *38*, 787. (d) Y. Liao, C. Xie, P. M. Lahti, R. T. Weber, J. Jiang, D. P. Barr, *J. Org. Chem.* **1999**, *64* (14), 5176.
6. (a) D. Shiomi, K. Ito, M. Nishizawa, K. Sato, T. Takui, K. Itoh, *Synth Met.* **1999**, 103**,** 2271. (b) J. Y. Bae, M. Yano, K. Sato, D. Shiomi, T. Takui, T. Kinoshita, K. Abe, K. Itoh, D. Hong, *Synth. Met.* **1999**, 103, 2261.(c) P. Turek, P. Wautelet, J. L. Moigne, J. L. Stanger, J. J. Andre, A. Bieber, P. Rey, A. D. Cian, J. Fischer, *Mol. Cryst. Liq. Cryst.* **1995**, 272, 99.
7. (a) P. Wautelet, L. Catala, A. Bieber, P. Turek, J. J. Andre, *Polyhedron*. **2001**, 20, 1571. (b) L. Catala, P. Turek, J. LeMoigne, A. De Cian, N. Kyritsakas, *Tetrahedron Lett*. **2000**, *41*, 1015. (c) S. Murata, H. Iwamura, *J. Am. Chem. Soc.* **1991**, *113*, 5547 (d) P. Wautelet, A. Bieber, P. Turek, J. L. Moigne, J. J. Andre, *Mol. Cryst. Liq. Cryst*. **1997**, 305, 55. (e) L. Catala, J. L. Moigne,

N. Kyritsakas, P. Rey, J. J. Novoa, P. Turek, *Chem. Eur. J.* **2001**, 7. 2466.

8. J. H. Osiecki, E. F. Ullman, *J. Am. Chem. Soc*. **1968,** 90, 1078.
9. a) V. I. Ovacharenko, S.V. Fokin, G.V. Romanenko, I. V. Korobkov, P. Rey, *Russ. Chem. Bull*. **1999**, 48, 1519. b) V. I. Ovacharenko, S.V. Fokin, P. Rey, *Mol. Cryst. Liq. Cryst*. **1999**, 334, 109.
10. a) K. Sonogashira, Y. Tohada, N. Hagihara, *Tetrahedron Lett*. **1975**, 4470. b) S. Thorand, N. Krause, *J. Org. Chem.* **1998**, 63, 8551. c) W. B. Austin, N. Bilow, W. J. Kelleghan, K. S. Y. Lau, *J. Org. Chem.* **1981**, 46, 2280.
11. X. Wang, P. Rabbat, P. O´Shea, R. Tillyer, E. J. J. Grabowski, P. J. Reider, *Tetrahedron Lett*. **2000**, 41, 4335.
12. BiRad- Programme available on request from D. Hinderberger, G. Jeschke (Prof. Spiess group, MPIP – Mainz).
13. a) K. Mukai, T. Tamaki, *Bull. Chem. Soc. Jpn*. **1977**, 50, 1239. b) K. Mukai, J. Sakamoto, *J. Chem. Phys*. **1978**, 68, 1432. c) K. Mukai, N. Inagaki, *Bull. Chem. Soc. Jpn*. **1980**, 53, 2695.

CHAPTER 4

Organic - Inorganic Hybrid Cluster, Supramolecular Chains and Networks

Abstract: *Exploitation of mononitronylnitroxide radicals as a ligands with $Cu(hfac)_2$ and $Mn(hfac)_2$ yielded 1-D extended polymeric magnetic chains and trinuclear copper cluster. The high spin biradical* ***1****, as described in Chapter 3, was successfully complexed with $Cu(hfac)_2$ to form an extended network structure.*

4.1 Backgrounds and design

Many *organic-inorganic* hybrid ferro-, ferri-, and antiferromagnetically ordered materials are reported in the literatures highlighting their importance with magneto-structural correlations to get spontaneous magnetization[1]. The goal to reach a real synthetic magnet is by the formation of highly ordered spin domains[1]. This can be achieved through strongly interacting dimensionalities (1 - 3D), which are very difficult to realize in pure organic magnetic materials owing to their weak non-bonded interactions in solid state. In this vein, organic spin molecules in combination with different spin metals are still a promising approach due to their cooperative interactions in higher dimensional states to yield bulk magnetic properties. One way of achieving this notion is an assembling of organic and inorganic spins in parallel, as chains in solid state, expecting strong intra and inter-chain magnetic interactions. Many successful efforts went into the construction of 1-D chains based on nitronyl-nitroxides (NIT)[2,3] and ^{t}Butyl nitroxides derivatives[4] owing to their ligating abilities with metals with $M(hfac)_2$ [hfac = hexafluroacetylacetonate]. In particular, NIT-**R** (R = H, methyl, ethyl and prophyl) based one-dimensional structures and adducts with different metals are interesting due to their available two coordinating oxygens in a monoradical to form higher dimensions with coordinatively doubly unsaturated paramagnetic metal ions[5]. The influence of the **R** group appended to NIT unit, in controlling the solid-state structures and the resulting magnetic properties are not really explored. Mainly, the extent of the magnetic interaction varies, depending on the relative geometry of the magnetic orbital of the metals to the coordinating radical. Increasing the bulkiness of the **R** group can minimize the extent overlap favoring ferromagnetic coupling. Particularly, when **R** is phenyl, no extended linear structures were observed with Cu and $Mn(hfac)_2$, it forms only adducts and clusters[6]. To extend the structures to 2 or 3 dimensions, phenyl group is useful, since it can be seen as a part of bi- and triradicals to form higher dimensional assemblies with metals. Our approach towards obtaining the higher dimensional motifs is given as cartoon diagram [Scheme.4.1]. Each circle depicts the individual ligand design. The higher motifs and cluster were realized using individual ligand design approach or combination of two designs.

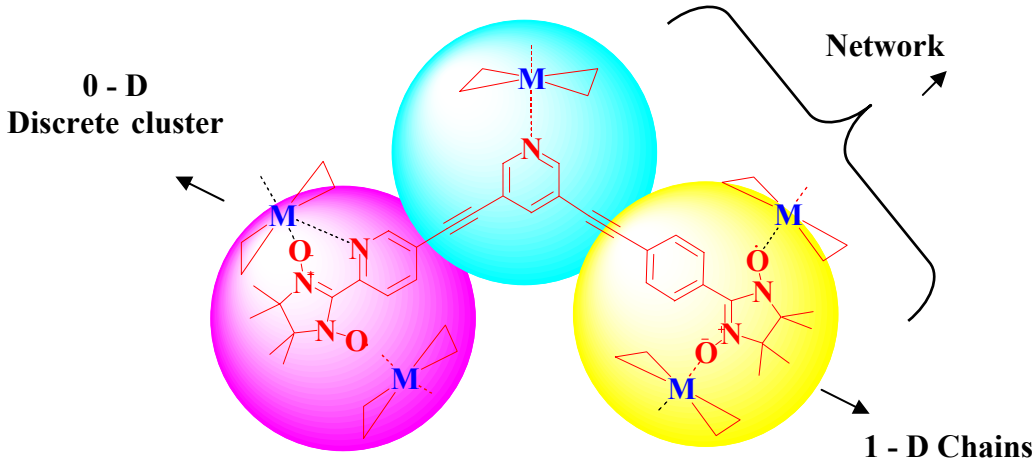

Scheme 4.1. *Cartoon of the ligands design and their different modes of coordination for extended architectures*

4.2 A discrete trinuclear copper cluster

The case in which, two types of coordination are involved in a molecule or cluster, the coordination geometry and the bond distances are very important in order to understand the exchange interactions and to address the magneto-structural correlation. In the literature, few trinuclear copper complexes are reported[7,8] with two different coordination modes with pyroxylimino nitroxides (PIMR) and imino nitroxides (IN) having penta- and hexacoordinated coppers exhibiting ferromagnetic behavior. Attempts to make an extended structures based on $Cu(hfac)_2$ and imino pyridine, yielded dimer in heptane[8]. This mixed coordinating type radical is one of the promising candidates to design bimetallic systems[9,10] due to the existing different binding properties in a ligand. In this regard, we have synthesized the spin ½ ligand **21**, with NIT radical attached ortho to the pyridine nitrogen making three coordination sites [Scheme 4.2]. The pyridyl nitrogen and the NIT oxygen act as a bidentate ligation site on the one side and the remaining NIT oxygen acts as a monodentate ligation site on the other side. The bromine attached to **21** can be further functionalized to extend the structure into two dimensions. In addition, these different binding properties are useful tool to understand magnetic interactions between the organic and inorganic spins. To our best knowledge no reports are available on a

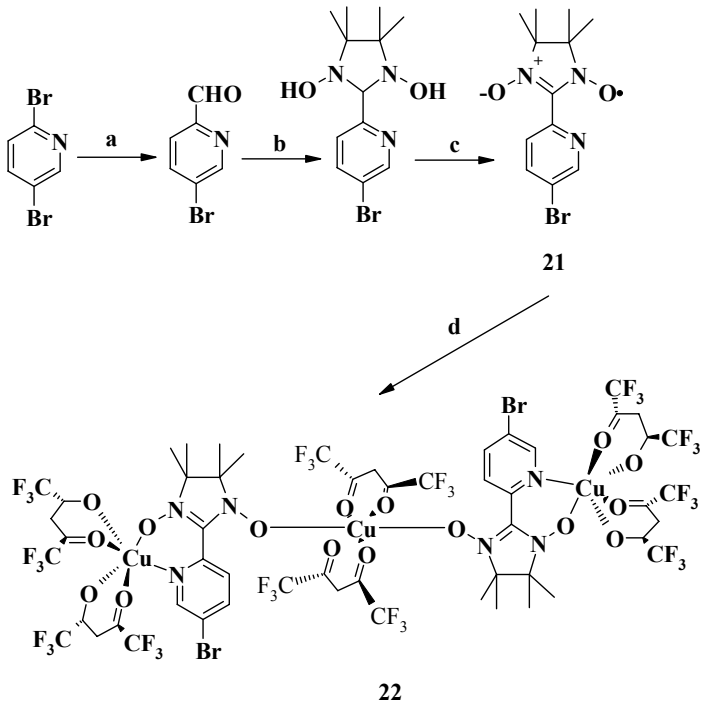

Scheme 4.2. *Synthesis of **21** and **22**. Reagents and Conditions: a) (i) n-BuLi / Toluene / -78°C (ii) DMF b) 2,3-Dimethyl-2,3-bis (hydroyamino)butane / MeOH c) $NaIO_4$ / $CHCl_3$ / H_2O d) $Cu(hfac)_2.x\ H_2O$ / Acetone*

hexacoordinated linear centrosymmetric trinuclear copper(II) complex with different binding modes to two pyridine based NIT radicals (**21**). where the radical oxygen and the pyridine nitrogen bites the $Cu(hfac)_2$ on one side (O-Cu-N) and on the other side, the next oxygen forms monodentate coordination (O-Cu-O).

4.2.1 Synthesis and characterization.

The synthesis of **21** and **22** are schematically represented in Scheme 4.2. The radical **21** was prepared in four steps from 2,5-dibromopyridine. The structure of **21** was confirmed by ESR, UV- Vis, and IR spectroscopy. X- Band ESR studies showed $\Delta Ms = \pm 1$ transition with five lines centered at $g_{iso} = 2.0067$ with $a_N = 7.4$ G characteristic for an organic radical. In the literature attempts made to prepare 2:1 crystalline complex of orthopyridine-NIT with $Cu(hfac)_2$ was unsuccessful in $CHCl_3$[11a]. Our attempts to grow single crystals of complex **22** by the reaction of **21** with $Cu(hfac)_2$ in dichloromethane and hexane were unsuccessful and yielded only

gummy precipitates. Dark green single crystals of the complexes of **22** were successfully obtained in acetone by slow evaporation of solvent from a mixture of **1** and $Cu(hfac)_2$ after 2 days. The structure of **22** was confirmed by X-ray crystallography.

4.2.2 Description of crystal structures

The X-ray studies revealed that, **21** is in the P-42_1c space group with one water molecule [Fig. 4.2.1.] and the complex **22** is centrosymmetric with *P*-1 space group with two typical coordination modes of **21** with $Cu(hfac)_2$ [see Fig. 4.2.2.]. The central copper is surrounded by six oxygen donor sets with tetragonal distortion and the terminal coppers are surrounded by one nitrogen and five oxygen donor sets forming a collinear trinuclear copper complex. The bidentate type coordination of the pyridyl nitrogen (N1) and oxygen (O1) of the nitronylnitroxide to the copper (Cu1) forms two octahedral structures at both end of the molecular complex.

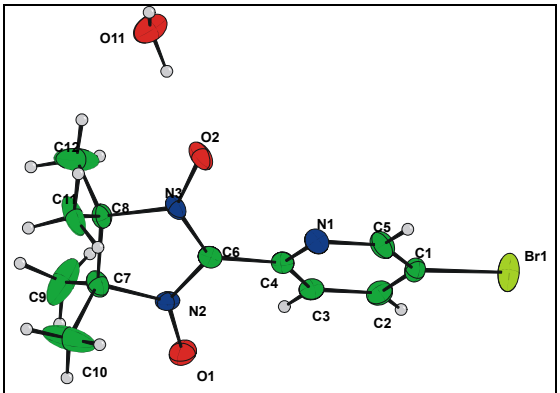

Figure 4.2.1. *ORTEP plot (50%) of* ***21***

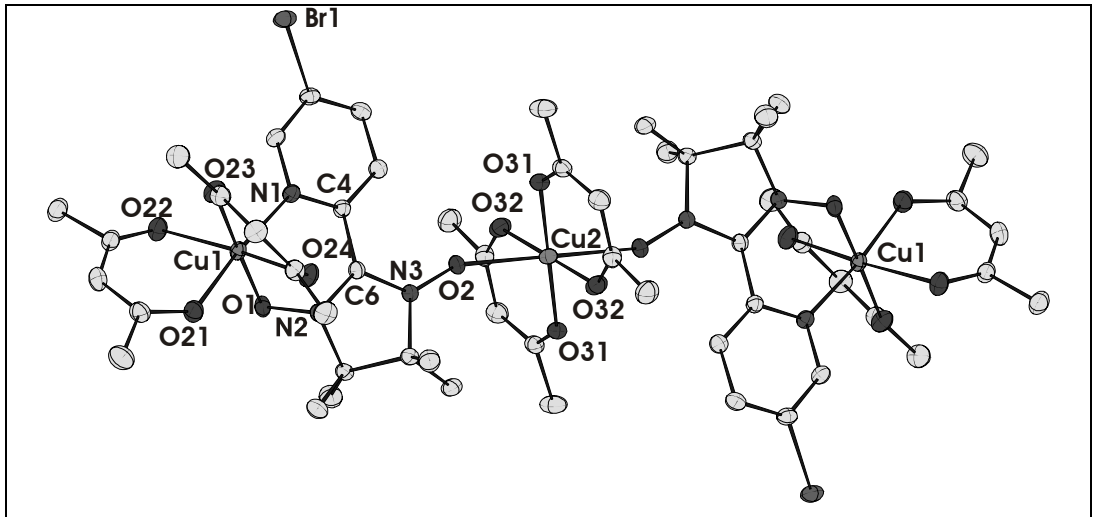

Figure 4.2.2. *ORTEP diagram (50% probability) of the complex* ***22****, hydrogen and fluorine atoms are omitted for clarity*

The Cu(2) occupies at the center of symmetry of the molecule. The two axial bonds (z-axis; O(24)-Cu(1)-O(22) 4.528 Å) formed between the copper and the hfac's oxygens have distances, Cu(1)-O(22): 2.238 Å; Cu(1)-O(24): 2.290 Å. The four equatorial bond distances are Cu(1)-O(1): 1.952 Å; Cu(1)-O(23): 1.958 Å, (O(1)-Cu(1)-O(23) 3.910 Å) and Cu(1)-O(21): 1.957 Å; Cu(1)-N(1): 2.047 Å, (O(21)-Cu(1)-N(1) 4.004 Å), which show that the radical chelating part takes equatorial binding. The comparison of bond distances between the copper (Cu1) with the pyridine nitrogen and the radical oxygen surprisingly shows stronger coordination of the radical oxygen with copper than the nitrogen. The monodentate coordination using the other oxygen of the NIT forms tetragonally distorted octahedral geometry at the center of the complex. Thus all the three coordination sites in **21** were used for coordination with copper. The two axial bonds in Cu(2) [Fig. 4.2.3. right] have Cu(2)-O(2) distance 2.517 Å (z-axis; O(2)-Cu(2)-O(2) 5.034 Å) which is much longer than the O(24)-Cu(1)-O(22) 4.328 Å [Fig. 4.2.3. left] suggesting the axially elongated copper (Cu(2); z-out). The four equatorial bonds forming the x and y-axis with bond distances O(32)-Cu(2)-O(32) 3.906 Å and O(31)-Cu(2)-O(31) 3.86 Å.

The bond angle between the Cu(2)-O(2)-N(3) is 142.85° which is higher than

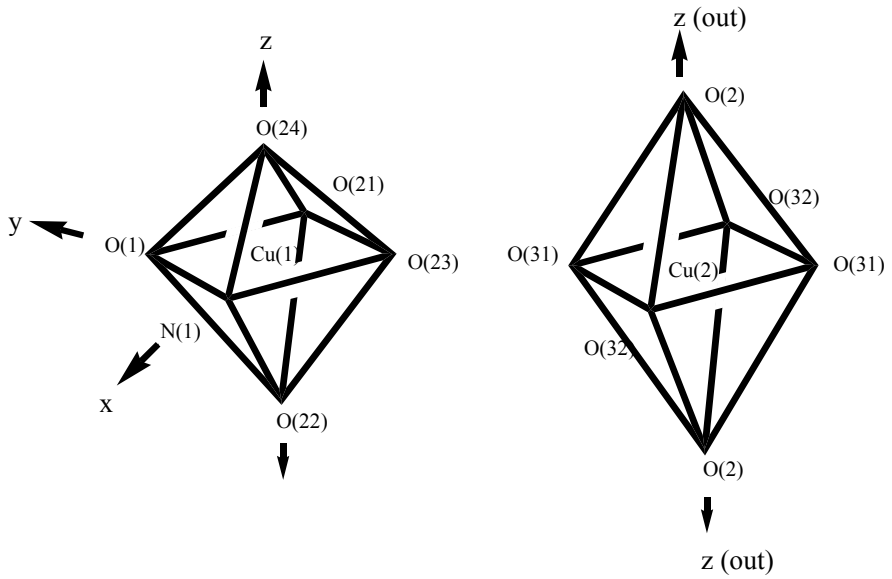

Figure 4.2.3. *Schematic representation of the two types coordination geometries of copper in* ***22***.

Cu(1)-O(1)-N(2) angle 111.25° indicating the significant overlap of N-O(1) π* orbital with Cu(1) *d* orbitals. The N(2)-O(1) and N(3)-O(2) of **22** has bond distances 1.294 Å and 1.272 Å which is different from **21**, 1.272 Å and 1.280 Å respectively due to the different modes of overlapping of the mono radical oxygens with coppers. In **22** the NIT is twisted out of plane of the pyridine with 4.02^{o} and –1.88^{o} differs considerably from the value of **21**, which are -2.64^{o} and -2.60^{o} respectively. The C(4)-C(6)-N(3) and C(4)-C(6)-N(2) bond angles of **22** reduced dramatically to 121.82^{o} and 115.77^{o} from 129.81^{o} and 124.70^{o} upon complexation from **21**. It is interesting to compare the bond distance between the two coppers with NIT oxygens; obviously the chelating type should have shorter bond length than the monodentate type. The Cu(1)-O(1) is 1.952 Å shorter than the Cu(2)-O(2) distance which is 2.517 Å, the

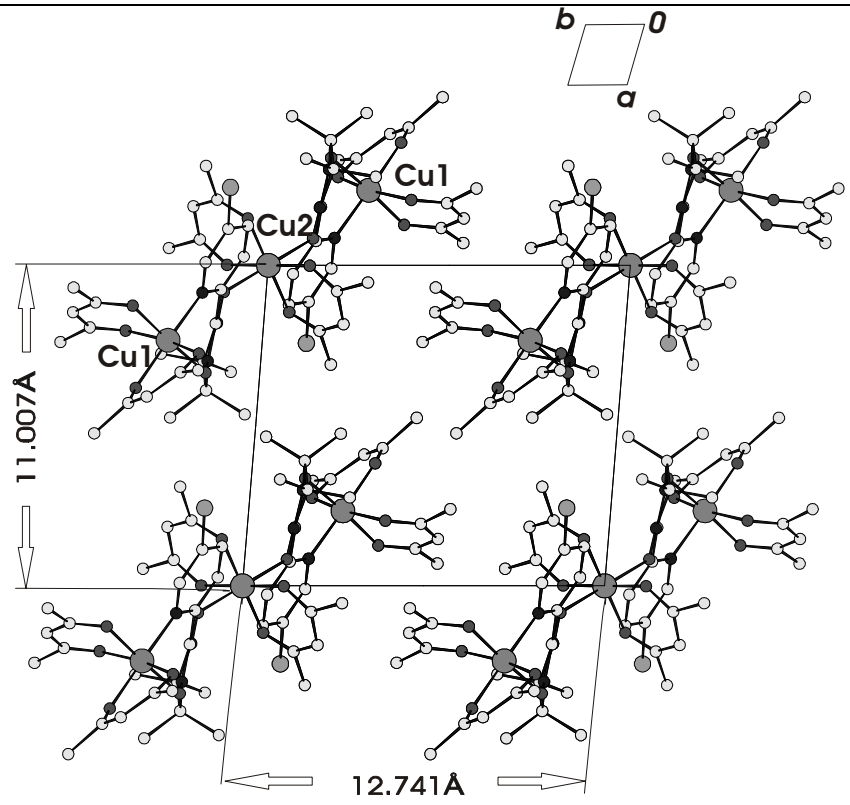

***Figure 4.2.4**. Projection of the unit cell of **22** along a, b axis*

Cu(1)-N(1)distance is 2.047 Å, which is longer than the Cu(1)-O(1) distance. The molecule is running along the *c*- axis of the unit cell, with four molecules per unit cell [Fig. 4.2.4.]. The intramolecular distances between the terminal Cu(1)-Cu(1) is 15.502 Å while for Cu(1)-Cu(2) is 7.751 Å. The shortest intermolecular Cu(2)-Cu(2) distance between the two neighboring molecule is 11.007 Å.

4.2.3 Magnetic properties

[The magnetic fitting analysis which is outlined below was done by Dr. Sergei Ostrovsky (Prof. Haase group).]

Magnetic data of **22** are shown in Fig. 4.2.5. as $\mu_{eff\ [\mu B]}$ versus T [K]. As the temperature decreases from 300 – 4.2 K, the μ_{eff} value decreases sharply from 2.63 μ_B to 1.86 μ_B. The room temperature value 2.63 μ_B is in between the S = ½ and S = 1 spin system suggesting a weak ferromagnetic interaction. Complex **22** can be regarded as a linear system with five spins S_i = ½ (i = 1, 2,...5) coupled by isotropic exchange interaction between nearest neighbors. From the structural point of view the existence of two different exchange coupling parameters J_1 and J_2 can be assumed.

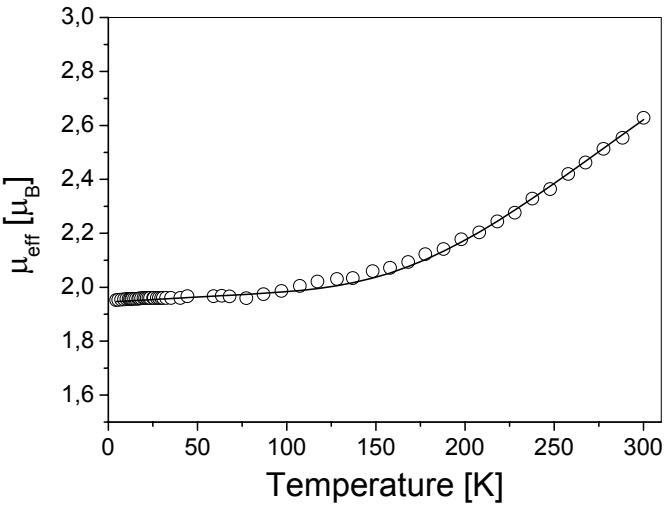

Figure 4.2.5. *Temperature dependence of the effective magnetic moment μ_{eff} [BM] of complex **22** (open circles represent the experimental values, solid curve is the best fit obtained with J_1 = -440 cm^{-1}, J_2 = 10 cm^{-1}, g = 2.25)*

The former describes the exchange process between the terminal Cu(1) ion and the neighboring radical while the latter is for the interaction between the central Cu(2) ion and the neighboring radicals. In the framework of the Heisenberg-Dirac-Van Vleck model the corresponding Hamiltonian describing the spin system of **22** can be written as follow:

$$H_{ex} = -2J_1\vec{S}_1\vec{S}_2 - 2J_2\vec{S}_2\vec{S}_3 - 2J_2\vec{S}_3\vec{S}_4 - 2J_1\vec{S}_4\vec{S}_5 \quad \ldots (37)$$

Thus the following successive spin-coupling scheme can be derived:

$$S_1 + S_2 = \widetilde{S}_2, \widetilde{S}_2 + S_3 = \widetilde{S}_3 \ldots \widetilde{S}_4 + S_5 = \widetilde{S}_5 \equiv S \qquad \ldots(38)$$

In the spin coupling Scheme 38 the terms $\widetilde{S}_2 = S_{12}, \widetilde{S}_3 = S_{12} + S_3 = S_{123} \ldots$ are intermediate spins (S_{12} could be $S_1 + S_2$, $S_1 + S_2 - 1$, … $| S_1 - S_2 |$; $S_{123} = S_{12} + S_3$, $S_{12} + S_3 - 1$, … $| S_{12} - S_3 |$ etc.), and $\widetilde{S}_5 \equiv S$ is the full spin of the system. The spin wave functions of the system are characterized by the full set of intermediate spins $\widetilde{S}_2 \widetilde{S}_3 \widetilde{S}_4$ (abbreviated as $(\widetilde{S})$), times the total spin of the system S and magnetic quantum number M:

$$\left| S_1 S_2 (\widetilde{S}_2) S_3 (\widetilde{S}_3) S_4 (\widetilde{S}_4) S_5 SM \right\rangle = \left| \widetilde{S}_2 \widetilde{S}_3 \widetilde{S}_4 SM \right\rangle \equiv \left| (\widetilde{S}) SM \right\rangle \qquad \ldots(39)$$

The matrix elements of Hamiltonian in eqn. 37 on the basis of eqn. 39 can be calculated by using the irreducible tensor operator technique, where each spin operator in (37) can be substituted by first-rank irreducible tensor $\hat{S}_q^{(1)}$ (where q is the component):

$$\hat{S}_{\pm 1}^{(1)} = \mp \frac{1}{\sqrt{2}} \left(S_x \pm i S_y \right), \; \hat{S}_0^{(1)} = S_z . \qquad \ldots(40)$$

The following relationship between the scalar product of spins and irreducible tensor product of zero-the rank holds as given in the eqn. (41):

$$\vec{S}_i \vec{S}_j = -\sqrt{3} \left\{ \hat{S}^{(1)}(i) \otimes \hat{S}^{(1)}(j) \right\}_0^{(0)} \qquad \ldots(41)$$

where $\otimes$ is the sign of the irreducible tensor product. Upon introducing a complex irreducible tensor operator $\hat{T}_0^{(0)}$ of the zero-th rank composed from the one-ion operators $\hat{S}_{q_i}^{(k_i)}(i)$ in the following way:

$$\hat{T}_0^{(0)} = \{\{\{\{ \hat{S}^{(k_1)} \otimes \hat{S}^{(k_2)} \}^{(\tilde{k}_2)} \otimes \hat{S}^{(k_3)} \}^{(\tilde{k}_3)} \otimes \hat{S}^{(k_4)} \}^{(\tilde{k}_4)} \otimes \hat{S}^{(k_5)} \}_0^{(0)} \qquad \ldots(42)$$

The irreducible tensor $\hat{T}_0^{(0)}$ operates in the spin space of the wave functions 39. In eqn.41 the coupling scheme for the tensor operators is the same as that adopted for the spin coupling in 37. The Hamiltonian in eqn. 37 can be then rewritten in terms of irreducible tensors $\hat{T}_0^{(0)}$ with different sets of (k) and ($\tilde{k}$). For example, the part

corresponding to the exchange interaction between centers Cu(1) and neighboring radical substitution can be made in $\hat{T}_0^{(0)}$ [Eqn. (41)] leading to $k_1=1$, $k_2=1$, $k_3=k_4=k_5=0$, all $\tilde{k}_i=0$; while for the exchange between Cu(2) and neighboring radical: $k_1=0$, $k_2=1$, $k_3=1$, $k_4=k_5=0$, $\tilde{k}_2=1$, all other $\tilde{k}_i=0$ etc.

The matrix elements of tensor operator 40 in the spin coupled representation 39 can be calculated using the Wigner-Eckart theorem and than the decoupling procedure for the irreducible tensors. The final term of the equation is as following:

$$\left\langle (\tilde{S}')S'\,M' \right| H_{ex} \left| (\tilde{S})S\,M \right\rangle = \delta_{SS'}\,\delta_{MM'} \frac{\sqrt{3}}{\sqrt{2S+1}} \sum_{k,\tilde{k}} J(k,\tilde{k}) \left\langle S_1 \left\| S^{(k_1)}(1) \right\| S_1 \right\rangle$$
$$\times \prod_{m=1}^{4} \sqrt{(2\tilde{S}'_{m+1}+1)(2\tilde{S}_{m+1}+1)(2\tilde{k}_{m+1}+1)} \left\langle S_{m+1} \left\| S^{(k_{m+1})}(m+1) \right\| S_{m+1} \right\rangle \begin{Bmatrix} \tilde{k}_m & k_{m+1} & \tilde{k}_{m+1} \\ \tilde{S}'_m & S_{m+1} & \tilde{S}'_{m+1} \\ \tilde{S}_m & S_{m+1} & \tilde{S}_{m+1} \end{Bmatrix} \qquad ...(43)$$

where $\begin{Bmatrix} \cdot & \cdot & \cdot \\ \cdot & \cdot & \cdot \\ \cdot & \cdot & \cdot \end{Bmatrix}$ is the 9j symbol and $J(k,\tilde{k})$ represents J_1 or J_2 depending on the set of k and $\tilde{k}$. The reduced matrix elements of $S^{(k)}$ are:

$$\left\langle S \left\| \hat{S}^{(0)} \right\| S \right\rangle = \sqrt{(2S+1)}$$
$$\left\langle S \left\| \hat{S}^{(1)} \right\| S \right\rangle = \sqrt{S(S+1)(2S+1)} \qquad ... (44)$$

From eqn. 44 the matrix of isotropic exchange interaction is diagonal with respect to the total spin of the system and the magnetic quantum number M, thus the states of the system (can be obtained as a result of matrix diagonalization) are characterized by the total spin value S and are independent of M. In this case the temperature dependent magnetic susceptibility of the compound can be obtained by using the well-known van Vleck equation:

$$\chi(T) = \frac{N_A g^2 \mu_B^2}{3kT} \cdot \frac{\sum_{S\nu} S\,(S+1)\,(2S+1)\ \exp\left(-E(\nu S)/kT\right)}{\sum_{S\nu} (2S+1)\ \exp\left(-E(\nu S)/kT\right)} \qquad ...(45)$$

where $E(\nu S)$ are the eigen-values of 37 in the basis 39 (ν enumerates different energy values for the same total spin).

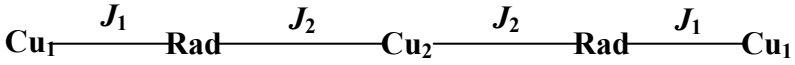

The experimental magnetic properties as well as the theoretical fit of complex **22** are presented in Fig. 4.2.4. The best-fit parameters are part of Figure caption. The magnetic behavior of the investigated complex is determined by the strong antiferromagnetic exchange interaction between the terminal Cu(1) ions and neighboring radicals with J_1 = -440 cm^{-1}. As a result the ground state and low-lying group of levels possess spin S = ½. The excited states with other larger values of total spin are high in energy and their effect on the magnetic properties of the system appears only at temperatures higher than 150 K. It should be mentioned that J_2 parameter cannot be determined exactly from the magnetic behavior of the compound. The same quality fit can be obtained for both small positive and small negative J_2 values as well as for J_2 = 0. The complex with the similar structure demonstrates small ferromagnetic exchange interaction (about 12 cm^{-1})[7]. Thus it is expected that the exchange interaction between the central Cu ion and neighboring radicals is ferromagnetic with J_2 = 10 cm^{-1}.

4.2.4 ESR and UV-Vis studies

The X- band ESR solution spectra of **22** measured in chloroform (c ~ 1 × 10^{-3}) from 288-120 K are shown in Fig. 4.2.6. At 288 K the spectrum of **22** shows an isotropic four line pattern, which is expected for Cu^{2+} (S = ½; I = 3/2) in solution with some dissociated radicals. A close look at the spectrum of **22** in comparison to $Cu(hfac)_2$ spectrum shows profound alteration of copper lines with narrow line pattern. The comparison of the *hfc* of the metal part and the radical part of the complex can give information about the operating exchange interaction between the radical and copper[11b] [Fig. 4.2.7]. It is generally assumed that the dipolar contribution averages to zero in solution due to rapid molecular tumbling[12]. The calculated isotropic g value is close to free copper, but with smaller *hfc* value of 49 G, which is lower than for the free $Cu(hfac)_2$ value 72 G. This can be accounted for the existing exchange interactions of the copper and the radical spins. A careful comparison of the simulated *hfc* value of the radical region of the complex **22** and monoradical **21** shows the

Figure 4.2.6. *ESR spectra of* ***22*** *at various temperature [288 – 120 K]*

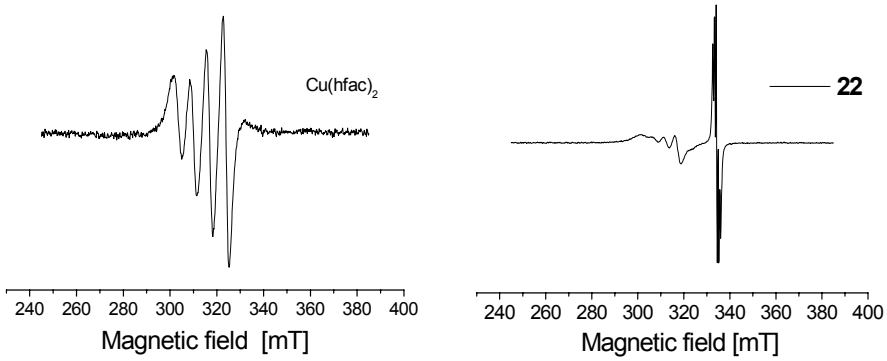

Figure 4.2.7. *X- band ESR solution spectra of $Cu(hfac)_2$ [left] and* ***22*** *at room temperature [right]*

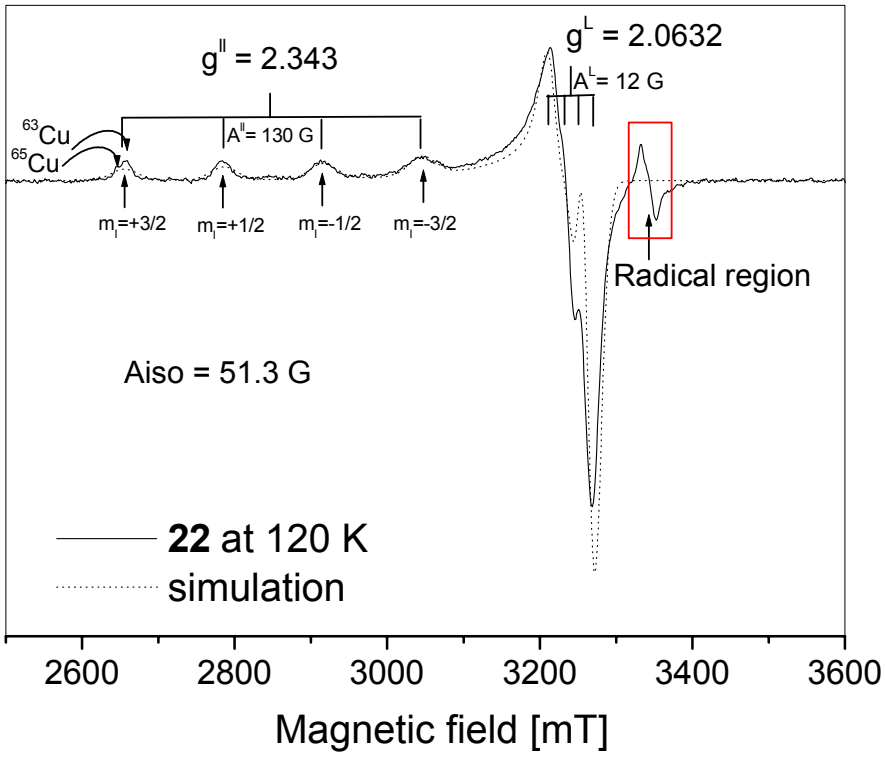

Figure 4.2.8. *Frozen ESR spectra of* ***22*** *in $CHCl_3$ (—— expt. and ....sim)*

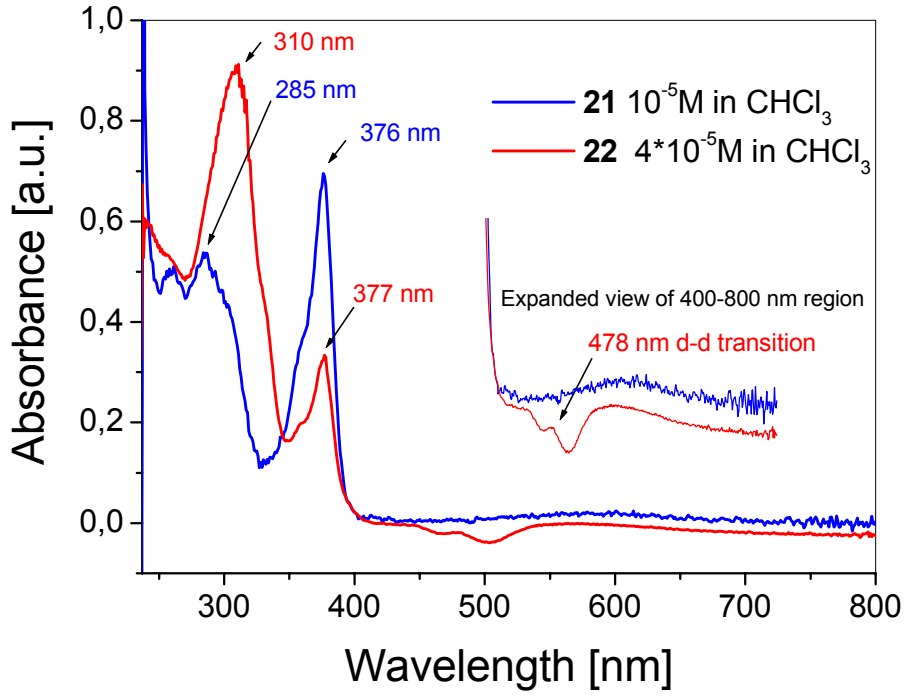

Figure 4.2.9. *UV-Vis spectra of* ***21*** *and* ***22*** *in* $CHCl_3$

same a_N value 7.4 G. UV/Vis study of the same solution shows new *d - d* transition at 478 nm, which is in accordance with the previous reports but with blue shift [Fig. 4.2.9.]. The π- π * transition of **21** at 285 nm is masked by the 310 nm band from $Cu(hfac)_2$ ruling out the possibility to see the shift of 285 nm band upon complexation. The observed *hfc* of copper shows that coppers are bound to the radicals in solution, most probably at the chelation site. ESR measurements at 288-120 K show, decreasing the temperature to 120 K, afford decrease in intensity of the radical part and increase in intensity of the copper part. This may be due to the difference in relaxation of copper and radical, or may be due to the increase in complexation at low temperature [Fig. 4.2.6.]. At 120 K a clear axial anisotropic spectrum was observed, which was simulated with $g^{\parallel} = 2.3430$ and $g^{\perp} = 2.0632$ with $g_{iso} = 2.156$. The simulated hyperfine parameters are $A^{\parallel}$ =130 G and $A^{\perp}$ = 12 G with A_{iso} = 51.3 G [Fig. 4.2.8.]. The general look at these copper spin Hamiltonian parameters indicates that, the g values are very close, where as A values differs in comparison with $Cu(hfac)_2$, attributing the interaction of copper with the radical in solution.

4.3 1- D Coordination polymers

The potential utility of 4-Trimethylsilylethynyl-1-(1-oxyl-3-oxo-4,4,5,5-tetramethylimidazoline-2-yl)benzene **4** as μ-1,5 bridging ligand in development of metal-radical hybrid magnets was exploited to make 1-D metal-radical alternating chain structures. The phenylacetylenic linker connected to monoNIT radical in **4**, act as a ferromagnetic coupler, if properly connected, according to topology to make bi or triradcals as explained in the Chapter 3. The protected acetylenic derivative carrying mononitronylnitroxide radical **4** [Scheme.4.3.] can be deprotected for further functionalization to act as candidate for extended architectures with metals, which will be discussed in section 4.4 of this chapter. To make an extended network of **23**, it it's vital to examine the complexation ability of **4** with different metals. Since as mentioned earlier no are reports available on a phenyl derivative carrying NIT

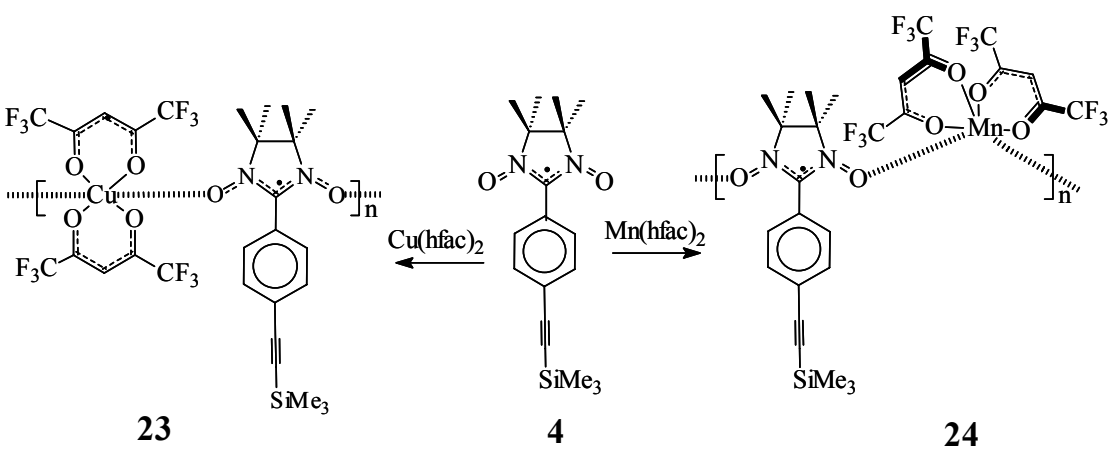

Scheme 4.3. *Reaction of **4** with M(hfac)$_2$ to form **23** and **24***

moiety, forming extended motifs with Cu(hfac)$_2$. In order to make an alternating linear chains of metals and mono radicals carrying protected phenylacetylenic linker, complexation behavior of **4** with Cu(hfac)$_2$ and Mn(hfac)$_2$ were studied as given in Scheme.4.3 and one dimensional extended chains were obtained with both metals.

4.3.1 Synthesis

The synthesis of **23** and **24** is given in Scheme 4.3. Monoradical **4** with Cu(hfac)$_2$ were taken in a mixed solvents of hexane: dichloromethane (20 mL: 5 mL). The formed brown solution was left at room temperature for crystallization. After a day,

the bluish green **23** plates were separated from the uncomplexed $Cu(hfac)_2$ plates. The same procedure was followed to obtain **24**, by mixing **4** with $Mn(hfac)_2$ in 5 mL each of acetone: heptane mixture. The solution was left at room temperature for 3 days for crystallization to get black needles of **24**.

4.3.2 Description of crystal structures.

In compound **23** [**4:**$Cu(hfac)_2$], **4** form 1-D linear polymeric chains upon coordination with $Cu(hfac)_2$, utilizing the two NIT oxygens, in $P2_1/n$ space group. The crystal structure [Fig. 4.3.1.] of the **4**: $Cu(hfac)_2$ shows that, the coppers are in the distorted octahedral environment. Each copper is bound to two hfac ligands and the two oxygens of the NIT are in the axial position forming a distorted octahedron. The four NIT methyl groups connected to C(10) and C(11) are in staggered conformation to minimize the repulsion energy due to the bulkiness of the methyl group. The five-member imidazole ring is slightly twisted from the planarity, locating the N(1) slightly away from the benzene and imidazole planes. The two NIT have different

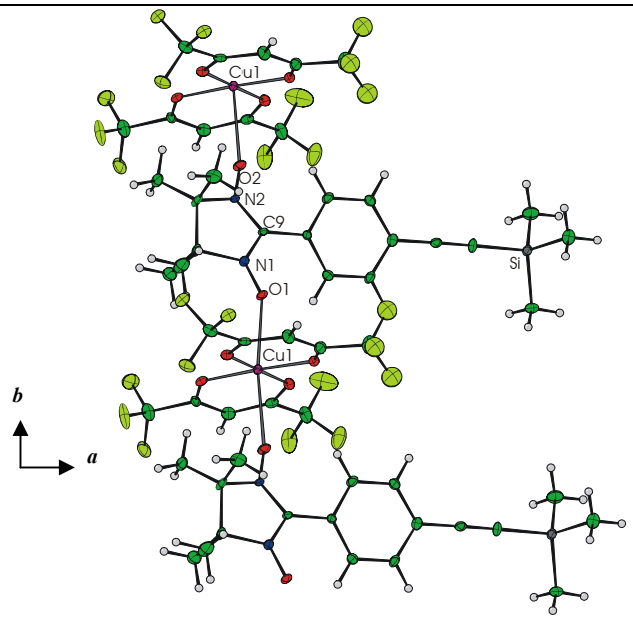

23

Figure 4.3.1. *Crystal structures of* ***23***

bond lengths to copper, Cu(1)-O(1) bond distance is longer than the Cu(1)-O(2) distance by 0.079 Å. The two-hfac groups are in plane taking the equatorial

coordination to the distorted copper. The bond angles of Cu(1)-O(1)-N(1) and Cu(1)-O(2)-N(2) are 148.02° and 150.72° longer than in $Cu(hfac)_2(NITPh)_2$ adducts, which are 135.7 and 132.8° [6]. This shows that the π^* orbital of the radical oxygen and nitrogen are nearly orthogonal to the magnetic orbital of the copper. This is one of the prime requirements for ferromagnetic interactions. The intrachain distance between Cu(1)-**4**-Cu(1) is 9.333 Å. Per unit cell four chains are running along the *b* -axis. [Fig. 4.3.2. and 4.3.3.].

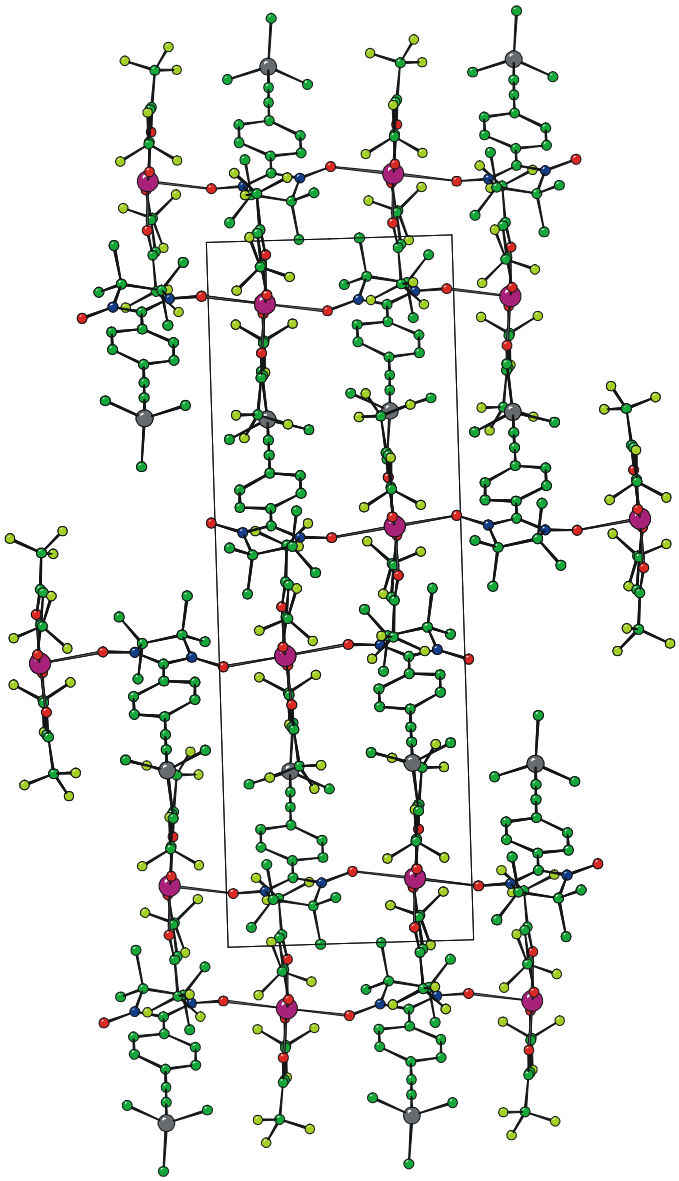

Figure 4.3.2. *Unit cell structure of* ***23***

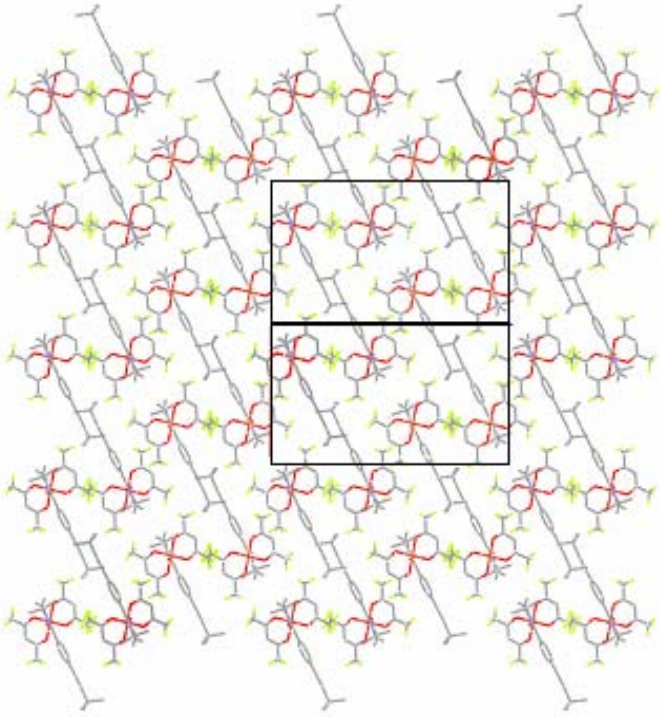

Figure 4.3.3. *Packing of* ***23*** *along the crystallographic chain axis [b - axis]*

In compound **24** [**4:**Mn (hfac)$_2$], the NIT is *cis*-coordinated to the Mn(hfac)$_2$ with O(1)-Mn(1)-O(2) bond angle 84.2° [Fig. 4.3.4.]. Each manganese ion is surrounded by two hfac´s taking distorted octahedron geometry with two axial Mn-O bond with distances, Mn(1)-O(1) 2.110 Å and Mn(1)-O(2) 2.124 Å. In comparison with **23**, the bond distances are shorter [**4**:Cu (hfac)$_2$] due to the stronger overlap of the radical oxygens with Mn ion. The overlap angles between Mn(1)-O(1)-N(1) and Mn(1)-O(2)-N(2) are 123.20° and 126.84° respectively. These angles are, in comparison to its copper analog are much shorter. The shortest intra and interchain distances between two Mn(II) ions are 7.483 Å and 10.68 Å respectively. The chains are running along the crystallographic *a*- axis with two chains per unit cell. The packing of **24** along the crystallographic *a* and *c*-axis are given in Fig. 4.3.5. and 4.3.6.

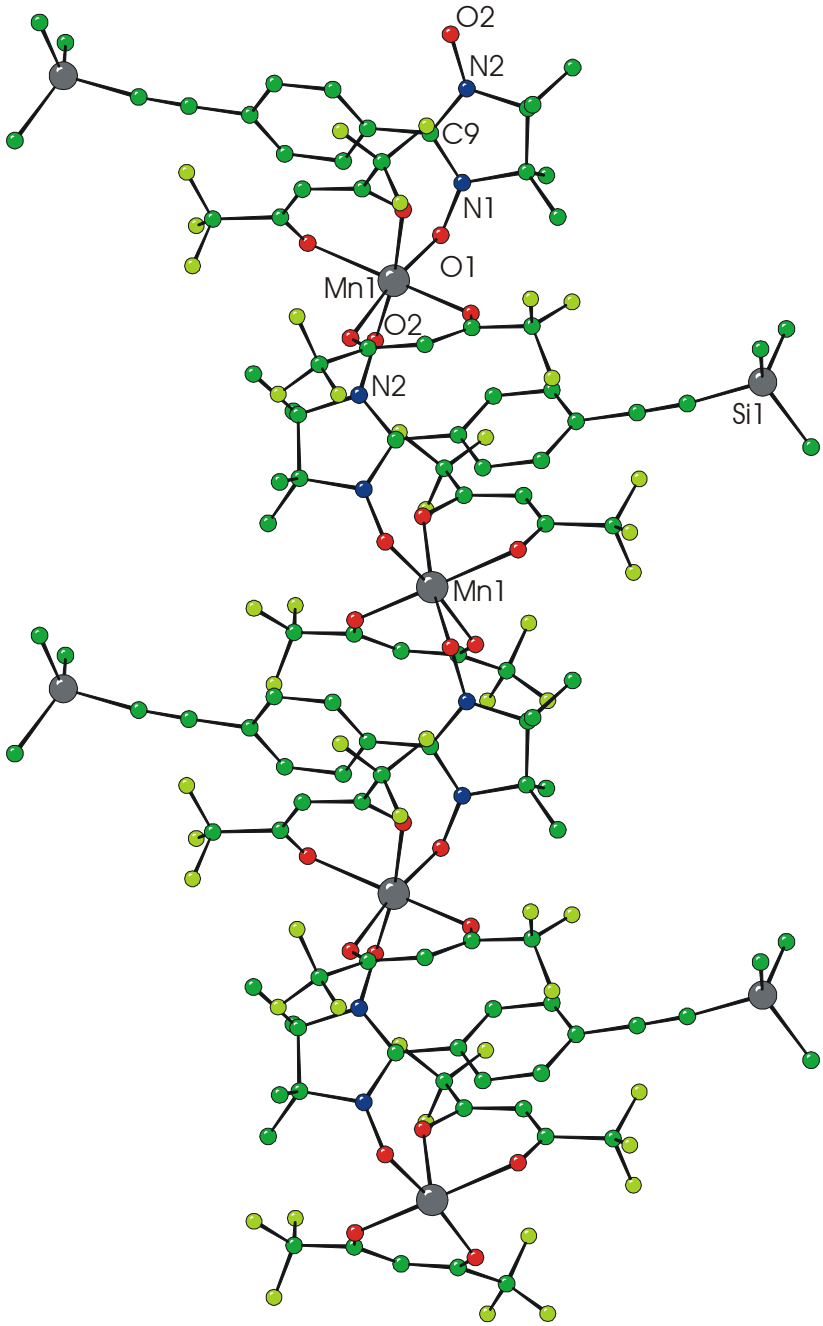

Figure 4.3.4. *ORTEP plot (50%) of a portion of a zig-zag single chain of* ***24*** *(hydrogen atoms are omitted for clarity)*

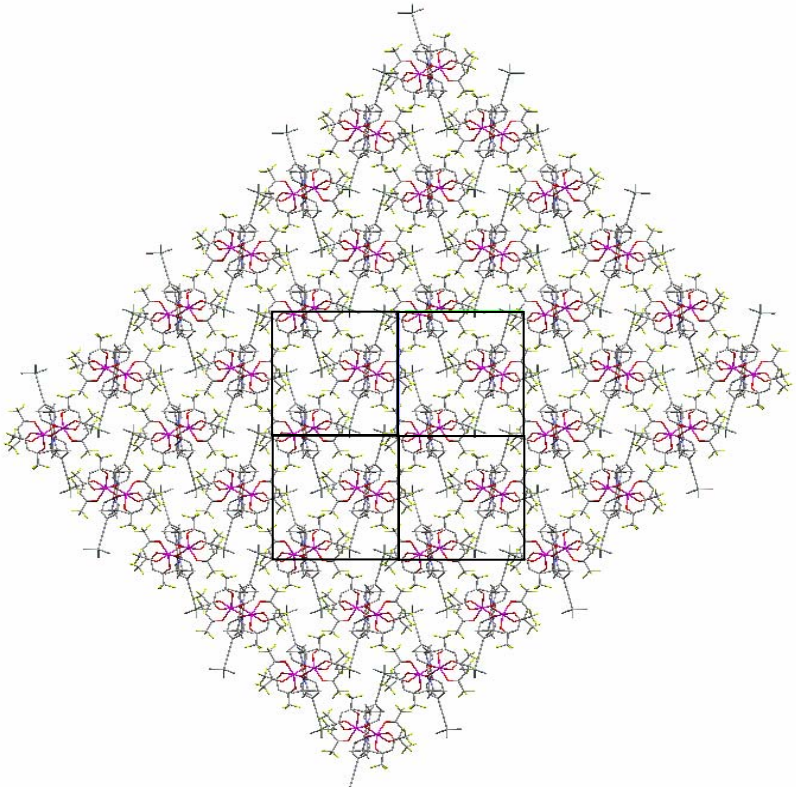

Figure 4.3.5. *Packing of* ***24*** *along the crystallographic chain axis [a- axis]*

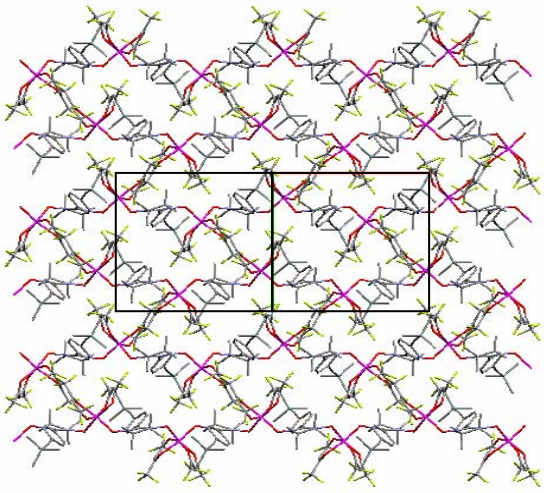

Figure 4.3.6. *Packing of* ***24*** *along the crystallographic c- axis*

4.3.2 Infrared studies:

A comparative Infrared analysis of **23** and **24** with **4** was made [Fig. 4.3.7.]. The hfac carbonyl stretching frequency of **23** and **24,** in comparison with the corresponding Metal(hfac)$_2$ show higher frequency band at 1653 cm^{-1} (+Δν 8 cm^{-1}) for **23**, and show two close carbonyl bands at higher frequencies at 1645 (+Δν 4 cm^{-1}) and 1652 (+Δν 11 cm^{-1}) for **24** demonstrating the existence of two types of carbonyl groups in the complex. Interestingly, the C≡C stretching band of **L** at 2158 cm^{-1} also shifted to higher wave number side by 10 cm^{-1} for **23** and 12 cm^{-1} for **24,** due to mechanical vibration coupling.

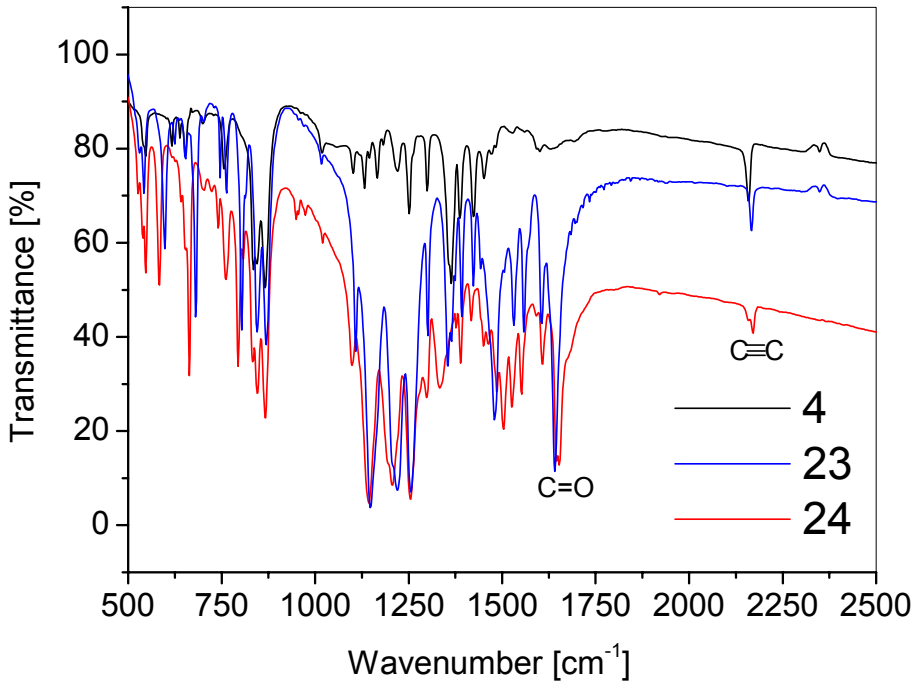

Figure 4.3.7. *FTIR spectra of* ***4****,* ***23*** *and* ***24***

4.3.3 ESR and magnetic studies:

Preliminary ESR investigation of the randomly oriented single crystals of **23** gave single broad line, the intensity of the signal increases linearly down to liquid helium temperature exhibiting the ferromagnetic interaction [Fig. 4.3.8.]. According to the ESR measurements the average g-value is 2.03. The X-band ESR studies of the randomly oriented single crystals of **24** at room temperature show a broad single line with a sharp radical line at the center [Fig. 4.3.9.].

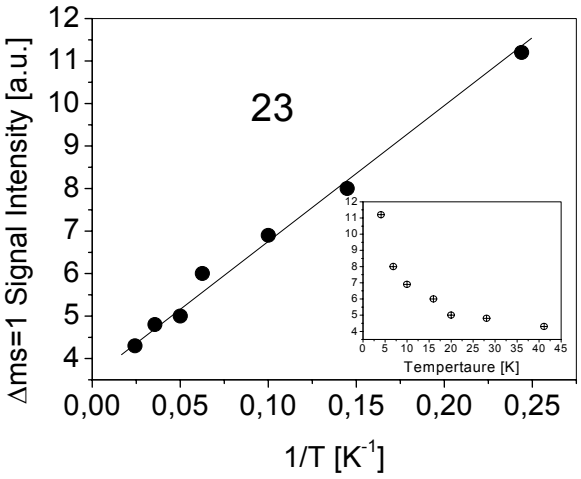

Figure 4.3.8. *Curie plot of the randomly oriented single crystals of* ***23*** *down to 4K*

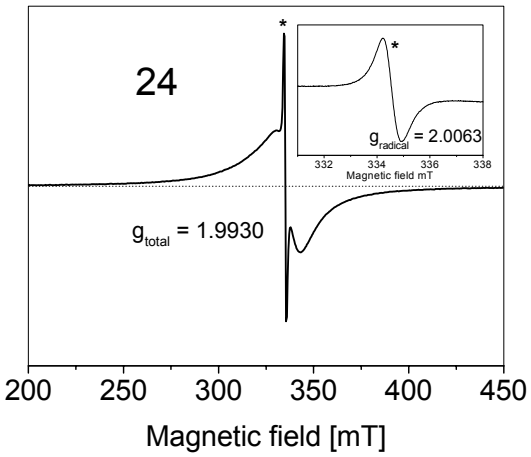

Figure 4.3.9. *ESR spectrum of* ***24*** *at room temperature, inset shows the central free radical signal*

The temperature dependent static molar magnetic susceptibilities [χ] and the effective magnetic moment [μ_{eff}] of **23** and **24** are given in Fig 4.3.10. At temperature higher than 50 K the effective magnetic moment of **23** is a constant value of about 2.5 μ_B that corresponds well to the paramagnetic mixture of two spins ½. Below 50 K μ_{eff} starts to increase. Low temperature magnetic behavior of **23** is typical of a ferromagnetically coupled linear chain. The Hamiltonian of the system is

$$\mathbf{H} = -2J\sum_{i=1}^{n-1}\mathbf{S}_i\mathbf{S}_{i+1} - 2J\mathbf{S}_1\mathbf{S}_n \qquad ...(46)$$

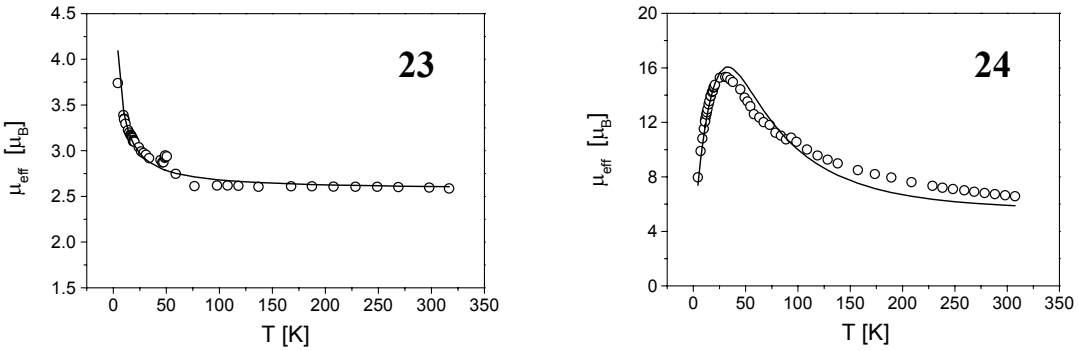

Figure 4.3.10. *Top figures show the static magnetic susceptibility and effective magnetic moment of* ***23*** *and* ***24*** *(the solid lines represent the theoretical fit)*

The magnetic properties of an infinite chain are calculated as follows: (i) a ring chain of n spins is considered. where J is the isotropic exchange parameter; (ii) a magnetic behavior of an infinite chain is extrapolated from the magnetic behavior of the ring chain in the limit $n \rightarrow \infty$. The theoretical fit is presented in Fig. 4.3.10. as a solid curve. The best-fit parameters are: $J = 6$ cm^{-1}, $g = 2.1$. The dynamic magnetic behavior of **23** shows no anomaly either in the real or imaginary part exhibiting the overall paramagnetic properties of the compound. Further more the dynamic magnetic susceptibility does not depend on the applied frequency or the amplitude of the oscillating field.

The magnetic behavior of **24** looks different [Fig. 4.3.10.]. In a plot of the effective magnetic moment vs. temperature μ_{eff}(T) a maximum at low temperatures could be

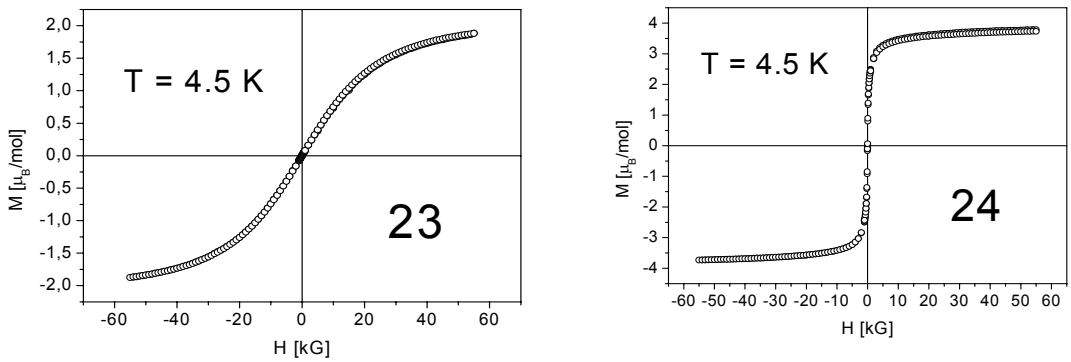

Figure 4.3.11. *Magnetization of* ***23*** *and* ***24*** *up to at 4.5 K*

observed reaching $\mu_{eff} \sim 15\ \mu_B$. Even at room temperature μ_{eff} is not a constant value indicating thus a strong coupling between the Mn^{II} ($S = {}^5/_2$) and the neighboring radical ($S = ½$). The question arises whether this intrachain interaction is of ferro- or antiferromagnetic type. To answer this question the magnetization measurements were performed. As can be seen from Fig. 4.3.11. the saturation magnetization tends to 4 μ_B/mol, which is the expected value for an antiferromagnetically coupled ${}^5/_2 - ½$ spin system. The fact that the typical minimum for a ferrimagnetic chain in μ_{eff} (T)[13a] is not observed is caused by the strong intrachain coupling. Like in the previous case the magnetic properties of **24** can be analyzed using the Hamiltonian (1) where $\mathbf{S}_i$ with odd and even subscripts corresponds now to Mn^{II} and radical respectively. It can be shown[13b] that the behavior of the infinite (½ - ${}^5/_2$) ferrimagnetic Heisenberg chain can be well described by the simple equation

$$\chi T_{ch} = P_1 x^a + 4.75 \exp(P_2 x)\ , \qquad ...(47)$$

where $P_1 = 4.1249$, $P_2 = -1.013$, $a = 1.72$ and $x = 2|J|/kT$.

The decrease of μ_{eff} at low temperatures can be explained by some interchain interaction. This interaction is taken into account in the molecular field approximation:

$$\chi T = \chi T_{ch} / (1 - 2zJ' \chi T_{ch} / Ng^2 \mu_B^2 T) \qquad ...(48)$$

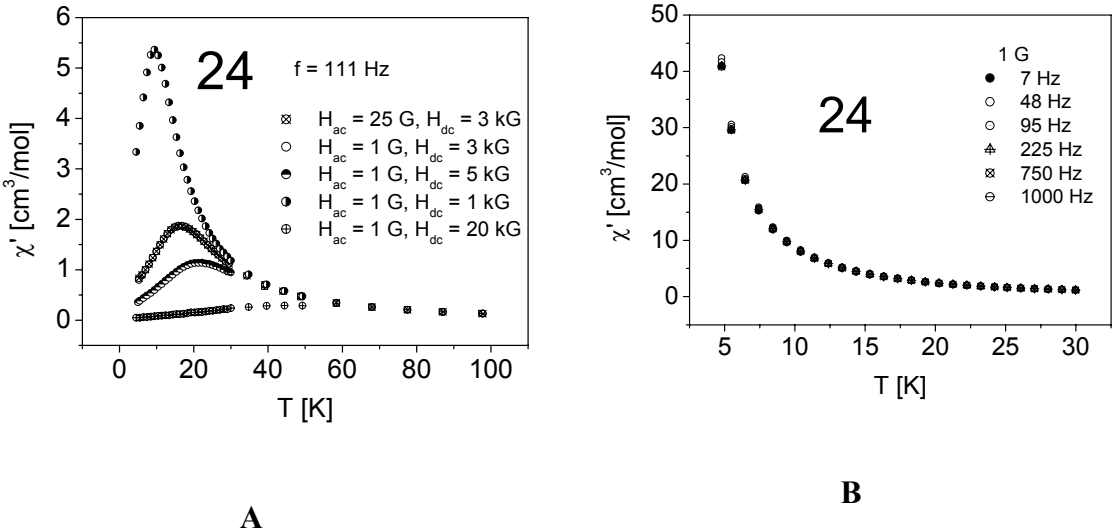

A **B**

Figure 4.3.12. *Dynamic magnetic susceptibility of **24** with (**A**) and without (**B**) an applied static magnetic field*

where χT_{ch} is given by eqn. (47). The theoretical fit is presented in Fig. 4.3.10. as a solid curve. The best-fit parameters are: J = - 67 cm^{-1}, zJ' = -0.33 cm^{-1}.

The origin of the interchain interaction could be the classical dipolar one, due to large interchain distances and the absence of interchain exchange pathways. Recently, it was shown[14,15] that the dipole-dipole interaction can be responsible for the bulk magnetic ordering of some Mn^{III}TPP – radical chain compounds[14-16]. To check the possibility of magnetic ordering in the investigated compound the dynamic magnetic susceptibility studies with and without an applied magnetic field were performed [Fig. 4.3.12.]. If no static magnetic field is applied during the measurement no anomaly can be observed and the value of χ_{ac} does not depend on the frequency or the oscillating field. If a static field H_{dc} = 1000 G is applied the situation changes dramatically. A maximum in the real part of the dynamic magnetic susceptibility occurs. The position and the amplitude of this maximum depend on the applied static magnetic field. The higher the field, the higher is the temperature and the lower is the amplitude. But for all cases no anomaly in the imaginary part of the dynamic magnetic susceptibility can be observed showing that there are no bulk magnetic properties in the material down to liquid He temperature. In accordance to this a measurement of magnetization yields no hysteresis at 4.5 K as can be seen in Fig. 4.3.11. The main difference between the compounds reported in[17] and the investigated one is that Mn^{II} has no single-ion anisotropy. For the ferrimagnetic Heisenberg chain the correlation length at low temperature diverges according to a power law [see eqn. (47)] and, as a consequence, the correlated spin blocks (superspins[14]) are not big enough to promote 3-D ordering through dipolar interaction.

4.4 1 - D Network of a high spin ligand with $Cu(hfac)_2$

As discussed earlier, in order to achieve higher spin domain formation, there is a need to design and to build a ligand with various available coordination sites which can bind with metals to form extended higher dimensional structure. In the field of molecular magnetism it is vital to construct higher dimensional magnetic motifs with strong exchange interactions for spontaneous magnetization. In order to extend the magnetic structure into higher dimensions following the metal-radical approach, it is

important to design multicoordinating ligand. Diamagnetic ligands are poor mediators of magnetic interactions; in this aspect high spin ligands are fruitful to enhance the magnetic communication. Not many extended structures are known, which are built from a well established high spin ligand building blocks based on nitronylnitroxide radical (NIT). NIT units are helpful in order to design complex network motifs and to understand the magneto-structural relationships due to the available two coordinating oxygen sites per radical unit. Heteroatom containing ligands carrying NIT have proven valuable building block for extended dimensions. In this context, we have designed a pyridine containing high spin ligand **1** (S=1) as described in Chapter.3. which has five coordinating sites, four NIT oxygens and one nitrogen from the pyridine. In **1** the two NIT moieties are separated by ~1.5 nm in distance. The pentadentate ligand **1**, react with $Cu(hfac)_2$ yielding compound **25**, with an extended structure [Scheme.4.4.1]. The complexation was done by using single crystals of **1** with $Cu(hfac)_2$ using diffusion technique [dichloromethane: hexane; 2:1 ratio] to yield blue green hair like crystals of **25** having composition $[Cu(C_5HO_2F_6)_2]_7(C_{35}H_{35}N_5O_4)_2$.

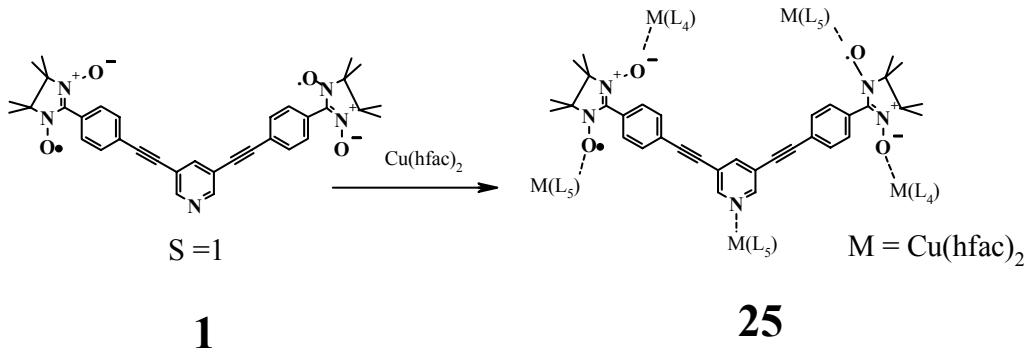

Scheme 4.4.1. *Reaction of a high spin ligand (**1**) with $Cu(hfac)_2$ to give **25***

In this case controlling the stoichiometry of the metals can define the structural dimension. For example using **1**: $M(hfac)_2$ in (2:1) ratio may yield zero dimensional structures using pyridine nitrogen as a coordination site due to its stronger coordination power than the radical oxygen.

4.4.1 Description of the crystal structure

X-ray structure analysis revealed the *P*-1 symmetry structure of **25**, with all the five coordination sites are occupied by the $Cu(hfac)_2$. Each repeating units [Fig. 4.4.2.] has two molecules of **1** in dimeric form carrying seven $Cu(hfac)_2$ molecules together, which extends in a linear fashion along the crystallographic *a* – axis. Here, Cu(2) and Cu(4) play an important role in extending the dimension of the structure. There are two types of coordination numbers of copper were found [octahedral (Oh) and square pyramidal (SP) geometry] in each repeating unit. Cu(2) and Cu(4) have coordination number six, and Cu(1) and Cu(3) have five coordination environment [Fig. 4.4.4.]. The extension of the total structure into higher dimension stops at Cu(1) and Cu(3).

Octahedral coppers: In Cu(2) one pyridyl nitrogen N(3) from **1** and one NIT oxygen O(11) from another molecule of **1** and the four oxygens from hfac (hexafluroacetyl acetonate) forms the octahedral [MO_5N_1 - type] geometry. N(3) and O(11) are *cis*– coordinated to the metal [N(3)-Cu(2)-O(11) bond angle: 95.95°]. Here, one oxygen from NIT O(11) and another oxygen from hfac O(72) are in the *z*-axis of the octahedron [O(11)-Cu(2)-O(72) bond distance: 4.718 Å], and N(3) bound to the Cu(2) in the x, y- plane with the Cu(2)-N(3) distance 2.013 Å. Importantly, Cu(4) plays an unique role of connecting the two NIT O(1) of the two molecules of **1**, forming a six oxygen coordinated tetragonally distorted octahedron geometry [MO_6 - type]. Here, the oxygens [π* - orbital] from the two NIT units have *trans*-coordination [O(1)-Cu(4)-O(1) bond angle: 180°] with a near orthogonal overlap [N(2)-O(1)-Cu(4) bond angle: 124.5°] to the Cu(4) dz^2 orbital, forming the *z*-axis of the distorted octahedron [O(1)-Cu(4)-O(1) bond distance: 4.718 Å] and the remaining hfac oxygens occupies the x- and y- axis plane.

Square pyramidal coppers: The two Cu(1) and Cu(3) have five coordination sites, where solely five oxygens are involved in making the square pyramidal [MO_5 - type] geometries. In Cu(3) the NIT oxygen O(12) forms the *z*-axis with the distance 2.254 Å and the rest of the four hfac´s oxygens bound to Cu(3) keeps the two hfac´s unit in the x, y-plane without distortion. The radical oxygen O(12) has a near

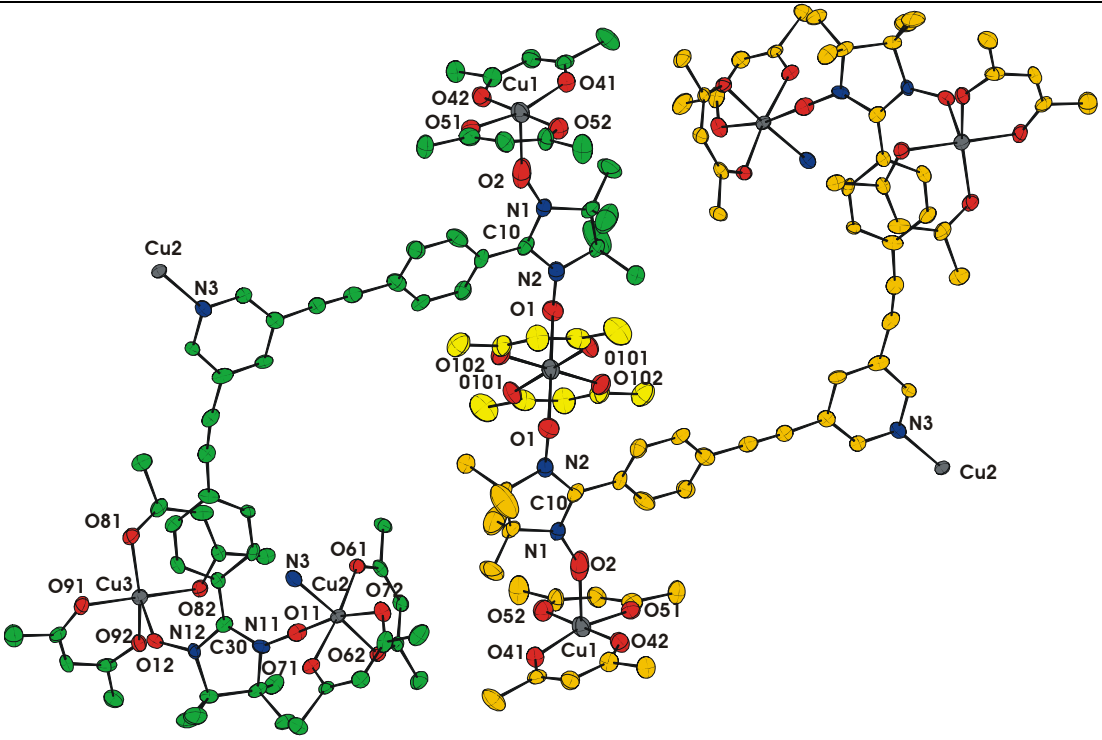

Figure 4.4.2. *ORTEP plot (50%) of a single repeating unit of* ***25*** *[hydrogen and fluorine atoms are omitted for clarity]*

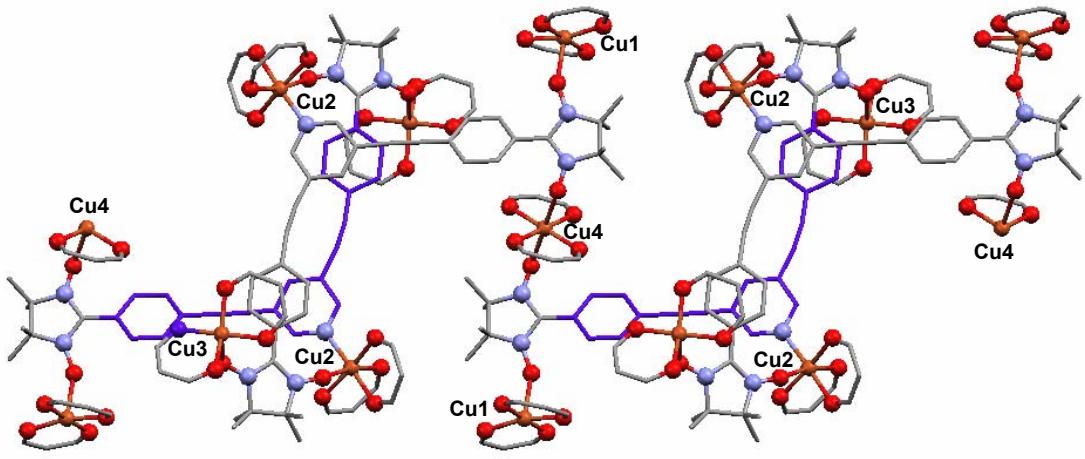

Figure 4.4.3 *Crystal structure of* ***25*** *showing a part of a single dimeric chain [hydrogen and fluorine atoms are omitted for clarity]*

orthogonal overlap with the copper dz^2 orbital [Cu(3)-O(12)-N(12) bond angle: 120.71°]. The Cu(1) has a NIT oxygen O(2) in the z-axis with the distance 2.218 Å, and the remaining four oxygens from hfac´s are in the x, y-plane. The overlap bond angle between the radical oxygen and the copper is [Cu(1)-O(2)-N(1): 150.81°].

The total repeating unit is a dimeric network with four types of copper. Where the two molecules of **1** form a kind of stack on top of each other at a distance ~3.3 Å [see Fig. 4.4.3.]. The highest z-axis length is 4.768 Å in the Cu(4) case forming the more Jahn-Teller distorted symmetry in the z-axis (out) than the Cu(2) case, where the distance is 4.718 Å. The Cu(4) bridges the two biradicals [**1**] forming an extended structure making the coppers Cu(1)-Cu(4)-Cu(1) in a linear fashion in the crystallographic *c* –axis. A model of diagram of four different types of coordination sites of copper in **25** is given in Fig. 4.4.4.

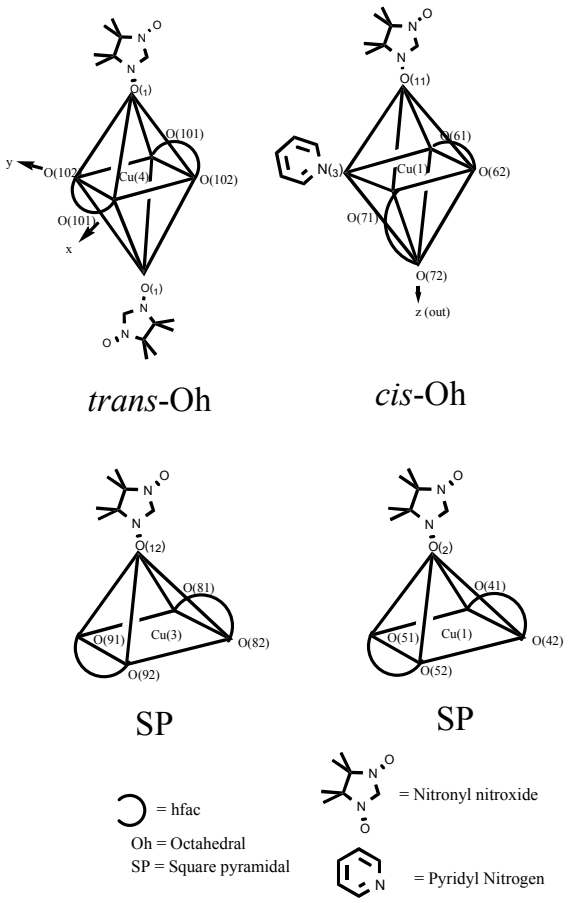

Figure 4.4.4. *Four types of coordination sites of copper in* ***25***

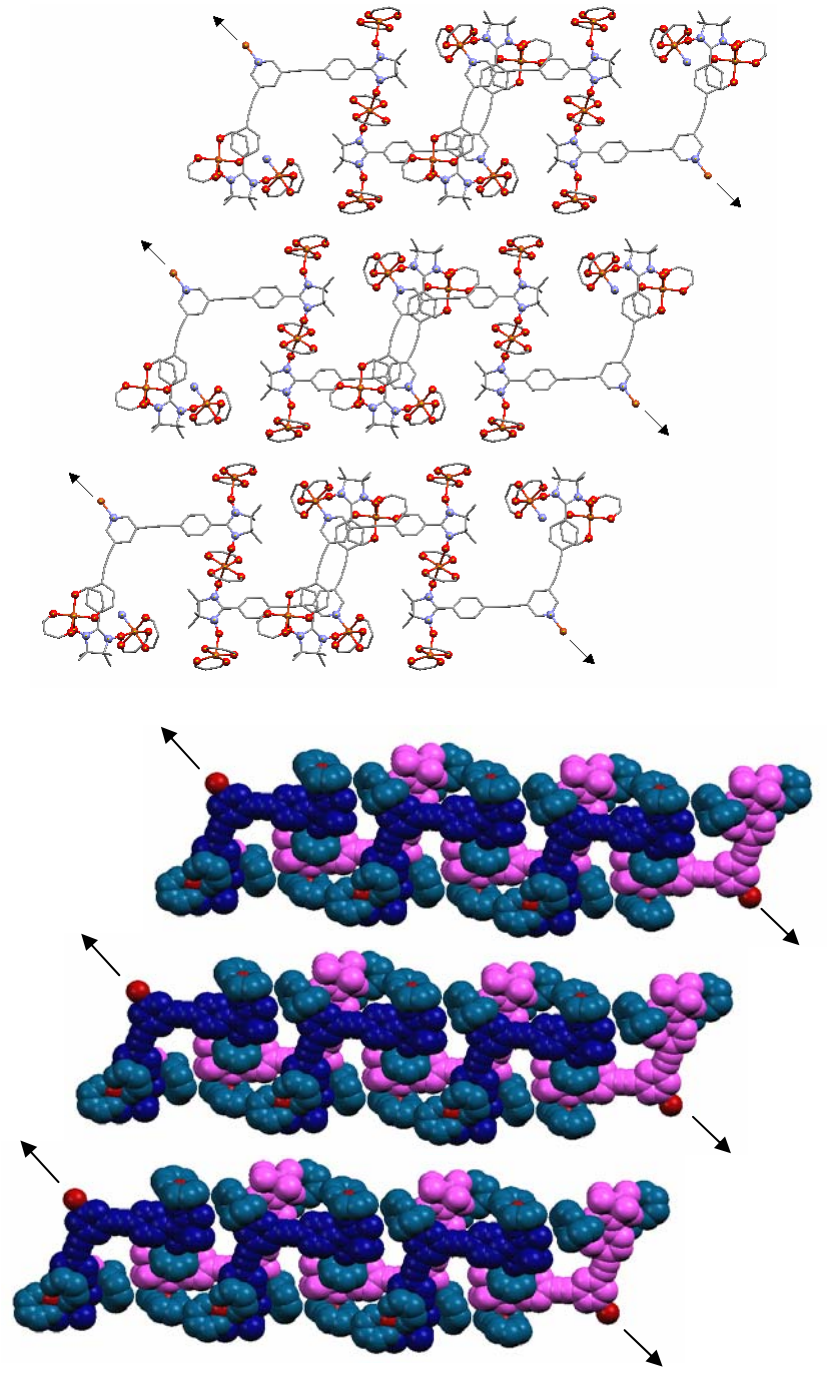

Figure 4.4.5. *Packing of* ***25*** *in the crystallographic, b, c- plane. Arrow marks denote the point of extension of each chain.(Top - Ball and Stick model, Bottom - Space fill model)*

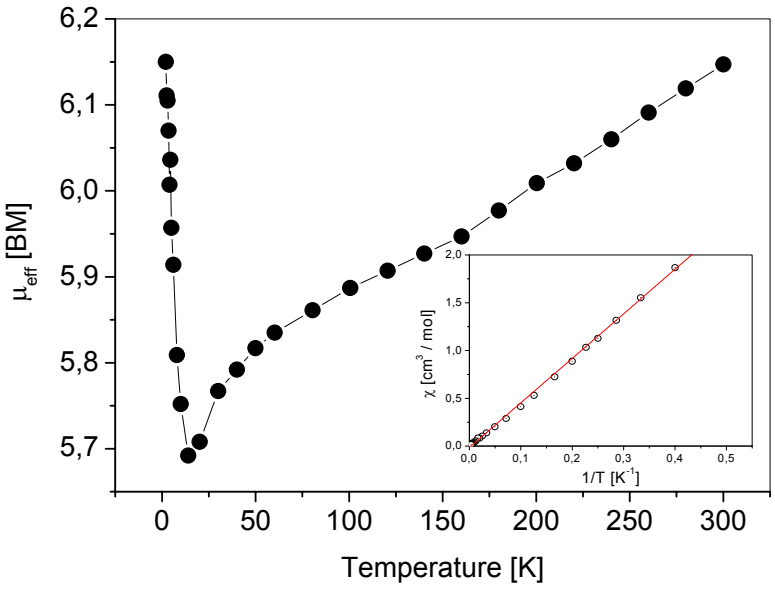

Figure 4.4.6. *Magnetic curve of **25**, inset show the low temperature behavior of **25** (inset χ cm^{-3}/mol^{-1} versus T^{-1})*

4.4.2 Magnetic studies

The temperature dependence of μ_{eff} and the χ (inset) measured at 0.5 T for **25** is shown in Fig. 4.4.6. The μ_{eff} value of **25** is 6.147 BM at 300 K, which is slightly lower than the calculated value of 6.21 BM for a non-coupled five spin system (g = 2.1). A negative Weiss temperature was obtained for **25** from the Curie-Weiss eqn. 4 with C = 4.823 cm^3 mol^{-1} K (g = 2.1) and $\theta \sim -24$ K. The C value is higher than the experimental value of 4.650 cm^3 mol^{-1} K for the five spin system. This finding implies that antiferromagnetic interaction is dominant in **25**. Upon cooling, the μ_{eff} values decreased to a 5.69 BM at 14 K below this temperature μ_{eff} increased to a maximum value of 6.15 BM at 2 K. The maximum μ_{eff} value at 2 K is close to the μ_{eff} at 300 K.

From the structural point of view the arrangement of Cu(1)-radical-Cu(4)-radical-Cu(1) is linear with near orthogonal overlap of the radical oxygen ($p\pi$) with the coppers. Where the radical unpaired electron can find less electron density of copper (when it is orthogonal) favoring minimum overlap integral and ferromagnetic

exchange integral. In addition to that, Cu(3) has pentacoordination with five oxygens, also with near orthogonal overlap leading to possible ferromagnetic interaction. In case of Cu(2) where the pyridyl nitrogen participates in the octahedral coordination sphere together with the NIT oxygen, (the NIT oxygen (O11) is in the *z*-axis of the octahedron) distorting the total hfac´s plane can be a probable reason for the observed antiferromagnetic interaction.

4.5 Conclusions

A novel stable dark-green trinuclear copper cluster was synthesized. The complex is linear and centrosymmetric in the triclinic *P*1 space group. The striking feature of the complex is the presence of two types of copper coordination geometries, a distorted octahedron at the center and two terminal octahedron structures, where the copper and the nitronylnitroxide oxygen binding is stronger in the latter case due to "chelation effect". The central copper is surrounded by O_6 donor sets and the terminal coppers are surrounded by NO_5 donor sets. The three copper ions in the complex are collinear with shortest intramolecular metal-metal distance ca. 7.75 Å. The magnetic behavior shows that the coupling is antiferromagnetic between the radical and the terminal coppers, with J_1 = -440 cm^{-1} and weakly ferromagnetic between the central copper and the neighboring radicals with J_2 = 10 cm^{-1}.

Two alternating linear metal-radical chains, the 1- D linear copper and zig-zag manganese chains bridged (μ–1,5) by 4-Trimethylsilylethynyl-1-(4,4,5,5-tetramethyl-3-oxylimidazoline-1-oxide)benzene exhibit ferro (J = 6 cm^{-1}) and ferrimagnetic (J = -67 cm^{-1}; zJ' = -0.33 cm^{-1}) behaviors respectively. Cryogenic magnetic measurements showed that there is no bulk magnetic ordering down to liquid helium temperature. In accordance to this a measurement of magnetization yields no hysteresis at 4.5 K.

Finally, the most challenging task of magnetic network formation of a high spin biradical with $Cu(hfac)_2$ was successfully realized. In a single repeating unit four different types of copper ions [two Oh, and two SP] were found. Magnetic susceptibility studies showed a strong antiferromagnetic behavior till 14 K and below this temperature a ferromagnetic transition. Modeling the magnetic data can yield four different exchange coupling *J* values.

4.5 References

1. O. Kahn, *Molecular Magnetism*; VCH; Cambridge, U.K., **1993**.
2. a) K. Fegy, D. Luneau, T. Ohm, C. Paulsen, and P. Rey, *Angew. Chem. Int. Ed*. **1998**, 37, 9, 1270. b) M. Minguet, D. Luneau, E. Lhotel, V. Viller, C. Paulsen, D. B. Amabilino, and J. Veciana, *Angew. Chem. Int. Ed*. **2002**, 41, 4, 586.
3. a) A. Caneschi, D. Gatteschi, R. Sessoli, *Acc. Chem. Res*. **1989**, 22, 392. b) A. Caneschi, D. Gatteschi, N. Lalioti, C. Sangregorio and R. Sessoli, *J. Chem. Soc., Dalton Trans*. **2000** 3907.
4. K. Inoue, F. Iwahori, A. S. Markosyan, H. Iwamura, *Coord. Chem.Rev.* **2000**, 198, 219.
5. (a) A. Caneschi, D. Gatteschi, R. Sessoli, P. Rey, *Acc. Chem. Res*. **1989**, 22, 392. (b) A. Caneschi, D. Gatteschi, J. Laugier, P. Rey, R. Sessoli, *Inorg. Chem*. **1988**, 27, 1553. (c) A. Caneschi, F. Ferraro, D. Gatteschi, P. Rey, R. Sessoli, *Inorg. Chem*. **1991**, 30, 3162. (d) A. Caneschi, D. Gatteschi, J. P. Renard, P. Rey, R. Sessoli, *Inorg. Chem*. **1989**, 28, 1976. (e) A. Caneschi, D. Gatteschi, J. Laugier, P. Rey, *J. Am. Chem. Soc*. **1987**, 109, 2191. (f) K. Inoue, F. Iwahori, H. Iwamura, *Chem. Lett*. **1998**, 737. (g) A. Caneschi, D. Gatteschi, P. Rey, R. Sessoli, *Inorg. Chem*. **1988**, 27, 1756. (h) K. Fegy, D. Luneau, T. Ohm, C. Paulsen, P. Rey, *Angew. Chem. Int. Ed.* **1998**, 37, 1270. (i) K. Griesar, W. Haase, I. Svoboda., H. Fuess, *Inorg. Chim. Acta*. **1999**, 287,181.
6. (a) D. Gatteschi, J. Laugier, P. Rey, and C. Zanchini, *Inorg. Chem*. **1987**, 26, 938. (b) J. Laugier, P. Rey, C. Benelli, D. Gatteschi, and C. Zanchini. *J. Am. Chem. Soc*. **1986**, 108 6931.
7. V. I. Ovcharenko, V. N. Ikorskii, N. V. Podberezskaya, N. V. Pervukhina, S. V. Larionov, *Russ. J. Inorg. Chem. (Engl. Tranl.)* **1987**, 32, 844.
8. D. Luneau, P. Rey, J. Laugier, P. Fries, A.Caneschi, D. Gatteschi, R.Sessoli, *J. Am. Chem. Soc*. **1991,** 113, 1245.
9. Y. Pei, M. Verdaguer, O. Kahn, J. Sletten, J. P. Renard, *J. Am. Chem. Soc*. **1986**, 108, 7428.
10. Y. Pei, Y. Journaux, A, Dei, D. Gatteschi, *J. Chem. Soc., Chem. Commun*. **1986**, 1300.

11. a) P. F. Richardson, R. W. Kreilick, *J. Am. Chem. Soc*. **1977**, 99, 8183. b) S. S. Eaton, G. R. Eaton, *Coordin. Chem. Rev.* **1978**, 26, 207.
12. P. M. Boymel, J. R. Chang, D. L. DuBois, D. J. Greenslade, G. R. Eaton, S. S. Eaton, *J. Am. Chem. Soc*. **1977**, 99, 5500.
13. (a) S. Gehring, P. Fleischhauer, H. Paulus, W. Haase, *Inorg. Chem*. **1993**, 32, 54. (b) J. S. Miller and M. Drillon, *Magnetism : Molecules to Materials - Models and experiments,* Wiley VCH, **2001**, 1.
14. S. Ostrovsky, W. Haase, M. Drillon, P. Panissod, *Phys. Rev. B* **2001**, 64, 134418.
15. S. Ostrovsky, W. Haase, M. Drillon, P. Panissod, in *"Relaxation Phenomena*" W. Haase, S. Wrobel., Springer, **2003**, 587.
16. K. Falk, W. Haase, *Phys. Stat. Sol. (a)* **2002**, 189, 979.

CHAPTER 5

Pure Organic Supramolecular 1 – Dimensional Hydrogen bonded Magnetic Polymers and π - π Stacks

Abstract: *This chapter describes the synthesis of hydrogen bonding synthons and their crystal structures, and ESR and magnetic susceptibility studies. Stacking of a monoradical and an approach towards π - π stacking of a sym-triradical together with its synthesis and ESR investigation will be discussed.*

5.1 Introduction

Building controlled supramolecular architectures adopting the concept of crystal engineering[1] in pure organic molecules is a challenging and fascinating area for its intriguing solid-state properties. In the field of molecular magnetism, H-bonding[2] and π-π stacking[3a,b] is the two promising approaches to design pure organic based higher dimensional motifs, and to explore the intermolecular magnetic communication. Many remarkable magnetic characterizations rely on specific intermolecular interactions.

5.2 1-D Hydrogen bonded chains

H-bond mediated magnetic interaction is a subject of great interest because of its unresolved mechanistic mysteries. Constructing magnetic chains in solids via this approach can be done in many ways using conventional supramolecular donor and acceptor synthons. Building 1- D chains using terminal acetylenic hydrogen and spin carrying nitronylnitroxide (NIT) oxygen atom is one of the routes to assemble magnetic polymer arrays in solid state[4]. The possible propagation of alternating spin waves of NIT to another molecule via H-bonding can lead to intermolecular ferro- or antiferromagnetic exchange interactions. In this chapter, a comparative analysis of ESR and magnetic studies of two structurally similar systems based on 2-(5-ethynyl-2-phenyl)-4,4,5,5-tetramethylimidazoline-1-oxyl (**26**) and 2-(5-ethynyl-2-pyridyl)-4,4,5,5-tetramethylimidazoline-1-oxyl (**27**) interacting via weak N-O···H-C≡C- hydrogen bonds exhibiting various intermolecular contacts will be provided.

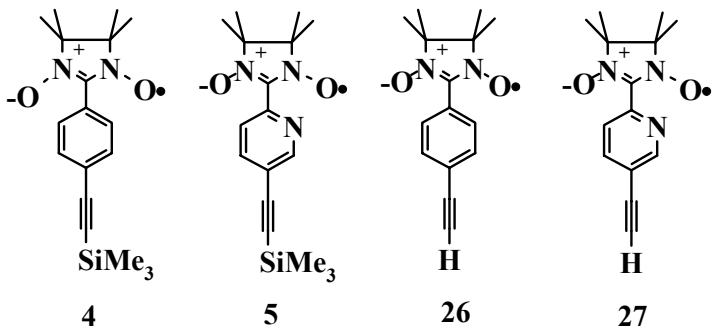

Scheme 5.2.1. *Protected (**4, 5**) and deprotected (**26, 27**) doublet radicals*

Compound **27** provide a potential complexation site that can be used to design novel magnetic system with transition metals. The striking evidence of intramolecular spin polarization from the radical moiety to acetylenic protons by ESR liquid state solution studies for the radicals **26** and **27** in comparison with **4** and **5** will also be discussed [see Scheme 5.2.1].

5.2.1 Synthesis

Previously, reported work on hydrogen bonded system is based on meta-pyrdineethynyl based nitronyl and imino-nitroxides were ferromagnetic behavior was

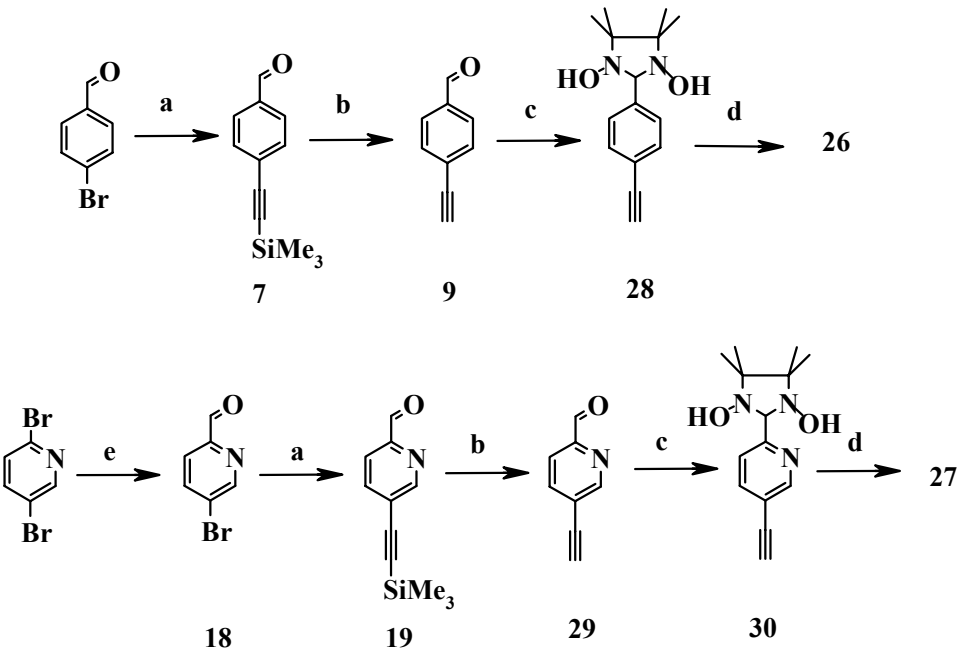

Scheme 5.2.2. *Deprotected monoradicals (**26** and **27**). Reagents and conditions: (a) Trimethylsilylacetylene (TMSA) / $Pd(PPh_3)_2Cl_2$ / CuI / Et_3N / THF (b)K_2CO_3 / MeOH (c) 2,3-Dimethyl-2,3-bis(hydroxylamino)butane / MeOH / THF (d) $NaIO_4$ / $CHCl_3$ / H_2O (e) n-BuLi / Toluene / DMF / -78°C*

observed and the polarization of spin densities to acetylenic protons were demonstrated by neutron diffraction studies[4]. With the aim of extending these ideas, two doublet mononitronylnitroxide radicals [**26** and **27**] carrying ethynyl functional groups were synthesized in nine steps. Sonogashira´s coupling reaction of 4-bromobenzaldehyde and 2-formyl-5-ethynyl pyridine with TMSA afforded

7 and **19**. Deprotection (for donor group) of trimethylsilylacetylene group, followed by Ullman´s condensation reaction with 2,3-dimethyl-2,3-bis(hydroxylamino)butane and subsequent oxidation (for acceptor group) [Scheme.5.2.2] yielded the desired doublet radicals **26** and **27**. The detailed description of the synthesis of compounds **4**, **5, 7, 9, 18** and **19** were discussed in Chapter 3. Compound **29** was synthesized from **19** by using K_2CO_3 / MeOH in 70% yield. Reaction of **9** and **29** with 2,3-dimethyl-2,3-bis(hydroxylamino)butane in dichloromethane and methanol respectively afforded condensed products **28** and **30**. Monoradicals **26** and **27** were synthesized by oxidation of the corresponding condensation products in phase transfer solutions (dichloromethane / water) using $NaIO_4$. Both **26** and **27** were crystallized in petroleum ether (b.p. 30 - 40°C): acetone mixture at room temperature to afford dark blue and blue needles respectively.

5.2.2 Molecular structures of 26 and 27 in solid state

X-ray structural analysis revealed that, both **26** and **27** are in P$2_1/c$ and P*bca* symmetries, respectively. Each monoradical has weak intermolecular hydrogen bonding interaction between the acetylenic hydrogen and the NIT oxygen of the adjacent molecule [O···H-C≡C-], forming head-to-tail chain like structures. In both **26** and **27**, each hydrogen bonded chains is propagating in alternating directions along the crystallographic *b* and *c* – axis with N-O···C≡C- distances 3.181 Å and 3.155 Å, respectively [Fig. 5.2.1. - 5.2.3.]. In **26** the five-membered imidazole ring is

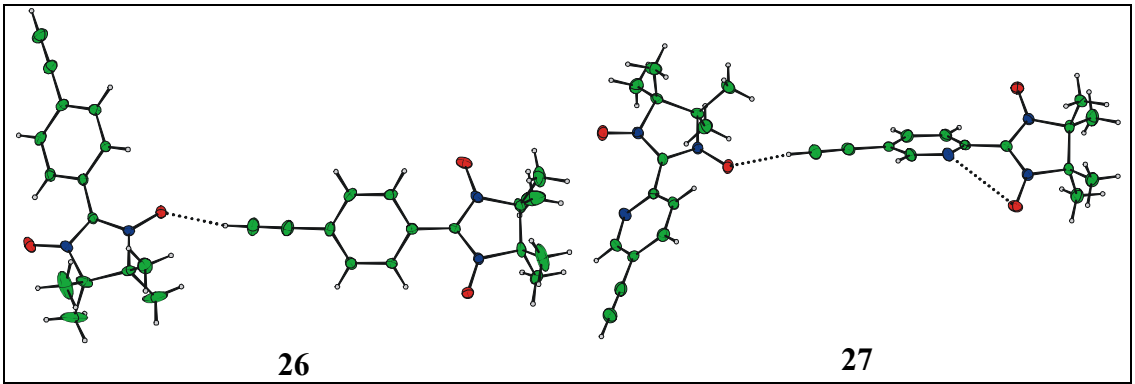

26 **27**

Figure 5.2.1. *H-bonded crystal structures of* ***26*** *and* ***27***

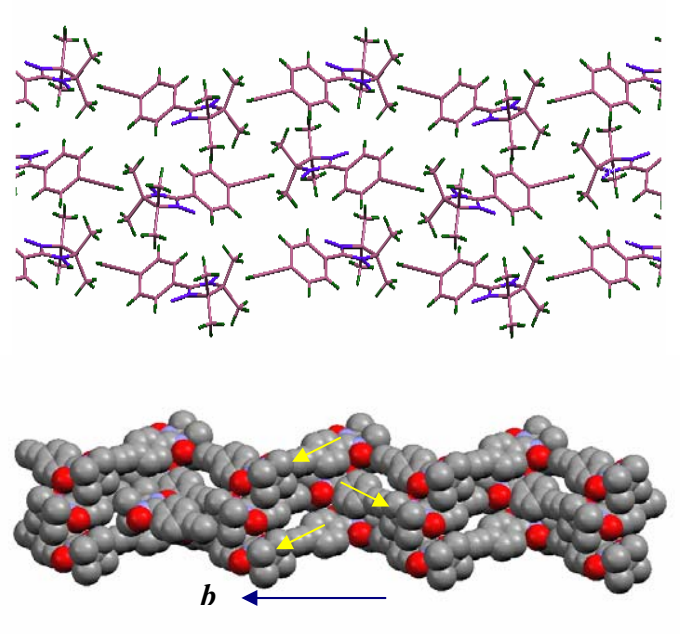

Figure 5.2.2. *Crystallographic projection of* ***26,*** *intermolecular head-to-tail 1-D H-bonded chains running along b – axis. Bottom figure shows the respective space fill models*

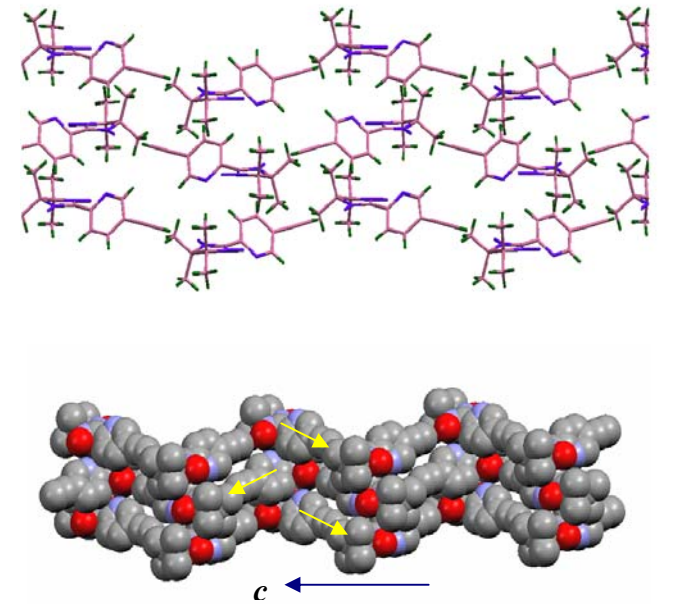

Figure 5.2.3. *Crystallographic projection of* ***27,*** *intermolecular head-to-tail 1-D H-bonded chains running along c – axis. Bottom figure shows the respective space fill models*

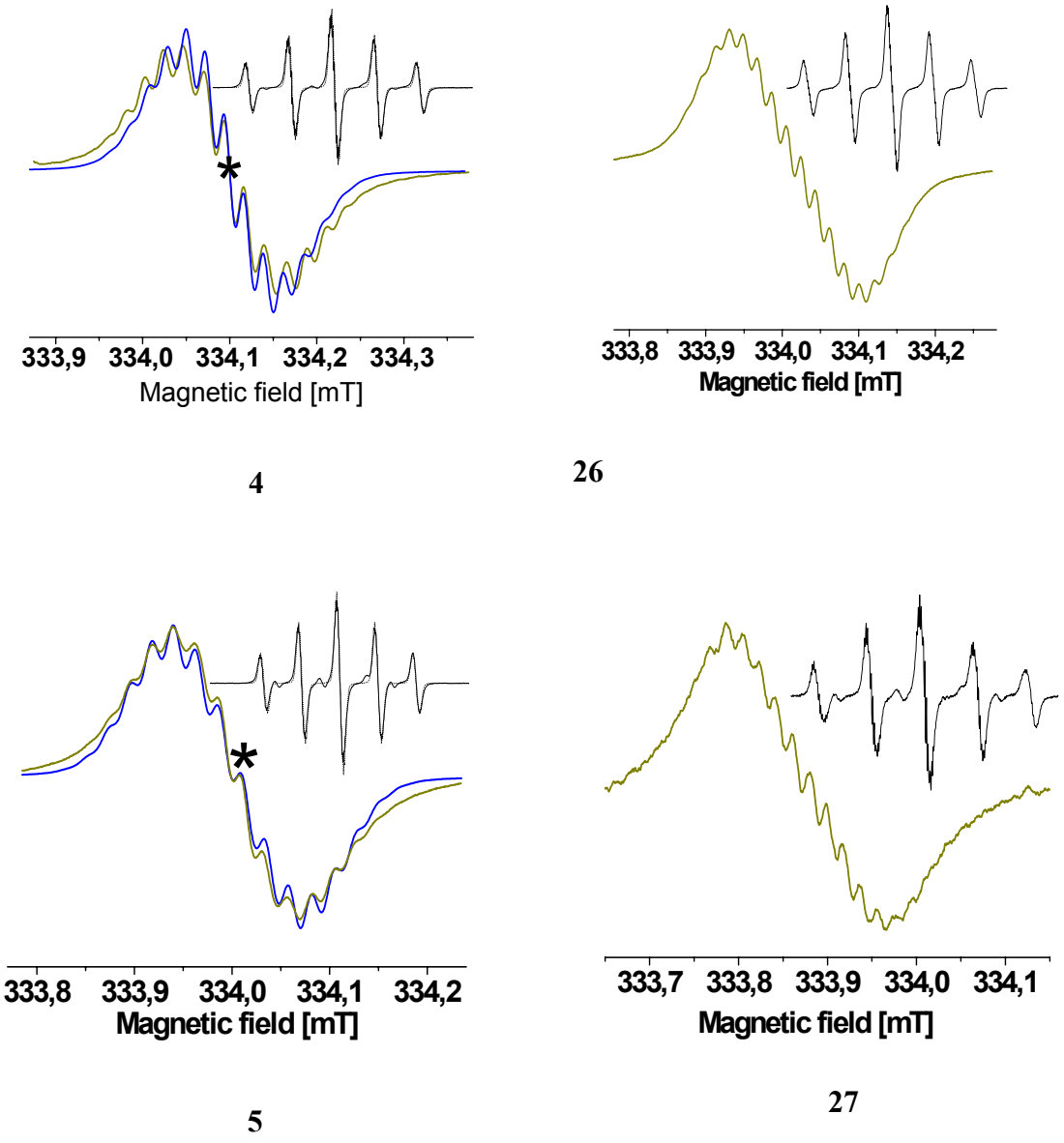

Figure 5.2.4. *Central lines of the solution ESR spectra of* ***4*** *and* ***26*** *(top left and right),* ***5*** *and* ***27*** *(bottom left and right); c ≤ 10^{-4}M in toluene, 1 scan, 5 mW, inset show the total five line spectra [green yellow- experimental and blue- simulated]*

planar and all the methyl groups are in eclipsed conformation, with a twisting from the benzene plane by an angle 1.75° [O2-N2-C9-C6]. In contrast, in **27** the five-membered imidazole ring is twisted from planarity due to the slightly staggered conformation of the four methyl groups [C14-C10-C9-C11: -21.60° and C13-C10-C9-C12: -22.43°]. The imidazole group also twisted from the pyridine plane with an angle of 3.57° [O1-N1-C8-C5].

5.2.3 ESR studies

High resolution liquid solution state ESR (X – band) studies of monoradicals in degassed toluene gave five major lines for two NIT nitrogens hyperfine coupling (*hfc*) with additional protons splitting of each line by 12 methyl protons and the aromatic protons. The five line spectra were best simulated[5] with *hfc* values for two nitrogen (a_N = 7.4 G and 7.36 G) for **4** and **5** respectively. A close study of the central line of five line spectra of **4** and **5** were made. Interestingly, in **4** the central resonance magnetic field is in the middle of a single line due to the *hfc* of benzene *ortho*-protons, while for **5** an extra splitting is observed and the central resonance field is in between two lines due to the coupling of two nuclei with different nuclear spin quantum numbers [*ortho*-pyridine proton (I = ½) and nitrogen (I = 1)]. Now comparison of **4** with **26** and **5** with **27** clearly ascertain, in addition to the 12 methyl and aromatic protons lines, some extra splitting due to the coupling of terminal acetylenic proton. Takui and his coworkers[6] have demonstrated experimentally, the magnitude and relative sign of the π-spin densities on the aromatic ring carbon sites of 4,4,5,5-tetramethyl-3-oxide-2-phenyl-2-imidaolin-1-yloxyl doublet radical by liquid-phase ENDOR/TRIPLE spectroscopy. The result shows the following proton hyperfine splitting constants [NIT methyl protons: 0.21 G, ortho aromatic hydrogens: 0.52 G, meta aromatic hydrogens: 0.298 G and the para aromatic hydrogen: 0.47 G]. Based on these values, the central line of the spectra of **4** and **5** were best simulated with the following *hfc* values, 12 methyl protons (a_H = 0.21 G) and 2 benzene ortho protons (a_H = 0.44 G) for **4**. For **5**, 12 methyl protons (a_H = 0.21 G), 1 pyridine ortho proton (a_H = 0.32 G) and 1 pyridine nitrogen (a_N = 0.45 G). Simulation of the central line of the spectra of **26** and **27** are not straight forward, due to the lack of knowledge of at least one defined proton coupling value. But, inspection of the spectra of **26** and **27** clearly show some extra lines, as a result of the involvement of acetylenic protons. This observed intramolecular spin polarization from the radical centre to the alkyne protons is important to understand the magnetic coupling between molecules in solid state particularly in H- bonded chains. Here we can anticipate an antiferromagnetic (AF) behavior in both **26** and **27** at low temperature in magnetic susceptibility studies, due to the H - bonding interaction between the atoms (H···O-N) carrying positive spin densities. The g values of **4**, **5**, **26** and **27** are 2.0067.

The ESR study of the randomly oriented single crystals of **26** down to liquid helium temperature follow Curie behavior.

5.2.4 Magnetic studies

The magnetic susceptibility data of **26** at 300 - 4K are shown in Fig. 5.2.5. Similar magnetic behavior was exhibited by **27**. Surprisingly the molecules exhibit paramagnetic behavior at wide range of temperature and show antiferromagnetic behavior close to liquid helium temperature. Even though ESR spectra of the **26** and **27** shows evidence of transmission of spin waves till acetylenic protons, the

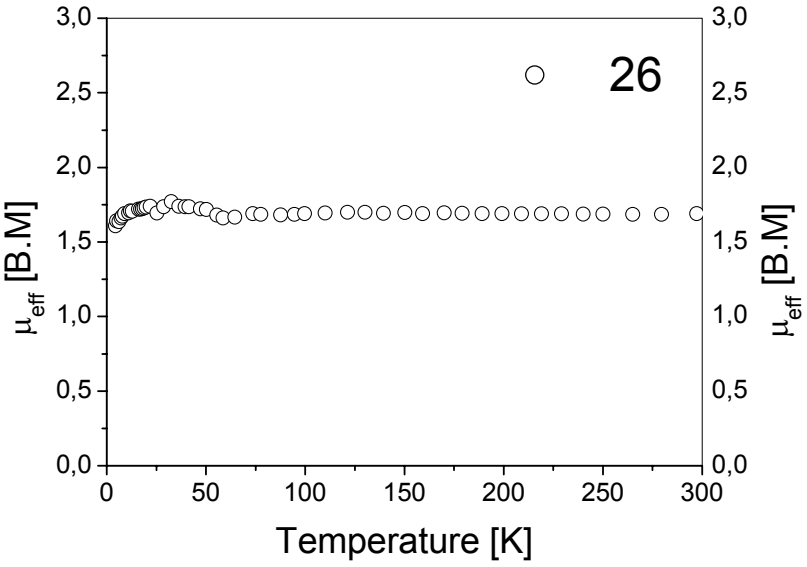

Figure 5.2.5. *Magnetic data of* ***26*** *at 300 - 4K range*

observed paramagnetic and low temperature AF behaviors probably arises as product of the balance between all the intermolecular interactions. According to McConnell I mechanism[7], in case of **26**, there are totally 16 intermolecular contacts, which are as follows, two interaction between the N-O···H-C≡C- (d = 2.245 Å), two H 81-H131 (d = 2.989 Å), and two H152-C5 (d = 2.843 Å) interactions are AF. It has two H152-H51 (d = 2.287 Å), two C7-H51 (d = 2.851 Å), two O2-H133 (d = 2.611 Å), two H121-C12 (d = 2.892 Å), and C1-O1 (d = 3.181 Å) interactions, which are ferromagnetic. In **27**, there are 14 intermolecular neighboring interactions, two N-O···C≡C- contacts per molecule H11-O2 (d = 2.209 Å), two O1-C12 (d = 3.178 Å) interactions are all AF.

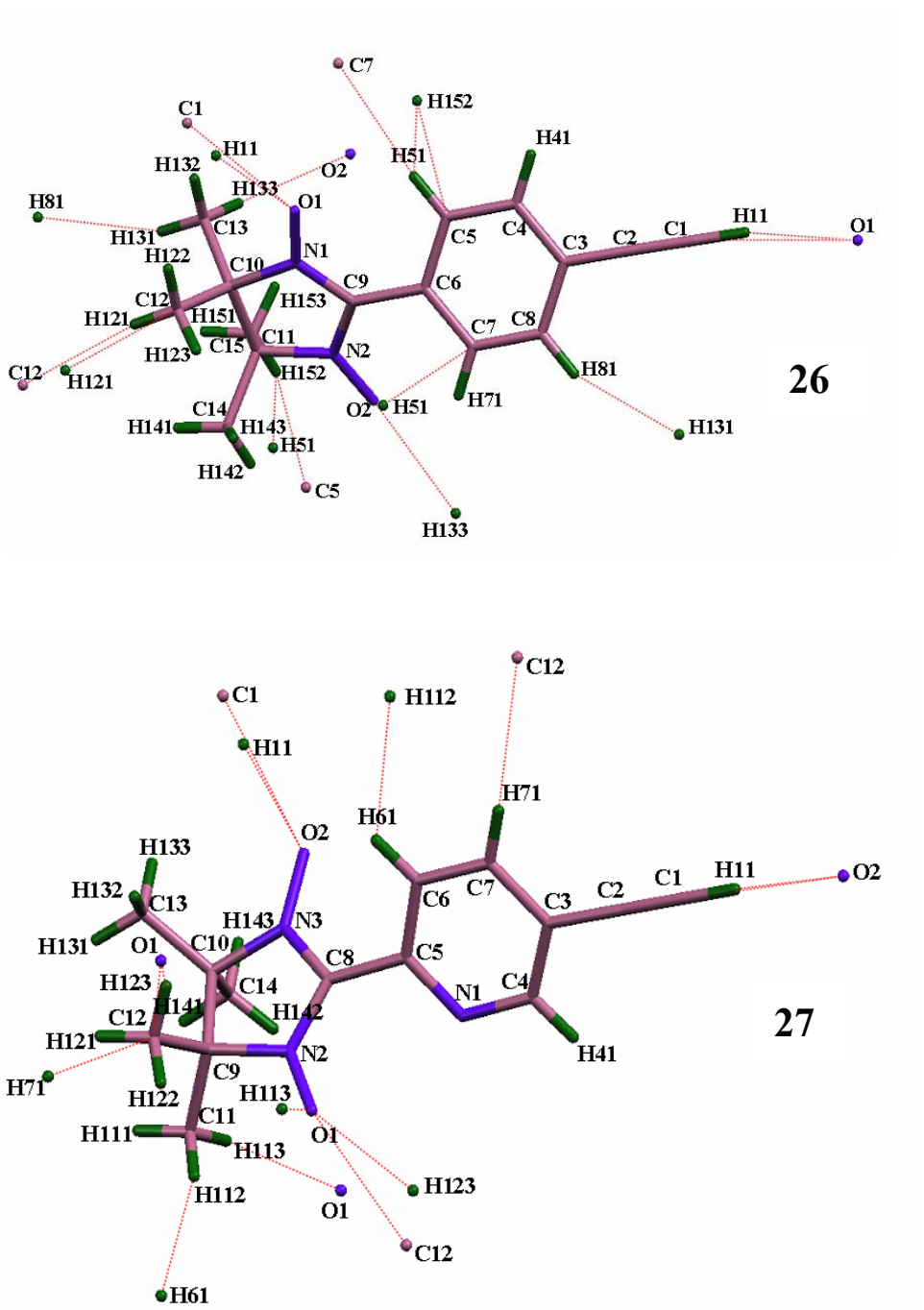

Figure 5.2.6. *Intermolecular contacts of* ***26*** *and* ***27***

Table 5.2.1. *Selected bond lengths (Å), torsion angles (°) and intermolecular distances (Å)*

26		**27**	
Intermolecular bond distances		**Intermolecular bond distances**	
H11···O1	2.245	H11···O2	2.209
H81···H131	2.989	C12···O1	3.178
H152···C5	2.843	H61···H112	2.375
H152···H51	2.287	H71···C12	2.894
H51···C7	2.851	O2···C1	3.155
H133···O2	2.611	O1···H123	2.531
H121···C12	2.892	O1···H113	2.602
Bond lengths	1.285	**Bond lengths**	1.288
N1-O1	1.279	N2-O1	1.289
N2-O2	1.181	N3-O2	1.191
C1-C2		C1-C2	
	1.75		3.57
Torsional angles	-5.57	**Torsional angles**	2.81
O2-N2-C9-C6		O1-N1-C8-C5	-21.60
O1-N1-C9-C6		O2-N3-C8-C5	-22.43
		C14-C10-C9-C11	
		C13-C10-C9-C12	

The rest of the two H61-H112 (d = 2.375 Å), two H71-C12 (d =2.894 Å), O2-C1 (d = 3.155 Å), two O1-H123 (d =2.531 Å), and two O1-H113 (d = 2.602 Å) interactions are ferromagnetic. Overall **26** and **27** have ten ferromagnetic interactions each, as compared to the six and four AF interactions in **26** and **27** respectively at 120 K. The observed AF interactions at low temperature can be due to the H-bonding connectivity between the atoms of same spin densities. Close to liquid helium temperature the AF interactions dominate probably due to the tightening of H-bonds.

These interactions reasonably well fit with the observed paramagnetic and antiferromagnetic behaviors of **26** and **27**. It is worth to mention here that, statistical analysis of close contact distances in the crystal structure of organic magnetic crystal do not confirm the argument of simple McConnell I model pictures[8]. Here, the observed bulk magnetic behavior appears to be determined by the interplay of vary different exchange interactions, since it is not clear which interactions will be dominant. In some cases, H-bonds act purely as molecular assembly interactions, even when it is plausible that they act as exchange linkers[3b]. It is therefore not entirely clear when H-bonds have an electronic role. Nevertheless, in the above analysis a decent magneto-structural correlation between the intra (by ESR) and intermolecular (solid state magnetic properties) interactions was found.

5.2.5 UV-Vis and IR studies

The UV-Vis spectra of the compounds **26** and **27** are given in Fig. 5.2.7. Which show, two π-π* transitions at 305 and 378 nm for **26**, and at 303 and 387 nm for **27**. It is important to mention here that the observed bands at 378 and 387 nm are a characteristic fingerprint for the nitronylnitroxide radicals. As explained in Chapter

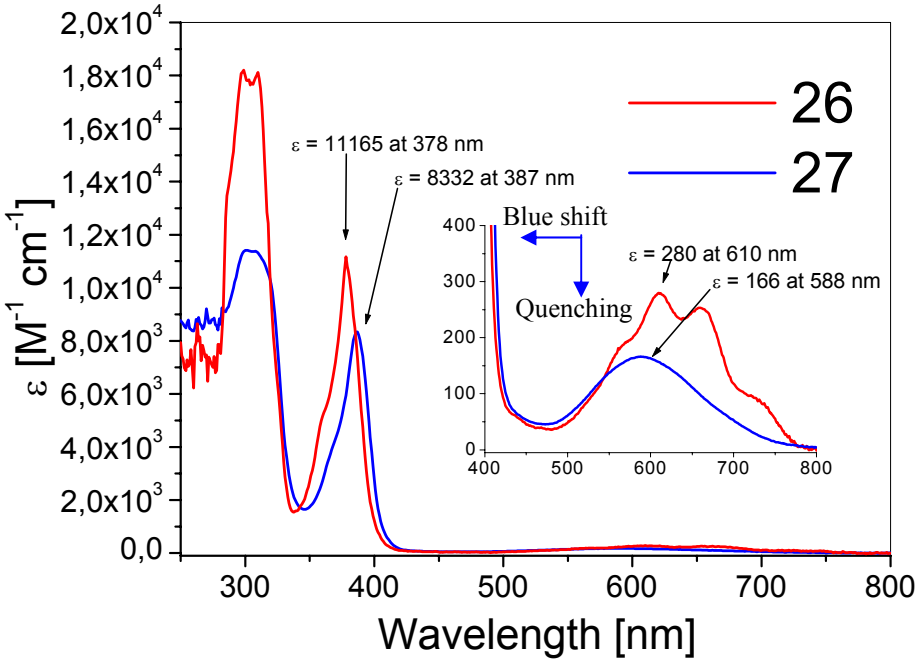

Figure 5.2.7. *UV-Vis spectra of* ***26*** *and* ***27***

3, comparison was made for **26** and **27**, to explore the influence pyridyl nitrogen on the n- π* transition extinction coefficient. As expected, the extinction coefficient of **27** is lower than that of **26**, besides that due to loss in symmetry in case of **27** no vibronic coupling was observed. Monoradical **26** gave extinction coefficient of 280 M^{-1} cm^{-1} at 610 nm with vibronic coupling, where as **27** exhibits extinction coefficient of 166 M^{-1} cm^{-1} with a blue shift to 588 nm.

The IR spectra of the H-bonded crystals of **26** and **27** are shown in Fig. 5.2.8. The compounds **26** and **27** were compared with ethynylbenzene and 4-ethynylpyridine respectively in order to diagnose the shift [Δν] of H-C≡C- stretching frequency band upon hydrogen bonding as per previous reports[4b]. The magnitude of H-C≡C- stretching frequency decreases in the order of ca. 80 cm^{-1} and 101 cm^{-1} for **26** and **27** respectively. It is likely that the hydrogen bonding observed between the ethynyl subunit and the NO is responsible for the head-to-tail 1-D hydrogen bonded structures.

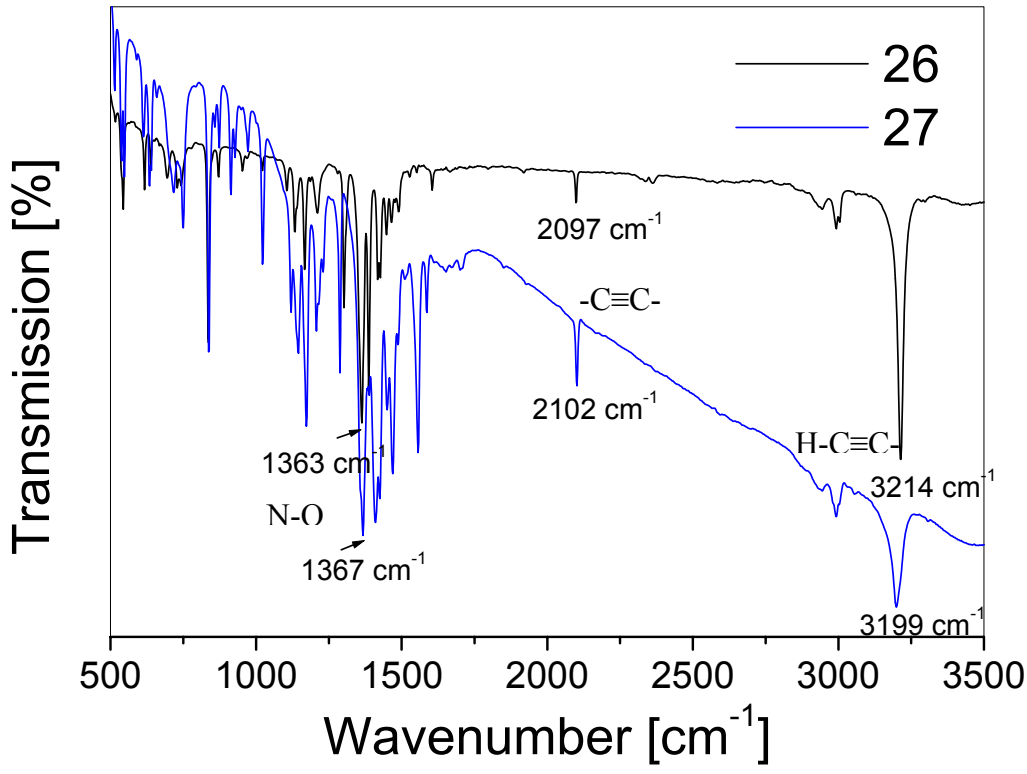

Figure 5.2.8. *IR spectra of the H-bonded crystals of* ***26*** *and* ***27***

5.3 π-π stacks

π-π stacking is another way of constructing supramolecular motifs besides hydrogen bonding. Appropriate stacking of organic spin carrying units in solid state can yield ferromagnetic interactions and low ordering temperature. While the goal has been defined, its accomplishment still presents a challenge in most cases. Not many examples are available in the literature regarding stacking of radical moieties. An elegant approach to a single component ferrimagnetic interactions of a triradical stacks was provided by Hosokoshi et al[3a], which exhibits 3-D ordering at 0.28 K [Fig. 5.3.1A.]. To achieve the challenging subject of π-π stacks, in this work, a model monoradical 2-(4,4,5,5-Tetramethyl-3-oxylimidazoline-1-oxide)-5-bromopyridine **21** was crystallized and nice stacking of the radical (S = ½) on top of each other was found. In order to extend the *π-π* stacking into higher spin units, a novel (S = 3/2) 1,3,5-Tris[4-(1-oxyl-3-oxo-4,4,5,5-tetramethylimidazolin-2-yl)phenylethynyl)]benzene was also synthesized in three steps. In this vein, earlier Siegel et al[3b]. have demonstrated the stacking of *sym*-triphenylethynylbenzene, where it forms a twisted rotor form [Fig. 5.3.1B.].

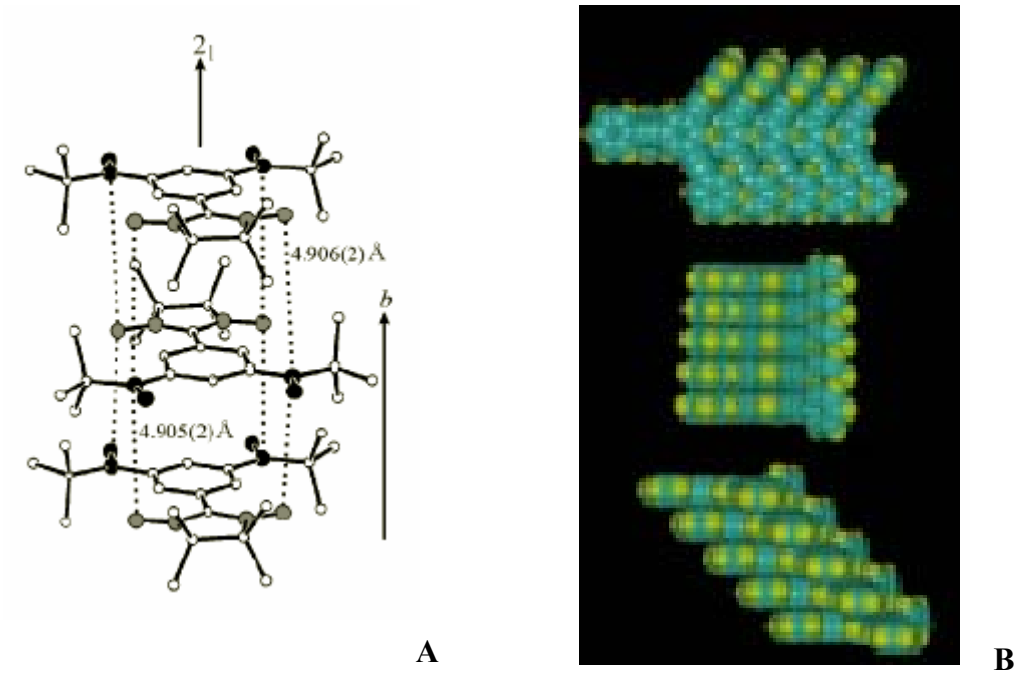

A **B**

Figure 5.3.1. *Stacking of A) a ferrimagnetic triradical[3a] B) sym-triphenylethynylbenzene[3b] [see from the top, top view, back view and side view]*

5.3.1 π-π stacking of monoradical 21

The synthesis of the doublet monoradical is described in Chapter 4. Recrystallization of **21** from the mixed solvents of dichloromethane: hexane [1:1] yielded blue needle shaped single crystals. X-ray analysis revealed the *P- 42$_1$c* space group of **21** with water molecules. Per unit cell eight molecules of **21** and eight molecules of water were found. Each radical stacks in a linear chain like fashion

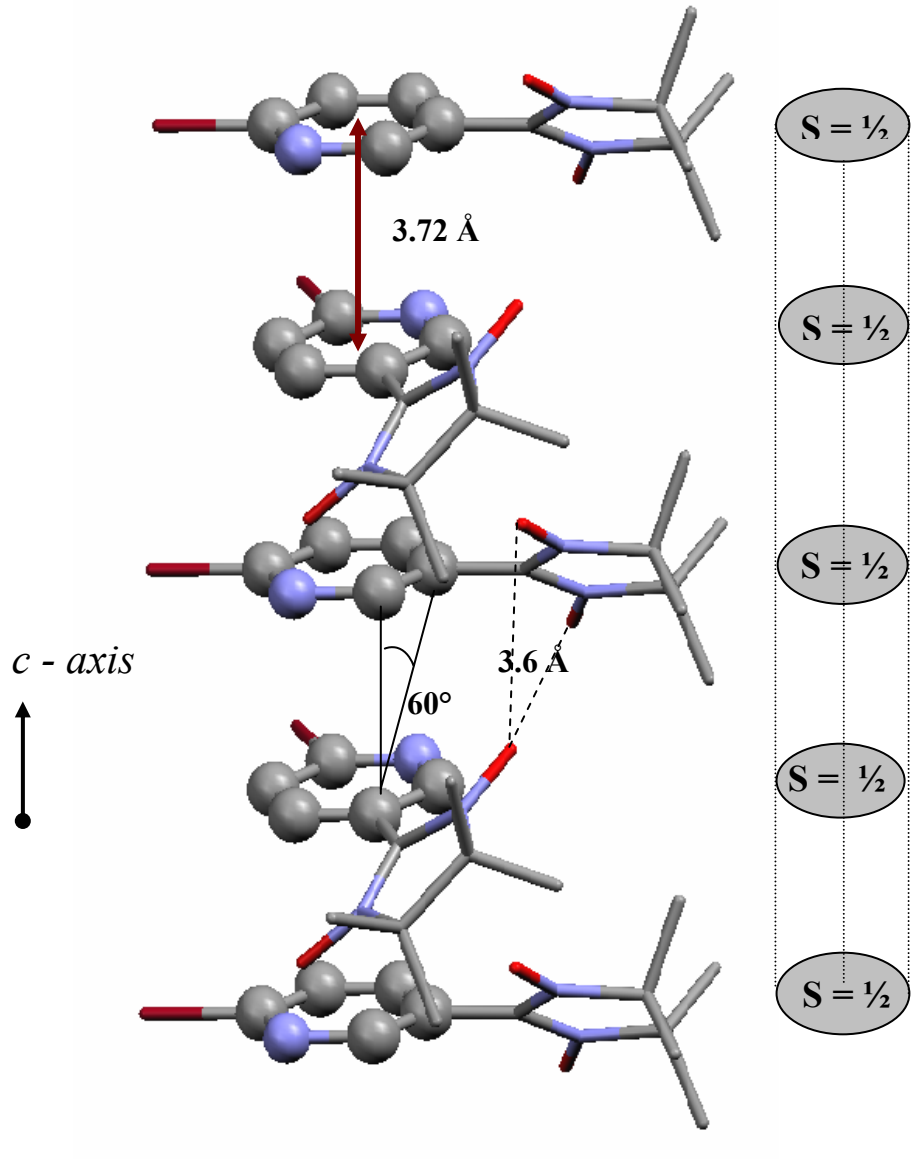

Figure 5.3.2. *Stacking of monoradical* ***21*** *along the crystallographic c-axis*

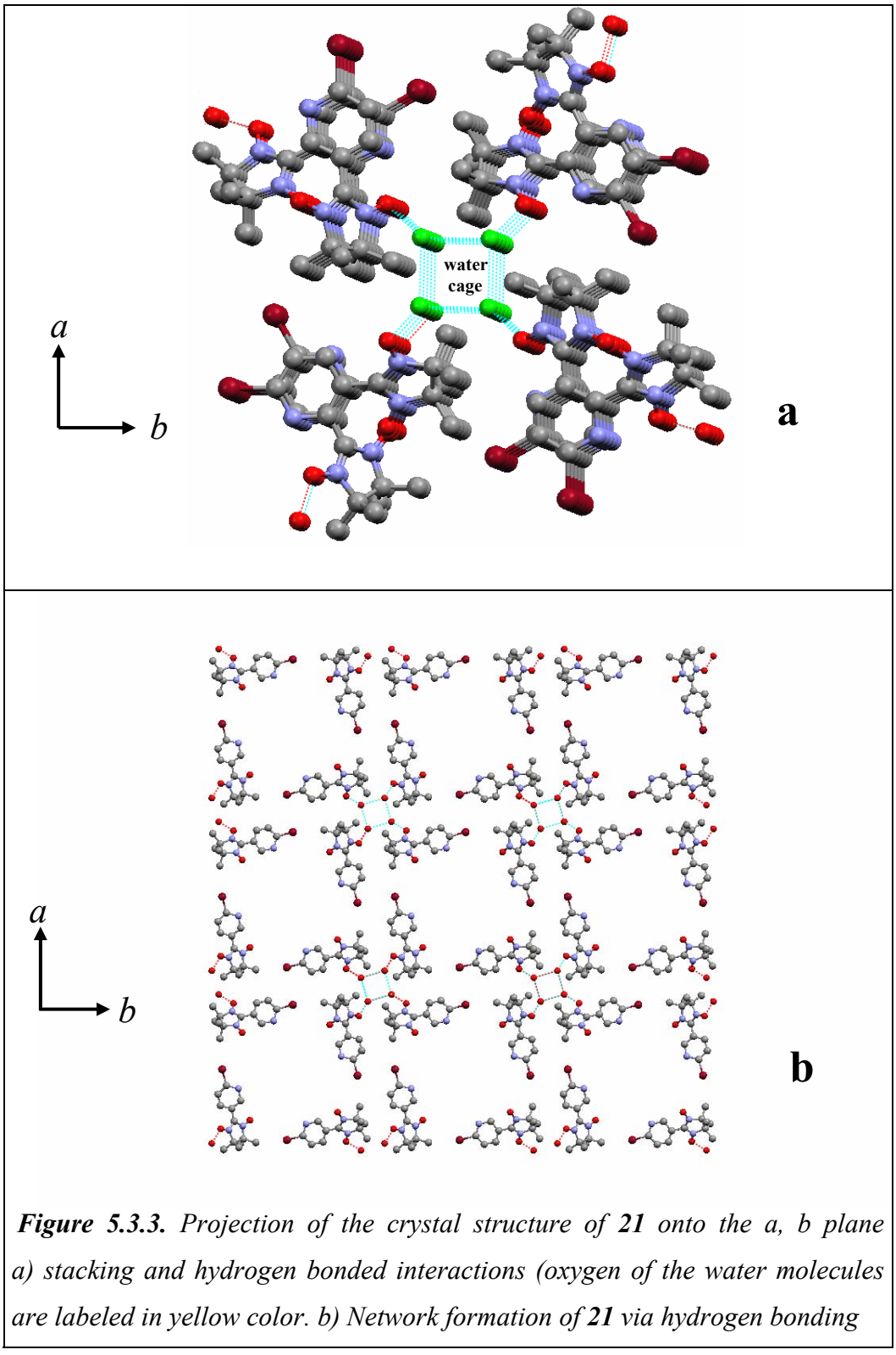

Figure 5.3.3. *Projection of the crystal structure of* ***21*** *onto the a, b plane a) stacking and hydrogen bonded interactions (oxygen of the water molecules are labeled in yellow color. b) Network formation of* ***21*** *via hydrogen bonding*

along the crystallographic c - axis. In **21** the torsional angles between the nitronyl nitroxide and the pyridine plane are 36.94° and 35.48°. The five-member imidazoline unit (NIT) is planar without any distortion. The distance between the stacks is 3.72 Å. Each radical unit forms twisted stack with a perfect rotation angle [θ] of 60° [Fig. 5.3.2.]. Besides that, the water molecules play an important role in forming hydrogen bonding with the nitronylnitroxide oxygen. The H – bonding distance between the oxygen atom of the water and the nitronylnitroxide oxygen [O···O-N] is 2.838 Å. Four water molecules by forming a perfect square onto the a, b - plane and extends as a square tubular cage along the c – axis [Fig 5.3.3a.]. Each water square exhibit hydrogen bonding interaction with four different nitronylnitroxide oxygens to produce pseudo-two-dimensional sheets [Fig. 5.3.3b.]. The observed stacking is a combined interplay between all non-bonded and hydrogen bonded interactions.

Earlier Zhang and Baumgarten[2a] have reported by AM1 calculation that the ferromagnetic coupling through space depends on the intermolecular vertical distance [d] and the alignment [rotational angle θ] of the dimeric radical stack. It was shown that the ferromagnetic coupling through space between stacked radicals under proper conformation is larger than the one through H – bonds in one plane. Larger triplet stabilization ΔE_{S-T} was observed when θ = 60° and 180°. Due to these angles, atoms of positive spin densities can be strongly exchange coupled with atoms of negative spin densities to yield ferromagnetic parallel total spin angular momentum on neighboring molecules with a stable high spin ground state. In our present case, the rotational angle θ and H - bonding interactions fulfill the requirement for a ferromagnetic interaction. The schematic diagram of the stacking along the c - axis and the H- bonding along the a, b - plane is given below [Scheme 5.3.1],

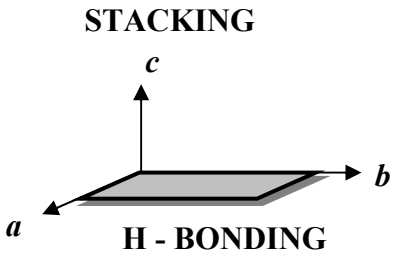

Scheme 5.3.1. *Illustration of stacking and H-bonding interactions of* ***21*** *along the crystallographic directions*

5.3.2 Magnetism

This experiment was performed using a Quantum Design SQUID magnetometer at an applied field of 0.5 T. The temperature dependence of the effective magnetic moment μ_{eff} [BM] is shown in Fig. 5.3.4. The observed μ_{eff} value 1.76 BM at room temperature is close to the spin quantum number S = ½ in accord with the radical nature of the spin bearing unit. It decreases slowly till 50 K then decreases sharply down to 3.5 K. This indicates dominant antiferromagnetic interaction. The μ_{eff} increases slightly below 3.5 K exhibiting a weak ferromagnetic interaction. The obtained results of the stacks are surprising since according to McConnell I[7] mechanism the through space interaction between the atom of positive spin density and atom of negative spin density should be ferromagnetic. In the magneto structural correlation

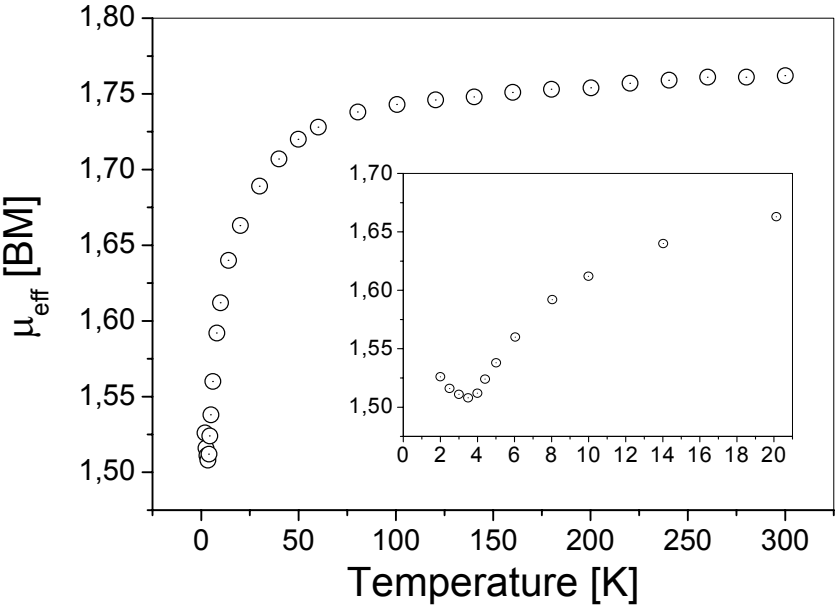

Figure 5.3.4. *Temperature dependence of the μ_{eff} [BM] of **21**. Inset shows the plot from 2- 21 K*

both stacking and H-bonding interactions were considered. In the stacking pattern, atoms of positive spin densities and atoms of negative spin densities are on top of each other leading to a ferromagnetic through space exchange interaction. A close look at the hydrogen bonded exchange pathway shows ferromagnetic interaction

since atoms of positive spin densities are connected via water molecules. Here, each water cage acts as a ferromagnetic exchange pathway between the four radical units. Since the ferromagnetic interaction should take place through space along the stacking gap of 3.7 Å in the *c* - axis and also via H bonded connection in the *a, b* - plane, we can anticipate total ferromagnetic exchange interaction. But still, it is questionable, whether water can act as a ferromagnetic exchange linker via hydrogen bonding or not.

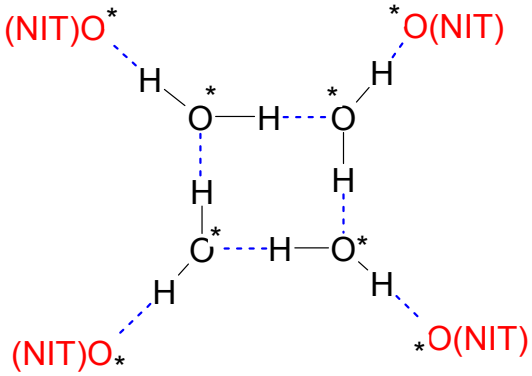

Scheme 5.3.2. *Spin polarization model for the water-radical connectivity in the crystal lattice of* ***21***

It is evident that the ferromagnetic interaction in the stack is exists below 3.5 K, because without intermolecular interaction, the value of the μ_{eff} should approach the constant value with decrease in temperature. This data suggest that the transition would be just below the experimental measured temperature of the apparatus. It is important to consider all possible close contact interactions for radicals interacting in a crystal lattice because; it is not necessarily clear by inspection what interaction dominant. Since the observed antiferromagnetic interaction above 3.5 K could also be as a result of other non-bonded interactions. Particularly, the distance between the nitronylnitroxide oxygens in between the two molecules in the stack is 3.67 Å and also the proton of the methyl group has also close contacts with the pyridine ortho and meta-protons in a distance of ~ 2.2 Å. It has recently been demonstrated that simplified models of solid-state interactions considering a single dominant interaction in a solid lattice are not well correlated with the overall exchange behavior[8]. Nevertheless, the analysis given above for **21** includes all of the important close contact interactions.

5.3.3 Approach towards π-π stacking of sym-triradical

Motivated by the stacking of monoradical **21** in solid state, in order to realize stacking of high spin triradicals, a 1,3,5-tris[4-(1-oxyl-3-oxo-4,4,5,5-tetramethylimidazolin-2-yl)phenylethynyl)]benzene **33** was designed and synthesized. The anticipated stacking fashion for the triradical is schematically represented in Fig. 5.3.5.

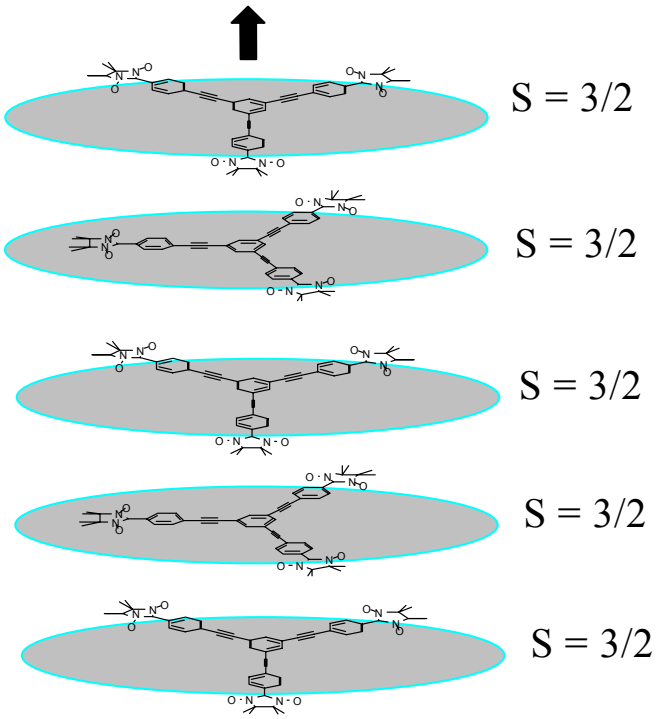

Figure 5.3.5 *Illustration of the stacking pattern of the sym-triradical* ***33***

5.3.4 Synthesis

The synthetic sequence towards the triradical is given in Scheme 5.3.1. *sym*-1,3,5-tris(4-formylphenylethynyl)benzene **31** was prepared by the Sonogashira coupling of the 1,3,5-triethynyl benzene with 4-bromobenzaldehyde using $Pd(PPh_3)_2Cl_2$ / CuI / Et_3N / THF reagents under reflux for 3 days at 70°C in argon atmosphere. The formed yellow precipitate of **31** is good soluble in dichloromethane, chloroform and insoluble in acetone.

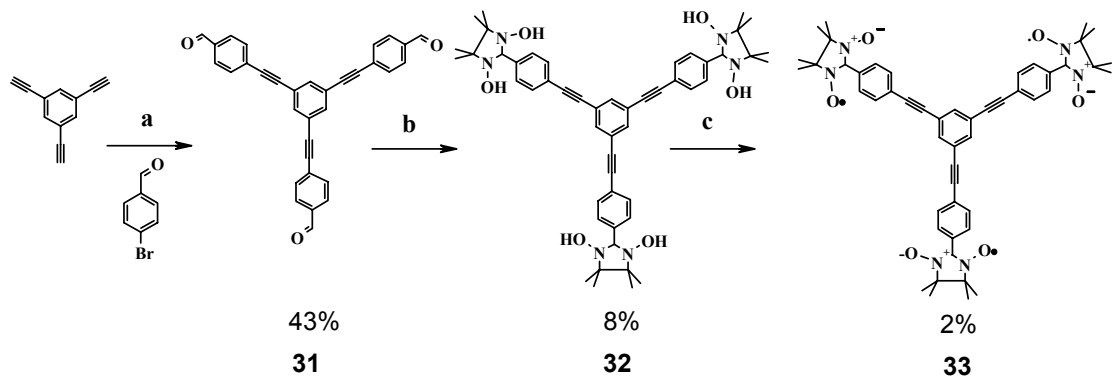

Scheme 5.3.1. *Reagents and conditions: (a) $Pd(PPh_3)_2Cl_2$ / CuI / Et_3N / THF/ 70°C /3 days (b) 2,3-Dimethyl-2,3-bis(hydroxylamino)butane / MeOH / Dioxane / 7 days (c) $NaIO_4$ / $CHCl_3$ / H_2O/ 5 min.*

The ^{1}H-NMR spectrum of the trialdehyde **31** is given in Fig. 5.3.2.

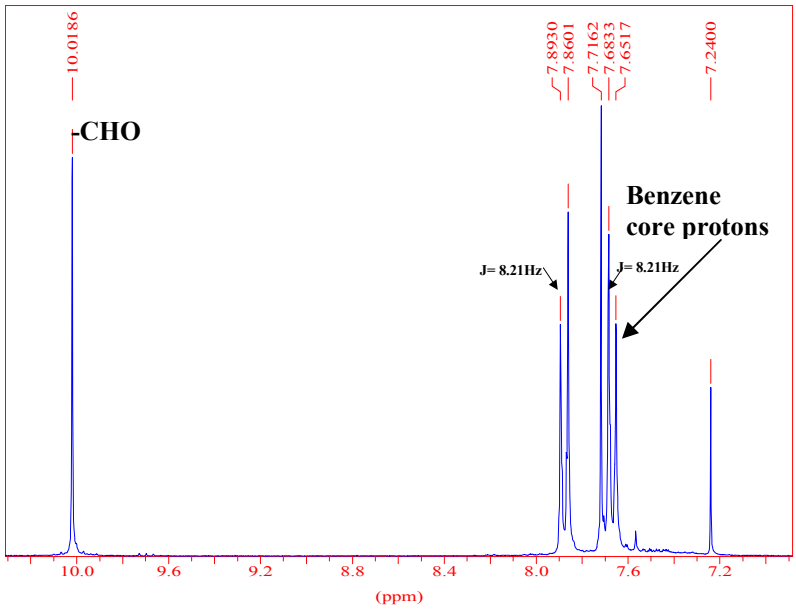

Figure 5.3.2. *^{1}H-NMR spectrum of the symmetrical trialdehyde **31** in $CDCl_3$ at rt.*

The central benzene core protons gave a singlet at δ 7.65 ppm and aromatic protons from three phenylethynyl arms gave two doublets at δ 7.88 ppm [^3J = 8.21 Hz] and δ 7.7 ppm [^3J = 8.21 Hz]. The condensation reaction of the trisaldehyde **31** with 2,3-dimethyl-2,3-bis(hydroxylamino)butane was unsuccessful in different solvents [Toluene (reflux), $CHCl_3$, CH_2Cl_2 with co-solvent MeOH] except in dioxane. The

reaction was followed by ^{1}H-NMR spectroscopy using the condensation precipitate formed in the turbid solution in order to confirm the complete condensation of the three aldehyde groups. The condensation reaction of **31** with 2,3-dimethyl-2,3-bis(hydroxylamino)butane was performed over one week in dioxane at RT to afford turbid solution, filtration of the solution gave precipitate of **32** in 8% yield. Most importantly, it is crucial to use very pure trialdehyde and 2,3-dimethyl-2,3-bis(hydroxylamino)butane for the condensation reactions, failure to use does not lead to any condensed products. The ^{1}H-NMR spectrum of the tricondensed product **32** is given in Fig. 5.3.3. The –OH peak from the condensed product appeared at δ 7.84 ppm and the signal from the core aromatic protons were shifted up field to δ 7.74 ppm.

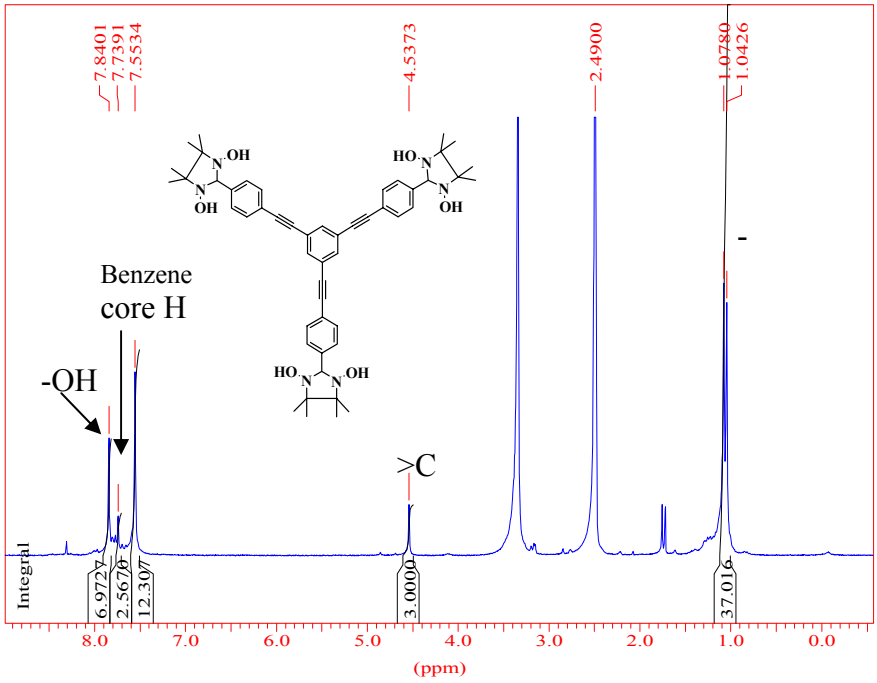

Figure 5.3.3. *^{1}H-NMR spectrum of the symmetrical **32** in DMSO-d_6 at RT.*

Surprisingly, the doublets from the three phenylethynyl side arms protons of **31** gave a singlet at δ 7.55 ppm with an integration value corresponds to 12 protons in **32**. The three imidazoline protons appeared at δ 4.53 ppm. Careful attention was taken during the oxidation of **32** into the triradical **33**. Oxidation of **32** with $NaIO_4$ gave mixture of bi and triradicals. During the oxidation, the reaction was controlled by TLC, by noting the lowest R_f [petroleum ether: acetone 7:3] value of the blue spot, which corresponds to the triradical ($R_f \sim 0.41$). Formation of mixture of radicals was

unavoidable. The spots were identified as mixture of imino and nitronylnitroxides (R_f ~ 0.56), bisnitronylnitroxide radical (R_f ~ 0.49) and trisnitronylnitroxide radical (R_f ~ 0.41). The yield of the desired blue triradical **33** was ~ 2 mg after purification by preparative chromatography.

5.3.5 ESR studies

The solution ESR spectrum [Δms = ±1] of the triradical **33** in chloroform gave 13 lines in the spectrum with an intensity ratio close to 1:6:21:56:96:132:141:132:96:56:21:6:1, due to the coupling of the electron spins with the symmetrically situated six nitrogen nuclei (I =1). These 13 lines pattern further indicates that, the three radicals are strongly exchange coupled within the ESR limit with $J >> hfc$. The temperature dependant ESR spectra from 300 - 200 K gave clear 13 lines pattern at all temperatures ruling out the possibility of any bi and monoradical impurities. The spectrum was best simulated with line spacing of $a_N/3$ = 2.5 G and isotropic g value centered at 2.007 [Fig. 5.3.4.]. Accidentally, the forbidden Δms = ±2 and Δms = ±3 transitions were not observed. From the structural point of view triradical **33** can be compared with biradicals **1** and **2** with the same intraradical distance of ~1.5 nm. As explained in chapter 3 both **1** and **2** have high spin ground states (S=1). Based on this consideration, **33** is also expected to have ground state quartet (S = 3/2) due to the topological symmetry requirement. Semi empirical [ROAM1/CAS(9,9)] calculations performed for the *sym*-triradical **33** predict that, the doublet-quartet gap is ΔE_{DQ} = 0.36504 kcal/mol. The AM1 optimized torsion angles [Θ_1= 22°; Θ_2 = 2°; Θ_3 = 0°] and CIS(19,19) calculated spin densities are given in Fig. 5.3.5.

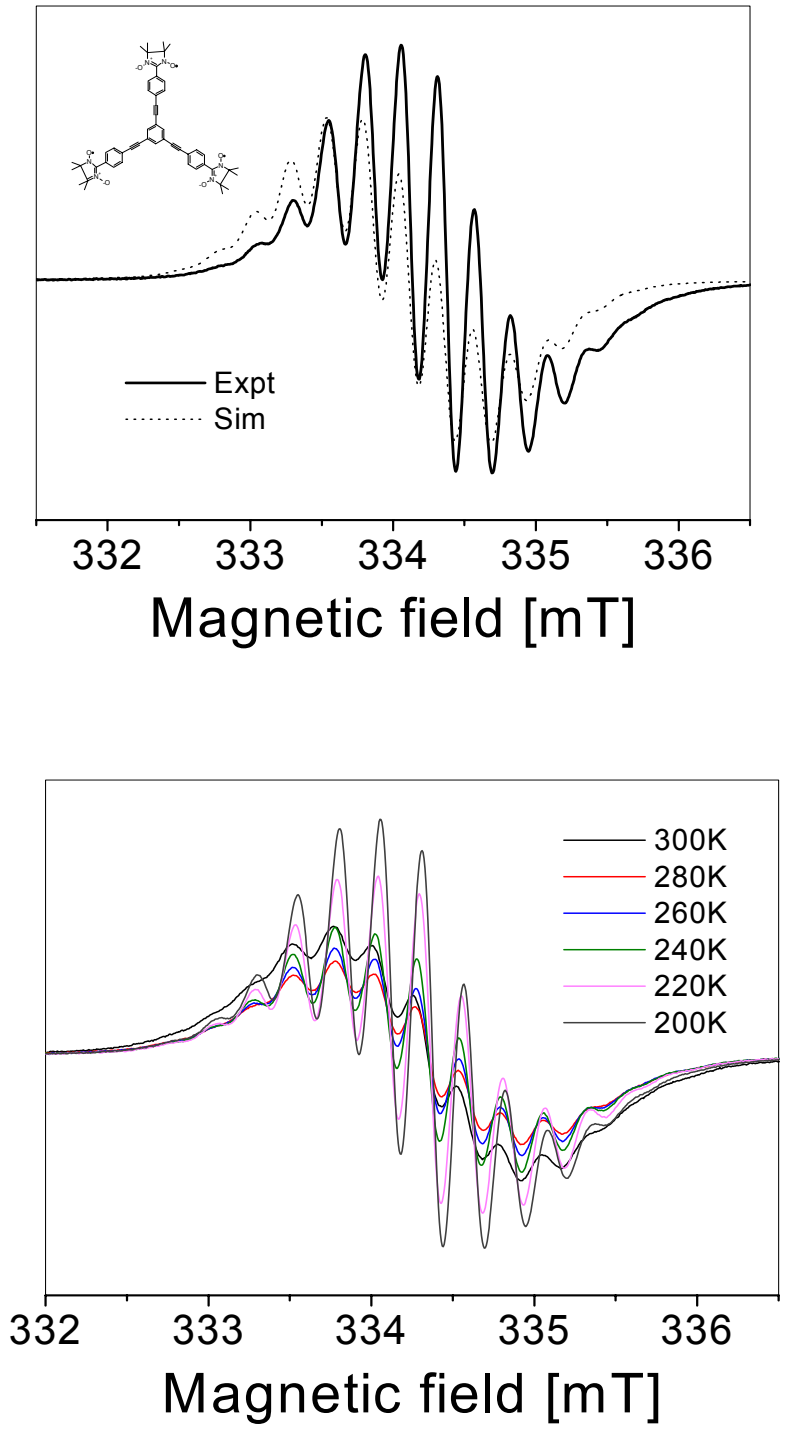

Figure 5.3.4. *ESR spectra of triradical* ***33*** *in* $CHCl_3$ *[ν = 9.407349 GHz; 2 scans; —— expt, ...sim]*

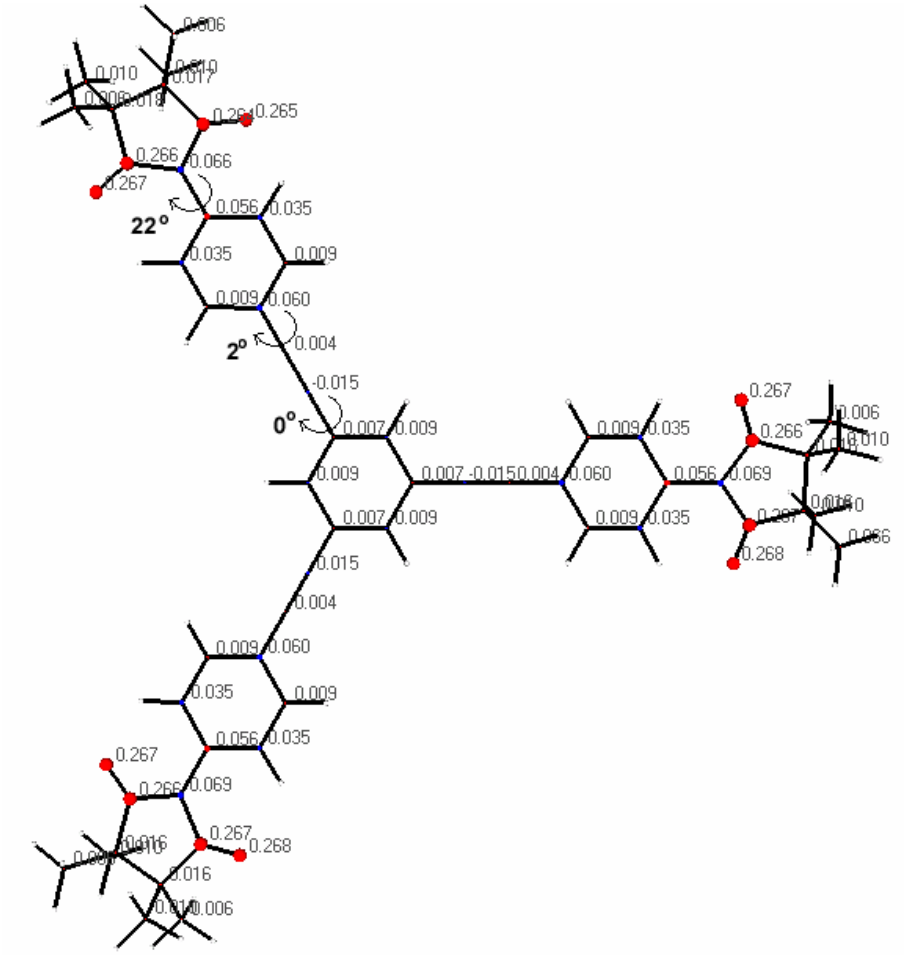

Figure 5.3.5. *AM1 optimized torsion angles and CIS (19,19) calculated spin densities.*

5.4 Conclusions

The two 1-D H-bonded polymeric chains are new members of hydrogen bonded stable organic radicals. The monoradical stacks are a good example of McConnell I postulates for ferromagnetic interactions. Their high degree of solid-state order is a demonstration of the possibilities of crystal engineering of molecular magnetic materials. Simplified approaches typically used to correlate molecular packing have shown not to be strongly predictive of experimental behavior. As a result more theoretical information is required to understand the relationship between crystal packing and the magnetic behavior.

5.4 References

1. G. R. Desiraju, *Angew. Chem*. **1995**, 107, 2541*, Angew. Chem. Int. Ed. Engl.* **1993**, 34, 2311.

2. a) J. Zhang, M. Baumgarten, *Chem. Phy.* **1997**, 222, 1. b) J. R. Ferrer, P. M. Lahti, C. George, P. Oliete, M. Julier, F. Palacio, *Chem. Mater.* **2001**; 13(7), 2447.

3. a) Y. Hosokoshi, K. Katoh, Y. Nakazawa, H. Nakano, K, Inoue, *J. Am. Chem. Soc*. **2001**, 123, 7921-7922. b) F. Ponzini, R. Zagha, K. Hardcastle, J. S. Siegel, *Angew. Chem. Int. Ed. Engl.* **2000**, 39, 13, 2323.

4. a) F. M. Romero, R. Ziessel, M. Bonnet, Y. Pontillon, E. Ressouche, J. Schweizer, B. Delley, A. Grand, C. Paulsen, *J. Am. Chem. Soc*. **2000**, 122, 1298 - 1309. b) F. M. Romero, R. Ziessel, M. Drillon, J. L. Tholence, C. Paulsen, N. Kyritsakas, J. Fisher, *Adv. Mater.* **1996**, 8, 826.

5. All the ESR spectral simulations were performed in WIN-SymFonia programme.

6. T. Takui, Y. Miura, K. Inui, Y. Teki, M. Inoue, K. Itoh, *Mol. Cryst. Liq. Cryst.* **1995**, 271, 55.

7. H. M. McConnell, *J. Chem. Phys.* **1963**, 39, 1916.

8. a) M. Deumal, J. Cirujeda, J. Veciana, J. J. Nova, *Adv. Mater.* **1998**, 10, 1461. b) M. Deumal, J. J.Nova, M. J. Bearoark, P. Celani, M. Olivucci, M. A. Robb, *J. Phys. Chem. A*. **1998**, 102, 8404.

6. SUMMARY

The result of the present work "High Spin Entities – A Supramolecular Approach via Pure Organic and Coordination Chemistry" can be summarized as follows:

Two novel high spin [S=1] ligands based on nitronylnitroxide **1** and **2,** monoradicals **3** - **5** and a symmetrical trisnitronylnitroxide **33** were synthesized. The preparation of the radicals involved mainly the following reactions: i) synthesis of bromoaldehyde ii) Sonogashira cross-coupling iii) deprotection of trimethylsilyl group iv) condensation reaction of aldehyde(s) with 2,3-dimethyl-2,3-bis(hydroxylamino)butane, and v) oxidation of the condensed products with $NaIO_4$. The structures of the radicals are given in Scheme 6.1.

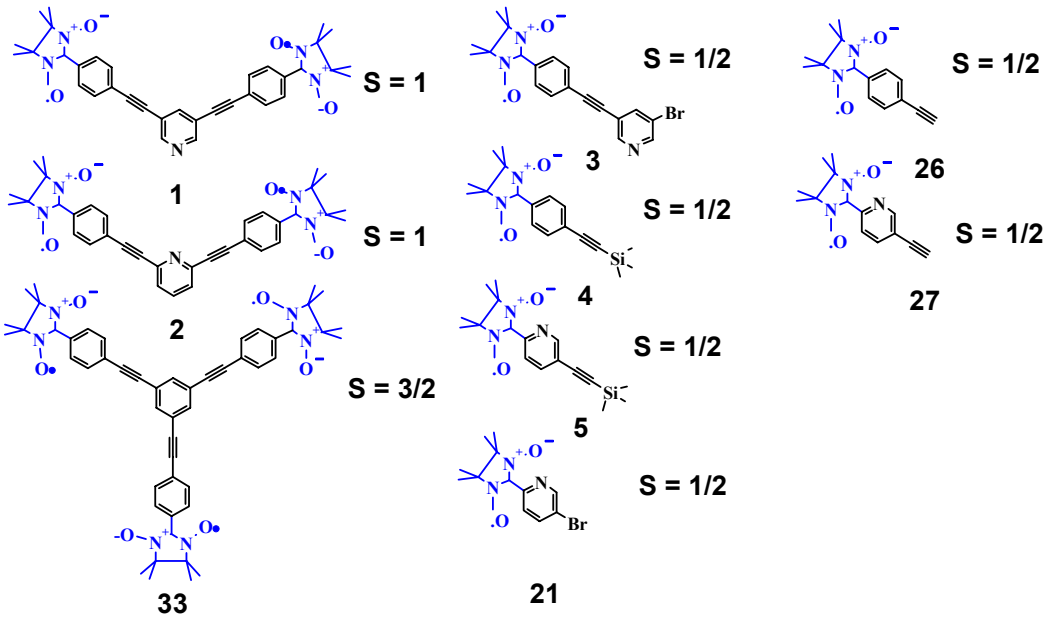

Scheme 6.1. *Mono- [**3-5**, **21**, **26**, and **27**], bi- [**1** and **2**], and trisnitronylnitroxide [**33**] radicals*

UV-Vis studies of the radicals were made to compare the influence of pyridine nitrogen on the extinction coefficients of the radicals where the backbones and functionalities are quite similar. In this scope, attempts were made to compare the extinction coefficients (n-π* transition) of all the radicals with and without pyridine moieties. As for the radicals **1**, **2**, **3**, **5**, **21** and **27** the extinction coefficients are lower

than for the corresponding benzene derivatives **4**, and **26**. In addition, the vibronic coupling patterns were also lost in the n-π* transition due to the loss of symmetry of the pyridine units compared to the benzene units.

Room temperature X-band ESR spectroscopic studies of the mono-, bis-, and trisnitronylnitroxide radicals in solution state displayed [Δms = ±1] five, nine, and thirteen line patterns with an intensity ratio close to 1:2:3:2:1; 1:4:10:16:19:16:10:4.1; and 1:6:21:56:96:132:141:132:96:56:21:6:1, respectively. The spacing between the lines are ~7.4 G [a_N]; 3.65 G [$a_N/2$], and 2.5 G [$a_N/3$] for the mono-, bi-, and triradicals with g_{iso} values centered at 2.0067. These results demonstrate that the bi-, and triradicals are strongly exchange coupled within the ESR limit ($J >> a_N$). Estimation of the *J* values by the fitting analysis of the isotropic spectra of **1** and **2** yielded the exchange interactions of 400 MHz as a minimum limit, further ascertaining that the $J >> a_N$. The frozen state samples of the biradicals **1** and **2** gave zero field splitting characteristic of a triplet state. From the measured D/hc values [~ 0.24×10^{-4} cm^{-1}] of the *zfs* spectra, the calculated average intraradical distance [r] between the two delocalized electron spin units using a point-dipolar approximation are ~ 1.02 nm. These distances were lower than those for the C-C spacing [r ~1.5 –1.3 nm] obtained from the single crystal X-ray diffraction studies. This indicates that some spin density is delocalized into the bridge. In order to ascertain the intraradical biradical nature of **1** and **2**, the temperature dependant signal intensity of the forbidden half field transitions [Δms = ±2] were followed down to liquid helium temperature, carefully avoiding saturation of the signals. The doubly integrated signal intensity followed a Curie pattern with strong increase in signal intensity down to liquid helium temperature indicating triplet ground state or its near degeneracy with the singlet state. Certainly the exchange coupling *J* cannot be very large, but a ferromagnetic exchange of *J* ~ 10-15 K is in line with the results, while an antiferromagnetic exchange could be as small as *J* < 2 K.

In order to determine more accurately ΔE_{ST}, single point energy calculations of the optimized structures with extended CI were made. The correlation included configurations resulting from the mixing of 8 electrons in 8 MOs (or CAS (8,8)). The effect of the out-of-plane rotation on the magnitude of the singlet - triplet splitting ΔE_{ST} was estimated by consideration of $\Theta_1 = 20^o$, $\Theta_2 = \Theta_3 = 3^o$ [from X- ray dihedral

angles of **1** were found to be $\Theta_1 = 21^o$, $\Theta_2 = 2.4^o$ and $\Theta_3 = 5.7^o$]. The calculations resulted in ΔE_{ST} of 4.1582 and 3.3262 KJ/mol for **1** and **2**. The triradical **33** also expected to have ground state quartet (S = 3/2) due to the topological symmetry requirement. Semi empirical [ROAM1/CAS (9,9)] calculations performed for the *sym*-triradical **33** predicts that the doublet-quartet gap is ΔE_{DQ} = 0.36504 kcal/mol. The AM1 optimized torsional angles are Θ_1= 22°; Θ_2 = 2°; Θ_3 = 0°.

Following the *organic-inorganic* hybrid approach to form a magnetic clusters, monoradical **21** was complexed with $Cu(hfac)_2$ and crystallized. X-ray studies showed a centrosymmetric linear trinuclear copper complex connected by two molecules of **21** forming a linear five half-spin system **22** [S_i = ½ (i = 1,2,...5)] coupled by isotropic exchange interaction between nearest neighbors. The magnetic susceptibility data displayed an antiferromagnetic behavior. The existence of two different exchange coupling parameters J_1 and J_2 were calculated by best fitting the magnetic data with the values J_1 = -440 cm^{-1}, J_2 = 10 cm^{-1}. To form extended linear coordination polymeric chains by exploiting the available two oxygens in a single radical, the monoradical **4** was successfully complexed with $Cu(hfac)_2$ and $Mn(hfac)_2$ to yield **23** and **24** respectively. Single crystal X-ray studies revealed the trans and cis coordinated 1-D alternating polymeric chains of **23** and **24**, respectively. The measured static magnetic susceptibility data of **23** and **24** show ferro-, and ferrimagnetic behaviors respectively, which were best fitted by using Heisenberg linear chain model with the isotropic *J* values for infinite chains. The extracted exchange coupling values of are *J* = 6 cm^{-1}, *g* = 2.1 for **23** and *J* = - 67 cm^{-1}, *zJ'* = -0.33 cm^{-1} for **24**. The ferrimagnetic nature of **24** was further confirmed from the saturation magnetization value 4 μ_B/mol, which is the expected value for an antiferromagnetically coupled $^5/_2$ – $^1/_2$ spin systems. To check the possibility of magnetic ordering in the investigated compound the dynamic magnetic susceptibility studies with and without an applied magnetic field were performed. But for all cases, no anomaly in the imaginary part of the dynamic magnetic susceptibility can be observed showing that there are no bulk magnetic properties in the material down to He temperature. In accordance with this observation, a measurement of magnetization yields no hysteresis at 4.5 K. Finally, the magnetic network formation was realized by reacting the high spin biradical **1** with $Cu(hfac)_2$. The challenging task of obtaining single crystals suitable for X- ray studies was successfully achieved. The crystal

structure revealed a complex dimeric network chain structure of **25**. The magnetic susceptibility data showed an antiferromagnetic behavior down to 14 K and below this temperature a ferromagnetic transition was observed. Due to the existence of four different types of copper, four exchange couplings [J_{intra}] within the chain can be expected.

Adopting the concept of *crystal engineering* and by following a *pure organic* approach, the designed doublet H-bonding synthons **26** and **27** were individually crystallized. X-ray analysis revealed that, both **26** and **27** are assembled in a linear 1-D polymeric chain like fashion via weak H- bonded intermolecular interactions [N-O···C≡C-H] of the radical oxygen and the acetylene hydrogen with N-O···C≡C- distances 3.181 Å and 3.155 Å, respectively. In order to establish the intramolecular spin wave propagation from the radical unit to the acetylene proton, solution ESR studies were undertaken to obtain well-resolved spectra. The proton hyperfine interaction values obtained from the well-resolved spectra of **26** and **27** were compared with those of **4** and **5**. The observed increase in the number of *hfc* lines of **26** and **27** in comparison to **4** and **5** showed that the extra lines originated from the interaction of acetylene protons with the electron spin. The obtained intramolecular magnetic data of **26** and **27** were well correlated with the bulk magnetic susceptibility data. From magnetic data, a decent magneto-structural correlation was made for the observed high temperature paramagnetic and low temperature antiferromagnetic behaviors.

Finally, crystallization of monoradical **21** followed by X-ray diagnosis revealed the π-π stacking arrangement of **21** with the stack distance [d] 3.7 Å and rotational angle [r] 60°. Besides stacking, H-bonding interaction mediated by water molecules between the radicals was also found. Magneto-structural correlation between the magnetic susceptibility data and the intermolecular contacts obtained from the crystal structure were made. The observed angle of rotation, stacking and H-bonding fulfilled the requirement of a ferromagnetic interaction according to McConnell I model, correlating well with the observed slight increase in μ_{eff} value below 3.5 K. The transition temperature would be just below the experimental measured temperature.
Extending the challenging notion of π-π stacking to the symmetrical triradical **33** [S = 3/2] was not possible due to low yield. Nevertheless, triradical **33** will definitely serve its purpose, if the final oxidation step is well optimized for high yield.

7. EXPERIMENTAL SECTION

7.1 Materials

P-Bromobenzaldehyde, 2,5-Dibromopyridine, 2,6-Dibromopyridine, 3,5-Dibromopyridine, Trimethylsilylacetylene (TMSA), Triphenylphosphine, $Pd(PPh_3)_2Cl_2$, CuI, 2,3-Dimethyl-2,3-bis(hydroxylamino)-butane sulphate salt $Cu(hfac)_2$ and $Mn(hfac)_2$ were purchased from Aldrich. n-BuLi (1.6 M in hexane), Triethylamine and dry Dimethylformamide (DMF) were purchased from Acros Organics. Tetrahydrofuran (THF) and toluene were distilled under argon in sodium and benzophenone before use. All the atmosphere-sensitive reactions were performed under argon using Schlenk line techniques. All the reactions were followed by thin-layer chromatography carried out on 0.25 mm ALUGRAM SIL G/ UV_{254} silica gel plates using UV detector. Column chromatography was performed on silica gel (E. Merck, 230-400 mesh). Purification of the radicals was done on PLC plates (20×20 mm) silica gel 60 F_{524} with concentrating zone (20×4 mm).

7.2 Physical Measurements

^{1}H NMR and ^{13}C NMR spectra were recorded on Bruker DPX250, 500DRX spectrometers with solvent proton or carbon signal as internal standards. UV/Vis spectra were recorded from Perkin Elmer spectrometer (UV/Vis/NIR Lambda 900). FD Mass spectra were obtained on a VG instruments ZAB-2-SE-FPD spectrometer. Infrared spectra were recorded using KBr pressed pellets on Nicolet 730 FT-IR spectrometer. ESR spectra were recorded on a CW X-band ESP 300 equipped with an NMR gauss meter (Bruker ER035), a frequency counter (Bruker ER 041 XK) and a variable temperature control continuous flow N_2 cryostat (Bruker B-VT 2000) or with Oxford system (ESR 910) helium continues flow cryostat. The solution ESR spectra were simulated using Bruker WINEPR - SimFonia programme. Melting points were measured on Büchi B-545 apparatus and are uncorrected. Elemental analysis carried out on Foss Heraeus Vario EL. Temperature dependent static susceptibilities of powdered samples were recorded using a Faraday-type magnetometer in a temperature range 4.2 to 300K. The measurements presented were done using a computer controlled Cahn D-200 microbalance and a Bruker B-MN 200/60 power

supply. The applied field was ~1.5 T .The diamagnetic corrections of the molar magnetic susceptibilities were applied using well-known Pascal's constants. The measurements of the dynamic magnetic susceptibility and the DC magnetization measurements were performed with a commercial Lake Shore AC/DC 7225 Susceptometer/Magnetometer. For compounds **22** and **25,** the magnetic susceptibility were measured on an MPMS-5S (Quantum Design) SQUID magnetometer over a temperature range of 2-300 K at 5 kOe.

7.3 Synthesis

7.3.1 Synthesis of 2,3-Dimethyl-2,3-bis(hydroxylamino)-butane (6)

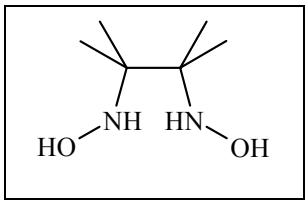

To an insoluble solution of 5 g of 2,3-dimethyl-2,3-bis(hydroxylamino)-butane sulphate salt (85%) in 40 mL of THF, 1.18 g of NaOH dissolved in 10 mL of distilled water was added in drop-by-drop to the insoluble sulphate salt in THF over 2 min and stirred for 10 min. The solid salt became soluble in THF /water mixture during the course of the reaction leaving Na_2SO_4 as insoluble mass. The solution was filtered off into the crystallizing disk and the solvents were evaporated. The formed dirty white precipitate was washed with hexane and cold acetone to get **6** as clean white crystalline powder. Yield 2.00 g (70%).

^{1}H NMR (250 MHz, D_2O, RT) δ: 1.25 (s, CH_3).
^{13}C NMR (62.5 MHz, D_2O, RT) δ: 21.5 (CH_3), 63.3 (CH_3-C-CH_3).
mp: 160-162 °C

7.3.2 Synthesis of 4-(Trimethylsilylethynyl)benzaldehyde (7)

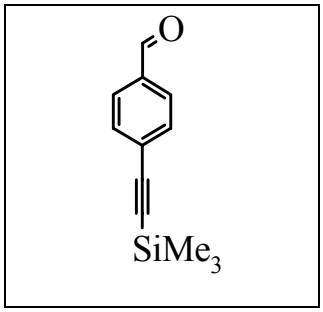

To a stirred suspension of 1.85 g (10.27 mmol) of 4-bromobenzaldehyde, 0.140 g of $Pd(PPh_3)_2Cl_2$, and 0.071 g of CuI in 20 mL of deaerated anhydrous Et_3N, was added 1.03 g (10.5 mmol) of trimethylsilylacetylene in 3 mL of desecrated THF by injecting through a rubber septum into

the dark brown reaction mixture within 20 min under argon. The formed black brown solution was heated to reflux at 70°C. After 3 hours the heating was stopped and just stirred for overnight. After evaporation of the solvents and column chromatography (petroleum ether (b.p. 30-40°C): acetone – 8:2), the resulting yellow fraction was left as such for crystallization for 3 days to give light yellow needle crystals of **7**. Yield 3.5 g (80%).

^{1}H NMR (250 MHz, $CDCl_3$, RT) δ: 9.85 (s, 1H, CHO), 7.60 (q, 4H, ^3J = 7 Hz, aromatic), 0.21 (s, 9H, $SiCH_3$).
FD MS (70 eV): m/z (%) 202.1 (100%).
FTIR (KBr disc; units in cm^{-1}): 2158 (s, C≡C); 1689 (s, C=O).
mp: 65 - 67°C (lit. 66-67°C)

7.3.3 Synthesis of 4-Ethynylbenzaldehyde (9)

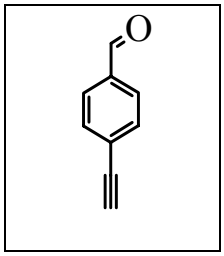

A solution of 1.0 g (4.94 mmol) of **7** and 0.2 g (1.45 mmol) of K_2CO_3 in 10 mL of deaerated anhydrous MeOH was stirred under argon atmosphere for 15 h. After evaporation of the solvent under reduced pressure the residue was treated with aq. $NaHCO_3$ (1 g in 10 mL of water). The formed light yellow organic layer was extracted with 20 mL of CH_2Cl_2, dried over $MgSO_4$ and filtered. The filtrate was evaporated to dryness to yellow mass and column chromatographed using petroleum ether: acetone (8:2) mixture and the resulted yellow solution was evaporated to give light yellow powder of **9**. Yield 0.65 g (100%).

TLC (8:2, petroleum ether: acetone): R_f ~ 0.6.
^{1}H NMR (250 MHz, $CDCl_3$, RT) δ: 10 (s, 2H, -CHO), 7.82 (d, 2H, ^3J = 6.95 Hz, H_2 and H_6), 7.62 (d, 2H, ^3J = 6.98 Hz, H_3 and H_5), 3.28 (s, 1H, -C≡H).
^{13}C NMR (62.5 MHz, $CDCl_3$, RT) δ: 191.4 (C=O), 135.9, 132.7, 129.5, 128.3, 82.6 (C≡C), 81.0 (C≡C).
FTIR (KBr disc; units in cm^{-1}): 3217 (C≡CH stretching); 2100 (w, C≡C); 1687 (s, C=O), 827 (CH out of plane deformation).
mp: 93 - 94°C (lit. 88-90°C).

7.3.4 Synthesis of 3,5-Bis(4-formylphenylethynyl)pyridine (10)

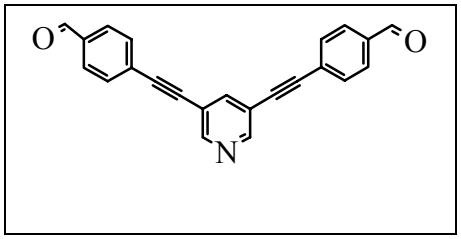

Twenty mililiters of freshly distilled triethylamine and 20 mL of THF were frozen in a Schlenk flask using liquid nitrogen, and 0.94 g (4 mmol) of 3,5-dibromopyridine, 0.141 g (0.2 mmol) of $Pd(PPh_3)_2Cl_2$, 1.3 g (10 mmol) of **9** and 0.0762 g (0.4 mmol) of CuI were added into the flask under argon over flow and deaerated by freeze-pump-thaw cycles for five times. The brown mixture was heated to reflux at 60°C for 4 days. After evaporation of the solvents the crude product was extracted with dichloromethane and evaporated to brownish yellow powder. In TLC ($CHCl_3$) the first spot from the top was dimer ($R_f \sim 0.75$) of **12** [m/z (%) 258.0 (100%)], the second was mono coupled product ($R_f \sim 0.5$) **11**, Yield 0.550 g (54%), and the third was the desired dialdehyde ($R_f \sim 0.2$) **10**. The fractions were separated by column chromatography ($CHCl_3$) to get yellowish monocoupled aldehyde and the desired yellow colored dialdehyde. Yield 0.335 g (27%).

TLC ($CHCl_3$): $R_f \sim 0.2$.

^{1}H NMR (250 MHz, $CDCl_3$, RT) δ: 10 (s, 2H, CHO), 9.7 (s, 2H, Py-H_2 and H_6), 7.95 (s, 1H, Py-H_4), 7.89 (d, 4H, ^3J = 8.21 Hz, Phenyl), 7.69 (d, 4H, ^3J = 8.22 Hz, Phenyl).

^{13}C NMR (62.5 MHz, $CDCl_3$, RT) δ: 191.26 (C=O), 151.39 (Py-C_2 and C_6), 140.87 (Py-C_4), 136.0 (Phenyl C-C=O), 132.3 (Phenyl C-H), 129.65 (Phenyl C-H), 128.29 (Phenyl C-acetylene), 119.57 (Py-C_3 and C_5), 92.38 (C≡C), 88.63 (C≡C).

FD MS (70 eV): m/z (%) 335.0 (100%).

UV (toluene, c = 10^{-4} M): 305 nm (ε = 32613 $M^{-1}cm^{-1}$).

FTIR (KBr disc; units in cm^{-1}): 3030 (s, Py-C-H), 2754 and 2856 (w, C-H, carbonyl), 1685 (vs, C=O), 825 (vs, aromatic CH out of plane deformation).

mp: 185 - 187°C (decomposed before melting).

7.3.5 Synthesis of 4-(5-Bromo-pyridine-3-ylethynyl)-benzaldehyde (11)

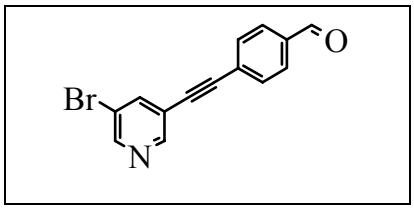

See the procedure for **10**.

TLC ($CHCl_3$): $R_f \sim 0.5$.

^{1}H NMR (250 MHz, $CDCl_3$, RT) δ: 10.02 (s, 1H, CHO), 8.68 (s, 1H, Py-H_2), 8.64 (d, 1H, Py-H_6, ^4J = 1.9 Hz), 7.99 (s, 1H, Py-H_4), 7.89 (d, 2H, ^3J = 8.21 Hz, phenyl), 7.38 (d, 2H, ^3J = 7.9 Hz, phenyl).

^{13}C NMR (62.5 MHz, DMSO-*d_6*, RT) δ: 191.98 (-CHO), 149.78 (Py-C_2 and C_6), 140.37 (Py-C_4), 135.53 (Phenyl **C**-C=O), 131.78 (Phenyl C-H), 129.19 (Phenyl C-H), 126.51 (Phenyl C-acetylene), 119.99 (Py-C_3 and C_5), 92.07 (C≡C), 87.48 (C≡C).

FD MS (70 eV): m/z (%) 285.2 (~89%) and 287.2 (100%).

FTIR (KBr disc; units in cm^{-1}): 3012 (w, Py CH stretching), 1680 (vs, C=O), 829 (s, aromatic CH out of plane deformation).

mp: 150-152^{o}C.

7.3.6 Synthesis of 4-(5-Bromo-pyridine-3-ylethynyl)-1-(1,3-dihydroxy-4,4,5,5-tetramethylimidazolin-2-yl)benzene (14)

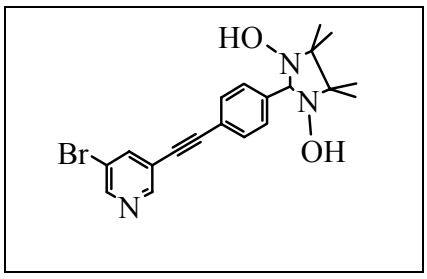

A 0.200 g (0.7 mmol) portion of **11** was taken in 10 mL each of toluene and methanol with 0.120 g (0.8 mmol) of 2,3-dimethyl-2,3-bis(hydroxylamino)-butane and refluxed at 90°C for three days under constant argon bubbling. The formed turbid yellow solution was filtered to obtain the condensation product **14** as yellow powder. Yield 0.134 g (46%)

^{1}H NMR (250 MHz, DMSO-*d_6*, RT) δ: 8.73 (s, 1H, Py-H_2), 8.72 (s, 1H, Py-H_6), 8.3 (s, 1H, Py-H_4), 7.55 (s, -OH), 7.23 (d, 2H, Phenyl), 7.16 (d, 2H, Phenyl), 4.54 (s, 1H, -CH-), 1.08 (-CH_3), 1.04 (-CH_3).

^{13}CNMR (62.5 MHz, DMSO-*d_6*, RT) δ: 150.1 and 149.7 (Py-C_2; C_6), 143.8 (Phenyl C- Imidazoline), 140.6 (Py-C_4), 130.99 (Phenyl C-H), 128.89 (Phenyl C-H), 128.21 (Phenyl **C**-acetylene), 120.1 and 119.94 (Py-C_3; C5), 93.98 (C≡C), 89.89 (C≡C), 84.40 (Imidazoline -CH-), 66.28 (Imidazoline -C-), 24.36 and 17.20 (-CH_3).

7.3.7 Synthesis of 4-(5-Bromo-pyridine-3-ylethynyl)-1-(1-oxyl-3-oxo-4,4,5,5-tetramethylimidazolin-2-yl)benzene (3)

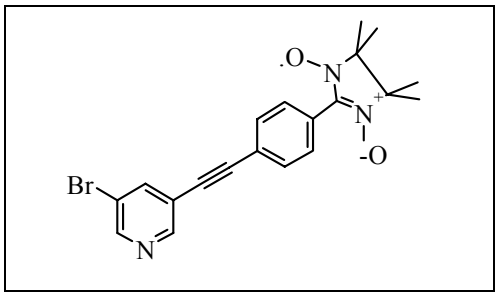

A 0.130 g (0.313 mmol) portion of **14** was taken with 0.069 g (0.32 mmol) of $NaIO_4$ in 25 mL each of chloroform and water. The solution was stirred for 20 min in an ice-cold bath. The formed blue organic layer was separated and dried over $MgSO_4$ and evaporated to give blue powder. The radical **3** was obtained as crystalline powder after column chromatography on silica gel (1:2 acetone / petroleum ether (b.p. 30-40°C); R_f ~ 0.74). Yield 26 mg (20%)

ESR (in toluene 10^{-3} M; RT; ν = 9. 397562 GHz; 2.01 mW power; 2 Scans): Five lines, g_{iso} = 2.0067, a_N = 7.40 G.

UV/Vis (toluene c = 10^{-5} M): 389 nm (ε = 9474 M^{-1} cm^{-1}), 620 nm (ε = 252 $M^{-1}cm^{-1}$). **FTIR (KBr disc; units in cm^{-1}):** 1354 (s, N-O).

mp: 167-169°C.

7.3.8 Synthesis of 3,5-Bis[4-(1,3-dihydroxy-4,4,5,5-tetramethylimidazolin-2-yl)phenylethynyl)]pyridine (13)

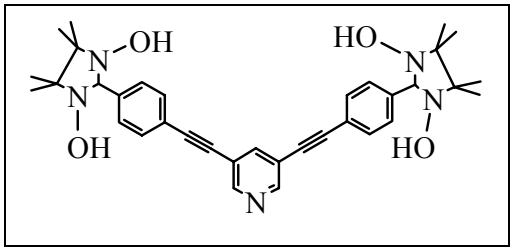

A 0.154 g (0.456 mmol) portion of **10** was dissolved in methanol and dichloromethane 15 mL each. After addition of 0,225 g (1.5 mmol) of 2,3-dimethyl-2,3-bis(hydroxylamino)-butane, the clear yellow solution was refluxed under argon bubbling at 60°C for 12 h. The light yellow precipitate of **13** was filtered and washed with chloroform and methanol, respectively. Yield 0.100 g (37%). Compound **13** was used for the next step without purification and characterization.

7.3.9 Synthesis of 3,5-Bis[4-(1-oxyl-3-oxo-4,4,5,5-tetramethylimidazolin-2-yl)phenylethynyl)]pyridine (1)

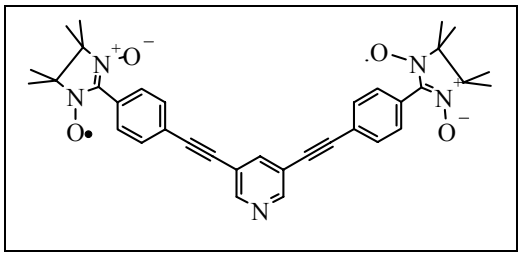

A 0.1 g (0.168 mmol) portion of **13** was taken in a phase-transfer solution of 10 mL each of chloroform and water. 0.1 g (0.465 mmol) of $NaIO_4$ was added into the solution and stirred for 10 min. The blue organic layer was separated and the aqueous layer was extracted with chloroform, the combined organic layers were concentrated into deep blue solution at 45°C under 75 mbar and purified by preparative chromatography (1:1 acetone: hexane) to yield **1** as blue powder. Yield 35 mg (35 %).

ESR (in toluene 10^{-3} M, RT, ν = 9.405596 GHz, 2.01 mW power, 2 Scans): Nine lines, g_{iso} = 2.0067, $a_N/2$ = 3.65 G.

UV/Vis (toluene, c = 10^{-5} M): 617 nm (ε = 470 $M^{-1}cm^{-1}$),387 nm(ε = 15972 $M^{-1}cm^{-1}$).

FTIR (KBr disc; units in cm^{-1}): 1390 (s, N-O).

Anal. Calcd. for $C_{35}H_{35}N_5O_4$: C 71.29; H 5.98; N 11.88. **Found:** C 70.28; H 6.20; N 11.49.

7.3.10 Synthesis of 2,6-Bis(4-formylphenylethynyl)pyridine (15)

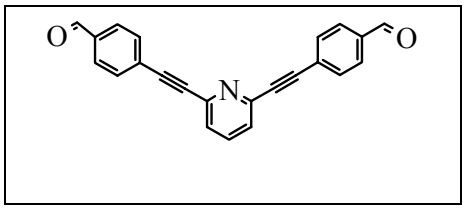

A 20 mL portion of triethylamine and 20 mL of THF were frozen in a dry Schlenk flask using liquid nitrogen, and 0.94 g (4.0 mmol) of 2,6-dibromo pyridine, 0.067 g (0.095 mmol) of $Pd(PPh_3)_2Cl_2$, 1.3 g (10 mmol) of **9**, and 0.0381 g (0.2 mmol) of CuI were added into the flask under argon over flow and deaerated using Schlenk line by freeze-pump-thaw cycles for 5 times. The brown mixture was refluxed with stirring at 60°C for 3 days under argon. The solvents from the crude reaction mixture were evaporated and extracted with dichloromethane and evaporated to brownish yellow powder. TLC (CH_2Cl_2): the first spot from the top was monocoupled [m/z (%) 285.2 (~89%) and 287.1 (100%)] and the second was the desired dialdehyde **15**. The fractions were

separated by column chromatography (CH_2Cl_2) to get yellowish dialdehyde. Yield 0.8 g (60%).

^{1}H NMR (250 MHz, $CDCl_3$, RT) δ: 10.02 (s, 2 H, CHO), 7.88 (d, 4 H, ^3J = 8.53 Hz, benzene), 7.74 (m, 5 H, the pyridine C_4-H and benzene protons also appears at the same ppm), 7.54 (d, 2 H, ^3J = 7.58, Py-H_3 and H_5).

^{13}C NMR (62.5 MHz, $CDCl_3$, RT) δ: 191.31 (C=O), 143.35 (Py-C_2 and C_6), 136.75 (Py-C_4), 136.09 (Phenyl **C**-C=O), 132.64 (Phenyl C-H), 129.56 (Phenyl C-H), 128.12 (Py-C_3 and C_5), 126.97 (Phenyl **C**-acetylene), 91.40 (C≡C), 88.52 (C≡C).

FD MS (70 eV): m/z (%) 335.3 (100%).

UV (toluene c = 10^{-4} M): 338 nm (ε = 28841 M^{-1} cm^{-1}).

FTIR (KBr disc; units in cm^{-1}): 3051 (w, Py-C-H), 2850 and 2736 (w, carbonyl C-H), 2210 (m, C≡C), 1697 (vs, C=O), 1601 (vs, aromatic C=C), 1558 (vs, aromatic C=N).

mp: 192-194 °C (decomposed before melting).

7.3.11 Synthesis of 2,6-Bis[4-(1,3-dihydroxy-4,4,5,5-tetramethylimidazolin-2-yl)phenylethynyl)]pyridine (17)

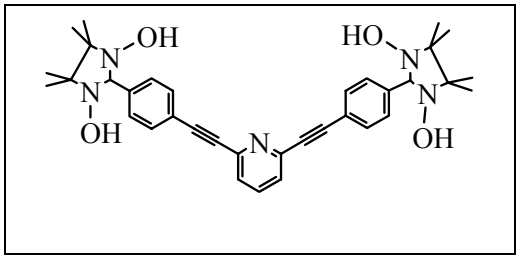

As described for the synthesis of **13**, 0.2 g (0.597 mmol) of **15** was dissolved in 10 mL of toluene and 5 mL of methanol, and after addition of 0.225 g (1.5 mmol) of 2,3-dimethyl-2,3-bis(hydroxylamino)-butane the turbid yellow solution was heated under argon bubbling to 80°C to get clear solution and then refluxed for 2 days. The formed yellow precipitate of **17** was filtered and washed with chloroform and methanol, respectively. Yield 0.215 g (61%).

^{1}H NMR (500 MHz, DMSO-d_6, RT) δ: 7.89 (t, 1 H, Py-H_4, ^3J = 8.01 Hz and ^3J = 7.78 Hz), 7.81 (s, -OH), 7.64 (d, 2H, Py-H_3 and H_5, ^3J = 7.86 Hz), 7.60 (d, 4 H, Phenyl, ^3J = 7.93 Hz), 7.58 (d, 4 H, Phenyl, ^3J = 7.99 Hz), 4.55 (s, 2 H, -CH-), 1.08 (s, 12 H, Si-CH_3) and 1.04 (s, 12 H, Si-CH_3).

7.3.12 Synthesis of 2,6-Bis[4-(1-oxyl-3-oxo-4,4,5,5-tetramethylimidazolin-2-yl)phenylethynyl)]pyridine (2)

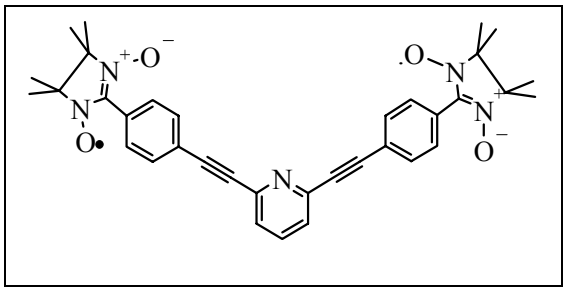

A 0.15 g (0.252 mmol) portion of **17** was taken in a phase-transfer solution of 15 mL each of chloroform and water. A 0.15 g (0.698 mmol) portion of $NaIO_4$ was added into the solution and stirred for 10 min. The blue organic layer was extracted with chloroform and concentrated into deep blue solution at 45°C under 75 mbar and purified by preparative chromatography (1:1 acetone: hexane) to afford blue powder of **2**. Yield 50 mg (34 %).

ESR (in toluene c = 10^{-3} M, RT, ν = 9.405379 GHz, 2.01 mW power, 2 Scans): Nine lines, $g_{iso} = 2.0067$, $a_N/2 = 3.65$ G.

UV/Vis (in toluene c = 10^{-5} M): 629 nm (ε = 499 M^{-1} cm^{-1}), 387 nm (ε = 19146 M^{-1} cm^{-1}).

FTIR (KBr disc; units in cm^{-1}): 1365 (s, N-O).

7.3.13 Synthesis of 4-Trimethylsilylethynyl-1-(1,3-hydroxy-4,4.5,5-tetramethylimidazoline-2-yl)benzene (8)

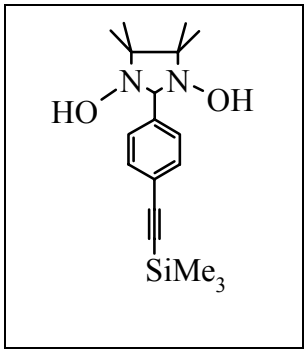

A 1.212 g (6 mmol) portion of **7** was dissolved in 10 mL each of THF and methanol. After addition of 0.975 g (6.5 mmol) of 2,3-dimethyl-2,3-bis(hydroxylamino)-butane, the solution was stirred at room temperature for 24 h. The formed white precipitate (**8**) was filtered and washed with chloroform and methanol, respectively. Yield 0.85 g (43%).

^{1}H NMR (250 MHz, DMSO-d_6, RT) δ: 7.82 (s, 2H, -OH), 7.46 (d, 2H, H_3 and H_5, ^3J = 8.21 Hz), 7.40 (d, 2H, H_2 and H_6, ^3J = 8.21 Hz), 4.49 (s, 1H, -CH-), 1.06 (s, 6H, -CH_3), 1.02 (s, 6H, -CH_3), 0.22 (s, 9H, Si-CH_3).

^{13}C NMR (62.5 MHz, DMSO-d_6, RT) δ: 142.63 (C_1), 130.47 (C_1), 128.17 (C_2), 120.57 (C_4), 105.02 (Imidazoline –CH-), 93.09 (C≡C), 89.39 (C≡C), 65.77 (Imidazoline-C-), 23.89, 16.72, 0.49 (Si-CH_3).

7.3.14 Synthesis of 4-Trimethylsilylethynyl-1-(4,4,5,5-tetramethyl-3-oxylimidazoline-1-oxide)benzene (4)

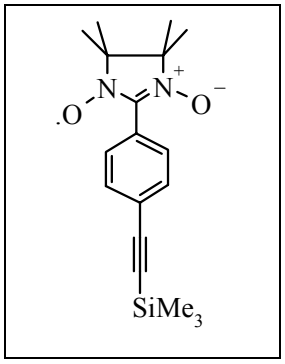

A 1.75 g (5.26 mmol) portion of **8** was taken with the phase-transfer solution of 80 mL of chloroform and 40 mL of water. A 2.16 g (1 mmol) portion of $NaIO_4$ was added into the solution and stirred for 1 h. The blue organic layer was extracted with chloroform and concentrated into deep blue oil and chromatographed on Al_2O_3. The dark blue layer was collected and evaporated to dryness to form blue crystals of **4**. Yield 1.37 g (79%).

ESR (in toluene, c = 10^{-3} M, RT, ν = 9.3984050 GHz, 2.01 mW power; 2 Scans): Five lines, g_{iso} = 2.0066, a_N = 7.41 G, a_H = 0.21 G (12 methyl protons) and a_H = 0.44 G (2 benzene ortho protons).

UV/Vis (in toluene, c = 10^{-5} M): 614 nm (ε = 339 M^{-1} cm^{-1}), 381 nm (ε = 12889 M^{-1} cm^{-1}).

FTIR (KBr disc; units in cm^{-1}): 2954 (m, broad, Si-C-H), 2158 (s, C≡C), 1363 (s, N-O).

Anal. Calcd. for $C_{18}H_{25}N_2O_2Si$: C 65.02; H 8.49 ; N 8.42. **Found:** C 64.82; H 8.23; N 8.52.

mp: 160-162 °C.

7.3.15 Synthesis of 2-formyl-5-bromopyridine (18)

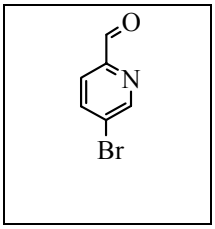

A solution of 10 g (41.2 mmol) of 2,5-dibromo pyridine in 500 mL dry toluene (distilled under argon) taken in a dry Schlenk flask was cooled to –78°C in a dry ice/ acetone bath. The flask was flushed with argon 3 times to ensure argon atmosphere. A 20 mL (50

mmol) portion of n-BuLi (1.6 M in hexane) was injected drop-by-drop into the flask within half an hour and stirred for 1 h at –78°C. After that, A 20 mL of dry DMF solution was injected immediately and the temperature was maintained at –78°C one more hour before the reaction mixture was allowed to warm up to room temperature overnight. The crude mixture was treated with saturated aqueous solution of NH_4Cl (100 mL) and the toluene organic layer was separated and evaporated to get viscous brown oil which became crystalline solid on standing. The solid was chromatographed on silica (3:2 CH_2Cl_2: Hexane, $R_f \sim 0.45$) to obtain compound **18** as cream powder. Yield 1.8 g (23%).

^{1}H NMR (250 MHz, DMSO-*d_6*, RT) δ: 9.95 (s, 1H, -CHO), 8.97 (s, 1H, Py-H_6), 8.31 (d, 1H, Py-H_3), 7.86 (d, 1H, Py-H_4, ^3J = 8.38 Hz).

^{13}C NMR (62.5 MHz, DMSO-*d_6*, RT) δ: 123.18 (Py-C_3), 125.53 (Py-C_5-Br), 140.38 (Py-C_4), 150.82 (Py-C_2), 151.1 (Py-C_6), 192.59 (C=O).

Anal. Calcd. for C_6H_4BrNO: C 38.74; H 2.17; N 7.53. **Found:** C 38.78; H 2.07; N 7.49.

mp: 96 - 98°C (lit. mp: 96.4 - 97.3°C).

7.3.16 Synthesis of 4-Trimethylsilylethynyl-1-formyl pyridine (19)

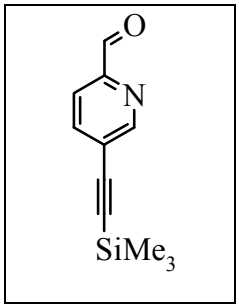

A total of 0.966 g of (5.30 mmol) of **18**, 0.141 g (0.2 mmol) of $Pd(PPh_3)Cl_2$, 0.0762 g (0.4 mmol) of CuI and 0.105 g (0.4 mmol) of PPh_3 was taken in a Schlenk flask fitted with rubber septum. 20 mL of deaerated triethylamine and 10 mL of THF were injected into the flask under argon atmosphere. A 1 mL (6.11 mmol) portion of trimethylsilylacetylene was injected into the flask drop-by-drop at room temperature and refluxed at 80°C for 5 h. The solvent from the crude mixture was evaporated and the crude mixture was extracted with chloroform and concentrated to dark brown mass. Which was chromatographed on silica using chloroform and the collected fractions were concentrated to solid mass.

The solid mass was washed with petroleum ether (b.p. 30-40°C) and the soluble fraction was evaporated to brown powder (**19**). Yield 0.69 g (64%).

In order to get very pure product alternatively sublimation was done for the crude product, the (light brown crystalline powder) yield was in the range of 30-33%.

^{1}H NMR (250 MHz, $CDCl_3$, RT) δ: 9.96 (s, 1H, -CHO), 8.86 (s, 1H, Py-H_6), 8.11 (d, 1H, Py-H_4), 7.9 (d, 1H, Py-H_3), 0.26 (s, 9H, Si-CH_3).

^{13}C NMR (62.5 MHz, $CDCl_3$, RT) δ: - 0.42 (-CH_3), 101.07 (C≡C), 101.87 (C≡C), 121.28 (Py-C_6), 123.3 (Py-C_5), 140.28 (Py-C_4), 150.93, (Py-C_1), 152.31 (Py-C_6) 192.74 (C=O).

FTIR (KBr disc; units in cm^{-1}): 2158 (w, C≡C); 1712 (s, C=O), 1576 (s, Py C=C stretching); 1559 (s, Py C=N).

mp: 79 - 81^{o}C.

7.3.17 Synthesis of 4-Trimethylsilylethynyl-1-(1,3-hydroxy-4,4.5,5-tetramethylimidazoline-2-yl) pyridine (20) and 4-Trimethylsilylethynyl-1-(4,4,5,5-tetramethyl-3-oxylimidazoline-1-oxide) pyridine (5)

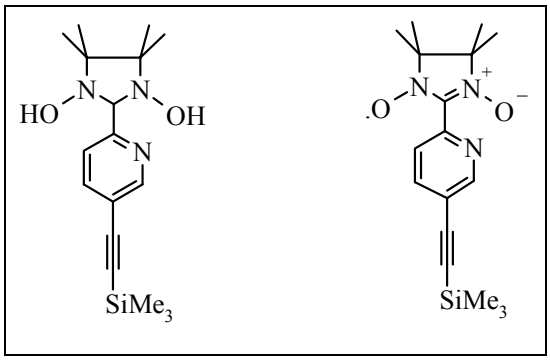

A suspension of 0.150 g of **19** (0.739 mmol) and 0.16g (1.07 mmol) of 2,3-dimethyl-2,3-bis(hydroxylamino)-butane in 20 mL of methanol was stirred at RT. After 2 days, no precipitate was found. Therefore the solvent was evaporated to get brown oily mass of **20** with initial aldehyde. Assuming 100% conversion (0.244 g) the brown mass was oxidized with 0.1 g (0.465 mmol) of $NaIO_4$ in chloroform/ water (50: 25) mixtures to give green solution. The monoradical **5** was separated using preparative chromatography (1:1 acetone: hexane, $R_f \sim 0.59$) to give violet crystals. Yield 76 mg (45 %)

ESR (in toluene, c = 10^{-3} M, RT, ν = 9.3984830 GHz, 2.01 mW, 2 Scans): Five lines, g_{iso} = 2.0067, a_N = 7.36 G, a_H = 0.21G (12 methyl protons), a_H = 0.32 G (1 pyridine ortho proton) and a_N = 0.45 G (1 pyridine nitrogen).

UV/Vis (in toluene, c = 10^{-5} M): 587 nm (ε = 277 M^{-1} cm^{-1}), 385 nm (ε = 12434 M^{-1} cm^{-1}).

FTIR (KBr disc; units in cm^{-1}): 3197 (s, Py-C-H stretching), 2991 (m, Si-C-H), 2100 (s, C≡C), 1362 (s, N-O), 1026 (Py ring breathing).

mp: 149 - 151°C.

7.3.18 Synthesis of 2-(5-Bromo-pyridin-2-yl)-4,4,5,5,-teramethyl-imidazolidine-1,3-diol

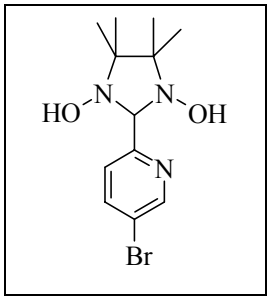

To a solution of 1.52 g (8.23 mmol) of **18** in benzene / methanol mixture (10 / 7.5 mL) was added 1.35 g (9.0 mmol) of 2,3-dimethyl-2,3-bis(hydroxylamino)butane. The mixture was stirred at room temperature under argon for 3 days. The formed light yellow precipitate was filtered and washed with benzene and methanol, respectively, to get a clear white powder. Yield 1.62 g (62.5%).

^{1}H NMR (250MHz, DMSO-d_6, RT) δ (ppm): 8.59 (s, 1H); 8.05 (d, 1H, ^{4}J = 2.21 Hz); 7.78 (s, 2H); 7.57 (d, 1H, ^{4}J = 2.53 Hz), 4.61 (s, 1H); 1.06 (s, 12H).

^{13}C NMR (62.5 MHz, DMSO-d_6, RT) δ (ppm): 160.48, 148.64, 138.77, 124.40, 119.06, 90.64 (-CH imidazoline), 66.47 (-C-$(CH_3)_2$), 23.99 (-CH_3), 17.46 (-CH_3).

7.3.19 Synthesis of 2-(4,4,5,5-Tetramethyl-3-oxylimidazoline-1-oxide)-5-bromopyridine (21)

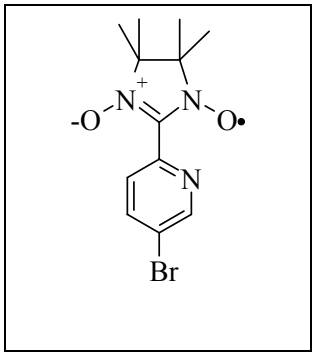

To a suspension of 1.62 g (5.14 mmol) of 2-(5-bromo-pyridin-2-yl)-4,4,5,5,-teramethyl-imidazolidine-1,3-diol in mixed solvents of 300 mL of $CHCl_3$ and 100 mL of water was added 1 g of $NaIO_4$ (5.1 mmol) and stirred for one and half hours to get dark blue solution. The blue organic layer was separated from the aqueous layer and dried over $MgSO_4$ and the solvent was evaporated to get blue powder.

Purification of the radical was done by recrystallization in petroleum ether (b.p. 40-65°C) to give blue crystalline powder. Yield 1.5 g (94%).

TLC (1:1; acetone: hexane): $R_f \sim 0.35$.

ESR (in $CHCl_3$, 10^{-3} M, RT, ν = 9.405026 GHz, 2 mW microwave power): Five lines; $g_{iso} = 2.0067$, $a_N = 7.4$ G, $\Delta B_{pp} = 2.8$ G, L/G = 0.33.

UV/Vis (in $CHCl_3$, values λ_{max} (ε)): 570 nm (437 M^{-1} cm^{-1}), 377 nm (17045 M^{-1} cm^{-1}).

FTIR (KBr disc; units in cm^{-1}): 2992 (ms, CH stretching), 1373 (vs, N-O), 1352 (vs), 1006 (vs, Pyridine ring breathing), 829 (CH out of plane deformation).

Anal. Calcd. for $C_{12}H_{16}BrN_3O_2$: C, 45.88%; H, 5.13%; N, 13.37%. **Found:** C, 45.61%; H, 5.12%; N, 13.18%.

7.3.20 Synthesis of Cu-complex of 2-(4,4,5,5 -Tetramethyl-3-oxylimidazoline 1-oxide)-5-Bromo pyridine (22)

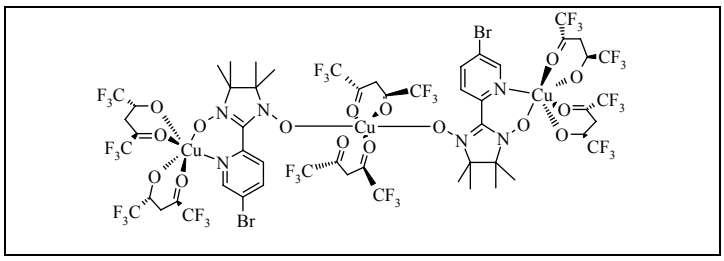

0.0156 g (0.05mmol) of **21** and 0.318 g (0.06mmol) of $Cu(hfac)_2$ as mono hydrate were dissolved in 20 mL of acetone and allowed to evaporate at room temperature, after 2 days dark brown crystals were found with colorless plates of $Cu(hfac)_2$. One of the crystals was selected for single crystal X-ray analysis. For magnetic measurements crystals of uniform quality were selected without contaminants. Yield 12.8 mg (~ 12%)

FTIR (KBr disc; units in cm^{-1}): 1376 (w, N-O), 1358 (vs).

Anal. Calcd. for $C_{54}H_{44}N_6Br_2Cu_3O_{16}F_{36}$: C, 31.37%; H, 2.15%; N, 4.07%. **Found:** C, 31.45%; H, 2.21%; N, 4.13%.

mp: 112-113°C.

7.3.21 Synthesis of Poly{[(4-Trimethylsilylethynyl-1-(4,4,5,5-tetramethyl-3-oxylimidazoline-1-oxide)benzene)]bis(hexafluoroacetylacetonato)copper(II) }(23)

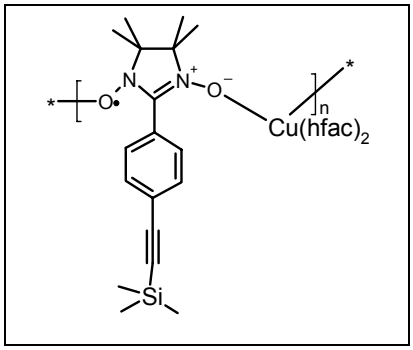

60 mg (0.12 mmol) of $Cu(hfac)_2.H_2O$ and 32.8 mg (0.1 mmol) of **4** were dissolved in hexane: dichloromethane (20 mL: 5 mL) mixture. The formed brown solution was left at room temperature for crystallization. After a day, the bluish green **23** plates were separated from the uncomplexed $Cu(hfac)_2$ plates. Careful microscopic examination showed that all the crystals formed were belonging to the same type. Yield 40 mg (49%).

FTIR (KBr disc; units in cm^{-1}): 1363 (ms, N-O); 1653 (vs, C=O); 2167 (ms, C≡C).

Anal. Calcd. for $C_{28}H_{27}N_2O_6F_{12}SiCu$: C 41.67%; H 3.37%; N 3.47%. **Found:** C 41.22%; H 4.14%, N 3.39%.

mp: 142- 143°C.

7.3.22 Synthesis of Poly{[(4-Trimethylsilylethynyl-1-(4,4,5,5-tetramethyl-3-oxylimidazoline-1-oxide)benzene)]bis(hexafluoroacetylacetonato)manganese(II)} (24)

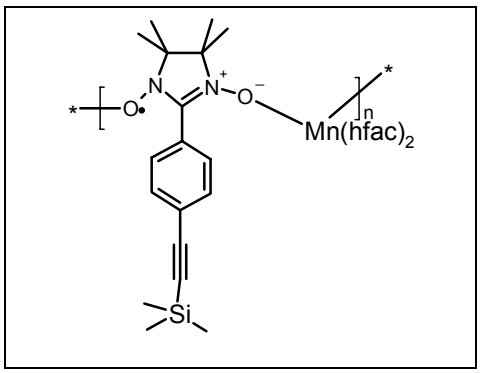

16.9 mg (0.052 mmol) of anhydrous $Mn(hfac)_2$ and 24.5 mg (0.052 mmol) of **4** were dissolved in acetone: heptane (5 mL each) mixture. The solution was left at room temperature for 3 days for crystallization to get black needles of **24**. Yield 10.5 mg (25%).

FTIR (KBr disc; units in cm^{-1}): 2171 (ms, C≡C); 1645 and 1652 (vs, C=O).

mp:117-120°C.

7.3.23 Synthesis of Network (25)

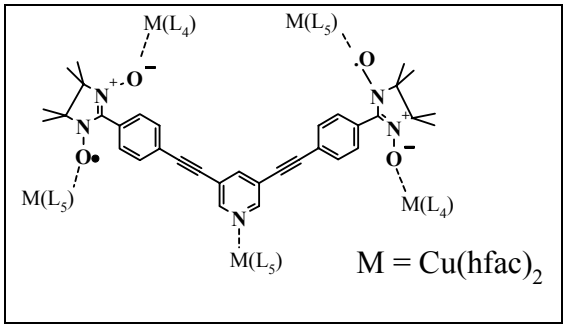

Recrystallization of 5.5 mg (0.0093 mmol) of biradical **1** and 31.05 g (0.095 mmol) of $Cu(hfac)_2.H_2O$ from dichloromethane via hexane diffusion gave micro crystals of **25**. The micro crystals were again recrystallized in dichloromethane: hexane mixture (1:2) by slow evaporation in a sample tube for two days to give **25** as hair like black needles. Yield 8.7 mg (21% calculated using M_r = 4522.9 for **25** in comparison with **1**).

mp: 150-152°C

7.3.24 Synthesis of 5-Ethynyl-pyridine-2-carbaldehyde (29)

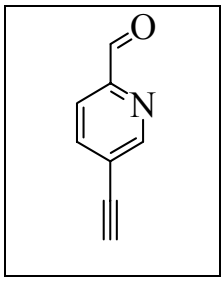

A 0.3 g (1.47 mmol) portion of **19** was taken in a dry Schlenk flask together with 0.1 g of K_2CO_3 and 10 mL of methanol was injected under argon atmosphere into the flask and stirred for 3 h. The solvent was evaporated and treated with 10 mL of $NaHCO_3$ solution (1 g in 10 mL) and than with 20 mL of dichloromethane. The organic layer was separated and evaporated to give **29** as yellow powder. Yield 0.134 g (70%).

TLC ($CHCl_3$): $R_f \sim 0.4$

^{1}H NMR (250 MHz, DMSO-d_6, RT) δ: 9.97 (s, 1H, -CHO), 8.89 (s, 1H, Py-H_6), 8.14 (d, 1H, Py-H_4, ^3J = 7.75 Hz), 7.91 (d, 1H, Py-H_3, ^3J = 7.90 Hz), 3.34 (s, 1H, C≡H).

^{13}C NMR (62.5 MHz, DMSO-d_6, RT) δ: 192.75 (C=O), 152.49 (Py-C_6), 151.07 (Py-C_1), 140.45 (Py-C_4), 122.99 (Py-C_5), 121.25 (Py-C_6), 87.52 (C≡C), 79.9 (C≡C).

FTIR (KBr disc; units in cm^{-1}): 3186 (vs, C≡C-H stretching), 2104 (vs, C≡C), 1689 (vs, -CHO).

mp: 121-122°C.

7.3.25 Synthesis of 2-(5-Ethynyl-pyridin-2-yl)-4,4,5,5-tetramethyl-imidazoline-1,3-diol (30)

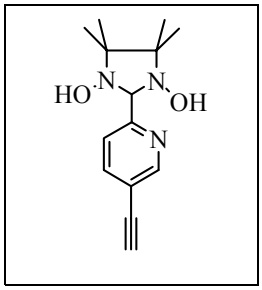

A 70 mg (0.53 mmol) portion of **29** was dissolved 10 mL of methanol. After addition of 0.100 g (0.67 mmol) of 2,3-dimethyl-2,3-bis(hydroxylamino)-butane, the solution was stirred at room temperature under argon atmosphere. After 3 days, the solvent from the flask were evaporated and the obtained yellow powder was washed with petroleum ether (b.p. 40-65°C) to remove the unreacted aldehydes to afford **30** as yellow powder. Yield 0.1 g (72.3%).

^{1}H NMR (250 MHz, DMSO-d_6, RT) δ: 8.58 (s, 1H); 7.89 (dd, 1H, ^4J = 1.9 Hz, ^3J = 8.2 Hz); 7.78 (s, 2H, -OH); 7.6 (d, 1H, ^3J = 8.21 Hz); 4.64 (s, 1H, imidazoline -CH); 3.16 (s, 1H, C≡CH); 1.06 (s, 12H, -CH_3).

^{13}C NMR (62.5 MHz, DMSO-d_6, RT) δ: 161.54 (C2); 150.56 (C6); 138.96 (C4); 122.12 (C3); 117.51 (C5); 90.99 (imidazoline –CH); 83.67 (C≡C); 80.71 (C≡C); 66.50 (imidazoline -C-(CH_3)$_2$); 24.01 (-CH_3); 17.44 (-CH_3).

7.3.26 Synthesis of 2-(5-Ethynyl-2-pyridyl)-4,4,5,5-tetramethylimidazoline- 1-oxyl (27)

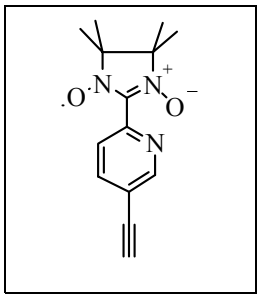

A 90 mg (0.345 mmol) portion of **30** was taken in a phase-transfer solution of 20 mL each of chloroform and distilled water and the flask was cooled in an ice bath. A 74 mg (0.345 mmol) portion of $NaIO_4$ was added into the flask and stirred rapidly for 5 min. The blue organic layer was separated, and the aqueous layer was extracted with 5 mL of dichloromethane repeatedly, and the combined organic layers were dried over $MgSO_4$, filtered and chromatographed on silica using acetone as an eluent (R_f ~ 0.8). The blue fractions from the column were collected and evaporated to blue powder and recrystallized in petroleum ether (b.p. 40-65°C): acetone mixture (5: 2) inside the refrigerator for a day to afford **27** as blue needles. Yield 0.53 mg (60%).

ESR (in toluene, c = 5*10^{-5} M, RT, ν = 9.401677 GHz, 1 Scan): Five lines, g_{iso} = 2.0068, a_N = 7.24 G.

FAB MS - (m/z): 259 (calcd. 259).

UV/Vis (in $CHCl_3$, c = 0.93*10^{-4} M): λ_{max} = 588 nm (ε = 166 M^{-1} cm^{-1}), λ_{max} = 387 nm (ε = 8332 M^{-1} cm^{-1}).

FTIR (KBr disc; units in cm^{-1}): 3199 (vs, C≡CH stretching), 2102 (w, C≡C), 1367(s, N-O), 837 (s, C-H out of plane deformation).

7.3.27 Synthesis of 2-(4-Ethynyl-phenyl)-4,4,5,5-tetramethyl-imidazolidine-1,3-diol (28)

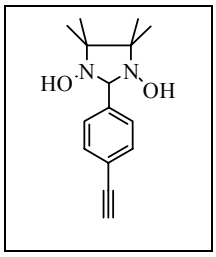

0.300 g (2.3 mmol) of **9** and 0.375 g (2.5 mmol) of 2,3-dimethyl-2,3-bis(hydroxylamino)-butane were taken together in a flask with 15 mL of methanol and strirred for 4 days at room temperature. The formed white precipitate was filtered to give the condensed product **28**. Yield 0.140 g (23%).

^{1}H NMR (250 MHz, DMSO-d_6, RT) δ: 7.8 (s, 2H, -OH); 7.45 (dd, 4H); 4.49 (s, 1H, imidazoline -CH); 4.43 (s, 1H, C≡CH); 1.06 (s, 6H, -CH_3); 1.02 (s, 6H, -CH_3).

7.3.28 2-(5-Ethynyl-2-phenyl)-4,4,5,5-tetramethylimidazoline-1-oxyl (26)

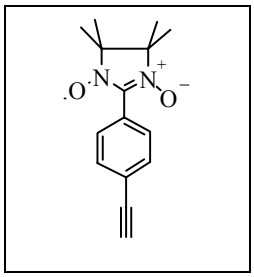

A 0.1 g (0.388 mmol) portion of **28** was taken with the phase-transfer solution of 10 mL each of dichloromethane and water. A 0.1 g (0.405 mmol) portion of $NaIO_4$ was added into the solution and stirred for 5 min. The dark blue organic layer was separated, dried over $MgSO_4$ and filtered. The blue powder was purified by preparative thin layer chromatography in 1:1 acetone: hexane (R_f = 0.88) and recrystallized at RT in acetone : petroleum ether (b.p. 40-65°C) mixture (1:1) to give **26** as blue needles. Yield 40 mg (40%).

ESR (in toluene, c = 10^{-4} M, RT, ν = 9. 399296 GHz, 1 Scan): Five lines, g_{iso} = 2.0068, a_N = 7.4 G.

FAB MS - (m/z): 258 (calcd. 258).

UV/Vis (in $CHCl_3$, c = 10^{-4} M): λ_{max} = 610 nm (ε = 280 M^{-1} cm^{-1}), λmax = 378 nm (ε = 11165 M^{-1} cm^{-1}).

FTIR (KBr disc; units in cm^{-1}): 3214 (s, ≡C-H), 2993 (ms, Si-CH), 2098 (ms, C≡C), 1363 (s, N-O), 837 (C-H out of plane deformation).

7.3.29 Synthesis of 1,3,5-Tris(4-formylphenylethynyl)benzene (31)

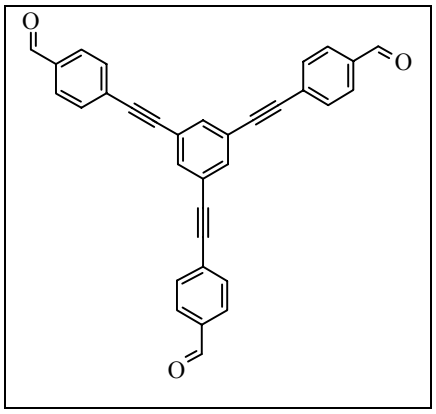

A total of 0.3 g (2 mmol) of 1,3,5-triethynyl benzene, 1.281 g (7 mmol) of p-bromobenzaldehyde, 0.14 g (0.2 mmol) of $Pd(PPh_3)Cl_2$, 0.76 g (0.4 mmol) of CuI, 0.210 g (0.4 mmol) of PPh_3, 20 mL each of Et_3N and THF was taken in a 100 mL Schlenk flask and frozen using liq.N_2 and deaerated using Schlenk line by freeze-pump-thaw cycles for 3 times. The mixture was refluxed under argon atmosphere at 70°C for 3 days. The crude was extracted with dichloromethane, after solvent evaporation to afford brownish yellow powder. The product was purified by column chromatography on silica using CH_2Cl_2 to remove the starting materials and finally washed with acetone to move the product from the top of the column (CH_2Cl_2; R_f ~ 0.53). The yield of the isolated yellow powder was 0.392 g (43%).

Alternatively purification was done by repeated washing of the crude product with acetone (the product is insoluble) to remove the starting materials. The separated trialdehyde was obtained as clean insoluble yellow powder.

^{1}H NMR (250 MHz, $CDCl_3$, RT) δ: 10.02 (s, 3H, -CHO), 7.88 (d, 6H, ^3J = 8.21 Hz), 7.72 (d, 6H, ^3J = 8.21 Hz), 7.65 (s, 3H, Phenyl core).

^{13}C NMR (62.5 MHz, $CDCl_3$, RT) δ: 191.29 (-CHO), 135.8, 134.81 (Phenyl core), 132.23, 129.63, 128.75, 123.67 (Phenyl core), 91.13 (C≡C), 89.98 (C≡C).

FD MS (70 eV): m/z (%) 462.4 (100%).

FTIR (KBr disc; units in cm^{-1}): 3055 (m, broad, aromatic C-H stretch), 2732 and 2825 (Carbonyl C-H), 2208 (w, C≡C), 1680 (vs, C=O), 1579 (vs, ring stretch), 823 (vs, 1,3,5-Trisubstituted benzene C-H out of plane deformation).

mp: 222°C (decomposed before melting).

7.3.30 Synthesis of 1,3,5-Tris[4-(1,3-dihydroxy-4,4,5,5-tetramethylimidazolin-2-yl)phenylethynyl)]benzene (32)

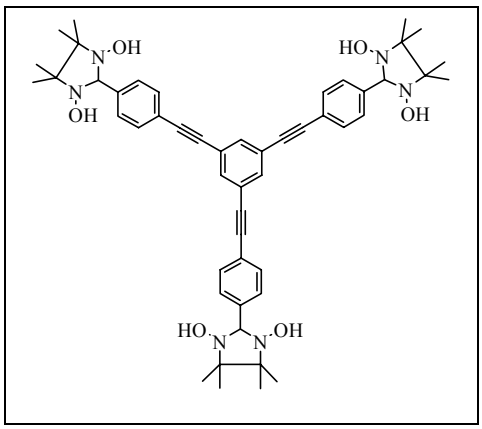

A 0.175 g (0.378 mmol) portion of **31** was dissolved by heating in 50 mL of dioxane and filtered to get a clean yellow solution. To this solution, 0.240 g (1.6 mmol) of 2,3-dimethyl-2,3-bis(hydroxylamino)-butane was added and stirred at RT for a week. The formed turbid solution was filtered to afford yellow powder of **32**. Yield 25 mg (8%)

^{1}H NMR (250 MHz, DMSO-d_6, RT) δ: 7.84 (s, 6H, -OH), 7.74 (s, 3H, Phenyl core), 7.55 (s, 12H), 4.54 (s, 3H, Imidazoline -CH-).
FD MS (70 eV): m/z (%) 834.0 (-OH$^+$) (100%).

7.3.31 Synthesis of 1,3,5-Tris[4-(1-oxyl-3-oxo-4,4,5,5-tetramethylimidazolin-2-yl)phenylethynyl)]benzene (33)

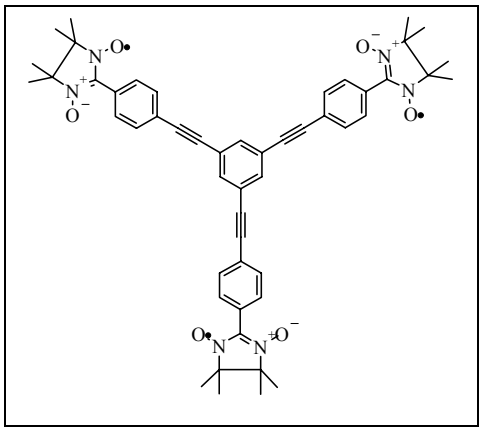

A portion of 22 mg (0.026 mmol) of **32** was taken in a phase-transfer solution of $CHCl_3$ / water [10/20 mL each]. A 100 mg portion of $NaIO_4$ (0.46 mmol) was added into the solution and stirred for 10 min. During the oxidation after 5 min the formed blue color solution turned into mixture of colors. The organic layer was separated from the aqueous layer and dried over $MgSO_4$. After evaporation of the solvent, TLC (petroleum ether (b.p. 40-65°C): acetone 7:3) was performed to identify the radicals formed. The spots were indentified as mixture of imino and nitronylnitroxides (R_f ~ 0.56), bisnitronylnitroxide radical (R_f ~ 0.49) and

trisnitronylnitroxide radical (R_f ~ 0.41). The crude product was purified by preparative chromatography. Yield ~ 2 mg (9%).

TLC ($CHCl_3$): R_f ~ 0.41

ESR ($CHCl_3$; ν = 9.407349 GHz; 200 K; 2 scans): g_{iso} = 2.007; $a_N/3$ = 2.5 G; ΔB_{pp} = 2.20 G; L/G = 0.33.

UV/Vis (in $CHCl_3$): λ_{max} = 608 nm, λ_{max} = 389 nm.

8. *APPENDIX*

8.1. Crystallographic Data for 1

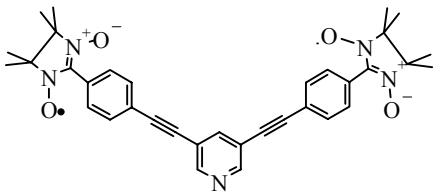

TABLE 8.1. *Crystal data and structure refinement for* ***1***

	1
Empirical Formula	$C_{17.5}H_{17.5}O_2N_{2.5}$
Formula weight	294.85
Temperature	293
Wavelength (Cu Kα), Å	1.5418
Crystal system, space group	Monoclinic, C2/c
a, Å	29.4916(1)
b, Å	8.3957(6)
c, Å	13.4508(7)
β (°)	112.9050(2)
Volume ($Å^3$)	3067.9
Z, ρ(g/cm^3)	8, 1.272
Absorption coefficient (cm^{-1})	6.479
F(000)	1251.958
Crystal size (mm)	0.53 × 0.21 × 0.14
Theta range for data collection (°)	0 to 65
Index ranges	-34<=h<=31, 0<=k<=9, 0<=l<=15
Reflections collected / unique	10092 / 2764
Refinement method	Full-matrix least-square on F
Data / restraints / parameters	1673 / 0 / 202
Goodness-of-fit on F^2	1.020
Final R indices [I>2σ (I)]	R1 = 0.046, R_w = 0.055
Largest diff. peak and hole	0.73 and -0.49 $Å^{-3}$

TABLE 8.2. *Atomic coordinates and Equivalent Isotropic Displacement Parameters*

Atom	x/a	y/b	z/c	U(iso)Occ
O(1)	0.11744(12)	0.0129(3)	0.4125(3)	0.0954
O(2)	0.19201(12)	0.4362(3)	0.3186(3)	0.1024
N(1)	0.0000	1.0941(5)	0.7500	0.0695
N(2)	0.14469(11)	0.0956(3)	0.3775(2)	0.0568
N(3)	0.17894(11)	0.2949(3)	0.3309(2)	0.0589
C(2)	0.01600(12)	0.8445(4)	0.6807(3)	0.0546
C(4)	0.03499(13)	0.7606(4)	0.6123(3)	0.0619
C(5)	0.05185(14)	0.6815(4)	0.5610(3)	0.0622
C(6)	0.07370(12)	0.5756(4)	0.5086(3)	0.0556
C(9)	0.12048(11)	0.3650(4)	0.4177(2)	0.0477
C(12)	0.14667(12)	0.2550(4)	0.3749(2)	0.0472
C(13)	0.17756(13)	0.0129(4)	0.3326(3)	0.0561
C(14)	0.20088(13)	0.1557(4)	0.2961(3)	0.0558
C(1)	0.01411(13)	1.0099(4)	0.6825(3)	0.0642
C(3)	-0.000000(7)	0.7613(6)	0.750000(7)	0.0537
C(7)	0.08068(13)	0.4174(4)	0.5397(3)	0.0618
C(8)	0.10343(14)	0.3131(4)	0.4955(3)	0.0589
C(10)	0.11263(15)	0.5222(4)	0.3852(3)	0.0649
C(11)	0.08914(15)	0.6264(5)	0.4287(3)	0.0711
H(11)	0.02291(13)	1.0674(4)	0.6319(3)	0.0715
H(31)	-0.000000(7)	0.6482(6)	0.750000(7)	0.0651
H(71)	0.06956(13)	0.3808(4)	0.5931(3)	0.0724
H(81)	0.10761(14)	0.2048(4)	0.5175(3)	0.0689
H(101)	0.12221(15)	0.5578(4)	0.3292(3)	0.0720
H(111)	0.08374(15)	0.7342(5)	0.4056(3)	0.0824
C(15)	0.21209(18)	-0.0883(6)	0.4207(4)	0.1041
H(151)	0.23342(18)	-0.1439(6)	0.3950(4)	0.1116
H(152)	0.23101(18)	-0.0225(6)	0.4797(4)	0.1116
H(153)	0.19388(18)	-0.1628(6)	0.4436(4)	0.1116
C(16)	0.14462(17)	-0.0930(6)	0.2417(4)	0.0925
H(161)	0.16395(17)	-0.1480(6)	0.2104(4)	0.1028
H(162)	0.12815(17)	-0.1679(6)	0.2688(4)	0.1028
H(163)	0.12104(17)	-0.0284(6)	0.1885(4)	0.1028
C(17)	0.25579(15)	0.1682(6)	0.3517(5)	0.1074
H(171)	0.27104(15)	0.0816(6)	0.3313(5)	0.1148
H(172)	0.26451(15)	0.1658(6)	0.4275(5)	0.1148
H(173)	0.26654(15)	0.2656(6)	0.3323(5)	0.1148
C(18)	0.1854(2)	0.1689(6)	0.1754(3)	0.1097
H(181)	0.1987(2)	0.0823(6)	0.1501(3)	0.1162
H(182)	0.1974(2)	0.2663(6)	0.1591(3)	0.1162
H(183)	0.1505(2)	0.1669(6)	0.1411(3)	0.1162

8.2 Crystallographic Data for 2

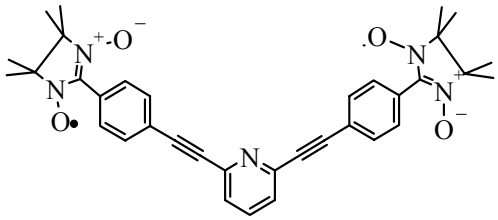

TABLE 8.3. *Crystal data and structure refinement for* ***2***

	2
Empirical Formula	$C_{42}H_{43}O_4N_{.5}$
Formula weight	681
Temperature	120
Wavelength (Cu Kα), Å	1.5418
Crystal system, space group	Monoclinic, P 2_1/a
a, Å	11.2915(8)
b, Å	18.5346(9)
c, Å	18.3792(9)
β (°)	101.929
Volume ($Å^3$)	3763.4(6)
Z, ρ(g/cm^3)	8, 1.205
Absorption coefficient (cm^{-1})	6.001
F(000)	1452.493
Crystal size (mm)	0.32 × 0.24 × 1.3
Theta range for data collection (°)	0 to 65
Index ranges	-13<=h<=12, 0<=k<=21, 0<=l<=21
Reflections collected / unique	26633 / 6589
Refinement method	Full-matrix least-square on F
Data / restraints / parameters	1864 / 0 / 385
Goodness-of-fit on F^2	1.012
Final R indices [I>2σ (I)]	R1 = 0.098, R_w = 0.114
Largest diff. peak and hole	0.76 and -0.53 $Å^{-3}$

Remark: Structure contains one molecule of toluene per asymmetric unit.

TABLE 8.4. *Atomic coordinates and Equivalent Isotropic Displacement Parameters*

Atom	x/a	y/b	z/c	U(iso)Occ
O(1)	-0.3744(6)	0.7073(4)	0.4532(6)	0.0462
O(2)	-0.6103(6)	0.5006(4)	0.4027(5)	0.0424
O(3)	-0.1548(7)	-0.1353(5)	-0.0238(5)	0.0519
O(4)	-0.4792(7)	-0.0534(6)	0.0711(7)	0.0777
N(1)	0.0501(6)	0.2890(4)	0.3006(5)	0.0169
N(3)	-0.4656(7)	0.6630(5)	0.4413(6)	0.0342
N(4)	-0.5794(7)	0.5670(4)	0.4149(6)	0.0313
N(5)	-0.2640(9)	-0.1252(5)	-0.0160(6)	0.0399
N(6)	-0.4168(8)	-0.0882(6)	0.0310(7)	0.0528
C(1)	0.1020(8)	0.3473(5)	0.3359(6)	0.0179
C(4)	0.1240(8)	0.2392(5)	0.2794(6)	0.0175
C(5)	0.0204(9)	0.3984(5)	0.3587(6)	0.0235
C(6)	-0.0544(9)	0.4377(6)	0.3743(6)	0.0281
C(7)	-0.1552(8)	0.4786(5)	0.3899(7)	0.0229
C(10)	-0.3572(8)	0.5515(6)	0.4150(7)	0.0309
C(13)	-0.4639(8)	0.5918(5)	0.4247(6)	0.0186
C(14)	-0.5898(8)	0.6895(6)	0.4461(7)	0.0293
C(15)	-0.6711(8)	0.6268(5)	0.4074(6)	0.0244
C(20)	0.0623(9)	0.1778(5)	0.2416(6)	0.0221
C(21)	0.0041(8)	0.1283(6)	0.2107(6)	0.0233
C(22)	-0.0666(9)	0.0725(5)	0.1686(6)	0.0264
C(25)	-0.2174(9)	-0.0290(6)	0.0819(6)	0.0293
C(28)	-0.295(1)	-0.0805(5)	0.0339(7)	0.0353
C(29)	-0.3718(13)	-0.1570(7)	-0.0674(9)	0.0634
C(30)	-0.4671(11)	-0.1490(8)	-0.0196(11)	0.0693
C(2)	0.2273(8)	0.3595(5)	0.3498(6)	0.0211
C(3)	0.2491(8)	0.2460(5)	0.2911(6)	0.0188
C(104)	0.2997(8)	0.3082(5)	0.3276(6)	0.0231
C(8)	-0.1414(8)	0.5357(5)	0.4374(7)	0.0255
C(9)	-0.2408(8)	0.5719(5)	0.4522(6)	0.0225
C(11)	-0.3710(9)	0.4954(5)	0.3660(7)	0.0289
C(12)	-0.2695(8)	0.4589(6)	0.3525(7)	0.0287
C(23)	-0.054(1)	0.0557(6)	0.0980(7)	0.0394
C(24)	-0.1260(11)	0.0053(7)	0.0537(7)	0.0409
C(26)	-0.229(1)	-0.0146(6)	0.1544(7)	0.0358
C(27)	-0.156(1)	0.0346(6)	0.1975(7)	0.0382
H(21)	0.2613(8)	0.4026(5)	0.3732(6)	0.0232
H(31)	0.2980(8)	0.2095(5)	0.2760(6)	0.0215
H(1041)	0.3849(8)	0.3149(5)	0.3376(6)	0.0255
H(81)	-0.0616(8)	0.5507(5)	0.4594(7)	0.0275
H(91)	-0.2317(8)	0.6092(5)	0.4883(6)	0.0229
H(111)	-0.4495(9)	0.4819(5)	0.3398(7)	0.0346
H(121)	-0.2776(8)	0.4201(6)	0.3180(7)	0.0338
H(231)	0.005(1)	0.0818(6)	0.0792(7)	0.0473
H(241)	-0.1125(11)	-0.0058(7)	0.0057(7)	0.0432
H(261)	-0.289(1)	-0.0401(6)	0.1732(7)	0.0402
H(271)	-0.167(1)	0.0443(6)	0.2465(7)	0.0414
C(16)	-0.587(1)	0.6968(8)	0.5288(9)	0.0543
H(161)	-0.662(1)	0.7144(8)	0.5361(9)	0.0602
H(162)	-0.524(1)	0.7294(8)	0.5503(9)	0.0602
H(163)	-0.571(1)	0.6508(8)	0.5517(9)	0.0602
C(17)	-0.611(1)	0.7614(7)	0.407(1)	0.0630
H(171)	-0.688(1)	0.7797(7)	0.410(1)	0.0588
H(172)	-0.550(1)	0.7949(7)	0.428(1)	0.0588

H(183)	-0.8107(9)	0.5639(6)	0.4201(8)	0.0356
H(173)	-0.607(1)	0.7540(7)	0.356(1)	0.0588
C(18)	-0.7725(9)	0.6059(6)	0.4438(8)	0.0406
H(181)	-0.8295(9)	0.6442(6)	0.4387(8)	0.0356
H(182)	-0.7427(9)	0.5961(6)	0.4951(8)	0.0356
C(19)	-0.7169(11)	0.6366(8)	0.3240(8)	0.0597
H(191)	-0.7757(11)	0.6740(8)	0.3167(8)	0.0765
H(192)	-0.6520(11)	0.6496(8)	0.3010(8)	0.0765
H(193)	-0.7529(11)	0.5932(8)	0.3025(8)	0.0765
C(31)	-0.393(2)	-0.1095(9)	-0.135(1)	0.1060
H(311)	-0.460(2)	-0.1247(9)	-0.172(1)	0.1212
H(312)	-0.406(2)	-0.0614(9)	-0.120(1)	0.1212
H(313)	-0.321(2)	-0.1113(9)	-0.154(1)	0.1212
C(32)	-0.3404(13)	-0.2319(8)	-0.088(1)	0.0800
H(321)	-0.4073(13)	-0.2524(8)	-0.122(1)	0.0835
H(322)	-0.3240(13)	-0.2593(8)	-0.044(1)	0.0835
H(323)	-0.2713(13)	-0.2323(8)	-0.110(1)	0.0835
C(33)	-0.4728(15)	-0.2122(8)	0.0320(12)	0.0928
H(331)	-0.5059(15)	-0.2530(8)	0.0036(12)	0.1031
H(332)	-0.5226(15)	-0.2000(8)	0.0660(12)	0.1031
H(333)	-0.3936(15)	-0.2233(8)	0.0587(12)	0.1031
C(34)	-0.5939(13)	-0.131(1)	-0.0608(15)	0.1437
H(341)	-0.6282(13)	-0.170(1)	-0.0916(15)	0.1010
H(342)	-0.6434(13)	-0.120(1)	-0.0262(15)	0.1010
H(343)	-0.5889(13)	-0.090(1)	-0.0907(15)	0.1010
C(41)	0.305(2)	-0.1070(14)	0.2097(11)	0.1275
C(42)	0.2366(18)	-0.1325(11)	0.2561(12)	0.1140
C(43)	0.110(2)	-0.1502(15)	0.2346(15)	0.1561
C(44)	0.058(2)	-0.1403(15)	0.1631(15)	0.1495
C(45)	0.136(2)	-0.1144(14)	0.1167(13)	0.1421
C(46)	0.255(2)	-0.1018(14)	0.1356(13)	0.1286
H(421)	0.2728(18)	-0.1346(11)	0.3075(12)	0.1424
H(431)	0.065(2)	-0.1673(15)	0.2694(15)	0.1822
H(441)	-0.024(2)	-0.1543(15)	0.1442(15)	0.2090
H(451)	0.096(2)	-0.1012(14)	0.0678(13)	0.1919
H(461)	0.301(2)	-0.0884(14)	0.0998(13)	0.1587
C(47)	0.433(2)	-0.0934(15)	0.2333(18)	0.1941
H(471)	0.466(2)	-0.0802(15)	0.1917(18)	0.1704
H(472)	0.475(2)	-0.1344(15)	0.2569(18)	0.1704
H(473)	0.442(2)	-0.0544(15)	0.2675(18)	0.1704

8.3 Crystallographic data for 21

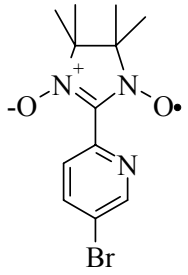

TABLE 8.5. *Crystal data and structure refinement for* ***21***

	21
Empirical Formula	$C_{12}H_{15}O_2N_3Br$
Formula weight	331.19
Temperature	120
Wavelength (Mo Kα), Å	0.7107
Crystal system, space group	Tetragonal, P-42_1c
a, Å	19.5394(5)
b, Å	19.5394(5)
c, Å	7.2742(4)
α, β, γ (°)	90
Volume ($Å^3$)	2777.2(1)
Z, ρ(g/cm^3)	8, 1.58
Absorption coefficient (cm^{-1})	2.968
F(000)	1349.592
Crystal size (mm)	0.44 × 0.18 × 0.11
Theta range for data collection (°)	0 to 28.95
Index ranges	0<=h<=26, 0<=k<=18, -9<=l<=9
Reflections collected / unique	31627 / 3936
Refinement method	Full-matrix least-square on F
Data / restraints / parameters	1974 / 0 / 172
Goodness-of-fit on F^2	1.078
Final R indices [I>2σ (I)]	R1 = 0.0403, R_w = 0.0471
Largest diff. peak and hole	0.69 and -0.49 $Å^{-3}$

TABLE 8.6. *Atomic coordinates and Equivalent Isotropic Displacement Parameters*

Atom	x/a	y/b	z/c	U(iso)	Occ
Br(1)	0.51713(3)	0.10840(3)	0.57729(11)	0.0396	
N(1)	0.3079(2)	0.09706(19)	0.5334(5)	0.0236	
N(2)	0.1904(2)	0.22747(19)	0.3894(5)	0.0214	
N(3)	0.16592(17)	0.14673(18)	0.5882(6)	0.0216	
O(1)	0.2241(2)	0.2694(2)	0.2897(6)	0.0408	
O(2)	0.17355(18)	0.09970(19)	0.7086(6)	0.0328	
C(1)	0.4242(2)	0.1337(2)	0.5486(7)	0.0228	
C(4)	0.2908(2)	0.1632(2)	0.5128(6)	0.0191	
C(6)	0.2169(2)	0.1780(2)	0.4965(7)	0.0191	
C(7)	0.1149(2)	0.2305(2)	0.3968(7)	0.0259	
C(8)	0.0963(2)	0.1755(2)	0.5432(7)	0.0214	
C(2)	0.4063(2)	0.2016(2)	0.5235(7)	0.0259	
C(3)	0.3374(3)	0.2159(2)	0.5040(6)	0.0212	
C(5)	0.3743(2)	0.0837(2)	0.5526(8)	0.0265	
H(21)	0.4398(2)	0.2368(2)	0.5232(7)	0.0221	
H(31)	0.3222(3)	0.2612(2)	0.4799(6)	0.0223	
H(51)	0.3879(2)	0.0375(2)	0.5704(8)	0.0234	
O(11)	0.0889(2)	0.0484(2)	0.9956(6)	0.0425	
H(1)	0.1168(2)	0.0658(2)	0.8994(6)	0.0300	
H(2)	0.0745(2)	0.0020(2)	0.9979(6)	0.0300	
C(9)	0.0951(3)	0.3024(3)	0.4484(16)	0.0687	
H(91)	0.1057(3)	0.3352(3)	0.3562(16)	0.0431	
H(92)	0.1213(3)	0.3116(3)	0.5555(16)	0.0431	
H(93)	0.0477(3)	0.3050(3)	0.4773(16)	0.0431	
C(10)	0.0894(5)	0.2139(5)	0.205(1)	0.0868	
H(101)	0.1017(5)	0.2504(5)	0.125(1)	0.0701	
H(102)	0.0414(5)	0.2064(5)	0.198(1)	0.0701	
H(103)	0.1129(5)	0.1735(5)	0.169(1)	0.0701	
C(11)	0.0531(3)	0.1174(3)	0.471(1)	0.0457	
H(111)	0.0440(3)	0.0853(3)	0.566(1)	0.0325	
H(112)	0.0110(3)	0.1342(3)	0.423(1)	0.0325	
H(113)	0.0781(3)	0.0957(3)	0.375(1)	0.0325	
C(12)	0.0679(5)	0.2049(4)	0.718(1)	0.0700	
H(121)	0.0590(5)	0.1687(4)	0.802(1)	0.0668	
H(122)	0.0990(5)	0.2364(4)	0.773(1)	0.0668	
H(123)	0.0263(5)	0.2277(4)	0.690(1)	0.0668	

8.4 Crystallographic data for 22

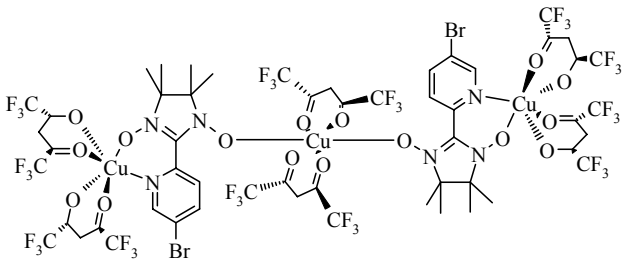

TABLE 8.7 *Crystal data and structure refinement for* ***22***

	22
Empirical Formula	$C_{54}H_{44}N_6Br_2Cu_3O_{16}F_{36}$
Formula weight	2068
Temperature	120
Wavelength (Mo Kα), Å	0.7107
Crystal system, space group	Triclinic, P-1
a, Å	11.0071(4)
b, Å	12.7406(5)
c, Å	13.6999(5)
α, β, γ (°)	72.610(1), 78.821(1), 82.330(1)
Volume ($Å^3$)	1792.8
Z, ρ(g/cm^3)	2, 1.907
Absorption coefficient (mm^{-1})	2.1438
F(000)	1011.432
Crystal size (mm)	0.38 × 0.16 × 0.09
Theta range for data collection (°)	0 to 32
Index ranges	-15<=h<=16, -17<=k<=18, 0<=l<=20
Reflections collected / unique	42231 / 12109
Refinement method	Full-matrix least-square on F
Data / restraints / parameters	7980 / 0 / 529
Goodness-of-fit on F^2	1.041
Final R indices [I>2σ (I)]	R1 = 0.032, R_w = 0.036
Largest diff. peak and hole	0.81 and -0.69 $Å^{-3}$

TABLE 8.8 *Atomic coordinates and Equivalent Isotropic Displacement Parameters*

Atom	x/a	y/b	z/c	U(iso)Occ
Cu(1)	0.23410(2)	0.26045(2)	-0.083969(18)	0.0170
Cu(2)	0.0000	0.0000	0.5000	0.0194
Br(1)	-0.24300(2)	0.122112(19)	-0.066469(18)	0.0247
O(1)	0.33520(14)	0.14941(12)	0.00538(11)	0.0212
O(2)	0.08350(14)	0.11702(15)	0.32207(11)	0.0253
O(21)	0.38240(16)	0.33899(14)	-0.15286(12)	0.0260
O(22)	0.27528(16)	0.17218(13)	-0.20697(12)	0.0255
O(23)	0.12624(15)	0.36580(12)	-0.17216(12)	0.0240
O(24)	0.20366(16)	0.37995(13)	0.01615(12)	0.0250
O(31)	-0.14600(14)	0.06758(13)	0.43973(12)	0.0226
O(32)	-0.00124(15)	0.11436(14)	0.56545(13)	0.0267
F(1)	0.4785(2)	0.53295(16)	-0.2501(2)	0.0625
F(2)	0.62407(17)	0.4051(2)	-0.23579(18)	0.0588
F(3)	0.5626(3)	0.4751(3)	-0.38175(16)	0.0859
F(4)	0.2961(3)	0.24763(18)	-0.46413(15)	0.0671
F(5)	0.43766(17)	0.12317(16)	-0.41320(13)	0.0430
F(6)	0.2484(2)	0.0935(2)	-0.35419(16)	0.0594
F(7)	0.15977(19)	0.52901(16)	-0.36692(13)	0.0489
F(8)	-0.02706(17)	0.49004(14)	-0.30001(13)	0.0429
F(9)	0.03656(17)	0.63927(12)	-0.29375(13)	0.0395
F(10)	0.2436(3)	0.66052(15)	-0.04211(18)	0.0678
F(11)	0.1705(3)	0.5592(3)	0.1049(2)	0.0885
F(12)	0.3536(2)	0.52531(19)	0.0353(2)	0.0741
F(31)	-0.38010(15)	0.11290(15)	0.40063(16)	0.0460
F(32)	-0.26229(19)	0.2256(2)	0.28563(14)	0.0583
F(33)	-0.38374(19)	0.27699(17)	0.40900(19)	0.0591
F(34)	-0.0028(3)	0.22754(18)	0.69723(16)	0.0662
F(35)	-0.1537(2)	0.3379(2)	0.6413(3)	0.0820
F(36)	0.0267(2)	0.34554(18)	0.55089(17)	0.0593
C(1)	-0.11391(18)	0.11925(16)	0.00721(16)	0.0195
C(4)	0.07593(18)	0.12556(16)	0.10510(14)	0.0175
C(6)	0.18184(17)	0.13215(16)	0.15270(14)	0.0172
C(7)	0.39012(18)	0.14409(17)	0.17041(15)	0.0205
C(8)	0.30015(18)	0.15814(18)	0.27020(15)	0.0208
C(21)	0.5243(3)	0.4435(3)	-0.2801(2)	0.0398
C(22)	0.4298(2)	0.35642(19)	-0.24678(17)	0.0263
C(24)	0.3335(2)	0.21874(19)	-0.29237(16)	0.0238
C(25)	0.3274(2)	0.1706(2)	-0.38208(18)	0.0315
C(26)	0.0695(2)	0.53294(19)	-0.28700(19)	0.0287
C(27)	0.1162(2)	0.46884(17)	-0.18515(16)	0.0226
C(29)	0.1936(2)	0.47904(17)	-0.03243(17)	0.0232
C(30)	0.2396(2)	0.55712(19)	0.01734(19)	0.0288
C(31)	-0.3094(2)	0.1942(2)	0.3862(2)	0.0312
C(32)	-0.20463(19)	0.15575(18)	0.45106(16)	0.0218
C(34)	-0.0808(2)	0.19537(19)	0.56133(16)	0.0245
C(35)	-0.0538(2)	0.2785(2)	0.6145(2)	0.0328
N(1)	0.08496(15)	0.17653(13)	0.00201(12)	0.0171
N(2)	0.29867(15)	0.14604(14)	0.10183(12)	0.0180
N(3)	0.17951(15)	0.12909(15)	0.25234(13)	0.0192
C(2)	-0.12355(19)	0.06521(17)	0.11189(17)	0.0219
C(3)	-0.02699(19)	0.06999(17)	0.16241(16)	0.0210
C(5)	-0.00950(19)	0.17387(16)	-0.04578(15)	0.0191
C(23)	0.4096(2)	0.3068(2)	-0.31904(17)	0.0305
C(28)	0.1462(2)	0.52907(17)	-0.12529(18)	0.0257
C(33)	-0.1841(2)	0.22033(19)	0.51106(18)	0.0261
H(21)	-0.19407(19)	0.02619(17)	0.14822(17)	0.0258
H(31)	-0.03082(19)	0.03546(17)	0.23462(16)	0.0265
H(51)	-0.00520(19)	0.21021(16)	-0.11770(15)	0.0249

H(231)	0.4482(2)	0.3338(2)	-0.38904(17)	0.0395
H(281)	0.1356(2)	0.60733(17)	-0.14821(18)	0.0323
H(331)	-0.2404(2)	0.28212(19)	0.51758(18)	0.0344
C(9)	0.4749(2)	0.2372(2)	0.11788(18)	0.0290
H(91)	0.5261(2)	0.2225(2)	0.05833(18)	0.0375
H(92)	0.5256(2)	0.2423(2)	0.16478(18)	0.0375
H(93)	0.4258(2)	0.3048(2)	0.09768(18)	0.0375
C(10)	0.4651(2)	0.0321(2)	0.18365(19)	0.0310
H(101)	0.5165(2)	0.0303(2)	0.11979(19)	0.0378
H(102)	0.5154(2)	0.0217(2)	0.23532(19)	0.0378
H(103)	0.4103(2)	-0.0251(2)	0.20407(19)	0.0378
C(11)	0.2759(2)	0.2765(2)	0.27728(19)	0.0294
H(111)	0.2211(2)	0.2776(2)	0.33981(19)	0.0358
H(112)	0.3520(2)	0.3042(2)	0.27694(19)	0.0358
H(113)	0.2391(2)	0.3213(2)	0.21983(19)	0.0358
C(12)	0.3326(2)	0.0801(2)	0.37146(17)	0.0285
H(121)	0.2742(2)	0.0943(2)	0.42787(17)	0.0369
H(122)	0.4136(2)	0.0909(2)	0.37894(17)	0.0369
H(123)	0.3299(2)	0.0061(2)	0.37073(17)	0.0369

8.5 Crystallographic data for 23

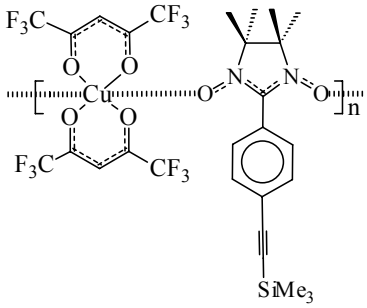

TABLE 8.9 *Crystal data and structure refinement for* ***23***

	23
Empirical Formula	$C_{28}H_{30}CuSiF_{12}O_6N_2$
Formula weight	810.14
Temperature	120
Wavelength (Mo Kα), Å	0.7107
Crystal system, space group	Monoclinic, $P2_1/n$
a, Å	13.8702(7)
b, Å	9.3331(5)
c, Å	26.854(1)
α, β, γ (°)	90, 90.291(1), 90
Volume ($Å^3$)	3476.3
Z, ρ(g/cm^3)	4, 1.542
Absorption coefficient (cm^{-1})	7.647
F(000)	1635
Crystal size (mm)	0.33 × 0.15 × 0.09
Theta range for data collection (°)	0 to 27.5
Index ranges	-17<=h<=18, 0<=k<=12, 0<=l<=34
Reflections collected / unique	26993 / 8021
Refinement method	Full-matrix least-square on F
Data / restraints / parameters	7980 / 0 / 529
Goodness-of-fit on F^2	0.961
Final R indices [I>2σ (I)]	R1 = 0.0821, R_w = 0.0875
Largest diff. peak and hole	1.31 and -0.61 $Å^{-3}$

TABLE 8.10. *Atomic coordinates and Equivalent Isotropic Displacement Parameters*

Atom	x/a	y/b	z/c	U(iso)	Occ
Cu(1)	0.24706(6)	1.23079(8)	0.08950(3)	0.0154	
F(4)	-0.0797(3)	1.2227(5)	0.18690(16)	0.0316	
F(5)	-0.0704(3)	1.3402(5)	0.11857(18)	0.0329	
F(6)	-0.0714(3)	1.1088(5)	0.11762(19)	0.0374	
F(7)	0.5699(4)	1.1757(9)	-0.0056(2)	0.0691	
F(8)	0.5627(4)	1.1174(9)	0.0694(2)	0.0689	
F(9)	0.5684(4)	1.3342(9)	0.0524(4)	0.1051	
F(10)	0.2298(6)	1.3372(6)	-0.0887(2)	0.0640	
F(11)	0.1395(4)	1.1632(9)	-0.06528(19)	0.0664	
F(12)	0.2772(4)	1.1221(6)	-0.09713(17)	0.0450	
O(11)	0.2783(3)	1.2110(5)	0.15906(17)	0.0230	
O(12)	0.1098(3)	1.2227(5)	0.10286(17)	0.0216	
O(13)	0.3847(3)	1.2392(5)	0.07695(17)	0.0218	
O(14)	0.2148(3)	1.2392(5)	0.01977(17)	0.0216	
C(21)	0.2653(6)	1.1881(11)	0.2464(3)	0.0487	
C(22)	0.2186(6)	1.2062(9)	0.1942(3)	0.0309	
C(24)	0.0728(5)	1.2202(8)	0.1451(2)	0.0213	
C(25)	-0.0391(5)	1.2221(9)	0.1421(2)	0.0264	
C(26)	0.5325(6)	1.2168(11)	0.0368(3)	0.0390	
C(27)	0.4211(5)	1.2222(8)	0.0345(3)	0.0253	
C(29)	0.2745(5)	1.2201(8)	-0.0155(2)	0.0203	
C(30)	0.2297(6)	1.2112(11)	-0.0672(3)	0.0378	
C(23)	0.1169(6)	1.2130(9)	0.1909(3)	0.0320	
C(28)	0.3756(5)	1.2086(9)	-0.0110(3)	0.0301	
H(231)	0.0792(6)	1.2146(9)	0.2203(3)	0.0443	
H(281)	0.4126(5)	1.1863(9)	-0.0396(3)	0.0389	
F(1)	0.3358(9)	1.0990(13)	0.2461(5)	0.0757	
F(2)	0.3025(9)	1.3092(13)	0.2612(5)	0.0719	
F(3)	0.2034(8)	1.1297(14)	0.2789(4)	0.0721	
F(21)	0.3465(14)	1.274(2)	0.2500(7)	0.0719	
F(22)	0.2089(14)	1.217(2)	0.2827(7)	0.0721	
F(23)	0.3096(16)	1.050(2)	0.2459(9)	0.0757	
Si(1)	0.85349(13)	0.7260(2)	0.24666(7)	0.0210	
O(1)	0.2784(4)	0.9730(5)	0.0760(2)	0.0263	
O(2)	0.2538(4)	0.4844(5)	0.1021(2)	0.0279	
N(1)	0.2467(4)	0.8431(6)	0.0779(2)	0.0177	
N(2)	0.2374(4)	0.6116(6)	0.0873(2)	0.0185	
C(1)	0.7337(4)	0.7274(9)	0.2172(2)	0.0235	
C(2)	0.6573(5)	0.7292(8)	0.1958(2)	0.0226	
C(3)	0.5667(5)	0.7290(9)	0.1702(2)	0.0237	
C(6)	0.3885(4)	0.7282(7)	0.1199(2)	0.0167	
C(9)	0.2934(4)	0.7277(7)	0.0956(2)	0.0173	
C(10)	0.1418(5)	0.8114(8)	0.0657(3)	0.0310	
C(11)	0.1510(5)	0.6484(8)	0.0550(3)	0.0306	
C(4)	0.5101(5)	0.8528(8)	0.1657(3)	0.0289	
C(5)	0.4233(5)	0.8538(8)	0.1403(3)	0.0284	
C(7)	0.4429(5)	0.6027(8)	0.1229(3)	0.0252	
C(8)	0.5302(5)	0.6042(8)	0.1476(3)	0.0269	
H(41)	0.5324(5)	0.9390(8)	0.1806(3)	0.0360	
H(51)	0.3881(5)	0.9403(8)	0.1364(3)	0.0352	
H(71)	0.4197(5)	0.5173(8)	0.1078(3)	0.0335	
H(81)	0.5668(5)	0.5183(8)	0.1498(3)	0.0317	
C(12)	0.1020(6)	0.9025(8)	0.0270(4)	0.0376	
H(121)	0.1422(6)	0.8984(8)	-0.0015(4)	0.0461	
H(122)	0.0995(6)	0.9982(8)	0.0390(4)	0.0461	
H(123)	0.0389(6)	0.8716(8)	0.0183(4)	0.0461	

C(13)	0.0864(6)	0.833(1)	0.1156(3)	0.0388
H(131)	0.0194(6)	0.816(1)	0.1108(3)	0.0525
H(132)	0.0960(6)	0.928(1)	0.1270(3)	0.0525
H(133)	0.1111(6)	0.768(1)	0.1395(3)	0.0525
C(14)	0.1833(7)	0.623(1)	0.0002(3)	0.0423
H(141)	0.1313(7)	0.646(1)	-0.0216(3)	0.0543
H(142)	0.2367(7)	0.683(1)	-0.0070(3)	0.0543
H(143)	0.2014(7)	0.526(1)	-0.0042(3)	0.0543
C(15)	0.0671(7)	0.556(1)	0.0658(4)	0.0502
H(151)	0.0144(7)	0.580(1)	0.0447(4)	0.0583
H(152)	0.0498(7)	0.572(1)	0.0995(4)	0.0583
H(153)	0.0833(7)	0.458(1)	0.0614(4)	0.0583
C(16)	0.8370(6)	0.708(1)	0.3150(3)	0.0377
H(161)	0.8980(6)	0.705(1)	0.3312(3)	0.0496
H(162)	0.8016(6)	0.788(1)	0.3266(3)	0.0496
H(163)	0.8024(6)	0.622(1)	0.3221(3)	0.0496
C(17)	0.9177(6)	0.5687(9)	0.2199(3)	0.0342
H(171)	0.9805(6)	0.5615(9)	0.2340(3)	0.0456
H(172)	0.9226(6)	0.5811(9)	0.1849(3)	0.0456
H(173)	0.8826(6)	0.4837(9)	0.2268(3)	0.0456
C(18)	0.9175(7)	0.8941(9)	0.2301(3)	0.0390
H(181)	0.9797(7)	0.8930(9)	0.2450(3)	0.0489
H(182)	0.8823(7)	0.9743(9)	0.2420(3)	0.0489
H(183)	0.9237(7)	0.9006(9)	0.1950(3)	0.0489

8.6 Crystallographic data for 24

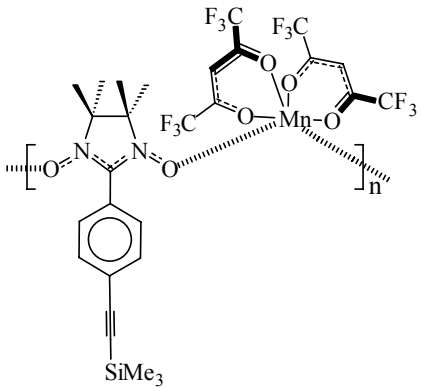

TABLE 8.11. *Crystal data and structure refinement for* ***24***

	24
Empirical Formula	$C_{28}H_{30}MnSiF_{12}O_6N_2$
Formula weight	798.52
Temperature	120
Wavelength (Mo Kα), Å	0.7107
Crystal system, space group	Orthorhombic, $P2_12_12_1$
a, Å	14.0062(5)
b, Å	15.0224(6)
c, Å	16.4600(6)
β (°)	90
Volume ($Å^3$)	3463.3(4)
Z, ρ (g/cm^3)	4, 1.531
Absorption coefficient (cm^{-1})	5.019
F (000)	1617.932
Crystal size (mm)	0.32 × 0.24 × 0.08
Theta range for data collection (°)	0 to 27.5
Index ranges	0<=h<=18, 0<=k<=19, -21<=l<=21
Reflections collected / unique	28573 / 7798
Refinement method	Full-matrix least-square on F
Data / restraints / parameters	5202 / 0 / 451
Goodness-of-fit on F^2	1.080
Final R indices [I>2σ (I)]	R1 = 0.043, R_w = 0.049
Largest diff. peak and hole	0.81 and -0.62 $Å^{-3}$

TABLE 8.12. *Atomic coordinates and Equivalent Isotropic Displacement Parameters*

Atom	x/a	y/b	z/c	U(iso)	Occ
Mn(1)	0.06727(4)	0.16718(4)	0.02643(3)	0.0193	
Si(1)	0.40150(8)	0.38978(8)	0.48396(7)	0.0338	
O(1)	0.14153(16)	0.26788(17)	-0.03845(15)	0.0223	
O(2)	0.46913(17)	0.23005(17)	-0.05229(15)	0.0217	
O(11)	0.01361(18)	0.09922(18)	-0.08012(15)	0.0253	
O(12)	-0.0263(2)	0.07554(18)	0.08648(16)	0.0282	
O(13)	0.18287(18)	0.07365(17)	0.01361(17)	0.0264	
O(14)	0.12827(18)	0.18250(17)	0.14569(16)	0.0257	
F(1)	0.0326(5)	0.0215(3)	-0.2201(2)	0.1262	
F(2)	0.0375(5)	-0.1020(3)	-0.1628(3)	0.1317	
F(3)	-0.0915(3)	-0.0432(4)	-0.1924(3)	0.1037	
F(4)	0.0087(3)	-0.1033(3)	0.1604(3)	0.0934	
F(5)	-0.1179(4)	-0.0316(2)	0.1866(3)	0.1147	
F(6)	-0.1184(3)	-0.1368(2)	0.1030(2)	0.0738	
F(7)	0.3116(3)	-0.1003(2)	0.10064(18)	0.0725	
F(8)	0.3197(2)	-0.04899(18)	-0.01881(18)	0.0499	
F(9)	0.1939(2)	-0.1157(2)	0.0179(3)	0.0874	
F(10)	0.2438(2)	0.0993(2)	0.31325(16)	0.0542	
F(11)	0.09133(18)	0.08757(18)	0.30528(15)	0.0419	
F(12)	0.1568(2)	0.21609(16)	0.29998(14)	0.0414	
N(1)	0.2269(2)	0.2568(2)	-0.06823(17)	0.0196	
N(2)	0.3807(2)	0.2393(2)	-0.07456(17)	0.0180	
C(1)	0.3667(3)	0.3612(3)	0.3797(3)	0.0380	
C(2)	0.3521(3)	0.3419(3)	0.3102(2)	0.0354	
C(3)	0.3379(3)	0.3173(3)	0.2258(2)	0.0317	
C(6)	0.3157(3)	0.2746(3)	0.0627(2)	0.0208	
C(9)	0.3079(2)	0.2562(2)	-0.0238(2)	0.0179	
C(10)	0.2450(3)	0.2555(3)	-0.1572(2)	0.0272	
C(11)	0.3488(3)	0.2173(3)	-0.1591(2)	0.0224	
C(21)	-0.0067(3)	-0.0259(3)	-0.1647(3)	0.0363	
C(22)	-0.0089(3)	0.0193(3)	-0.0814(3)	0.0291	
C(24)	-0.0427(3)	-0.0025(3)	0.0623(3)	0.0276	
C(25)	-0.0693(4)	-0.0675(3)	0.1296(3)	0.0368	
C(26)	0.2612(3)	-0.0603(3)	0.0433(3)	0.0370	
C(27)	0.2173(3)	0.0287(3)	0.0705(2)	0.0263	
C(29)	0.1708(3)	0.1238(3)	0.1836(2)	0.0241	
C(30)	0.1676(3)	0.1320(3)	0.2771(2)	0.0293	
C(4)	0.2741(3)	0.3651(3)	0.1777(2)	0.0300	
C(5)	0.2623(3)	0.3439(3)	0.0965(2)	0.0257	
C(7)	0.3790(3)	0.2259(3)	0.1112(2)	0.0255	
C(8)	0.3887(3)	0.2472(3)	0.1922(2)	0.0285	
C(23)	-0.0367(3)	-0.0344(3)	-0.0164(3)	0.0323	
C(28)	0.2165(3)	0.0470(3)	0.1531(2)	0.0264	
H(41)	0.2378(3)	0.4119(3)	0.2012(2)	0.0372	
H(51)	0.2188(3)	0.3768(3)	0.0640(2)	0.0322	
H(71)	0.4159(3)	0.1793(3)	0.0881(2)	0.0347	
H(81)	0.4312(3)	0.2142(3)	0.2256(2)	0.0330	
H(231)	-0.0524(3)	-0.0949(3)	-0.0269(3)	0.0392	

H(281)	0.2462(3)	0.0068(3)	0.1899(2)	0.0341
C(12)	0.1712(3)	0.1972(4)	-0.2005(3)	0.0494
H(121)	0.1830(3)	0.1971(4)	-0.2573(3)	0.0571
H(122)	0.1091(3)	0.2200(4)	-0.1903(3)	0.0571
H(123)	0.1755(3)	0.1381(4)	-0.1802(3)	0.0571
C(13)	0.2387(3)	0.3527(3)	-0.1844(3)	0.0422
H(131)	0.2492(3)	0.3564(3)	-0.2413(3)	0.0519
H(132)	0.2861(3)	0.3863(3)	-0.1568(3)	0.0519
H(133)	0.1774(3)	0.3758(3)	-0.1718(3)	0.0519
C(14)	0.3541(3)	0.1157(3)	-0.1656(3)	0.0328
H(141)	0.3350(3)	0.0972(3)	-0.2183(3)	0.0346
H(142)	0.4174(3)	0.0958(3)	-0.1554(3)	0.0346
H(143)	0.3122(3)	0.0909(3)	-0.1263(3)	0.0346
C(15)	0.4148(3)	0.2621(3)	-0.2209(2)	0.0263
H(151)	0.3950(3)	0.2484(3)	-0.2747(2)	0.0297
H(152)	0.4781(3)	0.2412(3)	-0.2127(2)	0.0297
H(153)	0.4129(3)	0.3247(3)	-0.2131(2)	0.0297
C(16)	0.4883(3)	0.3032(3)	0.5170(3)	0.0408
H(161)	0.5081(3)	0.3151(3)	0.5712(3)	0.0546
H(162)	0.5424(3)	0.3035(3)	0.4822(3)	0.0546
H(163)	0.4585(3)	0.2464(3)	0.5148(3)	0.0546
C(17)	0.4555(4)	0.5032(3)	0.4811(4)	0.0556
H(171)	0.4741(4)	0.5197(3)	0.5345(4)	0.0670
H(172)	0.5099(4)	0.5032(3)	0.4466(4)	0.0670
H(173)	0.4098(4)	0.5445(3)	0.4611(4)	0.0670
C(18)	0.2956(4)	0.3892(5)	0.5513(3)	0.0659
H(181)	0.3148(4)	0.4038(5)	0.6050(3)	0.0734
H(182)	0.2501(4)	0.4316(5)	0.5328(3)	0.0734
H(183)	0.2677(4)	0.3316(5)	0.5509(3)	0.0734

8.7 Crystallographic data for 25

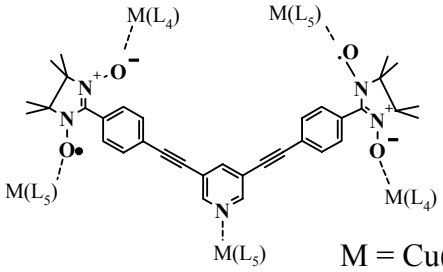

M = $Cu(hfac)_2$

TABLE 8.13 *Crystal data and structure refinement for* ***25***

	25
Empirical Formula	$C_{70}H_4Cu_{3.5}F_{42}O_{18}N_5$
Formula weight	2261.45
Temperature	120
Wavelength (Mo Kα), Å	0.7107
Crystal system, space group	Triclinic, P-1
a, Å	10.6191(4)
b, Å	19.6384(7)
c, Å	21.9418(8)
α, β, γ (°)	107.1117(14), 95.1078(12), 94.2080(12)
Volume ($Å^3$)	4331.93
Z, ρ (g/cm^3)	2, 1.734
Absorption coefficient (cm^{-1})	1.007
F (000)	2244.595
Crystal size (mm)	0.38 × 0.22 × 0.09
Theta range for data collection (°)	0 to 27.5
Index ranges	13<=h<=13, 25<=k<=24, 0<=l<=28
Reflections collected / unique	40178 / 19122
Refinement method	Full-matrix least-square on F
Data / restraints / parameters	7876 / 0 / 1189
Goodness-of-fit on F^2	1.174
Final R indices [I>2σ (I)]	R1 = 0.073, R_w = 0.047
Largest diff. peak and hole	1.28 and -0.53 $Å^{-3}$

TABLE 8.14. *Atomic coordinates and Equivalent Isotropic Displacement Parameters*

Atom	x/a	y/b	z/c	U(iso)	Occ
Cu(1)	0.9462(1)	0.91190(5)	0.10943(5)	0.0386	
F(41)	0.8197(7)	1.0607(3)	-0.0062(3)	0.0832	
F(42)	0.6319(6)	1.0628(3)	0.0250(4)	0.1014	
F(43)	0.7961(5)	1.1157(2)	0.0909(3)	0.0567	
F(44)	0.5300(5)	0.8100(3)	0.0987(3)	0.0664	
F(45)	0.6014(5)	0.7531(3)	0.0137(3)	0.0835	
F(46)	0.4747(5)	0.8307(3)	0.0124(3)	0.0618	
F(54)	1.2810(6)	0.7328(3)	0.1068(3)	0.0795	
F(55)	1.1416(6)	0.7279(3)	0.1676(3)	0.0817	
F(56)	1.0895(7)	0.6975(3)	0.0659(3)	0.0875	
O(41)	0.8839(5)	0.9888(3)	0.0847(3)	0.0345	
O(42)	0.7852(6)	0.8531(3)	0.0810(3)	0.0417	
O(51)	1.1093(5)	0.9700(3)	0.1385(3)	0.0431	
O(52)	1.0177(5)	0.8270(3)	0.1119(3)	0.0370	
C(41)	0.7740(8)	0.9888(4)	0.0606(4)	0.0327	
C(43)	0.6872(8)	0.8735(4)	0.0612(4)	0.0364	
C(44)	0.7533(8)	1.0595(5)	0.0430(5)	0.0484	
C(45)	0.5720(7)	0.8164(5)	0.0456(5)	0.0373	
C(51)	1.2126(8)	0.9448(4)	0.1443(4)	0.0394	
C(53)	1.1303(9)	0.8199(4)	0.1172(4)	0.0412	
C(54)	1.3287(8)	1.0021(5)	0.1656(5)	0.0584	
C(55)	1.164(1)	0.7439(5)	0.1143(5)	0.0525	
C(42)	0.6722(8)	0.9375(4)	0.0487(4)	0.0354	
C(52)	1.2328(8)	0.8748(4)	0.1322(4)	0.0386	
H(421)	0.5912(8)	0.9462(4)	0.0322(4)	0.0450	
H(521)	1.3172(8)	0.8623(4)	0.1362(4)	0.0451	
F(511)	1.335(1)	1.0275(6)	0.2310(6)	0.0559	0.494(8)
F(521)	1.3125(11)	1.0576(6)	0.1492(6)	0.0559	0.494(8)
F(531)	1.4349(11)	0.9734(6)	0.1464(6)	0.0559	0.494(8)
F(512)	1.339(1)	1.0344(6)	0.1158(6)	0.0559	0.506(8)
F(522)	1.310(1)	1.0587(6)	0.2090(6)	0.0559	0.506(8)
F(532)	1.4352(11)	0.9781(6)	0.1760(6)	0.0559	0.506(8)
Cu(2)	0.94876(8)	0.32506(4)	0.21372(4)	0.0206	
F(61)	1.1620(4)	0.2434(2)	0.3648(2)	0.0416	
F(62)	1.3069(4)	0.3075(2)	0.3394(2)	0.0469	
F(63)	1.2965(5)	0.1926(3)	0.3043(2)	0.0462	
F(64)	1.2312(5)	0.1944(4)	0.0695(2)	0.0758	
F(65)	1.1204(8)	0.1011(3)	0.0751(3)	0.0986	
F(66)	1.0389(5)	0.1705(3)	0.0301(2)	0.0595	
F(71)	0.8151(4)	0.4016(3)	0.0464(2)	0.0580	
F(72)	0.6852(5)	0.4515(3)	0.1102(3)	0.0545	
F(73)	0.6222(4)	0.3568(3)	0.0323(2)	0.0501	
O(61)	1.0574(4)	0.2938(2)	0.2751(2)	0.0232	
O(62)	0.9947(5)	0.2495(2)	0.1405(2)	0.0252	
O(71)	0.8630(4)	0.3675(2)	0.1539(2)	0.0235	
O(72)	0.7700(5)	0.2605(3)	0.2138(3)	0.0292	
C(61)	1.1389(7)	0.2505(4)	0.2589(4)	0.0248	
C(63)	1.0833(7)	0.2129(4)	0.1434(3)	0.0254	
C(64)	1.2263(8)	0.2476(4)	0.3172(4)	0.0310	
C(65)	1.1185(9)	0.1688(4)	0.0793(4)	0.0371	
C(71)	0.7529(7)	0.3448(4)	0.1224(3)	0.0230	
C(73)	0.6784(7)	0.2565(4)	0.1731(4)	0.0292	

C(74)	0.7176(8)	0.3892(5)	0.0777(4)	0.0352	
C(75)	0.5630(7)	0.2063(4)	0.1772(4)	0.0395	
C(62)	1.1593(7)	0.2093(4)	0.1984(3)	0.0268	
C(72)	0.6652(7)	0.2926(4)	0.1270(4)	0.0284	
H(621)	1.2233(7)	0.1774(4)	0.1939(3)	0.0326	
H(721)	0.5905(7)	0.2803(4)	0.0972(4)	0.0371	
F(741)	0.5800(13)	0.1403(7)	0.1545(8)	0.0589	0.394(6)
F(751)	0.4553(13)	0.2209(8)	0.1533(7)	0.0589	0.394(6)
F(761)	0.5449(14)	0.2159(8)	0.2387(7)	0.0589	0.394(6)
F(742)	0.5922(8)	0.1506(5)	0.1943(5)	0.0589	0.606(6)
F(752)	0.4865(8)	0.1798(5)	0.1230(5)	0.0589	0.606(6)
F(762)	0.4953(9)	0.2401(5)	0.2230(5)	0.0589	0.606(6)
Cu(3)	1.52667(9)	0.63217(5)	0.28298(5)	0.0307	
F(81)	1.4795(8)	0.6982(4)	0.4976(3)	0.0999	
F(82)	1.6675(7)	0.6777(5)	0.5010(3)	0.1255	
F(83)	1.5254(8)	0.6017(4)	0.5115(3)	0.0995	
F(84)	1.4390(4)	0.3912(2)	0.2566(2)	0.0308	
F(85)	1.5523(5)	0.3943(2)	0.3438(2)	0.0461	
F(86)	1.6411(4)	0.4076(2)	0.2631(2)	0.0421	
F(91)	1.3837(5)	0.8372(3)	0.2499(3)	0.0680	
F(92)	1.5716(6)	0.8816(3)	0.2452(3)	0.0665	
F(93)	1.5163(5)	0.8727(2)	0.3347(2)	0.0509	
F(94)	1.6621(6)	0.6075(3)	0.0788(3)	0.0747	
F(95)	1.8254(6)	0.6122(3)	0.1433(3)	0.0648	
F(96)	1.7848(5)	0.7050(3)	0.1159(3)	0.0618	
O(81)	1.5334(5)	0.6560(3)	0.3764(2)	0.0337	
O(82)	1.5320(5)	0.5313(2)	0.2735(2)	0.0293	
O(91)	1.5069(5)	0.7306(3)	0.2928(2)	0.0328	
O(92)	1.6243(5)	0.6210(3)	0.2092(2)	0.0306	
C(81)	1.5394(7)	0.6127(4)	0.4078(4)	0.0304	
C(83)	1.5394(6)	0.5048(4)	0.3187(4)	0.0211	
C(84)	1.5528(12)	0.6477(6)	0.4809(5)	0.0614	
C(85)	1.5420(7)	0.4242(4)	0.2968(4)	0.0276	
C(91)	1.5473(8)	0.7637(4)	0.2557(4)	0.0327	
C(93)	1.6517(7)	0.6709(4)	0.1867(4)	0.0318	
C(94)	1.5056(9)	0.8407(5)	0.2725(5)	0.0470	
C(95)	1.733(1)	0.6496(5)	0.1300(4)	0.0463	
C(82)	1.5437(7)	0.5383(4)	0.3844(4)	0.0314	
C(92)	1.6190(8)	0.7408(4)	0.2059(4)	0.0368	
H(821)	1.5487(7)	0.5110(4)	0.4136(4)	0.0393	
H(921)	1.6483(8)	0.7733(4)	0.1843(4)	0.0432	
Cu(4)	1.0000	1.0000	0.5000	0.0348	
F(101)	1.2873(7)	1.1310(5)	0.4206(4)	0.1266	
F(102)	1.3732(7)	1.1323(4)	0.5082(4)	0.1119	
F(103)	1.4307(8)	1.0655(4)	0.4264(5)	0.1571	
F(104)	1.1279(6)	0.7810(3)	0.4264(3)	0.0826	
F(105)	1.2274(7)	0.8074(3)	0.3572(3)	0.0941	
F(106)	1.3193(6)	0.8262(3)	0.4516(4)	0.1039	
O(101)	1.1315(5)	1.0546(3)	0.4723(3)	0.0422	
O(102)	1.0625(5)	0.9094(3)	0.4561(3)	0.0395	
C(101)	1.2314(9)	1.0293(5)	0.4516(4)	0.0478	
C(103)	1.1716(9)	0.9043(5)	0.4378(4)	0.0418	
C(104)	1.3314(11)	1.0895(7)	0.4497(7)	0.0681	
C(105)	1.213(1)	0.8287(6)	0.4179(5)	0.0548	
C(102)	1.2576(9)	0.9588(5)	0.4344(5)	0.0527	
H(1021)	1.3375(9)	0.9478(5)	0.4198(5)	0.0588	

O(11)	1.1529(5)	0.3807(3)	0.1933(2)	0.0313
O(12)	1.3365(5)	0.6099(3)	0.2225(2)	0.0294
N(11)	1.2002(5)	0.4368(3)	0.1826(3)	0.0234
N(12)	1.2837(5)	0.5448(3)	0.1957(3)	0.0232
C(22)	1.1554(7)	0.5596(4)	0.5435(4)	0.0273
C(23)	1.1763(6)	0.5601(4)	0.4909(4)	0.0267
C(24)	1.1975(6)	0.5488(4)	0.4258(3)	0.0266
C(27)	1.2273(6)	0.5183(4)	0.2955(3)	0.0204
C(30)	1.2374(6)	0.5006(4)	0.2271(3)	0.0231
C(31)	1.2387(7)	0.4343(4)	0.1175(3)	0.0291
C(32)	1.2545(8)	0.5146(4)	0.1249(4)	0.0326
C(25)	1.2054(6)	0.6034(4)	0.3970(3)	0.0259
C(26)	1.2214(7)	0.5897(4)	0.3335(4)	0.0256
C(28)	1.2226(6)	0.4637(4)	0.3252(3)	0.0238
C(29)	1.2078(6)	0.4796(4)	0.3883(3)	0.0198
H(251)	1.1993(6)	0.6513(4)	0.4222(3)	0.0312
H(261)	1.2286(7)	0.6273(4)	0.3146(4)	0.0301
H(281)	1.2311(6)	0.4158(4)	0.3007(3)	0.0240
H(291)	1.2026(6)	0.4421(4)	0.4075(3)	0.0261
C(33)	1.3651(7)	0.4004(4)	0.1130(4)	0.0360
H(331)	1.3948(7)	0.3980(4)	0.0729(4)	0.0421
H(332)	1.4269(7)	0.4283(4)	0.1469(4)	0.0421
H(333)	1.3510(7)	0.3535(4)	0.1165(4)	0.0421
C(34)	1.1402(7)	0.3882(4)	0.0654(4)	0.0342
H(341)	1.1632(7)	0.3868(4)	0.0242(4)	0.0401
H(342)	1.1331(7)	0.3411(4)	0.0690(4)	0.0401
H(343)	1.0610(7)	0.4074(4)	0.0709(4)	0.0401
C(35)	1.1280(9)	0.5418(5)	0.1076(4)	0.0526
H(351)	1.1041(9)	0.5242(5)	0.0626(4)	0.0558
H(352)	1.1382(9)	0.5927(5)	0.1208(4)	0.0558
H(353)	1.0638(9)	0.5256(5)	0.1292(4)	0.0558
C(36)	1.3617(9)	0.5407(5)	0.0919(4)	0.0515
H(361)	1.3428(9)	0.5216(5)	0.0466(4)	0.0615
H(362)	1.3699(9)	0.5915(5)	0.1038(4)	0.0615
H(363)	1.4390(9)	0.5250(5)	0.1052(4)	0.0615
O(1)	0.8817(6)	0.9275(3)	0.2021(4)	0.0793
O(2)	0.8330(6)	1.0031(3)	0.4227(3)	0.0469
N(1)	0.8724(6)	0.9708(3)	0.2641(3)	0.0357
N(2)	0.8460(7)	1.0031(3)	0.3648(3)	0.0427
N(3)	0.9164(5)	0.4075(3)	0.2874(3)	0.0249
C(1)	0.8896(6)	0.5321(4)	0.3323(4)	0.0256
C(2)	0.8864(7)	0.6008(4)	0.3258(4)	0.0270
C(3)	0.8807(7)	0.6605(4)	0.3236(4)	0.0326
C(4)	0.8758(7)	0.7325(4)	0.3209(4)	0.0340
C(7)	0.8660(7)	0.8731(4)	0.3173(4)	0.0289
C(10)	0.8610(7)	0.9462(4)	0.3152(4)	0.0315
C(11)	0.8255(9)	1.0690(4)	0.3461(4)	0.0414
C(12)	0.885(1)	1.0489(5)	0.2827(4)	0.0537
C(18)	0.8693(6)	0.4527(4)	0.3969(3)	0.0272
C(5)	0.9397(8)	0.7565(4)	0.2762(4)	0.0408
C(6)	0.9329(8)	0.8252(4)	0.2739(4)	0.0426
C(8)	0.8057(7)	0.8500(4)	0.3613(4)	0.0330
C(9)	0.8095(7)	0.7803(4)	0.3635(4)	0.0321
C(17)	0.8670(6)	0.5206(4)	0.3911(3)	0.0241
C(19)	0.8934(6)	0.3961(4)	0.3440(3)	0.0212
C(20)	0.9123(6)	0.4736(3)	0.2828(3)	0.0228
H(51)	0.9872(8)	0.7249(4)	0.2478(4)	0.0506
H(61)	0.9746(8)	0.8407(4)	0.2430(4)	0.0504
H(81)	0.7606(7)	0.8817(4)	0.3909(4)	0.0426

H(91)	0.7664(7)	0.7648(4)	0.3940(4)	0.0361
H(171)	0.8502(6)	0.5593(4)	0.4262(3)	0.0270
H(191)	0.8941(6)	0.3489(4)	0.3472(3)	0.0253
H(201)	0.9257(6)	0.4811(3)	0.2429(3)	0.0249
C(13)	0.8973(11)	1.1348(4)	0.3967(4)	0.0630
H(131)	0.8856(11)	1.1764(4)	0.3839(4)	0.0757
H(132)	0.9853(11)	1.1290(4)	0.4011(4)	0.0757
H(133)	0.8648(11)	1.1398(4)	0.4366(4)	0.0757
C(14)	0.6893(11)	1.0752(7)	0.3375(7)	0.0902
H(141)	0.6724(11)	1.1165(7)	0.3254(7)	0.1058
H(142)	0.6570(11)	1.0780(7)	0.3771(7)	0.1058
H(143)	0.6494(11)	1.0336(7)	0.3053(7)	0.1058
C(15)	1.0366(12)	1.0695(6)	0.2941(6)	0.0886
H(151)	1.0543(12)	1.1201(6)	0.3069(6)	0.0947
H(152)	1.0728(12)	1.0490(6)	0.2557(6)	0.0947
H(153)	1.0720(12)	1.0517(6)	0.3270(6)	0.0947
C(16)	0.8393(15)	1.0778(6)	0.2314(5)	0.1120
H(161)	0.8522(15)	1.1287(6)	0.2455(5)	0.0934
H(162)	0.8811(15)	1.0600(6)	0.1942(5)	0.0934
H(163)	0.7509(15)	1.0627(6)	0.2213(5)	0.0934

8.8 Crystallographic data for 26

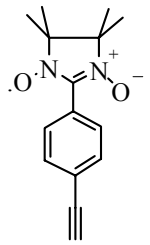

TABLE 8.15. *Crystal data and structure refinement for* ***26***

	26
Empirical Formula	$C_{15}H_{17}O_2N_2$
Formula weight	257.31
Temperature	120
Wavelength (Mo Kα), Å	0.7107
Crystal system, space group	Monoclinic, $P2_1/c$
a, Å	8.0924(3)
b, Å	19.9703(9)
c, Å	8.9068(4)
α, β, γ (°)	90, 109.079(2), 90
Volume ($Å^3$)	1360.3
Z, ρ (g/cm^3)	4, 1.264
Absorption coefficient (cm^{-1})	0.084
F (000)	548.232
Crystal size (mm)	0.53 × 0.26 × 0.12
Theta range for data collection (°)	0 to 27.5
Index ranges	-10<=h<=9, 0<=k<=25, 0<=l<=11
Reflections collected / unique	11119 / 3192
Refinement method	Full-matrix least-square on F
Data / restraints / parameters	1559 / 0 / 172
Goodness-of-fit on F^2	1.070
Final R indices [I>2σ (I)]	R1 = 0.04365, R_w = 0.04703
Largest diff. peak and hole	0.59 and -0.39 $Å^{-3}$

TABLE 8.16. *Atomic coordinates and Equivalent Isotropic Displacement Parameters*

Atom	x/a	y/b	z/c	U(iso)Occ
O(1)	0.2651(2)	0.36049(8)	0.2633(2)	0.0316
O(2)	0.6785(2)	0.2145(1)	0.1952(3)	0.0465
N(1)	0.4085(2)	0.33735(9)	0.2513(2)	0.0217
N(2)	0.6024(2)	0.2683(1)	0.2152(2)	0.0274
C(2)	0.0244(3)	0.04591(13)	0.2580(3)	0.0324
C(3)	0.1255(3)	0.10451(11)	0.2492(3)	0.0250
C(6)	0.3304(3)	0.21583(11)	0.2345(3)	0.0205
C(9)	0.4431(3)	0.27272(11)	0.2320(3)	0.0207
C(10)	0.5563(3)	0.38353(12)	0.2556(3)	0.0266
C(11)	0.6939(3)	0.33406(14)	0.2294(3)	0.0335
C(1)	-0.0558(4)	-0.00270(13)	0.2653(4)	0.0412
C(4)	0.1169(3)	0.16278(12)	0.3322(3)	0.0264
C(5)	0.2167(3)	0.21811(11)	0.3238(3)	0.0218
C(7)	0.3382(3)	0.15755(12)	0.1507(3)	0.0259
C(8)	0.2352(3)	0.10309(12)	0.1567(3)	0.0287
H(11)	-0.1201(4)	-0.04183(13)	0.2713(4)	0.0487
H(41)	0.0417(3)	0.16445(12)	0.3947(3)	0.0330
H(51)	0.2088(3)	0.25794(11)	0.3794(3)	0.0271
H(71)	0.4146(3)	0.15548(12)	0.0894(3)	0.0311
H(81)	0.2381(3)	0.06406(12)	0.0966(3)	0.0336
C(12)	0.4873(4)	0.43500(19)	0.1241(5)	0.0718
H(121)	0.5779(4)	0.46521(19)	0.1238(5)	0.0829
H(122)	0.3934(4)	0.45920(19)	0.1401(5)	0.0829
H(123)	0.4470(4)	0.41217(19)	0.0253(5)	0.0829
C(13)	0.6141(4)	0.41760(14)	0.4165(4)	0.0424
H(131)	0.7081(4)	0.44733(14)	0.4237(4)	0.0518
H(132)	0.5192(4)	0.44198(14)	0.4301(4)	0.0518
H(133)	0.6517(4)	0.38444(14)	0.4970(4)	0.0518
C(14)	0.7404(6)	0.34398(19)	0.0794(5)	0.0810
H(141)	0.7995(6)	0.38542(19)	0.0839(5)	0.1171
H(142)	0.8134(6)	0.30844(19)	0.0679(5)	0.1171
H(143)	0.6354(6)	0.34414(19)	-0.0088(5)	0.1171
C(15)	0.8605(4)	0.3282(2)	0.3725(5)	0.0745
H(151)	0.9243(4)	0.3690(2)	0.3873(5)	0.0806
H(152)	0.9309(4)	0.2927(2)	0.3560(5)	0.0806
H(153)	0.8288(4)	0.3191(2)	0.4642(5)	0.0806

8.9 Crystallographic data for 27

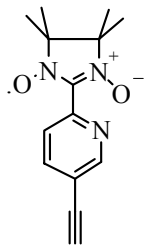

TABLE 8.17. *Crystal data and structure refinement for* ***27***

	27
Empirical Formula	$C_{14}H_{16}O_2N_3$
Formula weight	258.30
Temperature	120
Wavelength (Mo Kα), Å	0.7107
Crystal system, space group	Orthorhombic, Pbca
a, Å	8.5206(4)
b, Å	15.7718(6)
c, Å	19.9660(7)
α, β, γ (°)	90, 90, 90
Volume ($Å^3$)	2683.1
Z, ρ (g/cm^3)	8, 1.279
Absorption coefficient (cm^{-1})	0.088
F (000)	1095.918
Crystal size (mm)	0.38 × 0.20 × 0.09
Theta range for data collection (°)	0 to 27.5
Index ranges	0<=h<=10, 0<=k<=20, 0<=l<=25
Reflections collected / unique	17450 / 2992
Refinement method	Full-matrix least-square on F
Data / restraints / parameters	1326 / 0 / 173
Goodness-of-fit on F^2	1.048
Final R indices [I>2σ (I)]	R1 = 0.03898, R_w = 0.04379
Largest diff. peak and hole	0.68 and -0.39 $Å^{-3}$

TABLE 8.18. *Atomic coordinates and Equivalent Isotropic Displacement Parameters*

Atom	x/a	y/b	z/c	U(iso)	Occ
O(1)	0.1827(2)	0.35272(11)	0.28471(8)	0.0245	
O(2)	0.1838(2)	0.12278(11)	0.14010(9)	0.0257	
N(1)	0.0926(3)	0.17760(13)	0.3354(1)	0.0199	
N(2)	0.1692(3)	0.30866(13)	0.2307(1)	0.0179	
N(3)	0.1762(3)	0.19976(13)	0.1616(1)	0.0182	
C(2)	0.2395(3)	0.01286(18)	0.45364(13)	0.0233	
C(3)	0.2244(3)	0.06330(16)	0.39344(12)	0.0185	
C(5)	0.1926(3)	0.16500(15)	0.28384(11)	0.0166	
C(8)	0.1765(3)	0.22359(15)	0.22672(11)	0.0165	
C(9)	0.1754(3)	0.35035(15)	0.16256(11)	0.0175	
C(10)	0.1428(3)	0.27331(16)	0.11555(12)	0.0197	
C(1)	0.2561(4)	-0.02746(18)	0.50359(14)	0.0318	
C(4)	0.1099(3)	0.12621(17)	0.38841(12)	0.0203	
C(6)	0.3061(3)	0.10221(15)	0.28329(12)	0.0197	
C(7)	0.3237(3)	0.05046(16)	0.33870(12)	0.0216	
H(11)	0.2689(4)	-0.05957(18)	0.54347(14)	0.0391	
H(41)	0.0394(3)	0.13308(17)	0.42489(12)	0.0241	
H(61)	0.3699(3)	0.09441(15)	0.24474(12)	0.0253	
H(71)	0.4018(3)	0.00749(16)	0.33982(12)	0.0256	
C(11)	0.0547(3)	0.42110(17)	0.15929(14)	0.0269	
H(111)	0.0589(3)	0.44741(17)	0.11652(14)	0.0334	
H(112)	0.0773(3)	0.46184(17)	0.19298(14)	0.0334	
H(113)	-0.0472(3)	0.39845(17)	0.16643(14)	0.0334	
C(12)	0.3418(3)	0.38720(18)	0.15680(14)	0.0285	
H(121)	0.3535(3)	0.41497(18)	0.11488(14)	0.0339	
H(122)	0.3590(3)	0.42666(18)	0.19200(14)	0.0339	
H(123)	0.4160(3)	0.34243(18)	0.16009(14)	0.0339	
C(13)	0.2504(4)	0.26805(19)	0.05472(13)	0.0303	
H(131)	0.2298(4)	0.31444(19)	0.02568(13)	0.0375	
H(132)	0.3567(4)	0.27015(19)	0.06905(13)	0.0375	
H(133)	0.2320(4)	0.21637(19)	0.03159(13)	0.0375	
C(14)	-0.0281(3)	0.26471(18)	0.09400(13)	0.0278	
H(141)	-0.0549(3)	0.30999(18)	0.06477(13)	0.0343	
H(142)	-0.0942(3)	0.26626(18)	0.13231(13)	0.0343	
H(143)	-0.0417(3)	0.21224(18)	0.07136(13)	0.0343	

First of all, I would like to submit my sincere thanks to my thesis guru Priv. Doz. Dr. Martin Baumgarten for giving me an opportunity to pursue my Ph.D. in this elite institute and exposing me to the demanding field of Molecular Magnetism. Further, I am indebted to him for giving me, superb guidance, constant encouragement, crystal clear and quality discussions and full scientific freedom. I acknowledge the graduate college of Darmstadt [TU Darmstadt] for the support given to me for my Ph.D. I extend my sincere thanks to Prof. K. Müllen, [MPIP] for permitting me to work at the MPIP and his support during my final phase of my thesis.

I am grateful to Prof. W. Haase [TU Darmstadt] for his nice collaboration and the facilities he has made available for the magnetic measurements. Without his help, the magnetic characterization part of this thesis would not be possible. I also thank, Dr. K. Falk for his tireless magnetic measurements of my samples. My sincere appreciation also goes to Dr. S. Ostrovsky for his kindness in the fitting process of all my magnetic data of the complexes.

I thank Prof. H. Plenio [TU Darmstadt] for agreeing to monitor my work as one of the supervisor. I would like to extend my thanks to A. Ivanova [Bulgaria] for her quantum mechanical computational work for the high spin molecules.

I gratefully acknowledge all of my international male friends, G. Zoppellaro [Italy], Dr. A. Geies [Egypt], Dr. H. Adel [Egypt], Dr. A. Grimsdale [New zealand], Dr. M. Wagner [Germany], G. Mihov [Bulgaria], Dr. V. Hrenov [Russia], K. Vaislev [Bulgaria], P. Petkov [Bulgaria], M. Abdalla [Egypt], A. Al-Hussaini [Egypt], Dr. W. Wu [China], Dr. C. Wang [China], J. Wu [China], J. Qu [China], E. Erhan [Turkey], R. Bauer [Romania], F. Nolde [Germany], Y. J. Jang [S. Korea], Dr. N. Lucas [Australia] , Dr. P. Zmolek [USA], D. Wasserfallen [Switzerland], Dr. C. Clark [USA], G. Tomović [Yugoslavia], L. Oldridge [New zealand], F. Dierschke [Germany], and female friends Dr. I. Scheppelmann [Germany], L. Gherghel [Romania], Dr. N. Tchebotareva [Russia], Dr. S. Klyatskaya [Russia], Y. Fogel [Russia], E. Andreitchenko [Russia], D. Grebel-Köhler [Germany] for their friendliness and nice company.

I thank my amicable MPIP Indian gang, R.S. Prabaharan, N.R. Kundu, Dr. J. Jacob, Dr. P. Suresh, A.K. Mishra, P. Sonar, R.Thaokar, S. Pal, Dr. R.S. Sathish, for providing me the Indian feeling and flavor.

Last but not least I thank, J. Schnee for her help in the laboratory.

List of Publications

1. C. Rajadurai, A. Ivanova, V. Enkelmann, M. Baumgarten, **"A Study on the Heteroatom Influence in Pyrdine Based NitronylNitroxide Biradicals with Phenylethynyl Spacers on the Molecular Ground State"** *J. Org. Chem.* **2003**, 68 (26), 9907-9915.

2. C. Rajadurai, S. Ostrovsky, K. Falk, V. Enkelmann, W. Haase, M. Baumgarten, **"Synthesis, Crystal Structure and Magnetism of Centrosymmetric Linear Trinuclear Copper (II) Complex of Pyridine NitronylNitroxide Derivative"**, *Inorg. Chim. Acta.* **2004**, 357, 581-587.

Curriculum Vitae

PERSONAL DETAILS

Chandrasekar RAJADURAI
Date of birth: May 20, 1973.
Citizenship: Indian
Marital status: Single

SCHOLASTIC RECORDS

- **Dr.rer.nat.** [Chemistry], from May, 2001 – Nov, 2003.Thesis topic : **"**High Spin Entities – A Supramolecular Approach via Pure Organic and Coordination Chemistry", in Prof. Müllen´s subgroup, under the supervision of Priv. Doz. Dr. Martin Baumgarten, at **Max Planck Institute for Polymer Research**, Mainz, Germany.

- **Lecturer (Full time)** in Chemistry in **Bharathiyar University** (SRMV College of Arts and Science), Coimbatore, India from June 1999 - April 2001 (taught B.Sc. and M.Sc. courses).

- **M.Tech.** [Polymer Science and Technology], **Indian Institute of Technology, Delhi** in 1998, CGPA: 7.92/10.00 (Very Good), Thesis topic: "Intrinsically and Extrinsically Conducting Polymer Blends".

- **M.Sc.** [Chemistry] from **The American College**, Madurai, in 1997, Percentage: 65.00. Thesis topic: "Thermal Clasien Rearrangement of Aryl Propargyl Ethers".

- **B.Sc.** [Chemistry] from **Thiagarajar College**, Madurai in 1994, Percentage: 77.07.

- **H.Sc.** [Science] from **Al-Ameen Higher Secondary School**, Madurai in 1991, Percentage: 72.00.

NATIONAL LEVEL ACHIEVEMENTS

- Qualified **ICAR- NET' 98** examination with **Asst. Professorship / Lectureship** in organic chemistry.

- Qualified Graduate Aptitude Test in Engineering (**GATE' 97**) in chemistry.

- Qualified **CSIR - NET** – **Junior Research Fellowship** and **Lectureship** conducted by Council of Scientific and Industrial Research (CSIR'96).

HOBBIES

Gardening, Painting, Listening to music, Reading, Debating and Travelling.

Chandrasekar Rajadurai,
MPI für Polymerforschung, Postfach 3148, D-55021 Mainz
Telefon:+49 (0)1798358215
e-mail:chandrasekar100@yahoo.com
Ackermannweg 10
D-55128- Mainz den 03.12.03

Eidesstattliche Erklärung

Ich erkläre hiermit an Eides Statt, dass ich meine Dissertation selbständig und nur mit den angegebenen Hilfsmitteln angefertigt habe.

_____
Signature (C. Rajadurai)

Chandrasekar Rajadurai,
MPI für Polymerforschung, Postfach 3148, D-55021 Mainz
Telefon:+49 (0)1798358215
e-mail:chandrasekar100@yahoo.com
Ackermannweg 10
D-55128- Mainz den 03.12.03

Erklärung

Ich erkläre hiermit, noch keinen Promotionsversuch unternommen zu haben.

_____
Signature (C. Rajadurai)